Acta Morphologica et Anthropologica 31 (1–2)

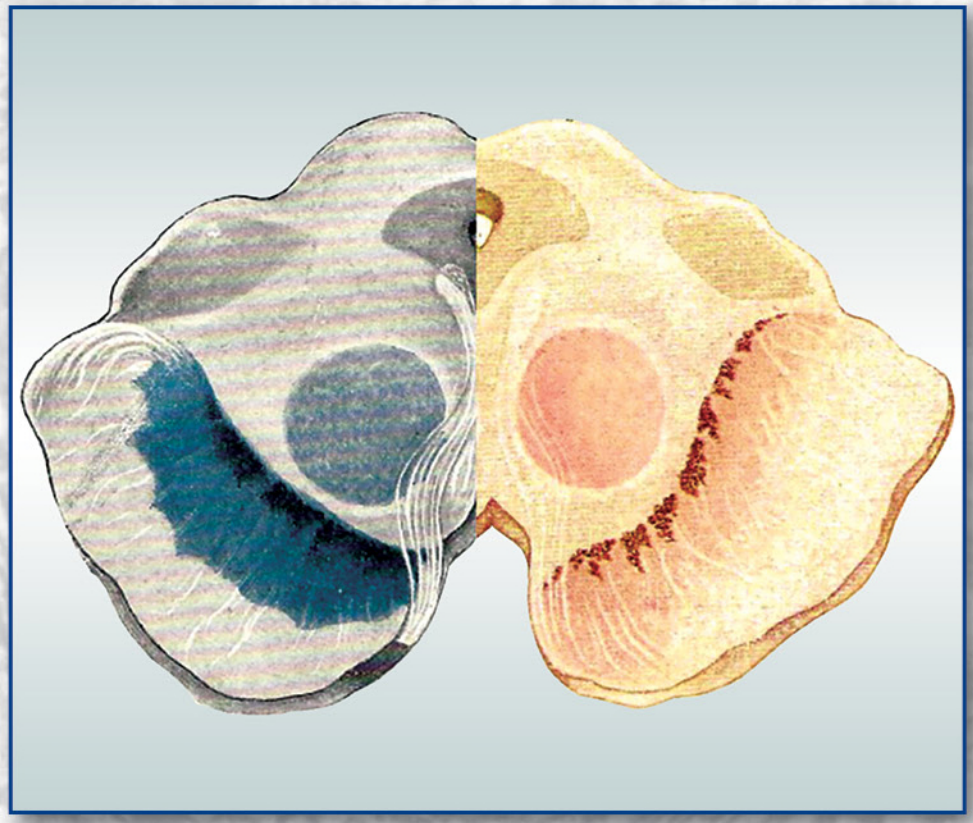

Prof. Marin Drinov Publishing House
of Bulgarian Academy of Sciences

Acta Morphologica et Anthropologica
is the continuation of Acta cytobiologica et morphologica

Indexed in:

Editorial Correspondence

Institute of Experimental Morphology, Pathology and Anthropology with Museum
Bulgarian Academy of Sciences
Acta Morphologica et Anthropologica
Acad. Georgi Bonchev Str., Bl. 25
1113 Sofia, Bulgaria

E-mail: ama.journal@iempam.bas.bg; yordanka.gluhcheva@iempam.bas.bg;
ygluhcheva@hotmail.com

Tel.: +359 2 979 2344

Издаването на настоящия том 31, книжки 1 и 2 е осъществено с финансовата подкрепа на Фонд „Научни изследвания“

Prof. Marin Drinov Publishing House of Bulgarian Academy of Sciences
Bulgaria, 1113 Sofia, Acad. Georgi Bonchev Str., Bl. 6

Graphic designer Veronika Tomcheva.

Format 70×100/16 Printed sheets 12,75

Printing Office of Prof. Marin Drinov Publishing House of Bulgarian Academy of Sciences
Bulgaria, 1113 Sofia, Acad. Georgi Bonchev Str., Bl. 5

Acta Morphologica et Anthropologica

ISSN 1311-8773 (print)
ISSN 2535-0811 (online)

Acta Morphologica et Anthropologica 31 (1-2)

31 (1-2) ● Sofia ● 2024
Institute of Experimental Morphology, Pathology and Anthropology with Museum
Bulgarian Anatomical Society

Contents

MORPHOLOGY 31 (1)

Original Articles

ANTHROPOLOGY AND ANATOMY 31 (2)

Institute of Experimental Morphology, Pathology and Anthropology with Museum
Bulgarian Anatomical Society

Acta Morphologica et Anthropologica, 31(1-2)
Sofia ● 2024

MORPHOLOGY 31 (1)

Original Articles

The GABAergic and Mixed GABAergic/glycinergic Neurons of the Murine Cerebellar Nuclei: What the Genes Tell Us

Karl Schilling

Anatomisches Institut – Anatomie und Zellbiologie, Rheinische Friedrich-Wilhelms-Universität Bonn, Bonn, Germany

Corresponding author e-mail: karl.schilling@uni-bonn.de

Our knowledge of the cellular composition and internal wiring of the cerebellar nuclei lags considerably behind our understanding of the cerebellar cortex. Here, we take advantage of publicly available data of gene expression in cells of the cerebellar nuclei and cortex to compare and contrast GABAergic and mixed GABAergic / glycinergic cells of these territories. We find that nucleo-olivary projection neurons are characterized by dichotomic expression levels of multiple genes, but in contrast to zebrin II-defined Purkinje cells, may not be separated into clearly distinct sets. The gene expression patterns of previously identified sets of inhibitory nuclear interneurons resemble those of Golgi, globular and Lugaro cells. Our analysis also suggests that the distinctive electrophysiological characteristic of inhibitory "interneurons" which also target the cerebellar cortex may be due to their quite specific expression of glycine receptors.

Key words: cerebellum, cerebellar nuclei, inhibitory interneuron, gene expression, scRNA

Introduction

The cerebellum is often used as a textbook paradigm to introduce students to basic principles of the structure, function, development and pathology of the central nervous system. Its cortex may be described as an extremely regular, quasi-crystalline, three-

layered ensemble of only a few cell types, with readily distinguishable morphologies, which are wired in a highly stereotyped manner. Purkinje cells arguably form the pivot of the cerebellar cortical circuitry. They directly receive extra-cerebellar input through climbing fibers, and indirectly through mossy fibers. The latter is mediated and modulated by granule cells. The cerebellar cortical circuitry is complemented by a set of inhibitory (i.e., GABAergic and/or glycinergic) interneurons, viz. Golgi cells in the granule cell layer, Lugaro cells, globular cells and candelabrum cells resident in the upper granule cell and Purkinje cell layers, and basket and stellate neurons in the molecular layer. Thus, cerebellar cortical inhibitory interneuron somata are located in quite distinct environments: whereas the molecular layer is formed primarily by a dense entanglement of granule cell axons, dendrites of inhibitory interneurons and Purkinje cells, and the processes of Bergmann glial cells, the granule cell layer and the Purkinje cell layer comprise a very dense matrix of granule cell and Purkinje cell somata. Cortical inhibitory interneurons may be further distinguished by their (primary) axonal projections to targets in the granule cell layer (i.e., Golgi cells), in the molecular layer (i.e., stellate cells, and Lugaro, candelabrum and globular cells), or in the molecular and Purkinje cell layers (basket cells; for a reviews, see [31, 33]). Lastly, cerebellar cortical inhibitory neurons may be classified by the transmitter(s), i.e., whether they are purely GABAergic (like basket, stellate, and a smaller subset of Golgi neurons), or also use glycine (most Golgi cells, Lugaro and globular cells; for an extended and detailed classification, see [35]).

A distinguishing characteristic of cerebellar cortical inhibitory interneurons is that their developmental diversification differs mechanistically from that of, say, inhibitory interneurons in other regions of the CNS (e.g., [24, 30]): they originate from a common pool of precursors characterized by the expression of the paired-box gene, Pax2. These precursors are programmed to their specific fate postmitotically by hitherto unknown, environmental signals while they migrate to their final destinations [18, 19], or even after arriving there [31].

In contrast to the cerebellar cortex, our understanding of the cerebellar nuclei is still rather fragmentary (for a recent review, see [14]). Typically, their role as the (sole) output gateway of the cerebellum is stressed. Output is realized through glutamatergic and glycinergic neurons, which target multiple areas in the CNS (see [14] for a detailed review), and through GABAergic cells projecting to the inferior olive. It is by now well established that cerebellar nuclei receive input not only from the cerebellar cortex, but also from extra-cerebellar sources. Importantly, they also comprise local interneurons. Thus, their cellular composition and structure strongly support the notion that they not only channel, but in fact process information.

Based on the data of Kebschull et al. [15], we may estimate that, in the mouse, inhibitory nuclear interneurons account for some 40% of all inhibitory nuclear neurons. Like inhibitory interneurons of the cerebellar cortex, inhibitory interneurons of the cerebellar nuclei are derived from Pax2-positive precursors. Yet in contrast to cortical inhibitory interneurons, the characterization of those of the cerebellar nuclei is still rather fragmentary, and essentially based on functional analyses [1, 39]. There is also evidence that some of the inhibitory neurons of the cerebellar nuclei may share characteristics of interneurons and projection neurons [1, 8, 39].

Here, we attempt to gain further insight into the diversity of cerebellar nuclear inhibitory (inter-) neurons by comparing them with those in the cerebellar cortex. We

take advantage of the fact that recent single cell gene expression studies of the [adult] cerebellum, notably those of Kebschull et al. [15] and Kozareva et al. [16], grant a novel and unique vantage point to do so. Combining these datasets allowed us to assess the affinities of cerebellar nuclear inhibitory (inter-) neurons with inhibitory neurons from the cerebellar cortex, but also to pinpoint some differences.

Materials and Methods

Gene expression data for murine cerebella published by Kebschull et al. [15] and Kozareva et al. [16] were obtained from the NCBI Gene Expression Omnibus (GEO; accession numbers GSE160471, sample GSM4873765, and GSE165371, file GSE165371_cb_adult_mouse.tar.gz). Of note, these data sets had already been subjected to stringent quality controls (see the original publications cited).

All further data processing was done using R (version 4.3.1 patched; R Core Team, 2023; available at https://cran.r-project.org/) and package Seurat (version 4.4; [10]) and visualized using package scCustomize (version 1.1.3; [23]).

From the adult expression data of the cerebellar cortex of Kozareva et al. [16], we extracted data for inhibitory neurons as per the annotation provided with this dataset. This resulted in a set comprising data for 66,390 cells. Random subsets of these cells comprising 9,000 cells were generated using the R function "sample". From the data published by Kebschull et al. [21] for cerebellar nuclei, we utilized only the subset classified by these authors as inhibitory (ventricular zone-derived), comprising 2363 cells. Before integrating these data (i.e., a given subset of inhibitory cortical neurons and inhibitory nuclear neurons), we trimmed them to those 25,134 features (genes) present in both data sets. Integration followed the standard procedure as recommended for the Seurat package (cf https://satijalab.org/seurat/articles/integration_introduction). Cell-type specific annotations shown are based on those given in the original publications describing these data.

Results

To compare gene expression in adult cerebellar inhibitory interneurons, we used data obtained for murine nuclear inhibitory cells [15] and subsets of the data reported by for cortical inhibitory neurons [16]. The decision to use only a subset of the latter dataset was motivated by fact that data for 2363 nuclear cells were available, and the consideration that these should not be outnumbered too extremely by cortical cells. We repeated the analyses reported below with several randomly selected subsets of the cortical inhibitory interneurons, and cortical subsets comprising neurons from male animals only, as did the nuclear sample. This did not appreciably affect the results reported (data not shown).

Cluster i1 (nucleo-olivary projection neurons)

Clustering of all inhibitory interneurons revealed that Purkinje cells and inhibitory nuclear neurons of cluster 1 (i1), which were previously tentatively identified as nucleo-

olivary projection neurons [15], clustered close together, with only a small overlap (**Fig. 1A**). As a group, Purkinje cells and nuclear cells of cluster i1 were well separated from all cortical inhibitory interneurons, i.e. interneurons from the molecular layer (in clusters Mli1_1, Mli1_2, and Mli_2), Golgi cells in clusters Golgi_1 and Golgi_2, and candelabrum cells, globular cells, and Lugaro cells [27]. They were also well separated from nuclear inhibitory neurons in clusters i2_2, i2_2, i2_3 and i3.

As expected, cells in the cluster representing Purkinje neurons strongly and selectively expressed known Purkinje cell-specific genes, like *Pcp2* (L7; [26]), *Calb1*, or *Car8*. They also (rather) selectively expressed *Ebf1, Arhgef33, Kcnab1, Itpr1, Stac, Sox5* and *Grid2ip*. Conversely, among the genes selectively expressed by cells of cluster i1, there were *Zfhx4* (cf [15]), *Drd2, Pou3f2, Syt6, Slc24a4, Fxyd6, Cntnap3* and, notably, *Dmbx1*. Yet in contrast to Purkinje cell specific genes *Pcp2, Calb1, Itpr1* or *Car8*, none of the i1-specific genes was expressed in all i1 cells. Indeed, they typically were expressed in some 20-50 % of the cells of this cluster. *Zfhx4* was expressed in almost all cells of i1 (1328/1401), and *Slc24a4* in 1144/1404 cells. However, no combination of any two of the genes specifically expressed in cluster i1 labeled more than 95% of its cells. To wit, the Purkinje cell markers mentioned *individually* were expressed in more than 99.7 of the cells in the Purkinje cell cluster (PC). Also, among the genes specific for cluster i1, we found no pair that was expressed in mutually exclusive subsets of this cluster. Rather, even for genes expressed in rather small subsets of cluster i1 (say, *Dmbx1*, expressed in 331 cells; and *Drd2*, expressed in 362 cells of a total of 1401 cells in cluster i1) co-expression was found in 83 cells, i.e. ~ 23% of the cells expressing either of the two genes.

Differential gene expression allows distinguishing spatially organized subsets of Purkinje cells during development (e.g., *Pcp2* / L7; cf. [25, 36] and allow defining compartments of functionally distinct subsets of Purkinje cells in the adult, as prominently documented for zebrin II / aldolase C, [3, 12]. Intriguingly, Purkinje cells positive or negative for zebrin II / aldolase C are rather well separated within the Purkinje cell cluster, attesting to the fact that levels of zebrin II expression signify a more fundamental difference in gene expression between these sets of Purkinje cells (**Fig. 1B).**

Compartmentation has also been reported for cerebellar nuclei [5, 37]. Of the (anti-) genes used to define nuclear compartments by Chung et al. [5], *Slc6a5, Tbr1* and *Ebf2* are not expressed in nucleo-olivary projection neurons (i.e., neurons of cluster i1; cf the online material associated with the publication by Kebschull et al., [15] at https://github.com/justuskebschull/CNcode_final). As documented in **Fig. 1B,** none of genes associated with nuclear clusters show a pattern of distribution in nucleo-olivary projection neurons comparable to that observed in Purkinje cells based on their differential expression of zebrin II (*Aldoc*). Rather, as visible primarily for genes expressed in smaller subsets of i1-cells, their distribution follows the overall cell density distribution in cluster i1.

To further explore this issue, we compared gene expression by cells of cluster i1 either positive or negative for *Dmbx1*. The rational for this inquiry was that *Dmbx1* is the earliest known marker for at least a subset of precursors of nucleo-olivary projection neurons (cf [14]). No appreciably significant, or suggestive, differences of gene expression, other than *Dmbx1* itself, could be ascertained in cells positive or negative for this marker.

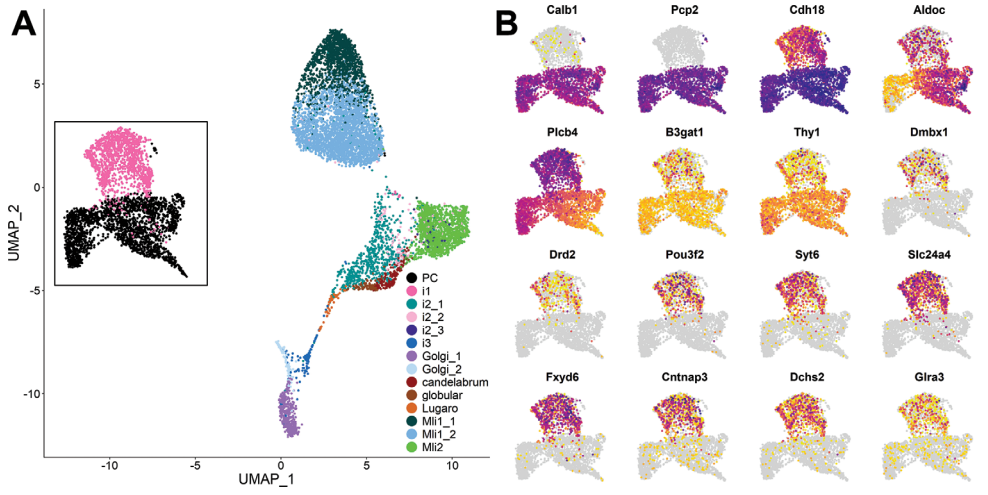

Fig. 1. Clustering of cortical and nuclear cerebellar interneurons and transcriptional heterogeneity in nucleo-olivary projection neurons. **(A)** Clustering of individual cells from adult cerebellar cortices and nuclei visualized by UMAP. Note that Purkinje cells and nucleo-olivary projection neurons (PC and i1, respectively) are well separated from nuclear and cortical inhibitory interneurons. **(B)** Examples of gene expression in clusters representing Purkinje cells and nucleo-olivary projection neurons (see boxed area in panel A) visualized by UMAP. Each dot represents an individual cell. Darker colors signify higher levels of gene expression; light gray marks negative cells. Purkinje cells can be unambiguously identified by classical markers (*Calb1, Pcp2*), and divided in two rather sharply separated sets defined by *Aldoc* (zebrin II) expression, and also by differential expression of *Plcb4*. Note also the differential expression levels in genes preferentially or exclusively expressed in nucleo-olivary neurons.

Cluster i2 and its subclusters, and cluster i3

Nuclear inhibitory neurons of clusters i2_1, i2_2, i2_3 and i3 are well separated from cells in the nuclear cluster i1 and Purkinje neurons. Strikingly, they are arrayed along a trajectory spanned out by molecular layer interneurons in cluster Mli2 and Golgi cells in clusters Golgi_1 and Golgi_2, closely following the arrangement of candelabrum cells, globular cells and Lugaro cells (**Fig. 1A**). A higher resolution view of these cells after removal of Purkinje cells, i1 cells and the molecular layer clusters Mli1_1 and Mli1_2 and re-clustering is shown in **Fig. 2**. Indeed, re-clustering of the cells of the combined datasets of cortical and nuclear inhibitory neurons typically results in clusters comprising Golgi and i3 neurons, and globular and candelabrum cells joined with i2 cells, unless the resolution parameter in the "FindClusters" function of the Seurat package was set to quite high values (not shown).

The rather small cluster i2_3 (39 cells) overlapped considerably with the molecular layer inhibitory interneurons of cluster Mli2. As may be seen in **Fig. 2**, next to cluster i2_3, clusters i2_2 and i2_3 closely abut the clusters of candelabrum and globular cells; then follows the cluster representing Lugaro cells, and, intercalated between the latter and the Golgi cell clusters, we find the nuclear cluster i3. A consistent arrangement of these clusters may be verified if data are embedded using t-distributed stochastic neighbor embedding (tSNE; not shown).

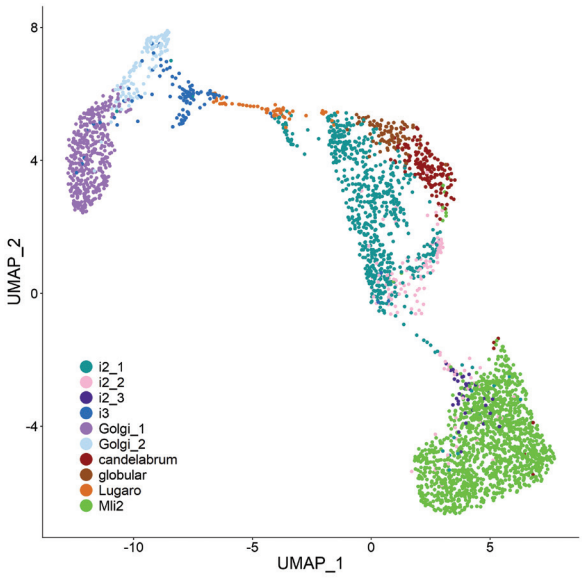

Fig. 2. Comparison of cortical and nuclear cerebellar interneurons based on their transcriptome. Cells were re-clustered after removal of projection neurons and molecular layer interneurons of clusters Mli1_1 and Mli1_2 and are visualized by UMAP. Clusters of nuclear cells are found along a line spanned out by cortical Golgi cells and molecular layer interneurons in cluster Mli2 and close to clusters of cortical candelabrum, globular, and Lugaro cells. Note also the position taken by cells of nuclear cluster i3 between Lugaro and Golgi cells.

The affinities between the cells in the individual clusters suggested by their arrangement may also be exemplified by selected markers and function-defining genes expressed by these cells as documented in **Fig. 3.** The genes shown were selected from those highly expressed in any one cluster distinguishing this cluster from all other clusters. The selection was primarily motivated by the (potential) functional significance and also includes known markers for cerebellar cells [15, 16, 22, 27, 32, 35].

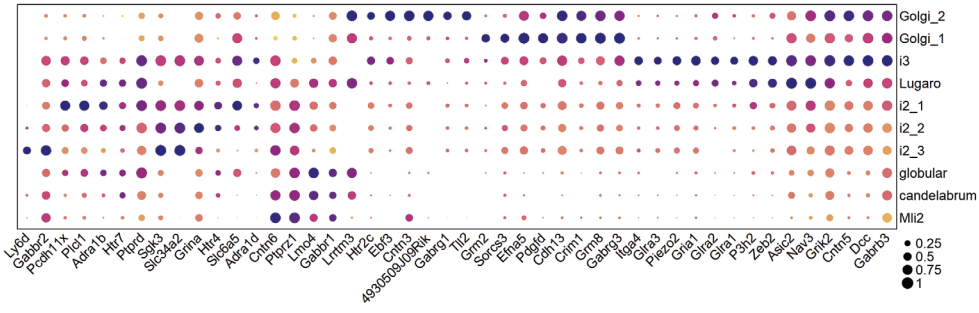

Fig. 3. Expression of selected genes documenting similarities and differences between nuclear inhibitory interneurons and cortical Golgi and Mli2 cells.While there are few genes that individually allow identifying the cell types compared (e.g., *Lyd6, Grm2*), combinations of two or three genes typically allow identification of individual cell types. Note also that in nuclear cell clusters, glycine receptor coding genes are strongly expressed rather selectively in cells of cluster i3. Among cortical cells, glycine receptor expression is more prominent in Lugaro cells. Darker colors signify higher levels of gene expression, and the symbol size indicates the fraction of cells expressing a gene (see scale at lower right corner of the figure).

As expected, there were hardly any markers that were individually specific for any one cluster *and* would label all of its cells. Yet this approach also identified small sets of genes that, when combined, allow to identify individual cell types, and to distinguish, e.g., nuclear form cortical cells. Moreover, the expression patterns of some genes also exemplify the similarities / parallels in gene expression between sets of cortical and nuclear cells as indicated, on a more encompassing scale, by the clustering patterns described above. E.g., cells of cluster i3, which are found next to the Golgi (_2) cell cluster and that of Lugaro cells **(Fig. 2)**, can be seen to share expression of *Cntn5* with the former, and *P3h2* and *Zeb2* with the latter. Yet the combined expression of either *Cntn5* and *P3h2* or *Zeb2* readily allows distinguishing i3 cells from Golgi and Lugaro cells.

A surprising and particularly intriguing result of our search for genes specific for individual cell clusters was the observation that cells of cluster i3 stand out due to their strong and broad expression of the mRNAs coding alpha subunits (primarily alpha2) and the beta subunit of glycine receptors (*Glra1, Glra2, Glra3, Glrb*). To follow up on this finding, we counted cells expressing any one of the *Glra* subunits, and the *Glrb* subunit, in all cells of our joint data set, and separately also in those cells positive for *Slc6a5*, i.e. glycinergic (inter-) neurons. The separate assessment of *Slc6a5*-positive cells was motivated by the findings of Uusisaari and Knöpfel [39], who have identified a subset of *Slc6a5*-positive cells in the cerebellar nuclei, traditionally considered to be interneurons, that also project to the cerebellar cortex. The numbers obtained are listed in **Table 1**.

Table 1. Total numbers of cells in defined clusters from the cerebellar cortex or nuclei, and of subsets positive for Slc6a5 or various glycine receptor subunits, or combinations thereof.

Cluster	Total #	*Slc6a5*+	*Glra*+	*Glra*+ and *Glrb*+	*Slc6a5*+, *Glra*+ and *Glyrb*+
GABAergic projection neurons					
PC	2342	16	345 (188)	290 (144)	1 (0)
i1	1401	42	720 (307)	555 (236)	22 (6)
nuclear GABAergic and/or glycinergic interneurons					
i2_1	675	548	235 (25)	201 (23)	166 (21)
i2_2	137	39	36 (5)	30 (3)	12 (0)
i2_3	39	1	11 (1)	7 (1)	0
i3	111	94	93 (69)	79 (59)	69 (52)
cortical GABAergic and/or glycinergic interneurons					
Golgi_1	435	379	97 (95)	84 (82)	72 (70)
Golgi_2	131	65	62 (61)	55 (54)	29 (28)
candelabrum	162	2	6	4	0
globular	90	51	4	3	3
Lugaro	59	44	30	28	22
Mli1_1	1409	6	63	47	0
Mli1_2	3003	23	140	82	2
Mli2	1369	7	63	45	0

Table legend: Cutoff levels for gene detection were set to zero unless otherwise indicated. Values in parenthesis give numbers of Glra positive cells if the cutoff for Glra was set to 0.3

(see main text for details), “Glra” stands for any of the Glra1, 2 or 3 receptor subunits. Glra4 was not expressed in the data analyzed.

As may be taken from this table, there are two major groups of nuclear GABAergic and/or glycinergic interneurons, in clusters i3 and i2_1, that express *Glra* subunits and subunit *Glrb*, i.e. are conceivably capable to express functional glycine receptors [21]. This holds for some 71 % of all i3 cells, and about 30 % of cells in cluster i2_1. Potentially glycine-sensitive cells in these clusters also differ by levels of *Glra* mRNA expression, which is much higher in i3 cells than in those of cluster i2_1 **(Fig. 3)**. Thus, average expression levels for *Glra1, 2* and *3* were ~ 6, 60, and 300 times higher in i3 than in i2_1 cells. Yet as expression values were not normally distributed, it may also be sensible to check for potential highly expressing outliers. If we focus on *Slc6a5*-positive cells and neglect, for the moment, cells with low expression of *Glra* expression (less than 0.3; average expression in i3 ~ 0.5, 1.6 and 0.9 of *Glra1, 2* and *3*, respectively), this difference becomes even more striking: thus, 55% of i3 cells (absolute number, 52), but only 3.8% of i2_1 cells (21 cells) meet these criteria, i.e. are both glycinergic and express substantial levels of *Glra* receptors, comparable to the levels also seen in Golgi cells.

Glycinergic (*Slc6a5*)-positive cells in clusters i3 and i2_1 not only differ by the levels of *Glra* subunits they express. A comparison of these groups also revealed highly significant differences in the expression of, inter alia, mRNAs coding for the adhesion molecules *Pcdh9, Pcdh15,* and *Dcc,* the calcium binding protein *Necab1*, the transmitter receptor subunits *Grik2* and *Gabarg3*, the microtubule binding protein, *Nckap5* , the zinc-finger transcription factor, *Zeb2* (all higher in i3 cells), or the adhesion molecules *Cdh18* and *Cdh22*, the actin associated protein *Whrn,* the protein tyrosine phosphatase receptor P*tprz1* and the phosphodiesterase *Pde4b* (all higher in i2_1 cells), to name but a few examples drawn from the 60 most differentially expressed genes.

Discussion

We integrated and compared gene expression data from the cortex and nuclei of adult murine cerebella with the principal goal to further characterize nuclear GABAergic and mixed GABAergic/glycinergic neurons. The results reported indicate that the molecular diversity of Purkinje neurons as revealed by their differential expression of zebrin II may not be translated into a comparable subdivision of nucleo-olivary projection neurons. Gene expression patterns of nuclear inhibitory interneurons were found to resemble those seen in inhibitory interneurons resident in the granule cell and Purkinje cell layers. Lastly, the present analysis suggests a rationale for the curious intrinsic electrophysiological silence, in slice preparations, of that subset of nuclear (inter-) neurons that also project to the cerebellar cortex [39].

Limitations

An obvious limitation of this study is that any functional interpretation presupposes that mRNA expression is indicative of the expression of functional proteins. Even if so, the data analyzed do not give any information about differential splicing,

posttranscriptional editing, let alone posttranslational modifications, all of which are known to significantly affect neural physiology (e.g., [7, 9, 11, 34]). However, while the findings reported do not inform about this post-transcriptional level of functional complexity, at a minimum they may help to focus future research.

Another point to keep in mind is that the samples analyzed comprise about 11% of all nuclear GABAergic and/or glycinergic cells (2363 of some 21500 cells; [2, 38]), and even a lower percentage of all cortical cells (~ 2.6%; estimated based on Purkinje cell numbers, cf [40]). This may arguably affect the precision of numerical estimates for smaller neuronal sets reported here.

Projection neurons

Cells in nuclear cluster i1, which comes to lie close to Purkinje cells in UMAP projection, are characterized by the differential expression of several RNAs, including that of *Dmbx1*.

During cerebellar development, *Dmbx1* is also expressed in at least a subset of cells positive for *Sox14* (KS, unpublished), a transiently expressed marker for a subset of nucleo-olivary projection neurons essential for their differentiation [28]. Together, these observations support the suggestion by [15] that this cluster comprises nucleo-olivary projection neurons.

Interestingly, while i1 cells form a rather tight cluster, they are also characterized by the differential expression of a sizable set of genes, including *Dmbx1* (**Fig. 1B**). Yet the expression pattern of none of these genes suggests a subdivision of i1 cells comparable to that of Purkinje cells revealed by expression of zebrin II (*Aldoc*). The significance, if any, of this heterogeneity for the function of the nucleo-olivary projection remains obscure. A so far unexplored issue is whether i1 cells also comprise neurons that project (also) to non-olivary targets of inhibitory nuclear neurons which have recently been described [4, 13, 20]. Unfortunately, no functional or molecular characteristics that would allow the alignment of the inhibitory, extra-cerebellar-projecting cells reported by Cao et al. [4] and Judd et al. [13] with the genetically defined subsets of cerebellar inhibitory neurons as defined by Kebschull et al. [15] have been reported so far. We cannot add to the characterization of D1 receptor-positive projection neurons reported by Locke et al. [20], as only nine cells expressing the mRNA for this receptor are present in the data for nuclear cells available, spread out across the inhibitory clusters identified.

Local inhibitory interneurons – and their not so local brethren

While the nuclear cells in clusters i2 (and all of its subclusters) and i3 are clearly separated from nucleo-olivary projection neurons and come to lie next to cerebellar cortical inhibitory interneurons in UMAP projections (and also when projected using tSNE), their global classification as “nuclear inhibitory interneurons” falls somewhat short of reality. Thus, Uusisaari and Knöpfel [39] and Ankri et al. [1] established that a subset of *Slc6a5*-positive nuclear neurons (also) projects back to the cerebellar cortex, where they innervate a *Slc6a5*-negative subset of Golgi neurons. It has been suggested that these inhibitory (GABA- and glycinergic) projections arise from cells of cluster i3 [14]. The genetic similarity / proximity of i3 cells to Lugaro neurons supports this view, as Lugaro cells also target Golgi cells [6] (for further references and discussion,

see also [33]). A somewhat anecdotal support for this view is further suggested by the observation that Lugaro cell axons – in contrast to the axons of all other cortical interneurons – have been observed to pass, occasionally, through the cerebellar white matter [17]. Yet the most intriguing argument in support of this view builds on the observation that these cells are strongly positive for mRNAs that predict the expression of functional glycine receptors. Uusisaari and Knöpfel [39] noted that the nuclear *Slc6a5*-positive cells projecting to the cortex, when analyzed in acute slices, did not show spontaneous activity and thereby could be functionally distinguished from local interneurons positive for *Slc6a5*. They also observed that blockade of GABA-receptors in the slices did not induce these cells to become active. The present findings suggest that it may not be GABAergic, but rather glycinergic input that suppressed spontaneous activity of the *Slc6a5*-positive nuclear neurons projecting to the cortex. The data reported here also reveal that i3 cells are the only inhibitory neuronal subgroup expressing substantial levels of mRNAs predicting the expression of functional glycine receptors (**Fig. 3**).

While we cannot exclude that cells from cluster i2_1 are also sensitive to glycine, the low levels of mRNAs for alpha subunits of the glycine receptor that these cells express suggests that this is a more remote possibility. More generally, differential expression of the mRNAs for glycine receptors suggests that cells of cluster i3 are the only population of inhibitory interneurons sensitive to glycine, and that i1 inhibitory interneurons may also differ in their sensitivity to glycine (**Fig. 1B**). In contrast, glycinergic cells are found in clusters i3 and i2_1, and rarely also in cluster i2_2. No *Slc6a5*-positive cells are found in cluster i2_3, which parallels the selective GABAergic nature candelabrum [27] and Mli2 cells, to which i2_3 cells resemble based on their position in UMAP-projections following clustering (**Fig. 2**).

Finally, a comment on the classification of the *Slc6a5*-positive nuclear cells that also target the cerebellar cortex identified by Uusisaari and Knöpfel [39] may be allowed. Clearly, these are no pure interneurons, with which they are usually classified, and which they very much resemble given their transcriptome. Yet it might be recalled that at least since the days of Birdsey Renshaw, it is appreciated that projection neurons also target local cells [29]. Are the cortically projecting nuclear cells of Uusisaari and Knöpfel [39] an example of local interneurons also targeting distant cells? It may be hoped that the distinct developmental history of classical projection neurons and interneurons in the cerebellum provide a paradigm to further study this blurry issue.

Conclusions

The present analysis reveals gene expression-based similarities and differences between sets to inhibitory (GABAergic and mixed GABAergic / glycinergic) cells of the cerebellar nuclei and cortex that hopefully allow focussing future research aimed at unravelling the molecular characteristics and identity, wiring and functional significance of the cells of the cerebellar nuclei.

Acknowledgements: My understanding of the cerebellar nuclei profited extensively from having been invited to join an outstanding group of colleagues for writing a review

on these quite special cells. I am also indebted to participants of the 26th Congress of the Bulgarian Anatomical Society for their encouraging and constructive discussion of a preliminary presentation of the present topic at that meeting. Obviously, any shortcomings of this manuscript are exclusively my responsibility.

References

1. **Ankri, L., Z. Husson, K. Pietrajtis, R. Proville, C. Lena, Y. Yarom, S. Dieudonne, Y. M. Uusisaari.** A novel inhibitory nucleo-cortical circuit controls cerebellar Golgi cell activity. – *eLife,* **4**, 2015, e06262.
2. **Bäuerle, J., U. Grüsser-Cornehls.** Differential number of glycine- and GABA-immunopositive neurons and terminals in the deep cerebellar nuclei of normal and Purkinje cell degeneration mutant mice. – *J. Comp. Neurol.,* **382**, 1997, 443-458.
3. **Beekhof, G. C., S. V. Gornati, C. B. Canto, A. M. Libster, M. Schonewille, C. I. D. Zeeuw, F. E. Hoebeek.** Activity of cerebellar nuclei neurons correlates with zebrin II identity of their Purkinje cell afferents. – *Cells,* **10**, 2021, 2686.
4. **Cao, B. B., Y. Huang, J. H. Lu, F. F. Xu, Y. H. Qiu, Y. P. Peng.** Cerebellar fastigial nuclear GABAergic projections to the hypothalamus modulate immune function. – *Brain Behav. Immun.,* **27**, 2013, 80-90.
5. **Chung, S. H., H. Marzban, R. Hawkes.** Compartmentation of the cerebellar nuclei of the mouse. – *Neuroscience,* **161**, 2009, 123-138.
6. **Dumoulin, A., A. Triller, S. Dieudonne.** IPSC kinetics at identified GABAergic and mixed GABAergic and glycinergic synapses onto cerebellar Golgi cells. – *J. Neurosci.,* **21**, 2001, 6045-6057.
7. **Farini, D., E. Cesari, R. J. Weatheritt, G. L. Sala, C. Naro, V. Pagliarini, D. Bonvissuto, V. Medici, M. Guerra, C. D. Pietro, F. R. Rizzo, A. Musella, V. Carola, D. Centonze, B. J. Blencowe, D. Marazziti, C. Sette.** A dynamic splicing program ensures proper synaptic connections in the developing cerebellum. – *Cell Rep.,* **31**, 2020, 107703.
8. **Gomez-Gonzalez, G. B., A. Martinez-Torres.** Inter-fastigial projections along the roof of the fourth ventricle. – *Brain Struct. Funct.* **226**, 2021, 901-917.
9. **Hannan, S., K. Gerrow, A. Triller. T. G. Smart.** Phospho-dependent accumulation of GABABRs at presynaptic terminals after NMDAR Activation. – *Cell Rep.,* **16**, 2016, 1962-1973.
10. **Hao, Y., H. Stephanie, E. Andersen-Nissen, W. M. Mauck, S. Zheng, A. Butler, M. J. Lee, A. J. Wilk, C. Darby, M. Zager, P. Hoffman, M. Stoeckius, E. Papalexi, E. P. Mimitou, J. Jain, A. Srivastava, T. Stuart, L. M. Fleming, B. Yeung, A. J. Rogers, J. M. McElrath, C. A. Blish, R. Gottardo, P. Smibert, R. Satija.** Integrated analysis of multimodal single-cell data. – *Cell,* **184**, 2021, 3573-3587.
11. **Hauser, D., K. Behr, K. Konno, D. Schreiner, A. Schmidt, M. Watanabe, J. Bischofberger, P. Scheiffele.** Targeted proteoform mapping uncovers specific Neurexin-3 variants required for dendritic inhibition. – *Neuron,* **110**, 2022, 2094-2109.
12. **Hawkes, R., K. Herrup.** Aldolase C/zebrin II and the regionalization of the cerebellum. – *J. Mol. Neurosci.,* **6**, 1995, 147-158.
13. **Judd, E. N., S. M. Lewis, A. L. Person.** Diverse inhibitory projections from the cerebellar interposed nucleus. – *eLife,* **10**, 2021, e66231.

14. **Kebschull, J. M., F. Casoni, G. G. Consalez, D. Goldowitz, R. Hawkes, T. J. H. Ruigrok, K. Schilling, R. Wingate, J. Wu, M. Y. U. Yeung.** Cerebellum Lecture: the cerebellar nuclei – core of the cerebellum. – *Cerebellum*, 2023, in press.
15. **Kebschull, J. M., E. B. Richman, N. Ringach, D. Friedmann, E. Albarran, S. S. Kolluru, R. C. Jones, W. E. Allen, Y. Wang, S. W. Cho, H. Zhou, J. B. Ding, H. Y. Chang, K. Deisseroth, S. R. Quake, L. Luo.** Cerebellar nuclei evolved by repeatedly duplicating a conserved cell-type set. – *Science*, **370**, 2020, eabd5059.
16. **Kozareva, V., C. Martin, T. Osorno, S. Rudolph, C. Guo, C. Vanderburg, N. Nadaf, A. Regev, W. G. Regehr, E. Macosko.** A transcriptomic atlas of mouse cerebellar cortex comprehensively defines cell types. – *Nature,* **598**, 2021, 214-219.
17. **Laine, J., H. Axelrad.** Morphology of the Golgi-impregnated Lugaro cell in the rat cerebellar cortex: a reappraisal with a description of its axon. – *J. Comp. Neurol.,* **375**, 1996, 618-640.
18. **Leto, K., A. Bartolini, F. Rossi.** The prospective white matter: an atypical neurogenic niche in the developing cerebellum. – *Arch. Ital. Biol.,* **8**, 2010, 137-46.
19. **Leto, K., A. Bartolini, Y. Yanagawa, K. Obata, L. Magrassi, K. Schilling, F. Rossi.** Laminar Fate and Phenotype Specification of Cerebellar GABAergic Interneurons. – *J. Neurosci.,* **29**, 2009, 7079-7091.
20. **Locke, T. M., M. E. Soden, S. M. Miller, A. Hunker, C. Knakal, J. A. Licholai, K. S. Dhillon, C. D. Keene, L. S. Zweifel, E. S. Carlson.** Dopamine D(1) receptor-positive neurons in the lateral nucleus of the cerebellum contribute to cognitive behavior. – *Biol. Psychiatry,* **84**, 2018, 401-412.
21. **Lynch, J. W.** Native glycine receptor subtypes and their physiological roles. – *Neuropharmacology,* **56**, 2009, 303-309.
22. **Maricich, S. M., K. Herrup.** Pax-2 expression defines a subset of GABAergic interneurons and their precursors in the developing murine cerebellum. – *J. Neurobiol.,* **41**, 1999, 281-294.
23. **Marsh, S.** Custom visualizations and functions for streamlined analyses of single cell sequencing, 2023. Available at *https://doi.org/10.5281/zenodo.5706430*
24. **Mayer, C., C. Hafemeister, R. C. Bandler, R. Machold, B. R. Batista, X. Jaglin, K. Allaway, A. Butler, G. Fishell, R. Satija.** Developmental diversification of cortical inhibitory interneurons. – *Nature*, **555**, 2018, 457-462.
25. **Oberdick, J.** Evidence for a genetically encoded map of functional development in the cerebellum. – *Histochem. Cell Biol.,* **102**, 1994, 1-14.
26. **Oberdick, J., F. Levinthal, C. Levinthal.** A Purkinje cell differentiation marker shows a partial DNA sequence homology to the cellular sis/PDGF2 gene. – *Neuron,* **1**, 1988, 367-376.
27. **Osorno, T., S. Rudolph, T. Nguyen, V. Kozareva, N. M. Nadaf, A. Norton, E. Z. Macosko, W. C. A. Lee, W. G. Regehr.** Candelabrum cells are ubiquitous cerebellar cortex interneurons with specialized circuit properties. – *Nature Neurosci.,* **25**, 2022, 702-713.
28. **Prekop, H. T., A. Kroiss, V. Rook, L. Zagoraiou, T. M. Jessell, C. Fernandes, A. Delogu, R. J. T. Wingate.** Sox14 is required for a specific subset of cerebello-olivary projections. – *J. Neurosci.,* **38**, 2018, 9539-9550.
29. **Renshaw, B.** Influence of discharge of motoneurons upon excitation of neighboring motoneurons. – *J. Neurophysiol.,* **4**, 1941, 167-183.

30. Sagner, A., J. Briscoe. Establishing neuronal diversity in the spinal cord: a time and a place. – *Development,* **146**, 2019, dev182154.
31. Schilling, K. Revisiting the development of cerebellar inhibitory interneurons in the light of single-cell genetic analyses. – *Histochem. Cell Biol.,* **161,** 2024, 5-27.
32. Schilling, K., J. Oberdick. The Treasury of the commons: Making use of public gene expression resources to better characterize the molecular diversity of inhibitory interneurons in the cerebellar cortex. – *Cerebellum,* **8**, 2010, 477-489.
33. Schilling, K., J. Oberdick, F. Rossi, S. L. Baader. Besides Purkinje cells and granule neurons: an appraisal of the cell biology of the interneurons of the cerebellar cortex. – *Histochem. Cell Biol.,* **130**, 2008, 601-615.
34. Seeburg, P. H., M. Higuchi, R. Sprengel. RNA editing of brain glutamate receptor channels: mechanism and physiology. – *Brain Res. Rev.,* 2**6**, 1998, 217-229.
35. Simat, M., F. Parpan, J. M. Fritschy. Heterogeneity of glycinergic and gabaergic interneurons in the granule cell layer of mouse cerebellum. – *J. Comp. Neurol.,* **500**, 2007, 71-83.
36. Smeyne, R. J., J. Oberdick, K. Schilling, A. S. Berrebi, E. Mugnaini, J. I. Morgan. Dynamic organization of developing Purkinje cells revealed by transgene expression. – *Science,* **254**, 1991, 719-721.
37. Sugihara, I. Compartmentalization of the deep cerebellar nuclei based on afferent projections and aldolase C expression. – *Cerebellum,* **10**, 2011, 449-463.
38. Sultan, F., T. Konig, M. Mock, P. Thier. Quantitative organization of neurotransmitters in the deep cerebellar nuclei of the Lurcher mutant. – *J. Comp. Neurol.,* **452**, 2002, 311-323.
39. Uusisaari, M., T. Knöpfel, T. GlyT2+ neurons in the lateral cerebellar nucleus. – *Cerebellum,* **9**, 2010, 42-55.
40. Wetts, R., K. Herrup. Direct correlation between Purkinje and granule cell number in the cerebella of lurcher chimera and wild-type mice. – *Dev. Brain Res.,* **10**, 1983, 41-47.

Institute of Experimental Morphology, Pathology and Anthropology with Museum
Bulgarian Anatomical Society

Acta Morphologica et Anthropologica, 31 (1-2)
Sofia ● 2024

Functional, Structural and Molecular Analyses Indicate that Injections of Trophic Factors into the Paralyzed Whiskerpad Muscles after Facial Nerve Injury Improve Vibrissal Motor Performance in Rats

Svenja Rink-Notzon[1], Jannika Reuscher[2], Laura Wollny[2], Stoyan Pavlov[3], Levent Sarikcioglu[4], Doychin N. Angelov[2], Marilena Manthou[5]*

[1]Department of Prosthetic Dentistry, School of Dental and Oral Medicine, University of Cologne, Germany;
[2]Department of Anatomy I, University of Cologne, Germany;
[3]Department of Anatomy, Histology and Embryology, Medical University, Varna, Bulgaria;
[4]Department of Anatomy, Akdeniz University, Antalya, Turkey;
[5]Department of Histology and Embryology, Medical School, Aristotle University Thessaloniki, Greece

*Corresponding author e-mail: angelov.anatomie@uni-koeln.de

Polyinnervation of neuro-muscular junctions (NMJs) in reinnervated mimic muscles is a major reason for poor motor recovery (vibrissal whisking) after transection and suture of the facial nerve. Recent own molecular biological analyses showed parallelism between better recovery of motor performance and increased amounts of brain derived neurotrophic factor (BDNF) and fibroblast growth factor 2 (FGF2) in denervated vibrissal muscles. The aim of the present study was therefore to test the effects of substitutive therapies with intramuscular injections of these trophic factors. Following transection and end-to-end suture of the buccal branch of the rat facial nerve (buccal-buccal anastomosis, BBA), we injected the paralyzed vibrissal musculature with different concentrations of BDNF and FGF2 at different postoperative periods. Video-based motion analysis of vibrissal whisking followed. We found that rats receiving BDNF over 14-28 days after injury showed the highest whisking amplitude.

Key words: nerve injury, motor recovery, motor endplates, BDNF, FGF2

Introduction

Three components of the misdirected regrowth of transected axons

Peripheral nerve transection results in poor function restoration and the inevitable development of a "post-paralytic syndrome" (paresis, synkinesis, and dysreflexia). It is widely accepted that incorrect reinnervation of the muscle targets is the cause of this insufficient recovery [43].

First, transected and regenerating axons are misrouted and fail to re-join their original nerve fascicles [47].

Second, each transected axon gives off up to 25 "collateral" branches within the nerve itself. Excessive collateral branching leads to reinnervation of several muscle groups, often with antagonizing action, by one single motoneuron or innervation of one muscle by more than one motoneuron, i.e. polyneuronal innervation [72]. It is thought that this kind of axonal misdirection is mostly responsible for abnormally associated movements.

The intramuscular axonal sprouting is a third issue. Axons divide again after they reach their target, reinnervating a large number of muscle fibers [39, 69]. Sprouting is thought to be an adaptive response to a decrease in functional capacity. It does, however, also have a "maladaptive" side, characterized by the enlargement of the motor units [21] and by the reinnervation of neuro-muscular junctions (NMJ) by more than one axon, a state known as "polyinnervation" [58].

Improved pathfinding by transected axons to reach the original fascicle

Little is currently known about potential solutions for this issue. The degree of collateral axonal branching at the lesion site was only slightly reduced by surgically guided axonal regrowth into a 3-way-conduit. However, neither an improvement in whisking performance nor a decrease in NMJ-polyinnervation accompanied this trend. When combined, the findings imply that the 3-way-conduit does not provide any further functional benefit following surgical reconstruction of the facial nerve, even if it is not an impediment for axonal regeneration [8].

Reduction of collateral branching does not enhance recovery

Utilizing a well-established technique for measuring vibrissae motor performance [27, 30], Streppel et al. investigated the possibility that a decrease in collateral axonal branching at the lesion site [70] may enhance function recovery. They discovered that whisking did not improve despite this reduction, indicating that functional performance was not primarily hampered by post-transectional collateral branching.

Reduced polyinnervation of NMJ promotes motor recovery

Further research revealed that the percentage of muscle endplates with polyneuronal reinnervation strongly correlated with the degree of functional recovery [29].

It has been demonstrated that motor endplate polyinnervation and intramuscular sprouting are reduced when denervated muscles are mechanically stimulated [3, 46]. Probably by activating cAMP signaling [52] or by restoration of neurotrophins and synaptic plasticity [73].

Muscle reinnervation's cellular correlates: the function of terminal Schwann cells

The issue which is currently addressed is, how mechanical stimulation reduces intramuscular axonal sprouting. Whereas it might be expected that the reduced number of axon terminals reaching one motor endplate after stimulation is a consequence of fewer cell processes emanating from the terminal Schwann cells (TSC; cellular correlate), the question about possible reduction of sprouting-inducing stimuli (molecular correlates) generated by the denervated muscle fibers and TSC is still open. This is why, current knowledge about the role(s) of TSC and expression of trophic factors/cytokines by denervated muscles are briefly reviewed in the following sections.

Adjacent still denervated motor endplates can be reached by processes that enlarge and sprout from just reenervated TSC [22]. TSC can reach, draw, and guide intramuscular axonal sprouts toward the denervated endplates by means of these bridges [33, 38, 57]. Interestingly, research has demonstrated that TSC processes emerge before sprouts from growing intramuscular axons do; in other words, TSC initiate intramuscular axonal sprouting [68]. Hence, by obstructing TSC processes' expansion and capacity to bridge between endplates, stimulation may have a positive effect on muscle reinnervation. Recent reports have shown similar findings with disrupted TSC bridge generation, albeit following running exercise [71] or electrical stimulation [46]. Therefore, any type of mechanically stimulated muscle contraction may prevent TSC from forming bridges and lessen intramuscular sprouting following a lesion.

Muscle reinnervation and molecular correlates: BDNF is a stimulus inducing sprouting

The low percentage of polyinnervated motor endplates found in the vibrissal muscles (e.g., *m. levator labii superioris*) following mechanical stimulation may be explained by decreased levels of sprouting-inducing stimuli [29]. Short-range diffusible sprouting stimuli have been demonstrated to be produced by denervated muscles [18, 54, 66, 75]. Numerous neurotrophic factors have been suggested as potential contenders for this function [23, 56, 63]. Muscle activity has an inverse relationship with their amount [10, 11]. Ultimately, peripheral nerve fibroblasts that produced high levels of BDNF were shown to accumulate in tissues from the proximal and distal nerve stumps following nerve transection, according to mRNA sequencing [34].

The brain-derived neurotrophic factor (BDNF) influences the dynamic branching of axonal arbors [14, 36, 75] and effectively promotes axonal outgrowth [17, 48, 49, 51, 67]. Application of BDNF has been shown to prevent neuronal cell death after nerve lesion [64] improving functional recovery of injured motor nerve after root avulsion [32], but not after transection of the rat sciatic nerve [65]. Three days after sciatic nerve transection in rats, mRNA sequencing showed that peripheral nerve fibroblasts accumulated in the proximal and distal nerve stumps and expressed large amounts of BDNF. *In vitro*, BDNF secreted from peripheral nerve fibroblasts increased the expression of **β**-actin and F-actin through the extracellular regulated protein kinase and serine/threonine kinase pathways, and enhanced motoneuron neurite outgrowth [34]. The neutralization of BDNF reduces the arborization of axons [15] and the length of regenerated nerves [74], decreases the average axon length [20, 50] and diminishes the nerve conduction velocity and muscle action potential duration [12].

The basic fibroblast growth factor (FGF-2) "stimulates *in vivo* neurite outgrowth from the proximal stump of transected peripheral nerves and contributes to the enlargement of axon caliber" [1, 2, 4, 24, 25, 37, 42, 53, 60]. Its neutralization causes a significant decrease in the number of regenerating axons [13]. Following transection of the buccal branch of rat's facial nerve there occurs a rapid upregulation of bFGF-immunoreactivity in the distal nerve stump and in the target muscles of the whisker pad at 1 day post lesion (DPL). This immunoreactivity reaches a first peak at 2 DPL, declines at 4 DPL, and climbs to a second peak at 5-6 DPL. A gradual decline follows at 8 DPL [70].

Quality of muscle reinnervation is decisive for recovery of function

To elucidate the mechanisms that may promote recovery of motor function the expression of trophic factors in denervated (after transection and suture of the buccal branch of the facial nerve) rat facial muscles has been analyzed by immunofluorescence and by *in situ* hybridization. As a rapid and strong increase was found, it has been supposed that this may correlate with the collateral axonal branching at the lesion site and hypothesized that a neutralization of those trophic factors could reduce collateral branching. After transecting the facial nerve trunk, Streppel et al. (2002) placed both ends into a silicon tube filled with collagen gel and antibodies to NGF, BDNF, FGF2, IGF-I, CNTF, and GDNF at neutralizing concentrations. The percentage of motor neurons, whose axons had split and projected concurrently into three primary fascicles of the facial trunk, was estimated two months later using retrograde labeling. Neutralizing concentrations of anti-neurotrophins, anti-FGF-2 and anti-IGF-I significantly reduced this collateral axonal branching [70].

Immediately thereafter another study checked whether reduced collateral branching would promote a better functional recovery. Surprisingly, the results of vibrissae whisking video-based motion analysis (VBMA) did not reveal any beneficial effects, indicating that collateral axonal branching at the lesion site is not the essential limiting factor for function recovery. This is why researchers decided to concentrate their work on the level of polyinnervation of NMJ. It was found that polyinnervated NMJ comprised 51%, whereas in blind RCS animals with a perfect recovery of motor performance they were only 10%. The conclusion learned from these experiments was that the quality of muscle reinnervation (poly- or mono-innervated NMJ) plays a decisive role for the recovery of function [29].

Manual stimulation of paralyzed muscles reduces NMJ-polyinnervation and improves recovery of function

Denervated muscles have few clinical alternatives for treatment. Electrical stimulation (ES) is one option, albeit there is a lot of debate over its application. Electrical stimulation of the denervated soleus muscle reduces motor-end plate polyinnervation and prevents intramuscular sprouting [10, 46]. Nevertheless, ES of denervated muscle fibers inhibits the generation of chemical mediators necessary for an axon branch to reconnect with its NMJ. It also lessens the spontaneous electrical activity of orphaned muscle fibers, known as fibrillation, which is believed to be a stimulus for the motor nerve that is starting to grow again. For the reasons listed above, ES is not a recommended treatment for facial paralysis and has not even been applied extensively.

We therefore decided to try a novel approach and used manual stimulation of muscles after nerve injury. Based on clinically established positive benefits of soft

tissue massage, supposed to promote muscle blood flow and to keep it in optimum condition whilst awaiting nerve regrowth, we gently stroked the vibrissal, the suprahyoid-sublingual and the orbicularis oculi muscles by hand for 5 minutes daily for two months after nerve injury. Video-based motion analysis showed that daily manual stimulation resulted in full recovery of whisking, tongue position and eye closure. Polyneuronal reinnervation of motor end-plates was reduced to 10% [3, 9, 19, 28]. This treatment's success was confirmed by other studies [31, 35, 41, 45].

Trophic factors play a key role in NMJ-reinnervation

Looking for the reasons for this very beneficial effect of manual stimulation we started to explore the role of trophic factors. We focused on IGF-1, BDNF and FGF-2 and studied the quality of reinnervation of vibrissal muscles and recovery of whisking function after FFA in mice deficient in

– IGF-1+/- (STOCKIgf1tmTs/ImJ,003258, Jacksons Laboratory),
– BDNF$^{+/-}$ (STOCK *Bdnf*^{tm1Jae}/J, 002267, Jackson Laboratory), and
– FGF2$^{-/-}$ (strain *Fgf2*^{tm1Zllr} C57/Bl6).

Controls were wild-type (WT) littermates and intact animals. We quantified vibrissal motor performance [5] and determined the percentage of NMJ bridged by S100-positive terminal Schwann cells (TSC).

We found that IGF-1 [40], BDNF [67] and FGF2 [61] are required for proper target muscle reinnervation and recovery of whisking function.

Orchestrated trophic factors´ expression regulates muscle reinnervation and the recovery of motor whisking function after FFA in blind rats

In situ hybridization studies showed that, till 1 week after the lesion, the main source of trophic factors´ release at the lesion site were the adjacent Schwann cells. Thereafter blood-borne immunoreactive macrophages invaded the lesioned nerve [70].

Likewise, in paralyzed muscles, the terminal Schwann cells (TSC) have been shown to produce short-range diffusible neurotrophic factors. To learn more about their effects we decided to determine which trophic factors may be responsible for the reinnervation of the neuro-muscular junctions (NMJs) in:

(i) the facial muscles in Sprague Dawley (SD)-rats with poor recovery of facial motor function (whisking) after facial nerve injury (50% of NMJs are poly-innervated) and in

(ii) the facial muscles of the blind SD/Royal College of Surgeons (RCS) rats with complete recovery of motor function (only 10% of NMJs are poly-innervated).

Our quantitative measurements showed that functioning reinnervation of mimic muscles in the blind SD/RCS rats was accompanied by (1) an early increase in FGF2 and IGF2 at 2 days after FFA, (2) reduced NGF between 2 and 14 days after FFA, (3) a late rise in BDNF at 14-28 days after FFA and (4) reduced IGF1 at 28 days [23]. These findings show that recovery of motor function after peripheral nerve injury is associated with a precisely orchestrated expression of regeneration-associated neurotrophic factors and cytokines in the denervated muscles [7]. The increase of FGF-2 protein and concomitant decrease of NGF during the first week following FFA in SD/

RCS blind rats possibly prevent the intramuscular (terminal) sprouting of regenerating axons resulting in reduced poly-innervation of motor endplates [23].

To investigate this hypothesis, we performed a buccal branch of the facial nerve transsection and suture (buccal-buccal anastomosis, BBA), and administered combinations of BDNF, anti-BDNF, and FGF2 at several intervals and doses following BBA operation into the levator labii superioris muscle, which moves the vibrissae. By surgically transecting and reconstructing just the buccal branch of the facial nerve, we were able to investigate the impact of BDNF suppression and FGF2 enhancement on NMJ reinnervation within a specific subset of axons.

Materials and Methods

Animals

For this investigation, thirty three-month-old female rats weighing 200–250 g (RjHan:WI-Wistar, Janvier Labs) were utilized, six in each group. Subsequent to unilateral transection and suture of the right buccal branch of the facial nerve (buccal-buccal anastomosis, BBA) under aseptic surgical settings, the rats were subcutaneously injected with various combinations and quantities of BDNF and FGF2.

Rats were given tap water at will and normal laboratory food (Sniff, Soest, Germany) both before and after surgery. They were also kept in an artificial light-dark cycle with 12 hours of light and 12 hours of darkness. The University of Cologne's Animal Welfare Committee gave its approval to all experimental methods, which were carried out in compliance with international law regarding animal protection.

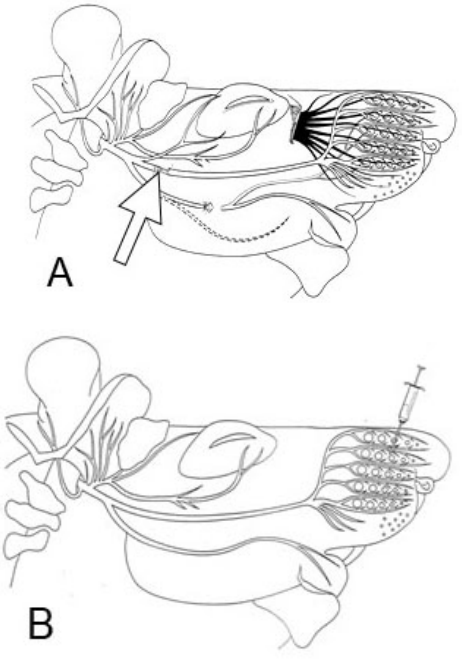

Fig. 1. A: Schematic drawing illustrating the site of transection and suture in the buccal branch (arrow) and of the transection and ligature of the marginal mandibular branch of the facial nerve. The cervical branch of the facial nerve is indicated by a dotted line. Adapted from Semba and Egger (1986) [62]. **B:** Schematic drawing of the extratemporal rat facial nerve indicating the site of intramuscular injections.

Buccal-buccal anastomosis surgery

Two 11-0 atraumatic sutures (Ethicon, Norderstedt, Germany) were used to suture the exposed buccal branch of the right facial nerve after an intraperitoneal injection of 200 µl of Xylazin (20 mg/kg body weight) and Ketamine (120 mg/kg body weight). To prevent subsequent reinnervation of the whisker muscles by nerve fibers from this branch of the facial nerve, the marginal mandibular branch was transected, and the proximal stump ligated (**Fig. 1**).

Post-operative injections of BDNF and FGF2

Daily subcutaneous injections of placebo, neurotrophic factors, and antibodies to brain-derived neurotrophic factor (anti-BDNF 2.0 µg/ml; PeproTech, 500-P84BT) were given 1-28, 1-13, and 14-28 days after BBA. Isoflurane (1.8% volume, Forene, Abbott), 0.6 l/min O_2 (Conoxia, Linde), and inhalation anesthesia with 1.2 l/min N_2O (Niontix, Linde) were also administered. The injections were performed using a micro-fine insulin syringe [U-100 (0.3 ml), 0.3 mm (30G) x 8.0 mm (Becton Dickinson, 324826)] at the same site halfway between the two dorsal vibrissal rows A and B of the whisker pad [6]. 30 µl of a saline placebo, fibroblast growth factor 2 (FGF2, PeproTech, 100-18C), or BDNF (PeproTech, 450-02) at low to high doses were injected. As an extension of our previous work with injections of trophic factors in 6 groups of rats [59], we performed a pilot study with the following 5 groups:

Group 1 Prelim "Placebo" consisted of 6 rats that received daily injections with 30 µl 0.9% NaCl from day 1 till day 28 after BBA.

Group 2 Prelim "anti-BDNF x 5" consisted of 6 rats that received daily injections with 30 µl anti-BDNF (10 µg/ml; Peprotech, Cat. Nr. 500-P84) into the LLS from day 1 till day 13 after BBA. Justification: the concentration of anti-BDNF was 5 times higher than the one used for Group 6 Publ of Rink et al., 2020 [59].

Group 3 Prelim "Late BDNF x 20" consisted of 6 rats that received daily injections with 30 µl BDNF (20 µg/ml; PeproTech, Cat. Nr. 450-02) into the LLS from day 14 till day 28 after BBA. Justification: since the dosage of 1 µg/ml did not improve whisking after BBA (amplitude of 21 ± 8 degrees for Group 3 Puble in Rink et al., 2020) [59], we tested the effect of 20 times higher dosage.

Group 4 Prelim "FGF-2 x 10 throughout " consisted of 6 rats that received daily injections with 30 µl FGF2 (100 µg/ml; PeproTech, Cat Nr. 100-18C) into the LLS from day 1 till day 28 after BBA. Justification: this concentration was ten times higher than the one which yielded in very good results in our pilot experiment (s. Group 10 Publ in Rink et al., 2020) [59].

Group 5 Prelim "early anti-BDNF x 5 plus late FGF-2 x 10" consisted of 6 rats that received daily injections with 30 µl anti-BDNF (10 µg/ml; Peprotech, Cat. Nr. 500-P84) into the LLS from day 1 till day 13 after BBA. From day 14 till day 28 rats received daily injections with with 30 µl FGF2 (100 µg/ml; PeproTech, Cat Nr. 100-18C) into the LLS. Justification: this combination yielded in the best results of our pilot experiment (s. Group 9 Publ in Rink et al., 2020) [59]. We repeated this experiment with increased dosages for anti-BDNF (2 times) and FGF2 (10 times).

Analysis of vibrissae motor performance during exploration

Video-based motion analysis (VBMA) of whisking behavior was conducted 56 days following BBA surgery to investigate the hypothesis that BDNF enhanced motor function.

Protraction (**Fig. 2a**) and retraction (**Fig. 2b**) are the two main vibrissal movements. As previously mentioned, just two of the C-row's big vibrissae on either side of the face were subjected to VBMA [16, 30]. Using a Panasonic NV DX-110 EG digital camcorder, the rats were videotaped while actively exploring for three to five minutes.

After watching the videos, 1.5-second segments featuring each animal were chosen for examination, with the animal's head posture being the determining factor. The following whisking parameters were assessed:

i) frequency, i.e. the number of times per second that an active forward vibrissal movement (protraction) and a passive backward movement (retraction) occur;

ii) the angle at maximal protraction of the whiskers, meaning the angle (in degrees) that is open rostrally between the mid-sagittal plane and the hair shaft. Maximal protractions have low angle values;

iii) amplitude - the difference between maximal retraction and maximal protraction (in degrees);

iv) angular velocity during protraction measured in degrees per second;

v) angular acceleration during protraction measured in degrees per second^2.

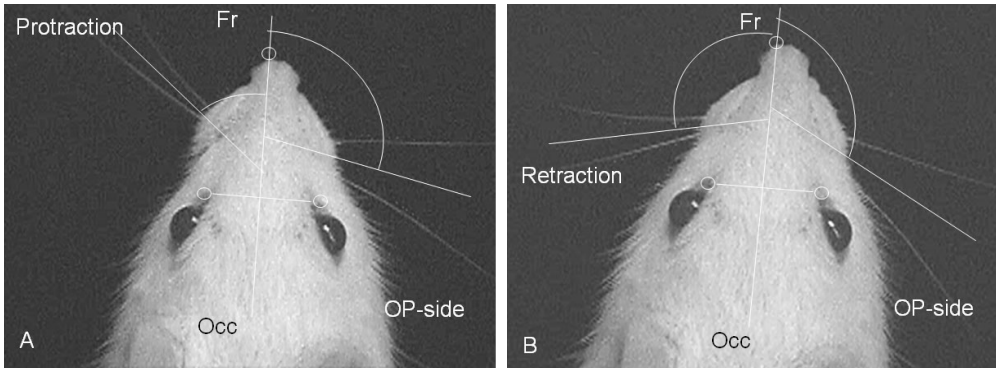

Fig. 2. "When the vibrissae are being protracted **(a)** and retracted **(b)**, the created spatial model enables accurate measurement of angles, angular velocity, and angular acceleration on the intact (left) and operated side (right). On the unaffected side, notice the marked change in angle between the sagittal line Fr-Occ during protraction and retraction. The operated side's vibrissae remain spastic. Figure and text adopted from Guntinas-Lichius et al. (2002) [30].

Tissue preparation for neuromuscular immunocytochemistry

The rats in all groups were thoroughly anesthetized 56 days after BBA, and their vessels were washed with phosphate buffered saline pH 7.4, transcardially, by perfusion. Tissues were then fixed by perfusion with 4% paraformaldehyde in the same buffer. After being dissected, the *levator labii superioris* (LLS) muscle was cryoprotected in sucrose and then sectioned longitudinally, 30 µm, using a cryostat (32–37 sections per muscle).

Every third section was used for immunostaining with a rabbit polyclonal antibody against neuronal class III β-tubulin (Covance, Richmond, CA, USA, No. PRB-435P, 1:1000; Cy3-conjugated anti-rabbit IgG; 1:400; Sigma), according to the fractionator section selection approach [26]. The sites of post-junctional acetylcholine receptors, labeled with Alexa Fluor 488-conjugated α-bungarotoxin (Molecular Probes, AZB13422, 1:500), were used to visualize the boundaries of the neuromuscular junctions (NMJ) in the LLS muscle.

As previously mentioned, the degree of non-, poly-, and mono-innervation of NMJs was assessed [29]. Mono-innervated NMJs are defined as muscle endplates innervated by a single axonal branch, whereas poly-innervated NMJs are defined as those innervated by two or more axonal branches (**Fig. 3**). The endplates without

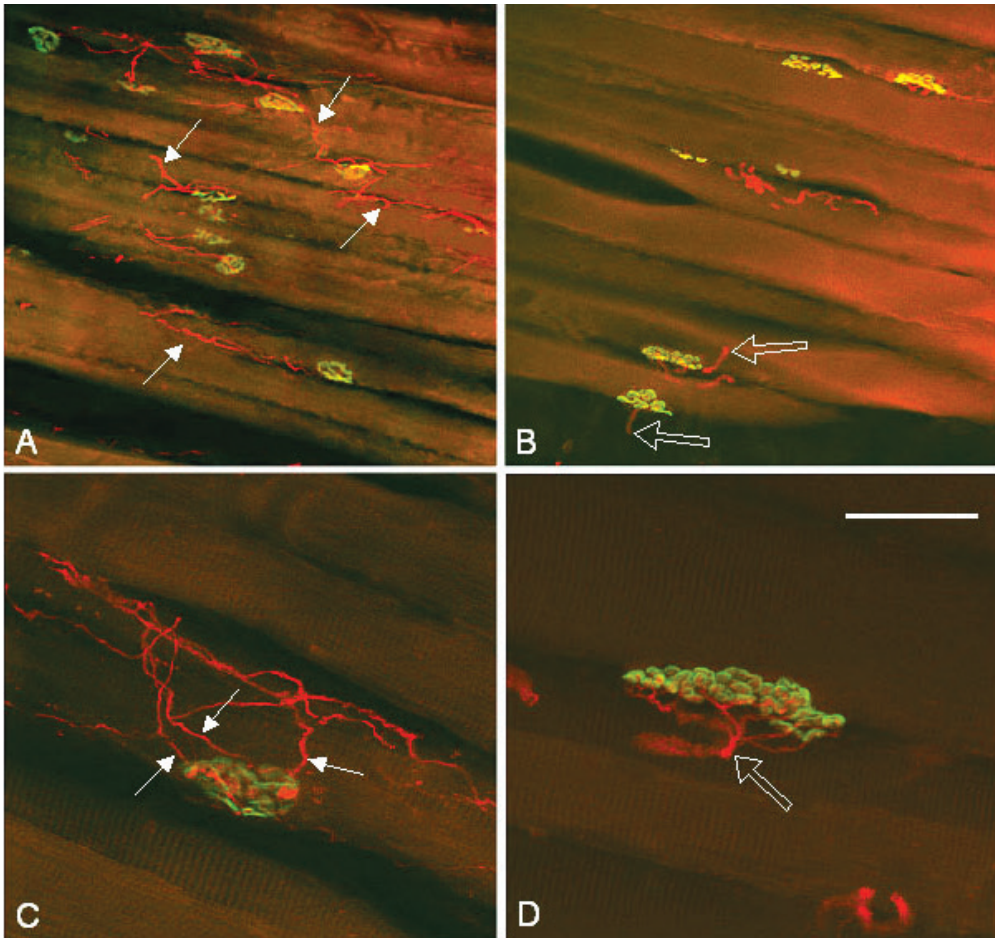

Fig. 3 A-D. "Stacks of superimposed confocal images of the end-plates in reinnervated LLS muscles visualized by staining of the motor endplates with Alexa Fluor 488 α-bungarotoxin (green fluorescence) and immunostaining of the intramuscular axons for neuronal class III β-tubulin (Cy3 red fluorescence). The innervation pattern is visible in the low magnification images presented in panels A and B. Note that while panel B lacks extensive intramuscular axonal branches, panel A exhibits them amongst endplates (arrows). Furthermore, it appears that the muscle fiber diameters in A have a smaller diameter than those in B. Panels C and D show examples of a polyinnervated and a monoinnervated endplate, respectively. The polyinnervated endplate boundaries, as indicated by the alpha-bungarotoxin staining, are reached by three axonal branches (arrows in C). On the other hand, a single axon with many preterminal rami (empty arrow in D) reaches the monoinnervated endplate. In both examples, the whole endplates are within the stack of confocal images. Scale bar shown in D indicates 125 μm for A, B and 40 μm for C, D." Adopted from Guntinas-Lichius et al. (2005) [29].

an apparent axonal branch were considered non-innervated. Observers blinded to allocation counted NMJs with and without innervation under a microscope at 40× magnification. Sections were examined using a Zeiss Axioskop 50 epifluorescence microscope and either "fluorescein" (Nr. 9, Carl Zeiss) or "rhodamine" (Nr. 15, Carl Zeiss) filter. An analysis was conducted on the number of β-tubulin positive axonal branches that enter or exit the borders of individual α-bungarotoxin positive endplates.

Statistical evaluation

For a given parameter, the data from all experimental groups were tested in a one-way analysis of variance (one-way ANOVA) procedure for overall experimental effects. If significant effects were detected ($p < 0.05$), comparisons of all groups with one control group (placebo) were performed using the post-hoc test of Dunnett at a significance level of 0.05. Statistica 6.0 software (StatSoft, Tulsa, OK, USA) was used for the analysis.

Results

In the following lines we place the suffix "Publ" to all groups groups which we have already published [59]. This is supposed to help to differentiate them from the groups of our preliminary results (indicated by the suffix "Prelim").

Quantitative estimates of vibrissal motor performance before and after buccal-buccal anastomosis (BBA) surgery and BDNF treatments

Pre-operative performance in intact rats

Mystacial vibrissae swept back and forth at ~6-7 Hz during active exploration, with a maximum protraction of ~50º, which is the rostrally open angle between the vibrissa shaft and the median sagittal plane. The difference between the maximal protraction and retraction in degrees, or the whisking amplitude, was around 60º. The movements were executed at approximately 1200º/sec sagittal angular velocity and ~40,000°/sec^2 sagittal angular acceleration [59].

Vibrissal motor function at 56 days after BBA surgery

The published results indicate that the mean amplitude of whisking was significantly higher in the groups receiving intramuscular injections of anti-BDNF alone for 1 to 13 days post-surgery (Group 6), anti-BDNF in combination for 28 days (Group 9), or FGF2 alone for 28 days (Group 10), compared to the placebo group 1 (ANOVA $F(9/50) = 7.6$; $p < 0.0001$) [59].

The present preliminary results on recovery of the whisking amplitude (histology is not ready yet) can be summarized as follows:

i) Injections with anti-BDNF in concentration 5x higher than in the previous study [59] did not result in an increased amplitude at 56 days after BBA (see Group 1 Prelim in **Fig. 4**).

ii) Injections with FGF-2 in concentrations 10x higher than in the previous study [59] also failed to promote further recovery of the whisking amplitude at 56 days after BBA (see Groups 4 Prelim and 5 Prelim in **Fig. 4**).

iii) Only the injections with BDNF in concentration 20 times higher than in the previous study [59] improved the amplitude significantly when compared to the one in Group 3 (see Group 3 Prelim in **Fig. 4**).

Quality of target reinnervation

With this evaluation, we anticipate to demonstrate whether daily trophic factor injections into the whisker pad muscles during the initial two weeks following BBB surgery, effect intramuscular axon sprouting at the NMJ by decreasing polyinnervation of the junctions and, consequently, enhancing the restoration of whisking behavior. Till the day of the EFEM lecture held on 30.09.2023 at the Congress of the Bulgarian Anatomical Society in Sofia this quantification was not completed.

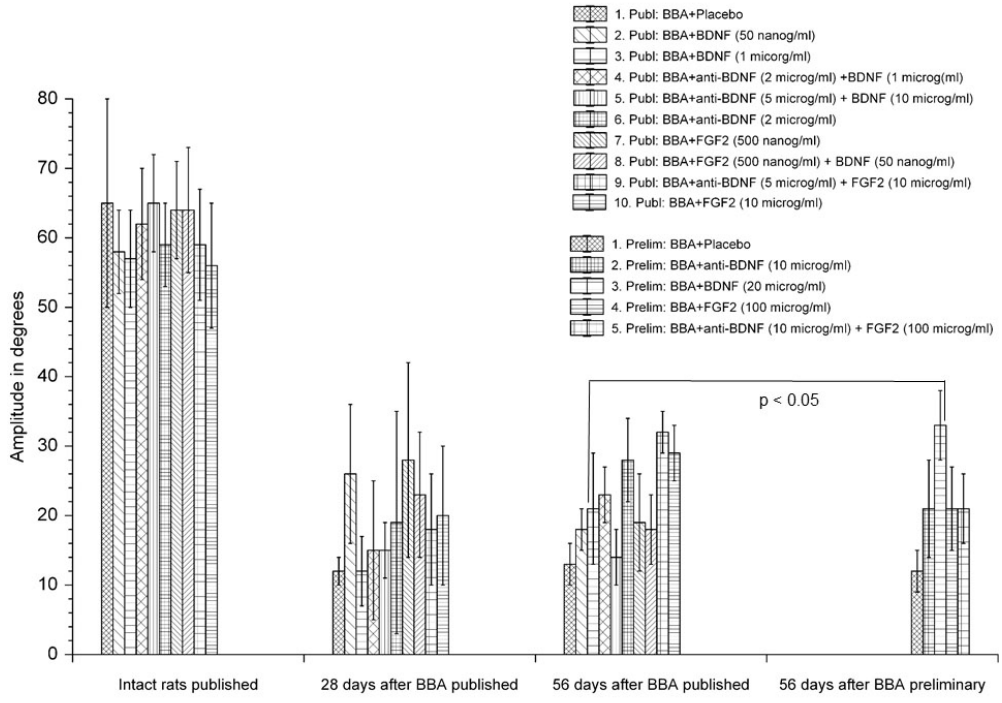

Fig. 4. Mean amplitude of vibrissal whisking in intact rats as well as on rats 28 and 56 days after transection and suture of the buccal branch of the facial nerve (buccal-buccal anastomosis, BBA). The amplitude in group 3 significantly increased. Prelim: BBA+ 20 µg/ml BDNF when compared to that in group 3 Publ; BBA+ 1 µg/ml BDNF is indicated.

Discussion

Justification of the approach

The application of the proposed trophic factors is justified by the results of three earlier published studies of our group [23, 59, 70]. Due to the rather short half-time life of the trophic factors, e.g. neurotrophins [55] injections will be performed every day.

The largest LLS muscle functioned as the main representative of the group whiskerpad muscles, even though it's possible that the injected solutions diffused towards the intrinsic follicular muscles that are innervated by the facial nerve as well as the extrinsic *maxillolabialis*, *transversus nasi*, *nasalis*, and *dilator naris muscles*.

Of course, we cannot claim that daily application will provide the optimal concentration (the amount of trophic elements that remain in the muscles of the whisker pad following injection is not quantifiable), but a 24 h interval between the injections is the minimum that was allowed by the Animal Welfare Committee (Az. 84-02.04.2021. A101 of 13.07.2021).

Unfortunately, the manufacturer (PeproTech) does not determine the half-life of its products under live conditions. Nevertheless, the activity bioassays are performed at 37°C with no media change. This is why, they know that the proteins are stable for: Human/Murine/Rat BDNF (Cat# 450-02) – 7 days, Anti-Human/Murine/Rat BDNF (Cat# 500-P84) – 7 days, Human IGF-II (Cat# 100-12) – 4 days and Human FGF-basic (Cat# 100-18C) – approx. 45 hours. We feel thus confident, that the proteins which we use will be long enough in an active state and exert their effects on the reinnervation of the vibrissal muscles.

Methodological considerations

Three possibilities are considered: The exogenous BDNF that was acquired from PeproTech (450-02) might be not effective at all or it might have been metabolized improperly or supplied in incorrect doses. Given that the identical BDNF formulation doses were utilized in a prior investigation that showed both in vitro and in vivo regeneration of motor and sensory axons, the first explanation is improbable [60]. Regarding the second argument, daily injections were administered to offset the growth factors' brief half-lives (30 minutes to 2 hours), at least in part [55]. Nevertheless, we cannot be sure that the daily application supplied the ideal concentrations since we were unable to determine the level of trophic elements still present in the whiskerpad muscles following injections. Furthermore, ethical constraints limited us to 24-hour intervals between injections. Although conditional measures would be needed to permit administration throughout certain time periods, delivery through viral transfection may be a future alternative [44].

We began with the lowest concentration of 50 ng BDNF/ml of distilled water, since this is the first study to inject neurotrophic factors into denervated muscles and as advised by the manufacturer (PeproTech) and Santos, et al. (2016) [60]. We also tested the effects of 1 µg/ml and 10 µg/ml. Lastly, it's possible that the 14–28-day window for applying BDNF following BBA surgery was not long enough.

Conclusions

The results of this study enable us to draw the conclusion that intramuscular administration of a complex mixture of trophic factors at particular post-operative times and concentrations can restore optimal muscle target re-innervation and vibrissal function following facial nerve injury and surgical repair in rats. To identify the best therapeutic approaches, further experimental research is needed.

References

1. **Ahmed, M. N., D. Shi, M. T. Dailey, K. Rothermund, M. D. Drewry, T. C. Calabrese, X. T. Cui, F. N. Syed-Picard.** Dental pulp cell sheets enhance facial nerve regeneration via local neurotrophic factor delivery. – *Tissue Eng. Part A*, **27**, 2021, 1128-1139.
2. **Allodi, I., V. Mecollari, F. González-Pérez, R. Eggers, S. Hoyng, J. Verhaagen, X. Navarro, E. Udina.** Schwann cells transduced with a lentiviral vector encoding Fgf-2 promote motor neuron regeneration following sciatic nerve injury. – *Glia*, **62**, 2014, 1736-1746.
3. **Angelov, D. N., M. Ceynowa, O. Guntinas-Lichius, M. Streppel, M. Grosheva, S. I. Kiryakova, E. Skouras, M. Maegele, A. Irintchev, W. F. Neiss, N. Sinis, A. Alvanou, S. A. Dunlop.** Mechanical stimulation of paralyzed vibrissal muscles following facial nerve injury in adult rat promotes full recovery of whisking. – *Neurobiol. Dis.*, **26**, 2007, 229-242.
4. **Angelov, D. N., O. Guntinas-Lichius, K. Wewetzer, W. Neiss, M. Streppel.** Axonal Branching and Recovery of Coordinated Muscle Activity after Transsection of the Facial Nerve in Adult Rats. – In: *Volume 180 of Advances in Anatomy, Embryology and Cell Biology* (Eds. Z. Kmiec, Michael J. Schmeisser, J.-P. Timmermans, S. Schumann), Heidelberg, Springer Berlin, 2005.
5. **Angelov, D. N., S. Waibel, O. Guntinas-Lichius, M. Lenzen, W. T. Neiss, T. L. Tomov, E. Yoles, J. Kipnis, H. Schori, A. Reuter.** Therapeutic vaccine for acute and chronic motor neuron diseases: implications for amyotrophic lateral sclerosis. – *Proc. Natl. Acad. Sci. USA*, **100**, 2003, 4790-4795.
6. **Arvidsson, J.** Somatotopic organization of vibrissae afferents in the trigeminal sensorynuclei of the rat studied by transganglionic transport of HRP. – *J. Comp. Neurol.*, **211**, 1982, 84-92.
7. **Bendella, H., S. Rink, M. Grosheva, L. Sarikcioglu, T. Gordon, D. N. Angelov.** Putative roles of soluble trophic factors in facial nerve regeneration, target reinnervation, and recovery of vibrissal whisking. – *Exp. Neurol.*, **300**, 2018, 100-110.
8. **Bendella, H., S. Rink, M. Manthou, T. Papamitsou, M. Nakamura, D. N. Angelov, L. Sarikcioglu.** Effect of surgically guided axonal regrowth into a 3-way-conduit (isogeneic trifurcated aorta) on functional recovery after facial-nerve reconstruction: Experimental study in rats. – *Restor. Neurol. Neurosci.*, **37**, 2019, 181-196.
9. **Bischoff, A., M. Grosheva, A. Irintchev, E. Skouras, K. Kaidoglou, J. Michael, S. K. Angelova, S. Kuerten, N. Sinis, S. A. Dunlop.** Manual stimulation of the orbicularis oculi muscle improves eyelid closure after facial nerve injury in adult rats. – *Muscle Nerve*, **39**, 2009, 197-205.
10. **Brown, M. C., R. L. Holland, W. G. Hopkins, R. J. Keynes.** An assessment of the spread of the signal for terminal sprouting within and between muscles. – *Brain. Res.*, **210**, 1981, 145–151.
11. **Brown, M. C., R. Ironton**. Motor neurone sprouting induced by prolonged tetrodotoxin block of nerve action potentials. – *Nature*, **265**, 1977, 459-461.

12. Byrne, P. J., R. M. Stuart, C. Fakhry, M. Lehar, P. W. Flint. An electrophysiologic model for functional assessment of effects of neurotrophic factors on facial nerve reinnervation. – *Arch. Facial Plast. Surg.*, **7**, 2005, 114-118.
13. Chen, Y. S., S. Murakami, K. Gyo, H. Wakisaka, S. Matsuda, M. Sakanaka. Effects of Basic Fibroblast Growth Factor (bFGF)-neutralizing antibody and Platelet Factor 4 on facial nerve regeneration. – *Exp. Neurol.*, **155**, 1999, 274-283.
14. Cohen-Cory, S. BDNF modulates, but does not mediate, activity-dependent branching and remodeling of optic axon arbors in vivo. – *J. Neurosci.*, **19**, 1999, 9996-10003.
15. Cohen-Cory, S., S. E. Fraser. Effects of brain-derived neurotrophic factor on optic axon branching and remodelling in vivo. – *Nature*, **378**, 1995, 192-196.
16. Dörfl, J. The innervation of the mystacial region of the white mouse: A topographica study. – *J. Anat.*, **142**, 1985, 173-84.
17. Eberhardt, K. A., A. Irintchev, A. A. Al-Majed, O. Simova, T. M. Brushart, T. Gordon, M. Schachner. BDNF/TrkB signaling regulates HNK-1 carbohydrate expression in regenerating motor nerves and promotes functional recovery after peripheral nerve repair. – *Exp. Neurol.*, **198**, 2006, 500-510.
18. English, A. W. Cytokines, growth factors and sprouting at the neuromuscular junction. – *J. Neurocytol.*, **32**, 2003, 943-960.
19. Evgenieva, E., P. Schweigert, O. Guntinas-Lichius, S. Pavlov, M. Grosheva, S. Angelova, M. Streppel, A. Irintchev, E. Skouras, S. Kuerten, N. Sinis, S. Dunlop, V. Radeva, D. N. Angelov. Manual stimulation of the suprahyoid-sublingual region diminishes polynnervation of the motor endplates and improves recovery of function after hypoglossal nerve injury in rats. – *Neurorehabil. Neural Repair*, **22**, 2008, 754-768.
20. Ghosh, A., J. Carnahan, M. E. Greenberg. Requirement for BDNF in activity-dependent survival of cortical neurons. – *Science*, **263**,1994, 1618-1623.
21. Gordon, T., J. Hegedus, S. L. Tam. Adaptive and maladaptive motor axonal sprouting in aging and motoneuron disease. – *Neurol. Res.*, **26**, 2004, 174-185.
22. Griffin, J. W., W. J. Thompson. Biology and pathology of nonmyelinating Schwann cells. – *Glia*, **56**, 2008, 1518-1531.
23. Grosheva, M., K. Nohroudi, A. Schwarz, S. Rink, H. Bendella, L. Sarikcioglu, L. Klimaschewski, T. Gordon, D. N. Angelov. Comparison of trophic factors' expression between paralyzed and recovering muscles after facial nerve injury. A quantitative analysis in time course. – *Exp. Neurol.*, **279**, 2016, 137-148.
24. Grothe, C., K. Haastert, J. Jungnickel. Physiological function and putative therapeutic impact of the FGF-2 system in peripheral nerve regeneration – lessons from in vivo studies in mice and rats. – *Brain Res. Rev.*, **51**, 2006, 293-299
25. Grothe, C., G. Nikkhah. The role of basic fibroblast growth factor in peripheral nerve regeneration. – *Anat. Embryol. (Berl.)*, **204**, 2001, 171-177.
26. Gundersen, H-JG. Stereology of arbitrary particles* a review of unbiased number and size estimators and the presentation of some new ones, in memory of William R. Thompson. – *J. Microsc.,* **143**, 1986, 3-45.
27. Guntinas-Lichius, O., D. N. Angelov, T. L. Tomov, J. Dramiga, W. F. Neiss, K. Wewetzer. Transplantation of olfactory ensheathing cells stimulates the collateral sprouting from axotomized adult rat facial motoneurons. – *Exp. Neurol.*, **172**, 2001, 70-80.
28. Guntinas-Lichius, O., G. Hundeshagen, T. Paling, M. Streppel, M. Grosheva, A. Irintchev, E. Skouras, A. Alvanou, S. K. Angelova, S. Kuerten, N. Sinis, S. A, Dunlop, D. N. Angelov. Manual stimulation of facial muscles improves functional recovery after hypoglossal-facial anastomosis and interpositional nerve grafting of the facial nerve in adult rats. – *Neurobiol. Dis.*, **28**, 2007, 101-112.
29. Guntinas-Lichius, O., A. Irintchev, M. Streppel, M. Lenzen, M. Grosheva, K. Wewetzer, W. F. Neiss, D. N. Angelov. Factors limiting motor recovery after facial nerve transection in the rat: combined structural and functional analyses. – *Eur. J. Neurosci.*, **21**, 2005, 391-402.

30. Guntinas-Lichius, O., K. Wewetzer, T. L. Tomov, N. Azzolin, S. Kazemi, M. Streppel, W. F. Neiss, D. N. Angelov. Transplantation of Olfactory Mucosa Minimizes Axonal Branching and Promotes the Recovery of Vibrissae Motor Performance after Facial Nerve Repair in Rats. – *J. Neurosci.*, **22**, 2002, 7121-7131.

31. Hadlock, T., R. Lindsay, C. Edwards, C. Smitson, J. Weinberg, C. Knox, J. T. Heaton. The effect of electrical and mechanical stimulation on the regenerating rodent facial nerve. – *Laryngoscope*, **120**, 2010, 1094-1102.

32. Haninec, P., P. Dubový, F. Šámal, L. Houštava, L. Stejskal. Reinnervation of the rat musculocutaneous nerve stump after its direct reconnection with the C5 spinal cord segment by the nerve graft following avulsion of the ventral spinal roots: a comparison of intrathecal administration of brain-derived neurotrophic. – *Exp. Brain Res.*, **159**, 2004, 425-432.

33. Hastings, R. L., M. Mikesh, Y. Il. Lee, W. J. Thompson. Morphological remodeling during recovery of the neuromuscular junction from terminal Schwann cell ablation in adult mice. – *Sci. Rep.*, **10**, 2020, 11132.

34. He, Q-R., M. Cong, F-H. Yu, Y-H Ji, S. Yu, H-Y. Shi, F. Ding. Peripheral nerve fibroblasts secrete neurotrophic factors to promote axon growth of motoneurons. – *Neural. Regen. Res.*, **17**, 2022, 1833-1840.

35. Heaton, J. T., C. J. Knox, J. S. Malo, J. B. Kobler, T. A. Hadlock. A System for Delivering Mechanical Stimulation and Robot-Assisted Therapy to the Rat Whisker Pad During Facial Nerve Regeneration. – *IEEE TNSRE,* **21**, 2022, 928-937.

36. Inoue, A., J. R. Sanes. Lamina-specific connectivity in the brain: regulation by N-cadherin, neurotrophins, and glycoconjugates. – *Science*, **276**, 1997, 1428-1431.

37. Jungnickel, J., P. Claus, K. Gransalke, M. Timmer, C. Grothe. Targeted disruption of the FGF-2 gene affects the response to peripheral nerve injury. – *Mol. Cell. Neurosci.*, **25**, 2004, 444-452.

38. Kang, H., L. Tian, W. Thompson. Terminal Schwann cells guide the reinnervation of muscle after nerve injury. – *J. Neurocytol.*, **32**, 2003, 975-985.

39. Kang, H., L. Tian, W. J. Thompson. Schwann cell guidance of nerve growth between synaptic sites explains changes in the pattern of muscle innervation and remodeling of synaptic sites following peripheral nerve injuries. – *J. Comp. Neurol.*, **527**, 2019, 1388-1400.

40. Kiryakova, S., J. Söhnchen, M. Grosheva, U. Schuetz, Ts. Marinova, R. Dzhupanova, N. Sinis, C. U. Hübbers, E. Skouras, J. Ankerne, J. W. U. Fries, A. Irintchev, S. A. Dunlop, D. N. Angelov. Recovery of whisking function promoted by manual stimulation of the vibrissal muscles after facial nerve injury requires insulin-like growth factor 1 (IGF-1). – *Exp. Neurol.*, **222**, 2010, 226-234.

41. Kleiss, I. J., C. J. Knox, J. S. Malo, H. A. M. Marres, T. A. Hadlock, J. T. Heaton. Whisking Recovery After Automated Mechanical Stimulation During Facial Nerve Regeneration. – *JAMA Facial Plast. Surg.*, **16**, 2014, 133-139.

42. Klimaschewski, L., P. Claus. Fibroblast growth factor signalling in the diseased nervous system. – *Mol. Neurobiol.*, **58**, 2021, 3884-3902.

43. Klimaschewski, L., B. Hausott, D. N. Angelov. The pros and cons of growth factors and cytokines in peripheral axon regeneration. – *Int. Rev. Neurobiol.*, **108**, 2013, 137-171.

44. Lalwani, A. K., J. J. Han, C. M. Castelein, G. J. Carvalho, A. N. Mhatre. In Vitro and in vivo assessment of the ability of adeno-associated virus-brain-derived neurotrophic factor to enhance spiral ganglion cell survival following ototoxic insult. – *Laryngoscope*, **112**, 2002, 1325-1334.

45. Lindsay, R. W., J. T. Heaton, C. Edwards, C. Smitson, K. Vakharia, T. A. Hadlock. Daily facial stimulation to improve recovery after facial nerve repair in rats. – *Arch. Facial Plast. Surg.*, **12**, 2010, 180-185.

46. Love, F. M., Y. Son, W. J. Thompson. Activity alters muscle reinnervation and terminal sprouting by reducing the number of Schwann cell pathways that grow to link synaptic sites. – *J. Neurobiol.*, **54**, 2003, 566-576.
47. Madison, R. D., M. V. Sofroniew, G. A. Robinson. Schwann cell influence on motor neuron regeneration accuracy. – *Neuroscience*, **163**, 2009, 213-221.
48. McGregor, C. E., A. W. English. The role of BDNF in peripheral nerve regeneration: activity-dependent treatments and Val66Met. – *Front. Cell Neurosci.*, **12**, 2019, 522.
49. Michalski, B., J. R. Bain, M. Fahnestock. Long-term changes in neurotrophic factor expression in distal nerve stump following denervation and reinnervation with motor or sensory nerve. – *J. Neurochem.*, **105**, 2008, 1244-1252.
50. Nawa, H., M. A. Pelleymounter, J. Carnahan. Intraventricular administration of BDNF increases neuropeptide expression in newborn rat brain. – *J. Neurosci.*, **14**, 1994, 3751-3765.
51. Novikov, L., L. Novikova, J-O. Kellerth. Brain-derived neurotrophic factor promotes axonal regeneration and long-term survival of adult rat spinal motoneurons in vivo. – *Neuroscience*, **79**, 1997, 765-774.
52. Pearse, D. D., F. C. Pereira, A. E. Marcillo, M. L. Bates, Y. A. Berrocal, M. T. Filbin, M. B. Bunge. cAMP and Schwann cells promote axonal growth and functional recovery after spinal cord injury. – *Nat. Med.*, **10**, 2004, 610-616.
53. Piehl, F., H. Hammarberg, T. Hökfelt, S. Cullheim. Regulatory effects of trophic factors on expression and distribution of CGRP and GAP-43 in rat motoneurons. – *J. Neurosci. Res.*, **51**, 1998, 1-14.
54. Pockett, S., J.R. Slack. Source of the stimulus for nerve terminal sprouting in partially denervated muscle. – *Neuroscience*, **7**, 1982, 3173-3176.
55. Pradat, P. F. Treatment of peripheral neuropathies with neutrotrophic factors: animal models and clinical trials. – *Rev. Neurol. (Paris)*, **159**, 2003, 147-161.
56. Raivich, G., M. Makwana. The making of successful axonal regeneration: genes, molecules and signal transduction pathways. – *Brain. Res. Rev.*, **53**, 2007, 287-311.
57. Reddy, L. V., S. Koirala, Y. Sugiura, A. A. Herrera, C-P. Ko. Glial cells maintain synaptic structure and function and promote development of the neuromuscular junction in vivo. – *Neuron*, **40**, 2003, 563-580.
58. Rich, M. M., J. W. Lichtman. In vivo visualization of pre-and postsynaptic changes during synapse elimination in reinnervated mouse muscle. – *J. Neurosci.*, **9**, 1989, 1781-1805.
59. Rink, S., C. Chatziparaskeva, L. Elles, S. Pavlov, K. Nohroudi, H. Bendella, L. Sarikcioglu, M. Manthou, S. Dunlop, T. Gordon, D. N. Angelov. Neutralizing BDNF and FGF2 injection into denervated skeletal muscle improve recovery after nerve repair. – *Muscle Nerve*, **62**, 2020, 404-412.
60. Santos, D., F. Gonzalez-Perez, X. Navarro, J. Del Valle J. Dose-dependent differential effect of neurotrophic factors on in vitro and in vivo regeneration of motor and sensory neurons. – *Neural Plast.*, **2016**, 2016, 4969523.
61. Seitz, M., M. Grosheva, E. Skouras, S. K. Angelova, J. Ankerne, J. Jungnickel, C. Grothe, L. Klimaschewski, C. U. Hübbers, S. A. Dunlop, D. N. Angelov. Poor functional recovery and muscle polyinnervation after facial nerve injury in fibroblast growth factor-2−/− mice can be improved by manual stimulation of denervated vibrissal muscles. – *Neuroscience*, **182**, 2011, 241-247.
62. Semba, K., M. D. Egger. The facial "motor" nerve of the rat: Control of vibrissal movement and examination of motor and sensory components. – *J. Comp. Neurol.*, **247**, 1986, 144-158.
63. Sendtner, M. Neurotrophic factors: effects in modulating properties of the neuromuscular endplate. – *Cytokine Growth Factor Rev.*, **9**, 1998, 1-7.
64. Sendtner, M., B. Holtmann, R. Kolbeck, H. Thoenen, Y-A. Barde. Brain-derived neurotrophic factor prevents the death of motoneurons in newborn rats after nerve section. – *Nature*, **360**, 1992, 757-759.

65. Simon, M., R. Porter, R. Brown, G. R. Coulton, G. Terenghi. Effect of NT-4 and BDNF delivery to damaged sciatic nerves on phenotypic recovery of fast and slow muscles fibres. – *Eur. J. Neurosci.*, **18**, 2003, 2460-2466.
66. Slack, J. R., S. Pockett. Terminal sprouting of motoneurones is a local response to a local stimulus. – *Brain Res.*, **217**, 1981, 368-374.
67. Söhnchen, J., M. Grosheva, S. Kiryakova, C. U. Hübbers, N. Sinis, E. Skouras, J. Ankerne, K. Kaidoglou, J. W. U. U. Fries, A. Irintchev, S. A. Dunlop, D. N. Angelov. Recovery of whisking function after manual stimulation of denervated vibrissal muscles requires brain-derived neurotrophic factor and its receptor tyrosine kinase B. – *Neuroscience*, **170**, 2010, 372-380.
68. Son, Y-J., W. J. Thompson. Nerve sprouting in muscle is induced and guided by processes extended by Schwann cells. – *Neuron*, **14**, 1995, 133-141.
69. Son, Y-J., J. T. Trachtenberg, W. J. Thompson. Schwann cells induce and guide sprouting and reinnervation of neuromuscular junctions. – *Trends Neurosci.*, **19**, 1996, 280-285.
70. Streppel, M., N. Azzolin, S. Dohm, O. Guntinas-Lichius, C. Haas, C. Grothe, A. Wevers, W. F. Neiss, D. N. Angelov. Focal application of neutralizing antibodies to soluble neurotrophic factors reduces collateral axonal branching after peripheral nerve lesion. – *Eur. J. Neurosci.*, **15**, 2002, 1327-1342.
71. Tam, S. L., T. Gordon. Mechanisms controlling axonal sprouting at the neuromuscular junction. – *J. Neurocytol.*, **32**, 2003, 961-974.
72. Vleggeert-Lankamp, C., G. C. W. De Ruiter, J. F. C. Wolfs, A. P. Pego, H. K. P. Feirabend, E. Lakke, M. J. A. Malessy. Type grouping in skeletal muscles after experimental reinnervation: another explanation. – *Eur. J. Neurosci.*, **21**, 2005, 1249-1256.
73. Ying, Z., R. R. Roy, V. R. Edgerton, F. Gómez-Pinilla. Exercise restores levels of neurotrophins and synaptic plasticity following spinal cord injury. – *Exp. Neurol.*, **193**, 2005, 411-419.
74. Zhang, J., X. Luo, C. J. Xian, Z. Liu, X. Zhou. Endogenous BDNF is required for myelination and regeneration of injured sciatic nerve in rodents. – *Eur. J. Neurosci.*, **12**, 2000, 4171-4180.
75. Zhao, C., K. Veltri, S. Li, J. R. Bain, M. Fahnestock. NGF, BDNF, NT-3, and GDNF mRNA expression in rat skeletal muscle following denervation and sensory protection. – *J. Neurotrauma*, **2**, 2004, 1468-1478.

Institute of Experimental Morphology, Pathology and Anthropology with Museum
Bulgarian Anatomical Society

Acta Morphologica et Anthropologica, 31 (1-2)
Sofia ● 2024

Neuronal Types in the Rat Spinal Trigeminal Nucleus

Andrey Ivanov [1,2], Dimitrinka Atanasova [1,3], Nikolai Lazarov [1,2]*

[1] Institute of Neurobiology, Bulgarian Academy of Sciences, Sofia, Bulgaria
[2] Department of Anatomy and Histology, Medical University of Sofia, Sofia, Bulgaria
[3] Department of Anatomy, Faculty of Medicine, Trakia University, Stara Zagora, Bulgaria

** Corresponding author e-mail: aivanov@medfac.mu-sofia.bg*

The spinal trigeminal nucleus (SpV) plays a crucial role in the modulation of pain processing. Understanding the morphology of neurons within the subnuclei is essential for unraveling its functional organization. This study aimed to examine the diversity of neuronal morphology in the oral, interpolar, and caudal subnuclei of the SpV. Neurons were characterized based on their soma size and shape using histological staining techniques with hematoxylin and eosin, toluidine blue, and neutral red. We found a broad spectrum of neuronal shapes of at least seven types including boat-shaped, lobulated, round, oval, elongated, pyramidal, triangular, and very large neurons. These findings provide insights into the structural heterogeneity of neurons within the SpV and contribute to our understanding of its complex organization, thus highlighting the significance of neuron shape diversity in sensory processing.

Key words: spinal trigeminal nucleus, neuronal morphology, histological staining, pain processing, rat

Introduction

Nestled within the intricate network of the brainstem lies a structure of paramount importance in sensory processing and pain modulation: the spinal trigeminal nucleus (SpV). This nucleus serves as a critical relay station for somatosensory information originating from the face and head, playing a pivotal role in various sensory and nociceptive pathways [17]. The SpV is anatomically and functionally divided into three distinct subnuclei: the caudalis (SpVc), interpolaris (SpVi), and oralis (SpVo) [13]. Each subnucleus exhibits unique cytoarchitectural features and receives inputs from specific regions of the face and head, thereby contributing to specialized sensory processing. Despite its relatively small size, the SpV plays a multifaceted role in sensory integration, nociception, and autonomic regulation. Sensory information from various modalities, including tactile, thermal, and nociceptive stimuli, converges upon the SpV, where it undergoes intricate processing and modulation [18].

Understanding the structural features, primarily the size and morphology of neurons in these subnuclei, is essential for unraveling the functional organization of the trigeminal sensory system. Prior research has investigated the neuronal architecture of the SpV, providing valuable information on the morphological heterogeneity within its subnuclei [18]. In particular, studies using various histological techniques and immunohistochemistry have repeatedly reported the morphological heterogeneity of neurons within the three subnuclei of the SpV in cats, rats, and humans [5, 6, 7, 9, 16]. The differences observed in these studies highlight the structural complexity of this brain nucleus in various animal species.

Despite the wealth of research on the neuronal size in the SpV, there remains a dearth of studies exploring neuronal shapes comprehensively. This study aims to fill this gap by examining the different shapes of neurons across the three subnuclei in the rat SpV. Utilizing staining techniques, we analyze the morphological heterogeneity of SpV neurons, shedding light on their structural diversity and potential functional implications.

Materials and Methods

The experiments were carried out on adult Wistar rats. A total of 12 male rats with a body weight of 180−300 g were used in our study. All experiments were conducted according to the regulations for work with experimental animals in Bulgaria in compliance with the rules of the Ethics Committee of the Institute of Neurobiology, BAS (registration FWA 00003059 US Department of Health and Human Services) and those of the Research Ethics Committee at the Medical University of Sofia following the Directive 2010/63/EU on the protection of animals used for scientific purposes.

Experimental animals were initially anesthetized with ether followed by an intraperitoneal injection of thiopental (Sigma-Aldrich) at 40 mg/kg dosage. Anesthesia was maintained as the ascending aorta was cannulated via the left ventricle for perfusion. The circulatory system was flushed with 0.05 M phosphate-buffered saline (PBS), pH 7.36, followed by fixation using 4% paraformaldehyde (Merck) in 0.1 M phosphate buffer (PB) for approximately 20 minutes. After brain removal, the region of interest spanning from the midbrain to the upper spinal cord was dissected. Tissue blocks were fixed overnight at 4°C in the same fixative, then washed thoroughly with tap water the following day and finally processed for embedding in paraffin. Tissue sections 7 μm thick were mounted on chrome-gelatinized slides and after rehydration were stained with toluidine blue (500 mg of dye to 100 ml of distilled water) for 5-10 min. This staining was used to describe the cytoarchitectonics of the nucleus and its parts. After dehydration sections were embedded into Entellan (Merck).

The specimens were viewed and photographed using an Olympus VS120-L100 Virtual Slide System research light microscope. the resulting digital images were then saved in TIF format, after which morphometric analysis of the digital images was conducted.

Results

Types of neurons in the spinal trigeminal nucleus

Brainstem sections at the level of SpVc, SpVi, and SpVo were stained to examine SpV subnuclear neurons. SpV neurons were categorized by the shape of their perikarya.

The three subdivisions of SpV were found to include similar types of neurons. Therefore, a general description of these neuronal types will be presented. According to the criteria of the study, each subdivision of the SpV had at least seven types of neurons.

Boat-like neurons

We revealed a unique neuronal phenotype in the rat SpV characterized by its boat-like soma (**Fig. 1A**). The neuronal perikarya resembled boats; they had a broad, elongated shape and a smooth surface viewed with light microscopy. Their somata were found to range in size between 20 and 30 μm, with an average diameter of 25 μm ± 3.8 (n = 11), indicating a significant level of variation among this group of neurons.

Elongated neurons

Other unique anatomical features were evident in medium-sized neurons in the SpV of rats, as shown in **Fig. 1B**. Fusiform or elongated cell bodies were present in these neurons and they belonged to the category of medium-sized neurons. The perikaryal diameter in this population of neurons ranged from 14 to 21 μm, with a mean diameter of 15 μm ± 2.1 (n = 24). This indicates a somewhat variable soma size.

Lobulated neurons

We have further observed another unique anatomical feature that appeared in lobulated neurons in the rat SpV, as shown in **Fig. 1C**. The cell bodies of these neurons were lobulated, meaning that they had irregular surface protrusions or depressions with an average diameter of 16 μm ± 1.3 (n = 9), while their soma diameters ranged from 15 to 21 μm.

Neurons with dilations/swellings at the axonal hillock

Our study also identified spinal trigeminal neurons with distinct morphological characteristics as shown in **Fig. 1D**. Specifically, we have seen neurons on whose cell bodies we observed dilated regions that were particularly visible near the branching points of their processes. There was likely significant dilation of the dendritic architecture at these points, as these dilated regions often exhibited widths that were similar or nearly identical to the diameter of the neuronal cell bodies. The perikarya of neurons with dilations differed significantly from each other in size and shape. This heterogeneity represented a distinctive morphological feature of this type of neuron within the SpV.

Pyramidal neurons

Other spinal trigeminal neurons in the rat SpV with unique morphological features were neurons that have a triangular soma (**Fig. 1E**). We found that this population of neurons exhibited apparent diversity in the mean diameter 17 µm ± 1.2 (n = 12) and a range of soma size from 13 to 21 µm. Dendritic morphology was determined by the presence of two basal and one apical processes in each neuron present in this staining type.

Neurons with an oval cell body and different sizes

We have also identified neurons with various oval or spherical cell bodies with different soma diameters. Their bodies varied from 6 to 20 µm with a mean diameter of 12 µm ± 1.1 (n = 509). This neuronal subtype appeared to have a very heterogeneous soma size (**Fig. 1F**).

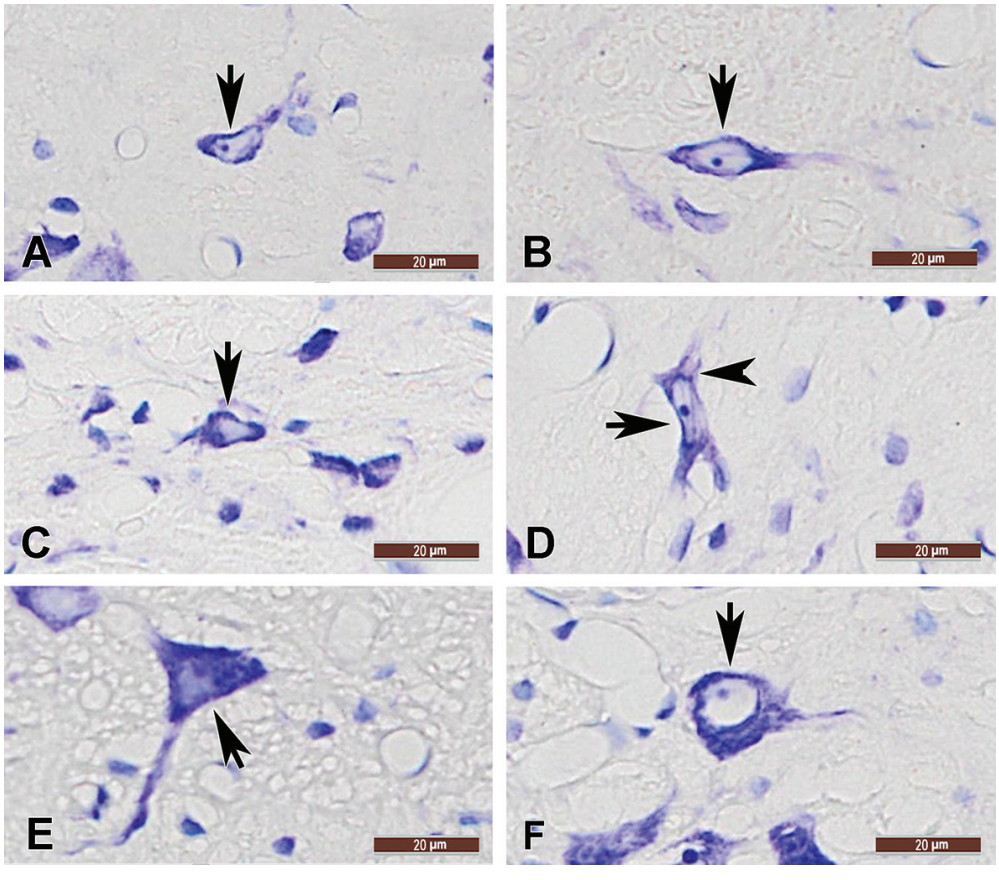

Fig. 1. Morphological types of neurons in the spinal trigeminal nucleus stained with toluidine blue. (**A**) Neuron with a boat-shaped body (arrow); (**B**) Neuron with a bipolar profile and elongated cell body (arrow); (**C**) Neuron with a lobulated cell body (arrow); (**D**) Neuron (arrow) with a dilatation (arrowhead) at the beginning of one of its processes; (**F**) Neuron with a characteristic pyramidal shape of its perikaryon; (**F**) Typical representative of neurons with an oval-shaped cell body (arrow). Scale bar = 20 µm.

Large neurons with different cell body shapes

Another cell population that we observed in the SpV of rats was very large neurons (**Fig. 2**). These neurons possessed large perikarya measuring over 21 µm in soma diameter. Within this population of neurons, the mean soma diameter was 26.7 µm ± 5.5 (n = 33), suggesting that soma size was quite variable. The largest cell body of a neuron that was measured had a diameter of almost 44 µm (43.92 µm). The diversity in somatic morphology among these neurons was reflected in the shape of their somata, which include round, oval, and pear-shaped cells.

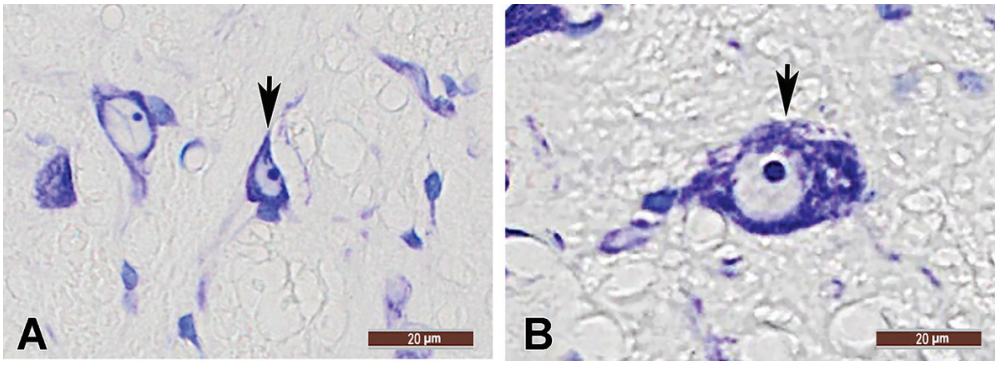

Fig. 2. Neurons with large perikaryal size. Notable diversity in somatic morphology with different shapes of cell bodies arrows described as pear-shaped (A) and oval shapes (B). Scale bar = 20 *µm*.

Discussion

This study represents the first comprehensive investigation of the morphology of neurons in the rat SpV. The results confirm the complex nature of neurons and provide an in-depth description of other neuron types, including fusiform, pyramidal, and multipolar cells, which have only been briefly described in previous reports. The study introduces new findings by describing neurons exhibiting characteristic features such as octopod-like, boat-like, and lobulated cells, and identifies and categorizes at least seven distinct neuronal cell types within the rat SpV, highlighting their similarity in its three parts. In addition, the study revealed pyramidal neurons resembling analogs in other species as well as small round or oval neurons likely correspond to small neurons reported in other species [5, 9, 11]. We also confirmed the similarity of the multipolar neurons in the rat SpV to those reported in previous studies [7, 11].

Prior studies of the morphology of neurons within the SpV, particularly in species such as rats [3, 4, 5, 9, 10], cats [7, 11], camels [2], and humans [15, 16], have primarily categorized these cells based on the size and shape of their bodies using a variety of techniques. In particular, the neuronal elements in the SpV have been identified in different species including rats, cats, monkeys and humans using various examination techniques such as Golgi impregnation, horseradish peroxidase (HRP), Nissl staining and immunocytochemistry, and multiple cell types have been described within the three subdivisions of the SpV [2, 3, 4, 5, 6, 7, 9, 11, 15, 16]. For instance, six distinct

neuron types have been identified in the feline SpV, including pyramidal neurons with spines, pyramidal neurons without spines, multipolar neurons characterized by a dense dendritic tree, and multipolar neurons with sparsely branching dendrites, cells characterized by small oval or round cell bodies and discrete clusters of spines on distal dendrites, and stalked cells showing multiple fine stalked branching and spines on their dendrites [5, 6, 7].

Studies on the human oral subnucleus have delineated two major categories of neurons [15, 16]. The first category consists of small rounded or fusiform cells (8-10 μm in diameter) clustered in small clusters or scattered. The second category comprises large neurons (22 μm in diameter) that have a pear-shaped, fusiform, multipolar, or bipolar morphology.

In addition, two of the subnuclei of the SpV have undergone extensive study in different species. In the feline interpolar subnucleus, for example, observation has revealed the presence of five distinct neuronal cell types [11]. These types exhibit different morphologies, including smooth pyramidal, smooth multipolar characterized by spherical dendritic arborizations, bipolar fusiform or oval with small nuclei, stalked neurons characterized by 2-4 extensively branched spiny dendrites, and cells with very small oval bodies and densely arranged dendrites. The diameters of these neurons range from 6-12 μm to 15-25 μm.

Conversely, three main types of nerve cells have been found in the rat oral subnucleus [3, 4], with reported forms including oval, fusiform, or pyramidal shapes. Cell body sizes of these neurons range from 5-15 μm to 25-50 μm in diameter. Previous studies of spinal trigeminal neurons have categorized them primarily based on the size of their cell bodies paying limited attention to the shape of their perikarya. Notable exceptions include detailed descriptions of stalked neurons in small animals such as rats and cats [5, 9, 11], where neurons were characterized as medium-sized neurons with many spiny stalk numbers. Although two previous studies have briefly outlined dendritic trees of nerve cells in the human oral subnucleus of the spinal trigeminal nucleus [15, 16], it should be noted that pain perception is generally associated with specialized sensory neurons that feature complex dendritic processes for detecting noxious stimuli [8, 12].

Previous studies, particularly those focused on stalk neurons, have provided detailed descriptions characterizing them as complex cells with spiny dendrites and a significant number of spiny dendritic stems [5, 6, 11]. It is noteworthy that the dynamics of spines influenced by neuronal activity and developmental age have been emphasized [14]. In contrast, other neuron types, including islet, fusiform, pyramidal, and multipolar cells, have been mentioned in earlier studies with limited details. In a study on cats, for example, pyramidal neurons were identified, and other neurons were described as small, round or oval with some spines on the dendrites [5]. However, detailed morphological data, such as the density of the dendritic tree and the types and distribution of the various appendages, have not been reported.

An interesting and similar study focused on the morphological characteristics of neurons in the SpV in camels, using the Golgi impregnation method [2]. Additionally, to look at the shape of the neuronal perikarya, the study also classified the cells based on cell body size and shape, dendritic tree density, and the morphology and distribution of appendages. The study identified at least 12 morphological types of neurons, including stalked, islets, octopus-like, lobulated, boat-like, pyramidal, multipolar, round, oval,

and elongated neurons [2]. These neurons exhibited diverse forms of appendages originating from both dendrites and cell bodies, with some featuring large dilatations at dendritic branching points. Taken together with our results, there are two pieces of research done by our awareness, that have successfully been able to show unique cell body morphology such as boat-like and lobulated neurons, one in rats and the other in camels.

Some previous reports emphasized the importance of small and stalked neurons to the exclusion of other types of neurons in the SpV [1, 5]. The present study, however, identified other neuronal types in significant numbers. In particular, the study reported large neurons with a body diameter of up to 44 μm in some cases, a characteristic not documented in the SpV of the rat. Furthermore, neurons with characteristic shapes, such as boat-like, and lobulated cells, were reported exclusively in the rat SpV from this study, with no precedent for similar neurons in this nucleus in rats in other work on this topic.

Conclusion

The neuronal morphologies outlined in this research serve as the foundation for our upcoming inquiries, which aim to elucidate the functional characteristics of these neurons, such as their connections, neurotransmitters, and neuropeptides. This endeavor is part of a broader project focused on compiling a comprehensive database of neuronal cell types across various regions of the rat brain. Within the scope of this study, we identified diverse morphological types of neurons within the rat SpV. Our classification of these neurons relied solely on the size and shape of their cell bodies. Notably, we identified three previously undocumented types of neurons in the rat SpV, known as the boat-like, lobulated, and neurons with dilations at the axonal hillock. We hypothesize that these neuron variations have emerged as adaptations within the rat sensory pathway to respond to painful stimuli. Comparative neuroanatomical investigations are pivotal for advancing our comprehension of the organization of the central nervous system.

References

1. **Bennett, G. J., M. Abdelmoumene, H. Hayashi, R. Dubner.** Physilogy and morphology of substantia gelatinosa neurons intracellularly stained with horserdish peroxidase. – *J. Comp. Neurol.*, **194**(4), 1980, 810-827.
2. **El-Dwairi Q. A., S. M. Al-Hussain, A. S. Banihani, Z. M. Bataineh, L. Djouhri, A. G. Mustafa, S. Zaqout.** Neuronal cell types in the spinal trigeminal nucleus of the camel brain. – *Brain Sci.*, **13**(2), 2023, 312.
3. **Falls, W. M.** A Golgi type II neuron in trigeminal nucleus oralis: A Golgi study in the rat. – *Neurosci. Lett.*, **41**(1–2), 1983, 1-7.
4. **Falls, W. M., R. E. Rice, J. P. Vanwagner.** The dorsomedial portion of trigeminal nucleus oralis (Vo) in the rat: Cytology and projections to the cerebellum. – *Somatosens. Res.*, **3**(2), 1985, 89-118.
5. **Gobel, S.** Golgi studies of the substantia gelatinosa neurons in the spinal trigeminal nucleus. – *J. Comp. Neurol.,* **162**(3), 1975, 397-415.

6. Gobel, S. Golgi studies of the neurons in layer I of the dorsal horn of the medulla (trigeminal nucleus caudalis). – *J. Comp. Neurol.,* **180**(2), 1978, 375-393.
7. Gobel, S. Golgi studies of the neurons in layer II of the dorsal horn of the medulla (trigeminal nucleus caudalis). – *Pain*, **6**(3), 1979, 386.
8. Kim, M. D., Y. J. Lily, N. J. Yuh. The bHLH-PAS protein spineless is necessary for the diversification of dendrite morphology of Drosophila dendritic arborization neurons. – *Genes Dev.*, **20**(20), 2006, 2806-2819.
9. Li, Y. Q., H. Li, T. Kaneko, N. Mizuno. Substantia gelatinosa neurons in the medullary dorsal horn: An intracellular labeling study in the rat. – *J. Comp. Neurol.,* **411**(3), 1999, 399-412.
10. Li, Y. Q., H. Li, K. Yang, Z. M. Wang, T. Kaneko, N. Mizuno. Intracellular labeling study of neurons in the superficial part of the magnocellular layer of the medullary dorsal horn of the rat. – *J. Comp. Neurol.*, **428**(4), 2000, 642-655.
11. Matthews, M. A., T. V. Hernandez, A. I. Romanska, K. D. Hoffman. Golgi and immunocytochemical analysis of neurons in trigeminal subnucleus interpolaris: Correlations with cellular localization of enkephalin. – *Neuroscience*, **32**(2), 1989, 463-480.
12. Moore, A. W., L. Y. Jan, Y. N. Jan. Hamlet, a binary genetic switch between single- and multiple-dendrite neuron morphology. – *Science*, **297**(5585), 2002, 1355-1358.
13. Olszewski, J. On the anatomical and functional organization of the spinal trigeminal nucleus. – *J. Comp. Neurol.*, **92**(3), 1950, 401-413.
14. Runge, K., C. Cardoso, A. de Chevigny. Dendritic Spine Plasticity: Function and Mechanisms. – *Front. Synaptic Neurosci.*, **12**, 2020, 1-26.
15. Rusu, M. C. The spinal trigeminal nucleus – Considerations on the structure of the nucleus caudalis. – *Folia Morphol. (Warsz)*, **63**(3), 2004, 325-328.
16. Schoenen, J. The dendritic organization of the human spinal cord: The dorsal horn. – *Neuroscience*, **7**(9), 1982, 2057-2087.
17. Singh, G. P. Anatomy of Trigeminal Nerve**.** – In: *Handbook of Trigeminal Neuralgia* (Eds. G. Rath), Singapore, Springer Nature, 2019, 11-22.
18. Usunoff, K. G., E. Marani, J. H. Schoen. The trigeminal system in man. – *Adv. Anat. Embryol. Cell Biol.*, **136**, 1997, 1-126.

Institute of Experimental Morphology, Pathology and Anthropology with Museum
Bulgarian Anatomical Society

Acta Morphologica et Anthropologica, 31 (1-2)
Sofia ● 2024

Adolescent Corticotropin Releasing Hormone Neuroplasticity in the Rat Bed Nucleus of Stria Terminalis

Albert Gradev [1], Pavel Rashev [2], Vasil Iliev [1], Angel Dandov [1]*

[1]Department of Anatomy, Histology and Embryology, Medical University, Sofia, Bulgaria
[2]Institute of Biology and Immunology of Reproduction "Acad. Kiril Bratanov", Bulgarian Academy of Sciences, Sofia, Bulgaria

* Corresponding author e-mail: a.gradev@medfac.mu-sofia.bg

The purpose of this study was to find out whether there was an adolescent neurochemical plasticity in the bed nucleus of stria terminalis (BNST), especially the laterodorsal nucleus (BNSTLD) that is involved in stress and anxiety responses. We also aimed to register if there was any difference between the sexes. We chose to investigate the corticotropin-releasing hormone (CRH), which is involved in stress responses. The laterodorsal nucleus has a lot of CRH-expressing neurons, which are GABA-ergic. We observed that there was a preadolescent sexual difference with a higher expression of CRH in females, while in males we found that the expression of CRH increased in the pubertal period. Nevertheless after puberty such a difference disappears. Our results suggest different stress susceptibility between sexes in the preadolescent period, and could explain the inadequacy of stress coping in males during puberty.

Key words: bed nucleus of stria terminalis, corticotropin-releasing hormone, anxiety, puberty, rat

Introduction

The bed nucleus of stria terminalis (BNST) is involved in a wide variety of limbic functions, in particular anxiety responses and addiction [1]. It is a complex structure, and is considered to be part of the extended amygdala, and according to various authors is made up of 12-18 subnuclei [6, 10]. The neurons of the BNST are mainly GABA-ergic, although some glutamate-ergic ones can also be found [11]. The complexity of the structure is further deepened by the co-expression of a variety of neuropeptides [10]. One of the most commonly co-expressed neuropeptide in the BNST is the corticotropin-releasing hormone (CRH). Indeed, the subnucleus with a major CRH expression is the laterodorsal nucleus of BNST (BNSTLD) [5]. The CRH function is to activate the hypothalamic-pituitary-adrenal axis in response to stress [4], albeit the sex and age differences in the CRH expression in the BNST are not well investigated.

Material and Methods

Adult (60 days old; female n=5 and male n=5) and pre-adolescent (20 days old; female n=5 and male n=5) Wistar rats were used for the aim of this study. Pre-adolescent rats were 25-35 g of weight, and adults 230-260 g. The experiments were conducted in accordance with the ethical guidelines of the EU Directive 2010/63/EU for the protection of animals used for scientific purposes and permission from the Bulgarian Food Safety Agency for working with the experimental animals with № 374 was issued. A minimum number of rats were used to reduce the suffering and to fulfill the requirements for a good statistical analysis. The animals were anesthetized intraperitoneally with Pentobarbital (35 mg/kg). After that they were transcardially perfused with phosphate-buffered saline at a volume of approximately 50 ml, which contained heparin at a concentration of 10 UI/ml, followed by 4% solution of formaldehyde at a volume of approximately 1L/kg. The speed of the infusion was 20 ml/min and the pressure was 80-120 mmHg. After the perfusion, the brains were excised, then sectioned, and put in the perfusion fixative for another 8-20 hours at 4°C for postfixation. Each brain was sectioned in two different planes, i.e. in the coronal plane 2 mm posterior to the olfactory bulbs, and through the horizontal fissure. Thereafter they were embedded in paraffin, and sliced on a microtome at a thickness of 6 μm. Then immunohistochemistry was performed, using kit with DAB-detection system (PolyQ Stain 2 step detection system goat anti-mouse/rabbit HRP, Peroxidase quench, DAB kit; quartet GmBH). Briefly, after deparaffinization of the sections, the endogenous peroxidase was blocked with the use of previously mentioned kit for 10 min, followed by antigen retrieval using citrate buffer at 95°C for 20 min, and applying the primary rabbit polyclonal antibody (dilution 1:50, Affinity Biosciences) incubated overnight at 4°C. Then the incubation with the secondary antibody from the kit was performed. The visualization of the reaction was with DAB. All slides were proceeded simultaneously to standardize the results. The ready slides were scanned using Olympus VS-ASW Image Acquisition software. 20 images were taken from the BNSTLD and an average number of 600 neurons were examined. The images were turned black and white, and the intensity of the immunoreaction was obtained using Fiji software, measuring the intensity of the grey (from 0-black, to 255-white). To illustrate the distributional data we used Box and Whiskers plot diagram, where the mean, the 75 and 25 percentile and the highest and lowest measurements are presented. Statistical analysis was performed using T-test for parametric data, which were checked with Kolmogorov-Smirnov test of normality. The differences in the means were considered as statistically important only when the p-value was under 0.05.

Results

By using immunohistochemistry in the BNSTLD, we found that reactivity for CRH in the nucleus of preadolescent females was increased compared to preadolescent males. Thus, expression was also seen in the males although to a lesser extent. The reaction was mainly confined to the perikaryal cytoplasm (**Fig. 1 a, b**). On the other hand, the immunoreaction for CRH in the nucleus of adult rats was evenly expressed in both sexes (**Fig. 1 c, d**). It should also be noted that in the adult males in particular the reaction was much more pronounced than in the younger species of the same sex.

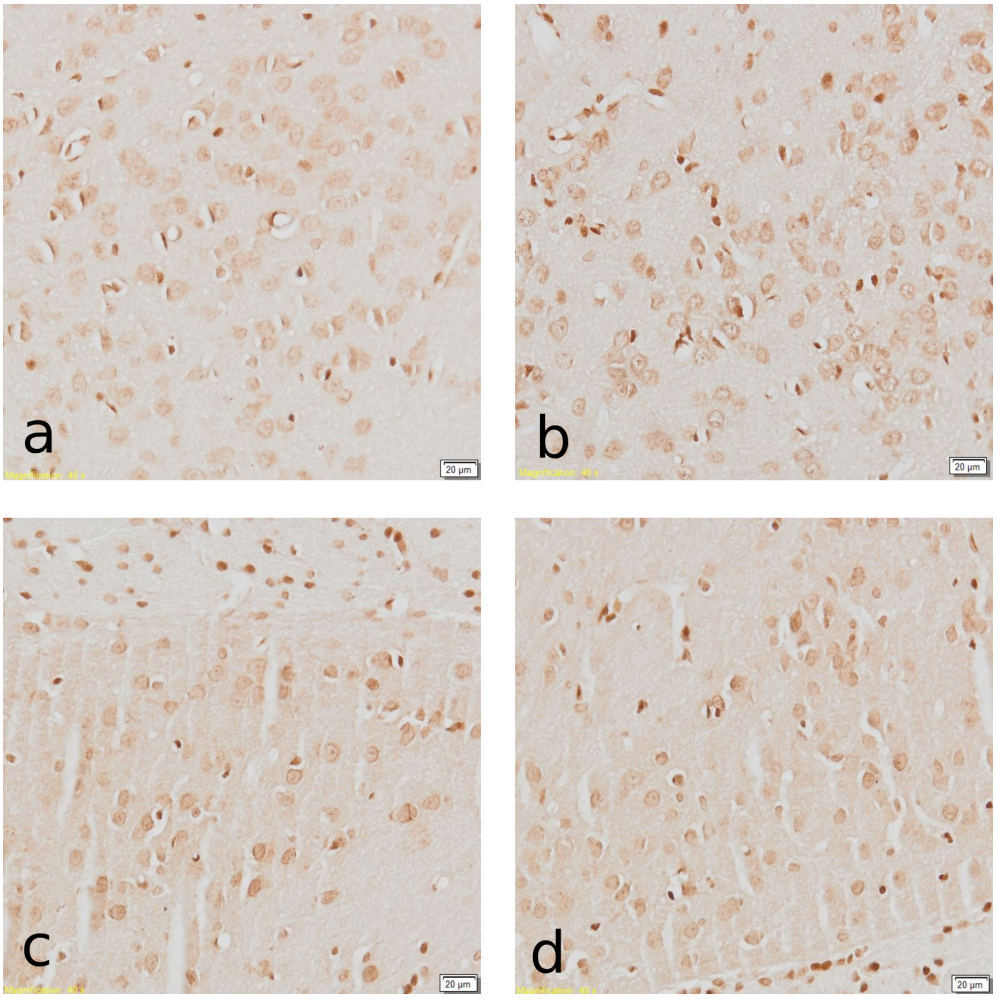

Fig. 1. Photomicrographs of immunohistochemical reaction for CRH at the level of BNSTLD. Images (a) and (b) are sections from preadolescent male and female rats respectively. Images (c) and (d) show sections of adult male and female animals respectively. It is clearly visible that the reaction in preadolescent males is weaker than the preadolescent females and also than adult males. In adults there is no visible sex difference in the CRH expression.

To check the statistical significance, we performed an analysis. The mean and the standard deviation of the expression of CRH (mean grey values) in the BNSTLD of the preadolescent male and female, and adult male and female rats were as follows: 193.59±3.71; 180.86±4.13; 182.06±6.54; 181.34±5.71 (**Fig. 2**). After the statistical analysis the following conclusions were made: the expression of CRH in the BNSTLD was higher in adult than in preadolescent rats, but only in males (**Fig. 3**). Also, the expression in preadolescent rats was higher in female than male rats, albeit in the adult rats we found no difference between sexes. The statistical data and measurements are presented in Table 1.

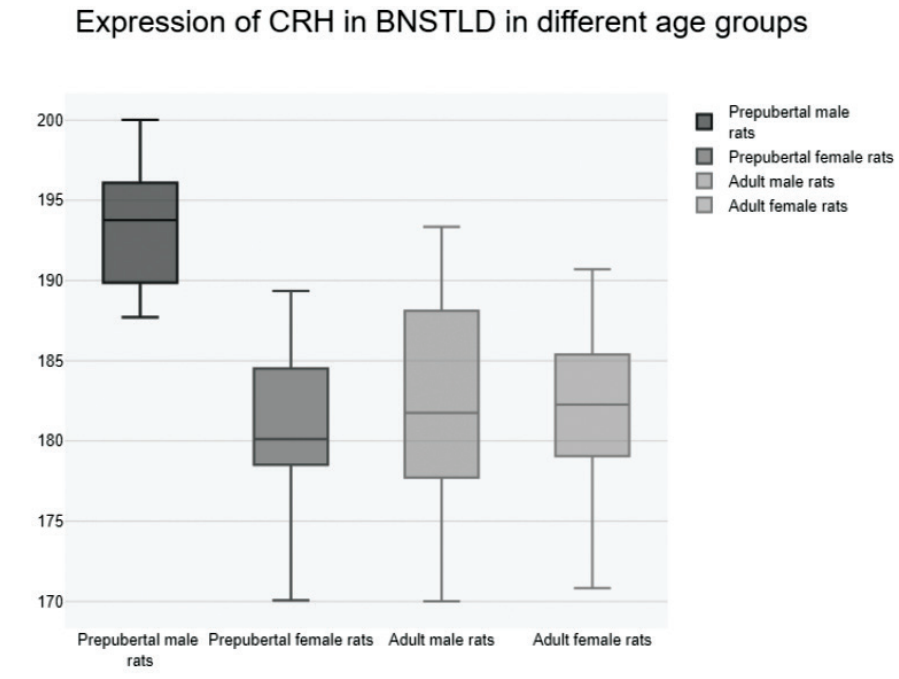

Fig. 2. Box and whiskers plot diagram representing the obtained data with the means, 25th and 75th percentile in the different age groups. On the vertical line the intensity of grey is shown (from 0-black to 255-white). There is statistical difference between preadolescent males and females and also between preadolescent males and adult males.

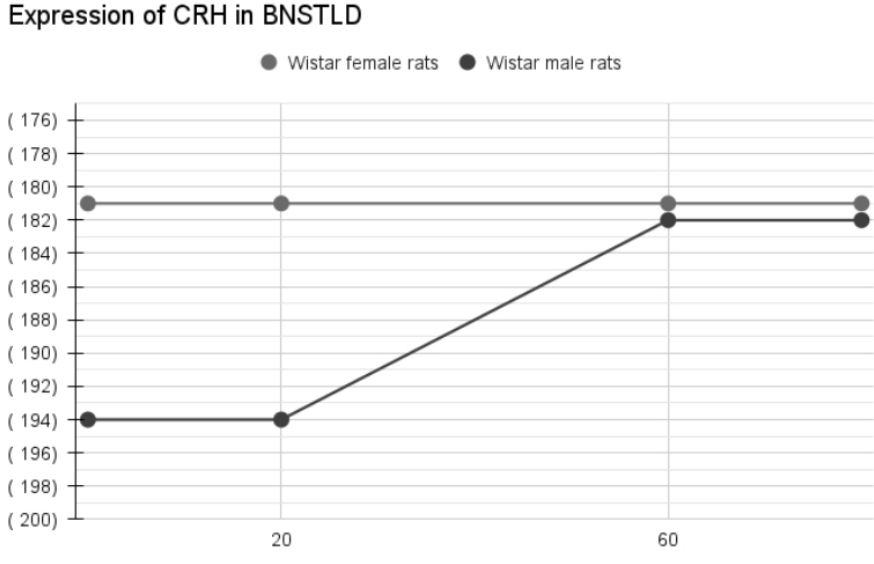

Fig. 3. Linear graph representing the periadolescent dynamics in CRH expression in BNSTLD. There is an obvious pubertal increase in CRH expression only in males, therefore the preadolescent sexual difference disappears after puberty.

Table 1. Statistical data from measurements of intensity of CRH imminoexpression of corticotropin-releasing hormone (CRH) in laterodorsal nucleus of bed nucleus of stria terminalis (BNSTLD).

Experimental group	Mean	Standard deviation	Kolmogorov-Smirnov-criteria
Pre-juvenile male	193.5992	3.71	0.11437
Pre-juvenile female	180.86063	4.13	0.12447
Adult male	182.05597	6.54	0.1067
Adult female	181.3364	5.71	0.10833

Compared groups	T-test value	P – value
Preadolescent male / Adult male	8.40813	<0.00001
Preadolescent female / Adult female	-0.36993	0.712781
Preadolescent male / Preadolescent female	7.70192	<0.00001
Adult male / Adult female	0.45408	0.65147

Discussion

BNST is the second major location of CRH-expressing neurons in the CNS after the hypothalamus [5] in rats. Unlike the latter, in the BNST the CRH-expressing neurons are GABA-ergic [5]. They are mainly located in the BNSTLD [3]. It is well documented that overexpression of CRH in these neurons is present in chronic stress [3, 12]. These cells are also implicated in reward responses since they send efferents to the ventral tegmental area [7]. Moreover, early maternal separation is involved in the overexpression of CRH [9]. Yu et al. [17] proved that CRH is overexpressed in the rat BNST after pain stimulation in a sex-specific manner. The study demonstrates that certain sex-specific peculiarities may exist in the CRH expression. Besides there is evidence for the different CRH response in males and females after stress [2]. The same review shows that females have a more increased anxiety-like behaviour after CRH-exposure than males. It should be noted that most of the studies, however, were performed in adult animals. Nonetheless, it is an emerging fact that the adolescent period is the second major period for neuroplasticity in the brain after the neonatal period [13] and it is also a period marked with significant behavioural changes [8]. Thus, we decided to check the periadolescent neuroplasticity in these neurons. Viau et al. [16] found out that various CRH-expressing sites in the rat brain are influenced differently by sex and age. The authors report age-related increased CRH mRNA expression in females in the paraventricular hypothalamic nucleus, while the same can only be observed in the central amygdala in males. Being part of the extended amygdala, BNSTLD is greatly associated with the central amygdaloid nucleus, classified as a central or lateral extended amygdala [6]. Therefore it is not surprising that our results are identical to the literature. Sterrenburg et al. [14] proved that there

is no sex difference in the CRH expression in BNSTLD in adult rats. In addition, early life stress can induce adult overexpression of CRH [16], so hyper-responsiveness to stress in females, proved in other brain areas [15], leads us to the conclusion that the preadolescent overexpression of CRH in female rats causes hypersensitivity to stress before puberty. Such hypersensitivity could have long-term effects. In addition, the CRH pubertal changes in males may impact on their stress coping during the adolescent period. Further experiments are needed in order to clarify the specific role of CRH before and during puberty, and how this influences stress susceptibility and coping in adult life.

Acknowledgements: This study was financially supported by the Medical Science Council at the Medical University of Sofia (Grant № Д-171/03.08.2023).

References

1. **Avery, S. N., J. A. Clauss, J. U. Blackford**. The Human BNST: Functional Role in Anxiety and Addiction. – *Neuropsychopharmacology,* **41(1),** 2016, 126-41.
2. **Bangasser, D. A., K. R. Wiersielis.** Sex differences in stress responses: a critical role for corticotropin-releasing factor. – *Hormones (Athens),* **17(1),** 2018, 5-13.
3. **Beyeler, A., J. Dabrowska.** Neuronal diversity of the amygdala and the bed nucleus of the stria terminalis. - *Handb. Behav. Neurosci*. **26,** 2020, 63-100.
4. **Caruso, A., A. Gaetano, S. Scaccianoce.** Corticotropin-Releasing Hormone: Biology and Therapeutic Opportunities. – *Biology (Basel),* **11(12),** 2022, 1785.
5. **Dabrowska, J., R. Hazra, J. D. Guo, S. Dewitt, D. G. Rainnie**. Central CRF neurons are not created equal: phenotypic differences in CRF-containing neurons of the rat paraventricular hypothalamus and the bed nucleus of the stria terminalis. – *Front. Neurosci.* **7**, 2013, 156.
6. **De Olmos, J. S., C. A. Beltramino, G. Alheid.** Amygdala and extended amygdala of the Rat: A cytoarchitectonical, fibroarchitectonical, and chemoarchitectonical survey. In: *The rat nervous system* (Ed. G. Paxinos) 3th ed., London, Elsevie Academis Press, 2004, 509-605.
7. **Dedic, N., C. Kühne, M. Jakovcevski, J. Hartmann, A. J. Genewsky, K. S. Gomes, E. Anderzhanova, M. L. Pöhlmann, S. Chang, A. Kolarz, A. M. Vogl, J. Dine, M. W. Metzger, B. Schmid, R. C. Almada, K. J. Ressler, C. T. Wotjak, V. Grinevich, A. Chen, M. V. Schmidt, W. Wurst, D. Refojo, J. M. Deussing.** Chronic CRH depletion from GABAergic, long-range projection neurons in the extended amygdala reduces dopamine release and increases anxiety. – *Nat. Neurosci*. **21(6),** 2018, 803-807.
8. **Holland-Hall, C., G. Burstein.** Adolescent physical and social development. In: *Nelson's textbook of paediatrics* (Eds. Kliegman R. M., B. F. Stanton, J. W. St Geme III, N. F. Schor, R. E. Behrman) 20th ed, Philadelphia, Elsevier, 2016; 926-931.
9. **Hu, P., I. Maita, M. L. Phan, E. Gu, C. Kwok, A. Dieterich, M. M. Gergues, C. N. Yohn, Y. Wang, J. N. Zhou, X. R. Qi, D. F. Swaab, Z. P. Pang, P. J. Lucassen, T. A. Roepke, B. A. Samuels.** Early-life stress alters affective behaviors in adult mice through persistent activation of CRH-BDNF signaling in the oval bed nucleus of the stria terminalis. – *Transl. Psychiatry,* **10(1),** 2020, 396.
10. **Lebow, M. A., A. Chen.** Overshadowed by the amygdala: the bed nucleus of the striaterminalis emerges as key to psychiatric disorders. – *Mol. Psychiatry*, **21**, 2016, 450-463.
11. **Nguyen, A. Q., J. A. Dela Cruz, Y. Sun, T. C. Holmes, X. Xu**. Genetic cell targeting uncovers specific neuronal types and distinct subregions in the bed nucleus of the stria terminalis. – *J. Comp. Neurol.,* **524(12),** 2016, 2379-2399.

13. **Olivera-Pasilio, V., J. Dabrowska**. Oxytocin Promotes Accurate Fear Discrimination and Adaptive Defensive Behaviors. – *Front. Neurosci*., **14,** 2020, 583878.
14. **Schulz, K. M., H. A. Molenda-Figueira, C. L. Sisk.** Back to the future: The organizational-activational hypothesis adapted to puberty and adolescence. – *Horm. Behav*., **55(5),** 2009, 597-604.
15. **Sterrenburg, L., B. Gaszner, J. Boerrigter, L. Santbergen, M. Bramini, E. W. Roubos, B. W. Peeters, T. Kozicz.** Sex-dependent and differential responses to acute restraint stress of corticotropin-releasing factor-producing neurons in the rat paraventricular nucleus, central amygdala, and bed nucleus of the stria terminalis. – *J. Neurosci. Res.*, **90**, 2012, 179-192.
16. **Toledo-Rodriguez, M., C. Sandi**. Stress before puberty exerts a sex- and age-related impact on auditory and contextual fear conditioning in the rat. – *Neural. Plast*., **2007**, 2007, 71203.
17. **Viau, V., B. Bingham, J. Davis, P. Lee, M. Wong.** Gender and puberty interact on the stress-induced activation of parvocellular neurosecretory neurons and corticotropin-releasing hormone messenger ribonucleic acid expression in the rat. – *Endocrinol*ogy, **146(1),** 2005, 137-46
18. **Yu, W., C. M. Caira, N. Del R Rivera Sanchez, G.A. Moseley, T. L. Kash**. Corticotropin-releasing factor neurons in the bed nucleus of the stria terminalis exhibit sex-specific pain encoding in mice. – *Sci. Rep*., ***11****(1),* 2021, 12500.

Institute of Experimental Morphology, Pathology and Anthropology with Museum
Bulgarian Anatomical Society

Acta Morphologica et Anthropologica, 31 (1-2)
Sofia ● 2024

Phyllanthus Amarus Mitigates against Potassium Dichromate-Induced Locomotion Posture and Coordination Impairment in Male Wistar Rats

Iteire Kingsley Afoke[1], Gbayisomore Tolulope Judah[1], Adunola Omosewa Victory[1], Babatunde Ogunlade[2], Dadeni Adeola Blessing[1]*

[1]Department of Anatomy, University of Medical Sciences, Ondo, Ondo State, Nigeria
[2]Department of Anatomy, Federal University of Technology Akure, Ondo State, Nigeria

*Corresponding author email: aiteire@unimed.edu.ng

The neuroprotective property of Phyllanthus amarus (AP) leaf extract was investigated in Potassium dichromate (PDCh)-induced cerebellar function impairment. The rats were divided into seven groups, including a control group, groups receiving different doses of AP, PDCh, and the drug donepezil (Dpz). Various tests assessed exploratory function, muscle strength, coordination, and spatial learning. The rats were examined, and their cerebellar tissues were analyzed. The PDCh group showed a significant decrease in body, brain, and cerebellar weight compared to the control, along with reduced grip strength, impaired locomotion, and increased freezing time in the open-field test. PDCh also affected T-maze and Morris water maze performance. Immunohistochemistry indicated cerebellar degeneration and altered expression of neuronal nuclear protein (NeuN) and Tissue Necrosis Factor TNF-α. GABA levels increased while Glutamate decreased, and Glutathione and Glutathione peroxidase were reduced in the PDCh group. Phyllanthus amarus treatment effectively countered these changes, offering protection against cerebellar degeneration and motor function impairment induced by PDCh toxicity.

Key words: Phyllantus amarus, neuroinflammation, neurotoxicity, motor function, cerebellum

Introduction

The cerebellum is responsible for the coordination of muscle movements, posture maintenance, and balance. For this reason, severe damage to the brain involving the cerebellum could impair its functions and result in ataxia. Cerebellar ataxia is a

progressive neurodegenerative disorder characterized by atrophy or degeneration of the cerebellum, leading to motor dysfunction, balance problems, and limb and gait ataxia [37]. Factors contributing to the pathophysiology of neurodegeneration of the cerebellum can be genetic, environmental such as (drugs, chemicals, metals, etc.), underlying chronic diseases, and multifactorial. Potassium dichromate (PDCh) is a heavy metal and widely recognized environmental pollutant linked to carcinogenic, teratogenic, and mutagenic effects [43]. It is mainly used as a precursor to potassium chromium alum in construction, photography, and printing. Like other hexavalent chromium compounds, PDCh is a strong oxidizer, acutely and chronically harmful to health. Widespread neurodegeneration has been observed in multiple studies involving the use of PDCh across multiple species, with significant toxicity to Purkinje cells of the cerebellum [9, 12]. This chemical compound generates reactive oxygen species (ROS), causing injury to the cellular proteins, lipids, and DNA and triggering a cascade of degenerating events leading to neuronal injury and neuroinflammation [38].

Moreover, neurodegeneration and neuroinflammation are intrinsically linked with associated inflammatory processes such as Alzheimer's disease (AD) and Parkinson's disease (PD). These two diseases of global importance, mainly to the elderly population, are estimated to have a death rate that has increased in both males and females within the last two to three years of the post-pandemic era [20]. Likewise, there is an overall ataxia prevalence rate of 26/100,000 in children, a prevalence rate of dominant hereditary cerebellar ataxia of 2.7/100,000, and a prevalence rate of recessive hereditary cerebellar ataxia of 3.3/100,000 [22]. Therefore, neurodegenerative diseases significantly impact the economy, and the risk of being affected increases with age, thus creating the need to improve our therapeutic approach towards them and adopt new ways to treat and prevent these neurological disorders. Besides, the use of plant materials as sources of medical compounds is rapidly emerging, and they have continued to play a dominant role in maintaining human health since antiquity.

Over 50% of all modern chemical drugs are of natural plant product origin and are essential in drug development programs of the pharmaceutical industry [40]. Therefore, intense research on the explorative use of orthodox medicine to treat neurodegenerative disorders (ND) is justified. Phyllanthus *amarus* (AP) is a widespread tropical plant known as the gale of the wind, stonebreaker, or seed-under-leaf. A link exists between its fruits as antioxidants, memory-enhancing, anticholinesterase, astringent, hepatoprotective, cytotoxic, and antimicrobial activity [28]. The phytochemical analysis of the plant extract revealed that it contains a high amount of saponins, tannins, flavonoids, and alkaloids [10]. Even though the neuroprotective nature of AP against oxidative stress has been identified in recent works, the specific dose range for its neuroprotective effect against neurotoxic agents is poorly understood, and its possible effect on potassium dichromate-induced neuronal cerebellar damage, about NeuN and TNFα expression, is yet to be documented. Therefore, this study will provide novel information on the neuroprotective effect of Phyllanthus *amarus* in PDCh-induced neurotoxicity in the cerebellum of male Wistar rats. Additionally, this study will further assess the neurobehavioral activity, oxidative stress level, GABAergic and Glutaminergic pathways, and immunohistochemically and histologically elaborate on new findings on the neuroprotective role of AP in the cerebellar impairment of rats treated with PDCh.

Materials and Methods

Aqueous extraction of Phyllanthus amarus leaves

Firstly, the fresh leaves were collected in bulk from a swamp around the Federal Housing Estate, Igba, Ondo City, Ondo State, Nigeria, and then immediately taken for identification by a plant Biologist at the Department of Plant Biology, Adeyemi Federal College of Education, with a Batch No: ACE/BIO/22/010. Plant authentication was carried out by a Herbarium Curator at the University of Medical Sciences, in the Department of Plant Biology and Biotechnology, with a herbarium Voucher label UNIMED/P.B.T.H/ 013, to preserve the voucher specimen for future reference. The harvested fresh leaves were then shade-dried for seven days with irregular sun drying for better grinding. The dried leaves were then ground into a coarse powder using a grinding machine and kept in air-tight conditions for extraction. The dried material (600 g) was macerated in 6 liters of distilled water for 48 hours at four °C in a refrigerator. The bottle's contents were sealed, kept at room temperature, and allowed to stand for seven days with irregular shaking. The extract was sieved, and the juice was filtered through Whatman (No. 1) filter paper. The filtrate was placed in a stainless-steel tray and concentrated in an air-circulating oven at 42°C until dry. The resulting extract (13 g) was placed into small glass dishes and stored at 28°C in an incubator for further studies. The different doses of 200, 300, and 400 mg/kg were reconstituted and stored in a stop-bottle for later administration via oral route to experimental animals [16].

Chemicals and reagents

Normal saline (100 ml) manufactured by Biomedical Limited, Nigeria, was purchased from Uche Care Pharmaceuticals Ondo City, Nigeria. Kermel Potassium dichromate (500g; molecular weight 294.18; UN number 3288) manufactured by Tianjin Kermel Chemical Reagent Co., LTD, China, was obtained from Pyrex Scientific Company, Benin Edo State, Nigeria. Donepezil hydrochloride 5mg tablets manufactured by Mutual Pharmaceutical CO., Inc., Philadelphia, USA, purchased from Uche Care Pharmacy LTD, Ondo City, Nigeria.

Experimental animals

The experiments were conducted at the Department of Anatomy, University of Medical Sciences (UNIMED), Ondo State, Nigeria. Animals were obtained from the Animal house's breeding colony of UNIMED and fed with standard rat chow (produced by Bendel livestock feed, Ibadan, Nigeria) and water throughout the study. Approval was granted by the Research Ethics Committee of the University of Medical Sciences, Ondo, Nigeria, with approval number NHREC/TR/UNIMED-HREC-Ondo St/22/06/21.

The animals received human care following the principle of human care and the use of laboratory animals. The rats were weighed weekly before the commencement and throughout the experiment using a Sunrise V-802 30Kg 1gm weighing scale manufactured by Sunrise Technology, USA, calibrated in grams, and recorded to the nearest whole number. Following acclimatization, seventy (70) young adult Wistar rats weighing between 100 g and 120 g were divided into seven groups of ten animals each. Experimental design and treatment protocol were shown on **Table 1**.

Table 1. Research design and treatment protocol.

S/N	Groups	Administration	Mode of Administration
A	Control	0.5ml of normal saline	Per Orally
B	Phyllanthus *amarus* only (AP)only	300mg/kg/day	Per Orally
C	Potassium Dichromate (PDCh)	17mg/kg/day	Per Orally
D	Donepezil only (Dpz)	5mg/kg/day	Per Orally
E	High Phyllanthus *amarus* + Potassium Dichromate	400mg/kg/day and 17mg/kg/day	Per Orally
F	Low Phyllanthus *amarus* + Potassium Dichromate	200mg/kg/day and 17mg/kg/day	Per Orally
G	Donepezil + Potassium Dichromate.	5mg/kg/day and 17mg/kg/day	Per Orally

Motor function tests: Neurobehavioral tests assessed how PDCh administration affects locomotor and exploratory activity.

Wire-hanging test: Commencing on the third day of the administration protocol, a wire-hanging test was conducted on rats to assess muscle strength following drug exposure. This wire suspension task gauges muscle strength and prehensile reflex, which is the animal's ability to grasp a tightly stretched horizontal wire with its forepaws and maintain suspension on the wire. The suspension time, which denotes the duration before the rat is released from the wire, was meticulously recorded. This parameter serves to identify neuromuscular abnormalities related to motor strength. A training session was conducted on the second day of the experiment to acquaint the rats with the task. Subsequently, the actual test started on the third day, as well as on days 7, 14, and 28. The cut-off time for the test was set at 180 seconds, indicating that rats were observed for a maximum of 180 seconds to remain suspended on the wire. If a rat dropped from the wire within this timeframe, the duration until the drop was noted [18].

Open field test (OFT): The OFT is a suitable measure of locomotion and anxiety in experimental animals (Millan, 2003). The OFT apparatus utilized in this study was a square wooden arena (72 cm × 72 cm × 20 cm) with lines on its floor dividing it into 18cm by 18 cm square [24]. The open field apparatus was cleaned with alcohol between each rat to avoid irritability due to odor. The rats were conveyed to the test room in their cages and tested for 5 minutes. Critical parameters of locomotor and exploratory activity, such as immobility (freezing time), rearing, ambulation, and grooming, were judiciously observed, and time spent executing each behavior was recorded.

T-maze spontaneous alternation test: T-maze spontaneous alternation is a behavioral test for measuring exploratory behavior in animals, especially in rodent models for CNS disorders. The test is based on the willingness of rodents to explore a

new environment, i.e., they prefer to visit a new arm of the maze rather than a familiar arm. Subjects were first placed in the start-arm of the T-maze. Upon leaving the start arm, subjects choose between entering the left or the right goal arm. With repeated trials, the animals should show less tendency to enter a previously visited arm. The percentage of alternation (number of turns in each goal arm) and total trial duration were recorded with a stopwatch. This test quantifies cognitive deficits in rats' transgenic strains and evaluates novel chemical entities for their effects on cognition [5].

Morris water maze: This test was carried out to assess the spatial learning and memory of the rats. A pool of water measuring about 100 cm in diameter and 30 cm in depth was used. An escape platform about an inch deep from the water's surface was placed outside one of the quadrants, which was a visual cue. The animals were trained 24 hours before the actual test. During the training, each rat was placed in the other three quadrants for a maximum of 60 seconds to find the escape platform at intervals of 15 minutes between quadrants until the escape latency period was reduced to less than 15 seconds. The time to find the escape platform was recorded as the escape latency period. The parameter measured in the Morris water maze is "Escape Latency" [8].

Determination of total brain and cerebellar weights

Morphometric analysis in this study involved the measurement of the rats' total brain weight (TBW) and cerebellar weight across experimental groups before brain dissection. The brain weight was measured using a sensitive weighing scale (HT-120 Electronic balance manufactured by AND Company Ltd, USA, 2014), and brain weights were recorded. Afterward, the brain was dissected into specific regions; the cerebellum was weighed using a sensitive weighing scale HT-120 Electronic balance manufactured by AND Company Ltd, USA, 2014). The mean ± SEM was calculated using the GraphPad Prism 8.0.1.244 x86 software.

Histological processing/biochemical analysis

After the conduct of the behavioral assessment, the rats were subjected to cervical dislocation; after the conduction of morphometric analysis, the brain tissues were then excised and dissected. Coronal sections of the cerebellum were obtained stereotaxically. For each group, three rat brain samples were chosen for the immunohistochemistry process, targeting NeuN and TNFα expression. Additionally, three brain samples per group were used for biochemical analyses, and another three brain samples per group were allocated for histochemistry to assess neurotransmitter levels. The cerebellum structures dissected from the brain samples were then embedded in an EDTA sampling bottle containing 10% neutral buffered formalin to preserve it. Subsequently, this part of the brain was processed to obtain a Paraffin wax-embedded block for H & E demonstration [15]. The homogenate of this tissue was obtained and then centrifuged at 12,000 rpm to obtain the supernatant containing tissue lysates. The supernatants were obtained and stored at very low temperatures. Glutathione peroxidase GPx activities in the tissue lysates were assayed using appropriate enzyme lysate immunosorbent assay kits.

Immunohistochemistry

NeuN: Immunohistochemistry analysis was performed to selectively identify antigens (proteins) on cells in a tissue section by exploiting the principle of antibody binding

specifically to antigens on biological tissues. The cerebellum was fixed in 10% neutral buffered formalin, dehydrated, and embedded in paraffin wax. Sections of 3 μm thicknesses were cut onto a charged-slides, deparaffinized, and rehydrated. Heat-mediated antigen retrieval was performed using a citrate-based antigen retrieval solution (pH 6.0) for 30 minutes. Endogenous peroxidase blocking (10 min) was performed before protein blocking (10 min). Immediately after, it was followed by incubation with the primary antibody's anti-NeuN antibody at 1:1000 for three hours at room temperature. Sections were then incubated in HRP (horse radish-peroxidase) micro-Polymer Goat Antirabbit HRP (Vector USA) for 30 minutes. The reaction was developed with DAB chromogen (Vector, USA). Sections were then rinsed in water, counterstained with Hematoxylin, dehydrated, cleared, and mounted with Dibutyl Phthalate Xylene (DPX). Thermofischer Scientific Inc. manufactured the enzyme immunoassay kit used (United Kingdom).

*TNF-alpha (α)***:** Levels of TNF-α were measured using a Tumor necrosis factor-alpha Assay kit (chemiluminescent assay) through the IMMULITE® 1000 system according to the manufacturer's instructions. The detection limit of the kits was obtained from the manufacturers as TNF-α (detection limit 1.7_1000pg/mL).

Assessment of neurotransmitters

Glutamate: Brain tissue was deproteinized according to a modification of the method of [2]. Each brain was rapidly weighed, and ground to a powder in a stainless-steel tissue grinder cooled in liquid nitrogen. Five hundred microliters of 2N HCO4 were frozen and ground in a separate stainless-steel tissue, grinder cooled in liquid nitrogen. The two frozen powders were combined in a plastic centrifuge tube and allowed to warm to 4°C. One and a half to two milliliters of Ice-cold deionized H_20 was added. Ten minutes later, the content was homogenized for 60 sec with a motorized. Teflon tissue grinder. The homogenate was centrifuged at 3000g for 15min at 0°C. The supernatant was removed. Neutralized with 2N KHC03 and centrifuged again under the same conditions. Half of the final supernatant was stored at -20°C for glutamate assays. The remaining supernatant for the α-KGA assays was stored on dry ice (-78.5°C). Glutamate concentrations were determined by modifying the method of [2]. The principle of this enzymatic spectrophotometric assay is that the reduction of 3acetylpyridine adenine dinucleotide (APAD) to APADH is proportional to the amount of glutamate present. The amount of APADH formed during the assay was determined by measuring the increase in absorbance at 363.

Gamma-aminobutyric acid (GABA): This assay employs the competitive inhibition enzyme immunoassay technique. The microtiter plate provided in this kit has been pre-coated with Gamma-Aminobutyric Acid (GABA) protein. Standards or samples are added to the appropriate microtiter plate wells with a biotin-conjugated antibody specific to Gamma-Aminobutyric Acid (GABA). Next, Avidin conjugated to Horseradish Peroxidase (HRP) is added to each microplate well and incubated. After the TMB substrate solution is added. Adding sulphuric acid solution terminates the enzyme-substrate reaction, and the color range is measured spectrophotometrically at a wavelength of 450nm ± 10nm. The concentration of Gamma-Aminobutyric Acid (GABA) in the samples is then determined by comparing the OD of the samples to the standard.

Determination of glutathione peroxidase (GPx) and GSH activity

GPx activity was determined according to the method of [31]. Glutathione peroxidase activity was observed by plotting a standard curve, and the concentration of the remaining GSH was extrapolated from the curve.

$$\text{GSH consumed} = 245.84 - \text{GSH remaining}$$

$$\text{Glutathione peroxidase activity} = \frac{\text{GSH consumed}}{\text{mg protein}}$$

Photomicrography and data analysis

Photomicrographs of slides obtained from histological and immunohistochemical processing of tissues were captured using a binocular microscope connected to a 5.0-megapixel camera. Data obtained from enzyme analysis was subjected to statistical analysis using the graph Pad Prism software (version 5). The results generated from the cognitive studies, immunoquantification of NeuN and TNF-α, and results of GPx, GSH Glutamate, and GABA concentrations were plotted as bar graphs with error bars (mean and standard error of the mean). One–way ANOVA followed by the Tukey test was used to determine any significant difference among the groups with a confidence limit of 95%. Data represent mean value ± SEM.

Results

The rats in the control group maintained a relatively average weight of 120-152 g throughout the experiment, similar to the positive control groups (AP and Dpz only). Rats treated with AP for 28 days showed no abnormal behavioral changes while handling and home-cage movement. After the dissection of the animals, the brain structure was observed to identify if the AP had caused any morphological effect on it. The animals from AP groups showed no edema or inflammatory changes in the brain structure.

Body weight and brain morphometric comparison (brain and cerebellar weight) across the groups were shown on **Fig. 1(a-c)**. Control and AP showed no significant difference in body weights. However, the body weight of PDCh group was significantly reduced compared to the control. Additionally, the Dpz group, AP (400 mg/kg) + PDCh and Dpz +PDCh showed a significant increase ($p < 0.001$) compared to the control group. In contrast, the AP (200 mg/kg) + PDCh was significantly reduced ($p \leq 0.001$) compared to the Dpz + PDCh. Noteworthy, is that the AP-treated group maintained an average weight throughout the study, and AP protected against weight loss in the PDCh-treated rats (**Fig. 1a**). Brain morphometric analyses also revealed a significant decrease ($p < 0.01$) in the brain weight of the PDCh-only-treated group compared to the Control group. Additionally, significant increments were observed at $p < 0.01$ and $p < 0.001$ when comparing the AP (400 mg/kg) + PDCh and the AP (200 mg/kg) + PDCh as well as Dpz groups to the PDCh group, respectively (**Fig. 1b**). Also, a significant decrease ($p < 0.01$) in cerebellar weight was observed in the PDCh-only group compared to the control group and Dpz (**Fig. 1c**). However, AP protective

treatment group (200mg/kg), comparably with Dpz, improved markedly in the brain and cerebellar weight loss caused by PDCh.

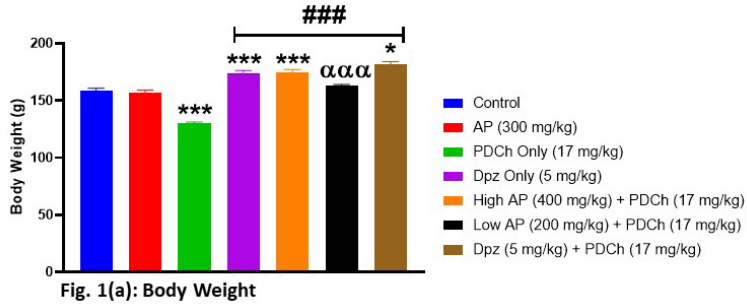

Fig. 1(a): Body Weight

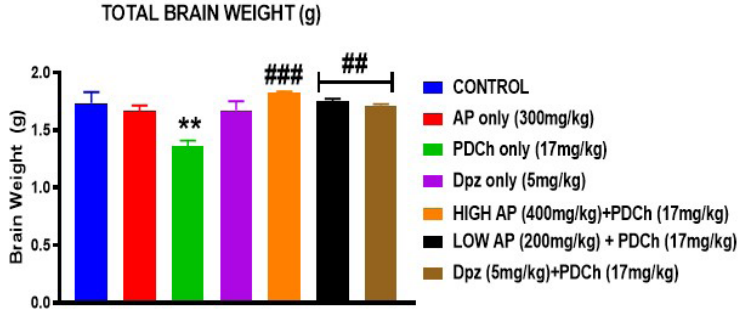

Fig. 1(b): Total Brain Weight

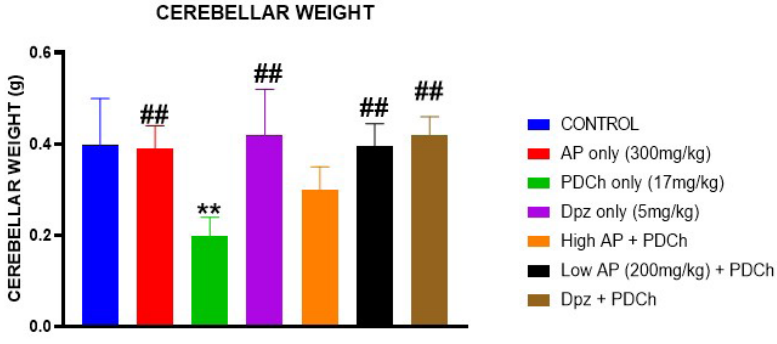

Fig. 1(c): Cerebellar Weight

Fig. 1. Changes in total brain and cerebellar weight. (a) body weight; (b) brain weight; (c) cerebellum weight.* denotes significant difference at $p<0.05$ when compared to control group, ** denotes significant difference at $p<0.01$ and *** at $p<0.001$ when compared to control group; ## denotes significant difference at $p<0.01$ and ### at $p<0.001$ when compared to PDCh only group; ααα denotes significant difference at $p<0.001$ when compared to Dpz + PDCh group.

Time spent hanging on a wire in the Wire hanging task was shown on **Figure 2**. There is no significant difference in time spent hanging on the wire ($p > 0.05$) between the control and PDCh group on the third day of administration, as well as other experimental groups. On day 7, a significant increase ($p < 0.01$) in the Wire hanging period was seen in the AP group compared to the Control group and the PDCh group. On day 14, no significant decrease ($p > 0.05$) in the Wire hanging period was seen in the PDCh group compared to the Control group. On day 28, a significant decrease ($p < 0.05$) in the Wire hanging period was seen in the PDCh group compared to the Control group. Nonetheless, a notable but statistically insignificant reduction was observed in the PDCh group when compared to the other experimental groups. Notably, AP treatment significantly improved the time spent hanging on the wire in the rats treated with PDCh, showing similar improvements as observed with Dpz across the experimental days.

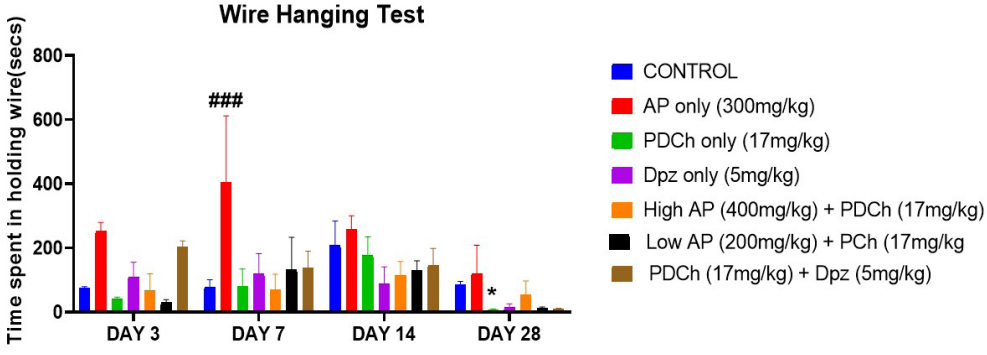

Fig 2. Wire Hanging test across administration days. * denotes significant difference at $p<0.05$ compared to control group; ### denotes significant difference at $p<0.001$ when compared to PDCh group.

The activities of experimental rats in the Open field task were shown on **Figure 3**. No significant variance ($p > 0.05$) was seen between the Control group and other experimental groups on day seven in the number of lines crossing as an exhibition of locomotive behavior **(Fig. 3a)**. On day 14, no significant difference ($p > 0.05$) in line crossings was observed in the PDCh group compared to the control group. On day 28, a significant reduction ($p < 0.01$) in line crossings was seen in the PDCh compared to Control and AP. A significant and noteworthy finding was the substantial reduction ($p < 0.001$) in the number of line crossings in the PDCh group in comparison to the High AP (400 mg/kg) + PDCh group. Also, in the rearing behavior, on days 14 and 28, a significant reduction ($p < 0.05$ and $p <0.01$, respectively) was seen in the PDCh group compared to the control group and the High AP (400 mg/kg) + PDCh (**Fig. 3b**). Also, there were significant decrease ($p < 0.05$) in number of rearings of PDCh group compared to the AP and Dpz groups. However, no significant difference was seen across the experimental groups compared to the Control in the Time spent in the centre square (**Fig. 3c**). In the frequency of entries into the center square, an obvious distinction was seen on day 28 in the PDCh group compared to other experimental groups, with a significant reduction ($p < 0.01$) in the PDCh group compared to the

AP only group (**Fig. 3d**). In the fecal boli count, no significant difference was seen across the groups (**Fig. 3e**). However, relatively high Fecal boli on day 14 and 28 can be observed in the PDCh and Dpz + PDCh groups compared to the control, indicating the exhibition of fear or anxiety. The freezing time indicates the period of immobility (**Fig. 3f**). A significant increase ($p < 0.05$) was observed in the PDCh group compared to the control group on day 14. Similarly, on day 28, a markedly significant increase ($p < 0.001$) was observed in the PDCh group compared to the control group and other experimental groups, indicating a deteriorating effect on the motor function of the treated rats as the administration progresses. The administration of AP demonstrated a protective effect against the motor function impairments induced by PDCh treatment in the rats. No significant difference ($p > 0.05$) in freezing time seen between AP + PDCh treatment groups and the Dpz + PDCh standard group was observed.

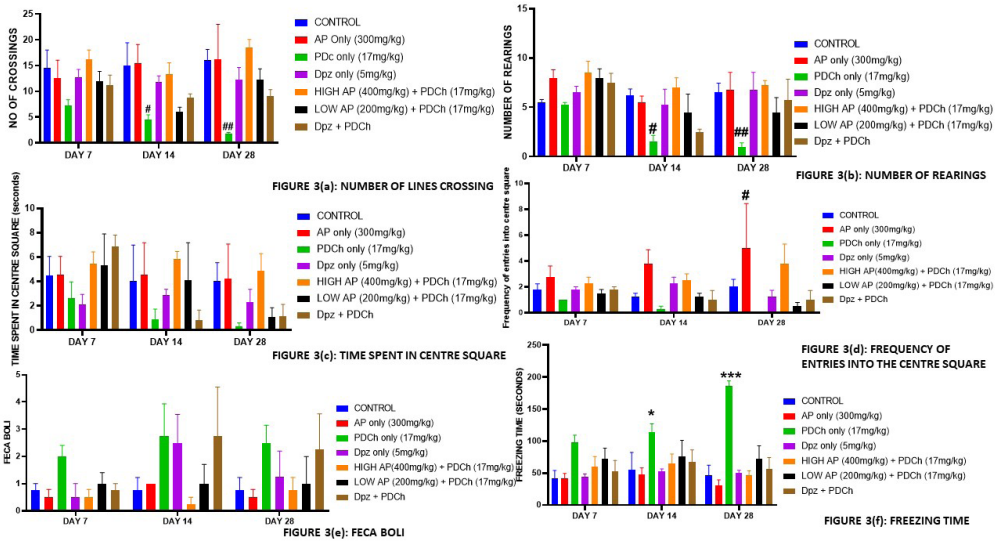

Fig. 3. The activities of experimental rats in the open field task. (a) number of lines crossing; (b) number of rearings; (c) time spent in center square; (d) frequency of entries into the center square; (e) fecal boli; 3(f) freezing time. * denotes a significant difference at $p<0.05$ and *** at $p<0.001$ when compared to control group; # denotes a significant difference at $p<0.05$ and ## at $p<0.01$ when compared to PDCh only group.

The frequency of entries in the T-maze task (a) and variations in Escape latency (EL) in the Morris water task (b) across treatment groups were shown on Figure 4. Significant difference ($p < 0.05$) was seen in the percentage frequency of arm entries on day seven between the PDCh group and the High AP + PDCh group**.** Although, no significant difference ($p > 0.05$) was seen across the experimental groups on days 7 and 14, a progressive reduction in the frequency of arm entries was noticed in the PDCh group on days 7and 14, with a significant reduction ($p < 0.05$) seen in PDCh compared to the control group on day 28 (**Fig.4a**)**.** However, no significant difference was seen between the Dpz + PDCh, High AP+ PDCh, and Low AP + PDCh groups compared to the control. This depicts the protective effect of AP against PDCh motor function

damage in rats seen on day 28 in both doses of AP. On day 7, a significant difference ($p < 0.05$) was seen in the Dpz + PDCh group when compared with the control group (**Fig. 4b**). Also, no significant differences were seen between the Dpz + PDCh group when compared with the High AP + PDCh group and the Low AP + PDCh group. On day 28, a significant difference ($p < 0.05$) was seen in the control group and AP group compared to the PDCh-only group, which reported the highest EL. Also, it's worth noting that a significant decrease ($p < 0.05$), reflecting a shorter escape latency, was observed in the 400 mg/kg AP group when compared to the Dpz + PDCh group. Interestingly, there was no significant difference between the 200 mg/kg AP and Dpz + PDCh treated groups, both of which maintained an average escape latency throughout the study.

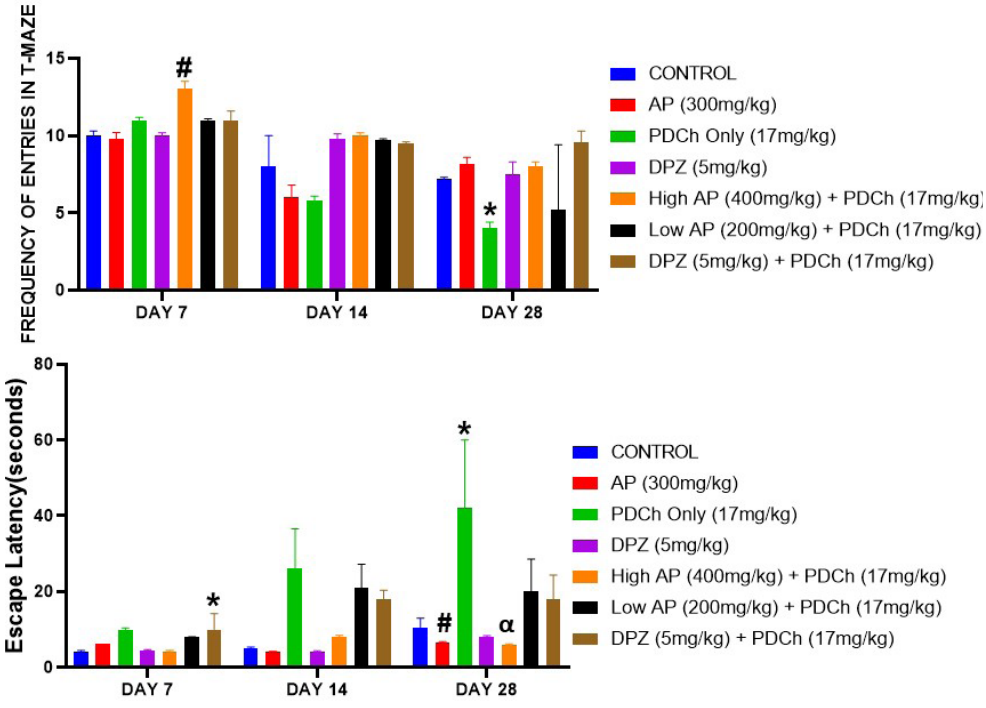

Fig. 4. (a). Frequency of arm entries in T maze; **(b).** Escape latency in Morris water maze

Fig. 4. Bar chart showing (a) Frequency of arm entries in T maze; (b) Escape latency in Morris water maze. *denotes significant difference at $p<0.05$ compared to the control group; # denotes significant difference at $p<0.05$ compared to PDCh only group; **α** denotes significant difference at $p<0.05$ when compared to Dpz + PDCh group.

Photomicrographs of the cerebellar histological architecture were presented on **Figure 5.** The cerebellar histology of the cerebellum shows three distinct layers: the granule layer with small, tightly packed rounded granular neuron; the Purkinje layer, which consist of a single layer of the large round nucleus and prominent nucleoli; the molecular layer with sparse cells. Control, AP, and Dpz groups show relatively intact cerebellar histology. Also, the High AP (400mg/kg) + PDCh and Dpz + PDCh

groups show typical cerebellar neuronal structures, depicting protection against PDCh cerebellar toxicity. The Low AP + PDCh shows normal neuronal structure but signs of cellular shrinking and scattered neurons. However, unlike other treatment groups, the PDCh group shows apparent degenerative features characterized by cellular shrinking, nuclear fragmentation, and neuronal degeneration.

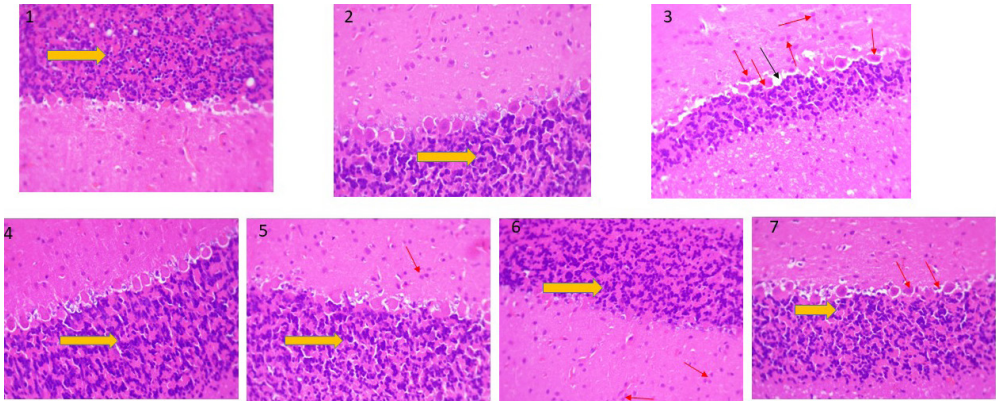

Fig. 5. Photomicrographs of Haematoxylin and Eosin staining of the cerebellum. Control (1), AP (2), PDCh (3), Dpz (4), High AP + PDCh (5), Low AP + PDCh (6), and Dpz + PDCh (7) groups (H and E, x400). Yellow arrows indicate a normal cerebellar neuronal structure. Black arrows indicate degenerating neurons at Purkinje layer with appearance of vacuolation. Red arrow denotes nuclear fragmentation.

Cerebellar immunohistochemical visualization of NeuN was presented on **Figure 6**. Chart shows the quantification of the percentage of NeuN expression in control and treated groups. The immunohistochemical localization of NeuN shows distinct expression in cerebellar neurons. PDCh-only groups show markedly reduced expression of NeuN immunoreactive neurons compared to the Control, AP, Dpz group, High AP PDCh, Low AP + PDCh, and Dpz + PDCh group. This result suggests that PDCh significantly reduced NeuN expression. In contrast, treatment with both Dpz, High and Low doses of AP significantly increased Neun expression compared to PDCh-only group.

Cerebellar immunohistochemical visualization of TNFα was presented on **Figure 7**. Chart shows the quantification of the percentage of TNFα immunoreactivity in control and treated groups. The percentage of TNFα immunoreactive cells in PDCh, Dpz, and Dpz + PDCh groups was significantly higher ($p < 0.001$) than in Control, AP, High AP + PDCh, and Low AP + PDCh groups. However, there is a significant reduction of TNFa expression ($p < 0.001$) in the AP group and AP + PDCh group compared to the PDCh group. Similarly, there was decreased expression ($p < 0.01$) in the PDCh + Low AP groups when compared to the PDCh group. Significantly, the expression of TNFα in both the 400 mg/kg and 200 mg/kg AP + PDCh groups showed a substantial reduction ($p < 0.001$) when compared to the Dpz + PDCh group. This result suggests that PDCh and Dpz or a combination of PDCh + Dpz may significantly increase TNFα expression. In contrast, treatment with high and Low doses of AP sufficiently reduced TNFα expression.

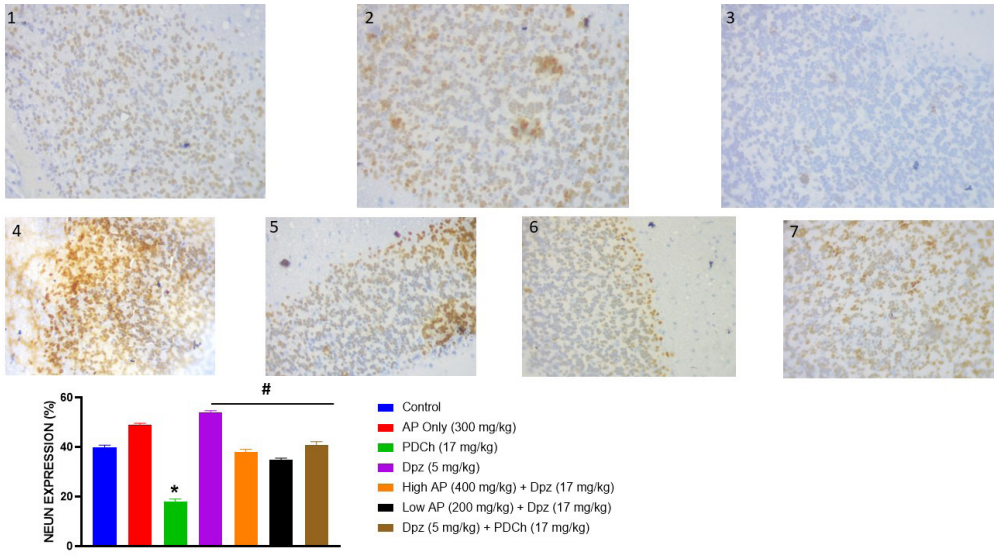

Fig. 6. Protein expression of NeuN in the cerebellum. (1-7) are photomicrographs as follow: Control (1), AP (2), PDCh (3), Dpz (4), High AP + PDCh (5), Low AP + PDCh (6), and Dpz + PDCh (7) groups (x400); Chart shows quantification of NeuN protein expression * denotes significant difference at $p<0.05$ when compared to the control group; # denotes significant difference at $p<0.05$ when compared to the PDCh only group.

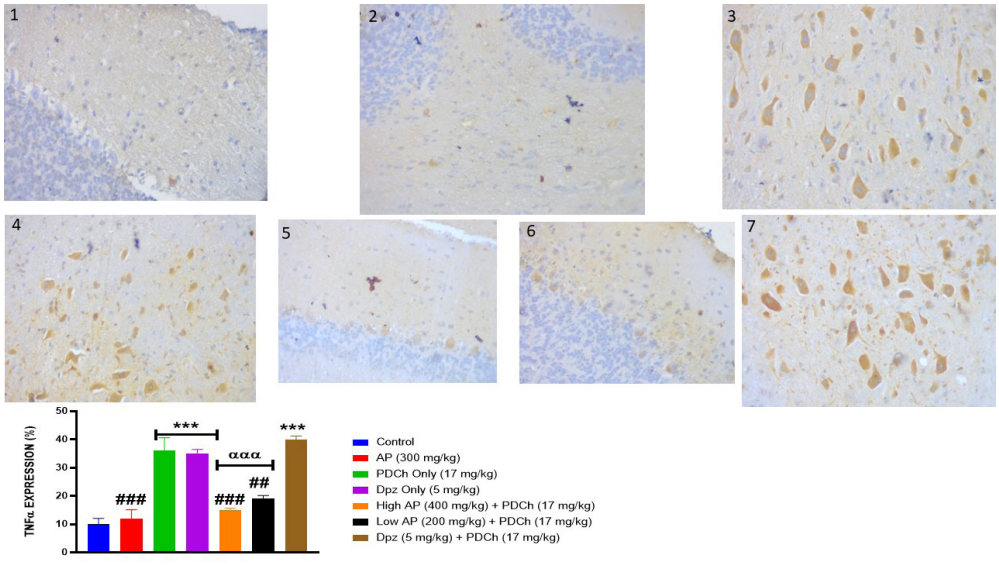

Fig. 7. Protein expression of TNF-ά in the cerebellum. (1-7) are photomicrographs as follow: Control (1), AP (2), PDCh (3), Dpz (4), High AP + PDCh (5), Low AP + PDCh (6), and Dpz + PDCh (7) groups (x400). Chart shows quantification TNF-ά expression in the cerebellum; *** denotes a significant difference at $p<0.001$ when compared to control; ## and ### denotes significant difference at $p<0.01$ and at $p<0.001$ when compared to PDCh only group; ααα denotes significant difference at $p<0.001$ when compared to Dpz+PDCh group.

Figure 8 demonstrated our data from measurements of Glutamine (a) and γ-aminobutyric (GABA) (b) levels across experimental groups. Significant difference ($p < 0.05$) in the Glutamate level in the control and AP groups was seen when compared to the PDCh group (**Fig. 8a**). Also, the result reveals no significant difference between High AP (400 mg/kg) + PDCh and Dpz + PDCh groups, but relatively reduced Glutamate level in the Low AP (200 mg/kg) + PDCh group compared to the control group, suggesting dose-dependent protection. Significant increase ($p < 0.001$) was found in GABA levels of the PDCh group compared to the control group and other experimental groups (**Fig. 8b**). However, no significant difference ($p > 0.05$) was seen between High AP + PDCh, Low AP +PDCh, and Dpz + PDCh.

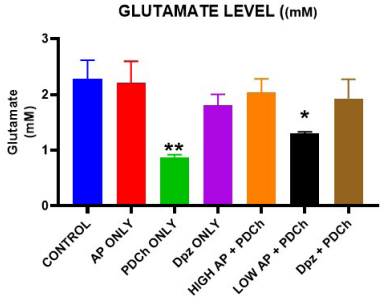

Fig. 8(a). Glutamate levels

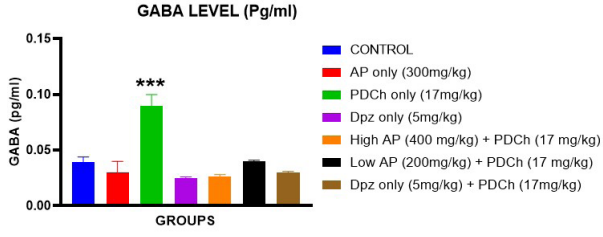

Fig. 8(b). GABA levels

Fig. 8. Quantification of glutamate (**a**) and GABA (**b**) levels across experimental groups. * denotes a significant difference at $p<0.05$, ** at $p<0.01$ and *** at $p<0.001$ when compared to the control group.

Figure 9 demonstrated concentration of Glutathione peroxidase (GPx) (a) and Reduced Glutathione level (GSH) (b) across experimental groups. No significant difference ($p > 0.05$) in the Glutathione peroxidase level was observed between the control and the PDCh groups (**Fig. 9a**). Also, the result reveals no significant difference between High AP (400 mg/kg), Low AP (200 mg/kg), and Dpz + PDCh group compared to the control group. Significant increase ($p < 0.001$) in the Reduced Glutathione level was observed in the control group and AP group when compared to the PDCh group. The result also reveals a significant increase ($p < 0.05$) between the Low AP + PDCh and control groups. The levels of Reduced Glutathione level across AP and Dpz groups are relatively average and similar to the Control group.

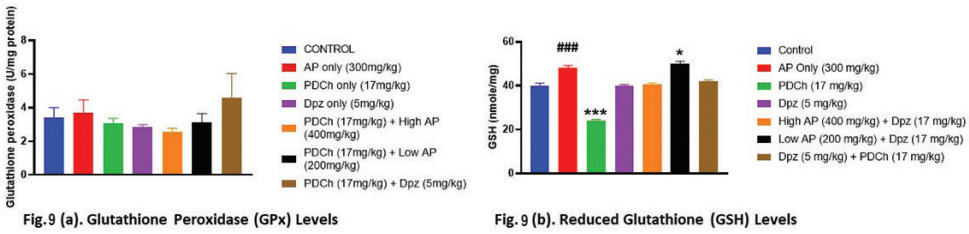

Fig.9 (a). Glutathione Peroxidase (GPx) Levels

Fig. 9 (b). Reduced Glutathione (GSH) Levels

Fig. 9. Quantification of Glutathione Peroxidase and Reduced Glutathione levels across experimental groups. * denotes significant difference at $p<0.05$ and *** at $p<0.001$ when compared to control group; ### denotes significant difference at $p<0.001$ when compared to PDCh only group

Discussion

In this study, the body weight was measured on the final day of administration to assess the differences in weight across experimental groups. Body weight is an indicator in examining motor balance and monitoring disease progression [6]. Moreover, reduction in body weight occurs frequently during advanced stages of spinocerebellar ataxia type 2(SCA2) [30]. In our study, a significant reduction in body weight was observed in the PDCh group when compared to both the control group and the other experimental groups. This suggests an early onset of ataxia, which notably impacted body weight. However, the AP-treated groups provided protection against changes in body weight in a dose-dependent manner, countering the deteriorating effect of PDCh on body weight.

Furthermore, total brain weight and cerebellum were weighed to assess brain morphological changes. The results showed a significant reduction in the total brain and cerebellar weights in the PDCh group compared to the control group. Reduction in brain weight is an apparent cause of disruption of the cerebellar hemispheres and dentate nuclei, which may result in limb ataxia, hypotonia, terminal and intention tremor, and dysarthria [3] — in addition, reduced cerebellar weight results from cerebellar degeneration, which leads to difficulty in balancing and coordination. Hence, this claim establishes that PDCh groups affected the total brain weight with edema changes seen morphologically and cerebellar weight reduction. Furthermore, in this study, AP and Dpz protected against cerebellar degeneration and brain toxicity caused by PDCh.

The wire-hanging test is widely used to measure rats' motor activity, coordination, and endurance [18]. The cerebellum, known as the "little brain, maintains balance and motor coordination. The wire hanging test was employed after a pre-determined treatment with PDCh and, subsequently, AP to ascertain its motor function. Findings showed marked reduced motor coordination and balance after PDCh exposure in rats. This reflects underlying progressive cerebellar dysfunction because the time of hanging to the suspension reduced as the administration of PDCh progressed. However, AP treatment improved the motor coordination and balance of the PDCh-induced rats, similar to the Dpz protective treatment group, as indicated by an increased time hanging on the wire. This observation was further supported by the open field test (OFT).

For instance, rearing and line-crossing behavior and activities in the centre-square have been reported to be potent indicators of locomotor and exploratory behaviors, respectively; immobility (freezing time) and fecal boli count are positively correlated to fear or anxiety [33]. Our findings on increased freezing time (immobility) agree with the findings of other studies, which demonstrated increased immobility following metal exposure in rats [25, 36].

Furthermore, impairment of locomotor and exploratory functions in the experimental rats is confirmed with the decreased crossing and rearing behaviors and fewer activities in the center square of the OFT apparatus. This finding also resonates with that of [41], who observed a positive correlation between line crossings and rearing. The findings revealing the motor function-enhancing effect of AP are supported by claims that plant extracts can mitigate metal toxicity in experimental rats [26, 32]. Besides, existing studies reported that aqueous Phyllanthus *amarus* extract (100 and 200 mg/kg) and methanolic extract of Phyllanthus *nuriri* enhanced neuromuscular coordination and balancing [1]. Nonetheless, this study explores the doses 200 and 400mg/kg dose, and new parameters were used in the OFT test, including Fecal boli count, to examine coordination. This study's findings show that PA attenuated PDCh-induced neurotoxicity; we suspect the plant's antioxidant properties as an antioxidant and acting as a neuroprotective agent in a dose-dependent manner.

The T-maze results show that PDCh affected the locomotive activity of the treated rats, exhibited by the significant reduction in the frequency of arm entries on between days 14 and 28. This correlates with the findings of [14], who reported that Hexavalent chromium caused hypo locomotive behavior in Hexavalent chromium-treated mice. About other experimental groups, our results show that AP possesses great locomotive-enhancing activity comparable with Dpz, which also demonstrated a cognitive protecting effect, as seen in the peak of arm entry frequency on day 7 in the AP + PDCh group. Similarly, in the Morris water maze task, an elevated level of escape latency was observed in the PDCh-treated rats, indicating cognitive impairment in decision-making and spatial awareness. PDCh rats swam for extended periods and traveled farther before locating the platform. These impairments were not improved when treated with Low AP (200 mg/kg) + PDCh group; however, when the dose was increased to 400 mg/kg and 300 mg/kg), there was enhanced cognitive function to exit the maze in PDCh-treated rats, which exhibited reduced levels of escape latency comparably better than Dpz (5mg/kg) treatment. These findings correlate with [27], which reports the neuroactive effects of Phyllanthus *amarus* (400 and 200 mg/kg) assessed under the Morris water maze task. However, this present study also supports the claim and asserts the cognitive-enhancing effect of 300 mg/kg Phyllanthus amarus aqueous extract in the Morris water maze task. Therefore, AP sufficiently protected against cognitive dysfunction induced by PDCh in rats.

The study also revealed that H & E stained cerebellar sections disclosed intact Purkinje neurons for both the control and the AP Only group. However, the PDCh-only group showed marked neurodegenerative changes in the Purkinje and granular layers. Additionally, signs of cell death and a faint nuclear outline of the Purkinje cell indicated early signs of neuronal nuclei destruction. These features observed by staining with H & E are consistent with reports of [9], and further correlated with the findings of our NeuN immunohistochemistry. Neuronal nuclear protein (NeuN) is a well-known marker found exclusively in post-mitotic neurons. It is found in the nucleus

of mature neurons and readily visualized with immunostaining. Thus, the current study used NeuN expression to demonstrate the effect of PDCh on the number or health of mature neurons in the cerebellar neuronal population. Our findings revealed that NeuN expression was significantly down-regulated in PDCh-treated rats, indicating occurring degenerative changes in the cerebellum or, neuronal development or maturation being disrupted, and neurons not reaching their mature state. Surprisingly, AP and Dpz maintained the regular expression of this protein relative to the control group.

Furthermore, it has been proven that chronic inflammation in specific brain areas is common in patients with cerebellar dysfunction. This led to the investigation of some anti-inflammatory drugs, such as Indomethacin, to halt inflammatory diseases [29]. Likewise, in our study, TNF-α expression was assessed, and AP was shown to exhibit a protective effect against an inflammatory factor (TNF-α) in the cerebellum, which is known to damage neurons to a certain extent. TNF-α in the Dpz + PDCh and PDCh groups were highly expressed compared with the control group, which suggested that the cognitive decline might have been caused by PDCh triggering microglial activation. However, the highly expressed TNF-α seen in the Donepezil-treated group is not correlated with past findings. Although Dpz has not been observed to augment the mRNA expression of anti-inflammatory phenotypes in primary microglial cells as a neuroprotective drug, it is expected to suppress the expression of TNF-α [13, 39]. This opens a research knowledge gap on the possible astrocytic mechanism involved in the anti-inflammatory effects of Dpz.

Glutamate is the most abundant excitatory neurotransmitter in the brain, and GABA is an inhibitory neurotransmitter. Glutamate/GABA concentration imbalance leads to progressive cognitive disorders [11]. Thus, Glutaminergic/GABAergic system balance is needed to attain optimal cognitive function and to keep the brain functioning correctly. This study observed that the glutamate concentration was markedly reduced in the PDCh-treated group compared to the control group. There is a link to cognitive deficits being associated with glutaminergic hypofunction [21].

Moreover, Ciacci et al. [4] reported that hexavalent chromium induces neurotoxicity by inhibiting Acetylcholine through alteration in its synthesis. Hence, it is imperative to note that PDCh caused glutaminergic hypofunction in this study and confirms the claim that PDCh causes inhibition of glutamine neurotransmitters. Surprisingly, AP protective treatment groups [300mg/kg and 400mg/kg] maintained balanced glutamate levels similar to the control. Also, this study demonstrated a reduction in GABA levels in the PDCh-only treated group compared to the control. Behavioral analysis revealed that reduced GABA+ levels were associated with decreased cognitive function. This proves that dysfunction of the GABAergic inhibitory circuits in the cerebellum contributes to changes in cerebellum neuronal excitability and cognitive impairment, leading to the inability to execute normal adaptive behavioral responses. Therefore, treatment with AP protected maintained balance in Glutamate/GABA signaling, and PDCh distorted Glutamate/GABA signaling, resulting in decreased motor activity in the OFT.

Glutathione peroxidase is an antioxidant-dependent enzyme important in the antioxidant defense mechanism. Oxidative stress and antioxidant levels are markers in inflammatory reactions. Glutathione peroxidase has been extensively examined in the cerebellum of PD, and there is wide variability in its reported levels and activity. This enzyme has been localized exclusively in the glial cells and down-regulated in astrocytes and neurons due to oxidative stress [35]. However, its levels and activity in

our study are generally not markedly elevated. There was no significant variability in Glutathione peroxidase across the experimental groups.

Conversely, Glutathione peroxidase level was similar across all the other AP and Dpz-treated rats and in the control group, suggesting oxidative stress support. Similar results were obtained on administering Phyllanthus *amarus* extract against neurotoxic agents [19, 23], although the studies only considered AChE inhibitors on the oxidative pathways.

GSH plays a vital role in neuronal defense against damage caused by oxidative agents like ROS and RNS [42]. Its depletion is implicated in cerebellar dysfunction, cerebral palsy, spinocerebral degradation, and ataxia [7]. Moreover, decreased GSH levels elevate cellular vulnerability towards oxidative stress and accumulating oxidative stressors in the substantia nigra of PD patients, brains of epileptic humans, and genetically epileptic transgenic mice [17]. Consequently, this antioxidant is vital in the onset and progression of neurological disorders and neurodegenerative diseases and serves as a biomarker for diagnostic screening. This present study showed a markedly significant reduction in the GSH level of the PDCh group, indicating oxidative stress and reduced antioxidant levels. However, GSH was significantly increased in the Low AP + PDCh group compared to the control group. This finding implies that at low doses of AP, GSH is neuroprotective. However, at high (Mm) concentrations, GSH may affect the redox state of glutamate receptors via its free thiol group [34]. This result corroborates earlier glutamate findings in which Low AP (200 mg/kg) + PDCh was distorted with substantially reduced Glutamate levels compared to other AP and Dpz treated groups. However, the Glutathione peroxidase level was maintained across all other AP and Dpz-treated rats in the control group, suggesting an anti-oxidative maintaining property of AP.

Conclusion

In conclusion, this study provides behavioral, histological, immunohistochemical, and neurotransmitter evidence that the aqueous extract of Phyllanthus *amarus* leaves extract is anti-inflammatory and significantly reduces the neurotoxic effect of potassium dichromate by mitigating locomotion, posture, and coordination impairment.

Acknowledgment: The authors appreciate The NeuroLab, Federal University of Technology Akure, for technical support.

References

1. **Ambali, S. F., A. O. Makinde, M. Shittu, S. A. Adeniyi, F. O. Mowuogwu.** Mitigating effects of *Phyllanthus niruri* on sensorimotor and cognitive impairments induced by subacute chlorpyrifos exposure in Wistar rats. – *Am. J. Med. Med. Sci.*, **2**, 2012, 50-58.
2. **Bernt, E., H.-U. Bergmeyer.** l-Glutamate: Determination with glutamic dehydrogenase. In: *Methods of enzymatic analysis* (Eds. H. U. Bergmeyer), Academic Press Inc, 1965, 384-397.
3. **Bodranghien, F., A. Bastian, C. Casali, M. Hallett, E. D. Louis, M. Manto, P. Mariën, D. A. Nowak, J. D. Schmahmann, M. Serrao, K. M. Steiner, M. Strupp, C. Tilikete, D. Timmann, K. van Dun.** Consensus paper: Revisiting the symptoms and signs of cerebellar syndrome. – *Cerebellum*, **15(3)**, 2016, 369-391.

4. **Ciacci, C., C. Barmo, G. Gallo, M. Maisano, T. Cappello, A. D'Agata, L. Claudio, M. Angela, F. Salvatore, C. Laura.** Effects of sublethal environmentally relevant concentrations of hexavalent chromium in the gills of *Mytilus galloprovincialis*. – *Aquat. Toxicol.*, **120-121**, 2012, 109-118.
5. **d'Isa, R., G. Comi, L. Leocani.** Apparatus design and behavioural testing protocol for the evaluation of spatial working memory in mice through the spontaneous alternation T-maze. – *Sci. Rep.*, **11**, 2021.
6. **Diallo, A., H. Jacobi, T. Schmitz-Hübsch, A. Cook, R. Labrum, A. Durr, A. Brice, P. Charles, C. Marelli, C. Mariotti, L. Nanetti, M. Panzeri, M. Rakowicz, A. Sobanska, A. Sulek, L. Schöls, H. Hengel, B. Melegh, A. Filla, A. Antenora, J. Infante, J. Berciano, B. P. van de Warrenburg, D. Timmann, S. Boesch, M. Pandolfo, J. B. Schulz, P. Bauer, P. Giunti, L. Baliko, M. H. Parkinson, J. Kang, T. Klockgether, S. T. du Montcel.** Body mass index decline is related to spinocerebellar ataxia disease progression. – *Mov. Discord. Clin. Pract.*, **4(5)**, 2017, 689-697.
7. **Dringen, R., J. M. Gutterer, J. Hirrlinger.** Glutathione metabolism in brain metabolic interaction between astrocytes and neurons in the defense against reactive oxygen species. – *Eur. J. Biochem.*, **267(16)**, 2009, 4912–4916.
8. **Faes, C., M. Aerts, H. Geys, L. De Schaepdrijver.** Modeling spatial learning in rats based on Morris water maze experiments. – *Pharm. Stat.*, **9(1)**, 2010, 10–20.
9. **Fahmy, A.** A histological study on the possible ameliorating effect of selenium on chromium (VI) induced neurotoxicity in the adult male Guinea pig cerebellar cortex. – *J. Am. Sci.*, **13(5)**, 2017, 8–17.
10. **Geethangili, M., S. Ding.** A review of the phytochemistry and pharmacology of *Phyllanthus urinaria* L. – *Front Pharmacol.*, **9**, 2018, 1109.
11. **Guerriero, R. M., C. C. Giza, A. Rotenberg.** Glutamate and GABA imbalance following traumatic brain injury. – *Curr. Neurol. Neurosci. Rep.*, **15(5)**, 2015, 27.
12. **Hao, P., Y. Zhu, S. Wang, H. Wan, P. Chen, Y. Wang, Z. Cheng, Y. Liu, J. Liu.** Selenium administration alleviates toxicity of chromium (VI) in the chicken brain. – *Biol. Trace. Elem. Res.*, **178(1)**, 2017, 127–135.
13. **Haraguchi, Y., Y. Mizoguchi, M. Ohgidani, Y. Imamura, T. Murakawa-Hirachi, H. Nabeta, H., H. Tateishi, T. A. Kato, A. Monji.** Donepezil suppresses intracellular Ca2+ mobilization through the PI3K pathway in rodent microglia. – *J. Neuroinflammation*, **14(1)**, 2017, 258.
14. **Hegazy, R., D. Mansour, A. Salama, A. Hassan, D. Saleh.** Exposure to intranasal chromium triggers dose and time-dependent behavioral and neurotoxicological defects in rats. – *Ecotoxicol. Environ. Saf.*, **216**, 2021, 112220.
15. **Igho, O., I. Afoke**. Histomorphological analysis of pyrethroid pesticide effects on the cerebrum and cerebellum in adult albino rats. – *J. Exp. Clin. Anat.*, **13(2)**, 2014, 54-59.
16. **Iteire, K. A., E. C. Osigwe, V. O. Ukwenya, F. U. Enemali, E. I. Odokuma.** *Carica Papaya* leaf crude-extract ameliorates lipopolysaccharide-induced neurotoxicity in mice cerebellum by downregulating GFAP and IBA-1 expression. – *J. Exp. Clin. Anat.*, **13(2)**, 2022, 275-288.
17. **Gawryluk, J. W., J. Wang, A. C. Andreazza, L. Shao, L. T. Young.** Decreased levels of glutathione, the major brain antioxidant, in post-mortem prefrontal cortex from patients with psychiatric disorders. – *Int. J. Neuropsychopharmacol.*, **14(1)**, 2011, 123–130.
18. **Klein, S.M, J. Vykoukal, P. Lechler, K. Zeitler, S. Gehmert, S. Schreml, E. Alt, U. Bogdahn, L. Prantl.** Noninvasive in vivo assessment of muscle impairment in the mdx mouse model – A comparison of two common wire hanging methods with two different results. – *J. Neurosci. Methods*, **203(2)**, 2012, 292–297.
19. **Kumar, K. B. H., R. Kuttan.** Protective effect of an extract of Phyllanthus amarus against radiation-indued damage in mice. – *J. Radiat. Res.*, **45(1)**, 2004, 133–139.

20. Li, S., L. Han, H. Shi, M. K. C. Chong, S. Zhao, J. Ran. Excess deaths from Alzheimer's and Parkinson's disease during the COVID-19 pandemic in the USA. – *Age Ageing*, **51(12)**, 2022, 1-6.
21. Merritt, K. P. McGuire, A. Egerton. Relationship between glutamate dysfunction and symptoms and cognitive function in psychosis. – *Front. Psychiatry*, **4(151)**, 2013, 1-8.
22. Musselman, K., C. T. Stoyanov, R. Marasigan, M. E. Jenkins, J. Konczak, S. M. Morton, A. J. Bastian. Prevalence of ataxia in children: a systematic review. – *Neurology*, **82(1)**, 2014, 80–89.
23. Nwankpa, P., M. U. Eteng, M. Akpamabiatu, G. Oze, H. Nwanjo. Effects of *Phyllanthus amarus* on serum lipid profile and oxidative stress status in Salmonellae typhi infected Wistar rats. – *J. Nat. Prod. Plant Resour.*, **2(5)**, 2012, 574–578.
24. Olopade, F. M. T. Shokunbi, A. Siren. Correlation of ventricular dilatation with neuropathological and neurobehavioral alterations in hydrocephalic rats. – *Fluids Barriers CNS*, **9(19)**, 2012, 1–10.
25. Omeiza, N. A., H. A. Abdulrahim, A. I. Alagbonsi, P. U. Ezurike, T. K. Soluoku, H. Isiabor, A. A. Alli-oluwafuyi. Melatonin salvages lead-induced neuro-cognitive shutdown, anxiety, and depressive-like symptoms via oxido-inflammatory and cholinergic mechanisms. – *Brain Behav.*, **11(8)**, 2021, e2227.
26. Owoeye, O., M. O. Gabriel. Protective effects of aqueous extract of Telfairia occidentalis on mercury-induced histological and oxidative changes in the rat hippocampus and cerebellum. – *Afr. J. Biomed. Res.*, **19(3)**, 2016, 241–247.
27. Oyeleye, S. I., T. A. Olasehinde, O. W. Fasakin, G. Oboh, J. A. Saliu. *Phyllanthus amarus* Schumach. & Thonn. and *Momordica charantia* L extracts improve memory function, attenuate cholinergic and purinergic dysfunction, and suppress oxidative stress in the brain of doxorubicin–treated rats. – *Phytomed. Plus.*, **2(2)**, 2022, 100283.
28. Patel, J., P. Tripathi, V. Shama, N. Chauhan, V. Dixit. Phyllanthus amarus: Ethnomedicinal uses, phytochemistry and pharmacology: a review. – *J. Ethnopharmacol.*, **138(2)**, 2011, 286–313.
29. Rao, S. K., C. Andrade, K. Reddy, K. N. Madappa, S. Thyagarajan, S. Chandra. Memory protective effect of indomethacin against electroconvulsive shock-induced retrograde amnesia in rats. – *Biol. Psychiatry*, **51(9)**, 2002, 770-773.
30. Rodriquez-Graña, T., R. Rodríguez-Labrada, S. Santana-Porbén, L. Reynaldo-Cejas, J. Medrano-Montero, N. Canales-Ochoa, Y. Silva-Ricardo, R. Torres-Vega, Y. González-Zaldivar, D. Almaguer-Gotay, G. Auburger, L. Velázquez-Pérez. Weight loss is correlated with disease severity in spinocerebellar ataxia type 2: a cross-sectional cohort study. – *Nutr. Neurosci.*, **25(8)**, 2022, 1747–1755.
31. Rotruck, J. T. A. L. Pope, H. E. Ganther, A. B. Swanson, D. G. Hafeman, W. G. Hoekstra. Selenium: biochemical role as a component of glutathione peroxidase. – *Science*, **179(4073)**, 1973, 588-590.
32. Seddik, L., T. M. Bah, A. Aoues, M. Brnderdour, M. Silmani. Dried leaf extract protects against lead-induced neurotoxicity in Wistar rats. – *Eur. J. Sci. Res.*, **42(1)**, 2010, 139-151.
33. Seibenhener, M. L., M. C. Wooten. Utilization of the open field maze for the assessment of locomotor and anxiety-like behavior in mice. – *J. Vis. Exp.,* **96**, 2015, 52434.
34. Shen, X. M., G. Dryhurst. Oxidation chemistry of (-)-norepinephrine in the presence of L-cysteine. – *J. Med. Chem.*, **39(10)**, 1996, 2018–2029.
35. Sian, J., D. T. Dexter, A. J. Lees, S. Daniel, Y, Agid, F. Javoy-Agid, P. Jenner, C. D. Marsden. Alterations in glutathione levels in Parkinson's disease and other neurodegenerative disorders affecting basal ganglia. – *Ann. Neurol.*, **36(3)**, 1994, 348-355.
36. Singh, N. A., V. Bhardwaj, C. Ravi, N. Ramesh, A. K. A. Mandal, Z. A. Khan. EGCG nanoparticles attenuate aluminum chloride-induced neurobehavioral deficits, beta-amyloid, and tau pathology in a rat model of Alzheimer's disease. – *Front. Aging Neurosci.*, **10(244)**, 2018.

37. **Smeets, C. J. L. M., D. S. Verbeek.** Cerebellar ataxia and functional genomics: Identifying the routes to cerebellar neurodegeneration. – *Biochim. Biophys. Acta*, **1842(10)**, 2014, 2030–2038.
38. **Soudani, N., A. Troudi, I. B. Amara, H. Bouaziz, T. Boudawara, N. Zeghal.** Ameliorating effect of selenium on chromium (VI) induced oxidative damage in the brain of adult rats. – *J. Physiol. Biochem.*, **68(3)**, 2012, 397–409.
39. **Tobinick, E., H. Gross, A. Weinberger, H. Cohen.** TNF-alpha modulation for treatment of Alzheimer's disease: a 6-month pilot study. – *Med. Gen. Med.*, **8(2)**, 2006, 25.
40. **Veeresham, C.** Natural products derived from plants as a source of drugs. – *J. Adv. Pharm. Technol. Res.*, **3(4)**, 2012, 200–201.
41. **Vidal, J.** Consistent individual differences in some behaviors in mice of the C57Bl/6J inbred strain. – *UB. J. Psy.*, **46(2)**, 2016, 83–89.
42. **Wilkins, H. M., D. Kirchhof, E. Manning, J. W. Joseph, D. A. Linseman.** Mitochondrial glutathione transport is a key determinant of neuronal susceptibility to oxidative and nitrosative stress. – *J. Biol. Chem.*, **288(7)**, 2013, 5091-5101.
43. **Wise Jr, J. P., J. L. Young, J. Cai, L. Cai.** Current understanding of hexavalent chromium [Cr(VI)] neurotoxicity and new perspectives. – *Environ. Int.*, **158**, 2022, 106877.

Institute of Experimental Morphology, Pathology and Anthropology with Museum
Bulgarian Anatomical Society

Acta Morphologica et Anthropologica, 31 (1-2)
Sofia ● 2024

Gastric Mucosal Mast Cell Activity in Children on Longitudinal Enteral Feeding with Percutaneous Endoscopic Gastrostomy, PEG

Nadya Penkova[1], Pepa Atanassova[1], Ivan Yankov[2], Vasilena Yankova[3], Petar Hrischev[4]

[1]*Department of Anatomy, Histology and Embryology, Faculty of Medicine, Medical University-Plovdiv, Bulgaria*
[2]*Department of Pediatrics and Medical Genetics, Faculty of Medicine, Medical University-Plovdiv, Bulgaria*
[3]*Student. Faculty of Medicine, Medical University-Plovdiv, Bulgaria*
[4]*Department of Physiology, Faculty of Medicine, Medical University, Plovdiv-Bulgaria*

*Corresponding author e-mail: nadja_penkova@abv.bg

Longitudinal enteral feeding via percutaneous endoscopic gastrostomy (PEG) challenges the gastric mucosa. The aim of our study is to make a morphological analysis of the gastric mucosa in PEG-children with an emphasis on the inflammatory component. The biopsy specimens from stomach of 37 children without GIT disease, age 0-18 years (20 with oral feeding – controls; 17 – with PEG; duration 24–48 month) are examined with histological and morphometric methods. In gastric mucosa of PEG children we find scanty amount of loose connective tissue, glands next to each other and hyperemic capillaries. In cases with cerebral palsy is noticeable an increased number of mast cells. Longitudinal enteral feeding via PEG doesn‘t cause significant morphological disorders in the structure of the stomach. Regarding increased mast cell activity further studies are needed to clarify whether this finding is related to the PEG or to the child‘s neurological disorder.

Key words: percutaneous endoscopic gastrostomy, cerebral palsy, gut, parietal cells, mast cells

Introduction

Enteral nutrition is a process of substrate satisfaction of the body’s needs for nutrients and energy, using the gastrointestinal tract (GIT) through a specially introduced probe of specially prepared medicinal foods. It is a type of nutritional therapy administered by gavage or stoma directly into the GIT, distal to the oral cavity. Enteral feeding probes can be placed through the mouth - orogastric, nasal, ie. naso-gastral, naso-

jejunal or naso-postpyloric feeding tube, or through an endoscopically placed stoma, percutaneous endoscopic gastrostomy or with an extension in the jejunum or in the jejunum.

Longitudinal enteral feeding via percutaneous endoscopic gastrostomy (PEG) challenges the gastric mucosa. It is carried out in conditions of disturbed physiology - all stages of the digestive process until the food enters the stomach are absent. There is a risk of infection of the GIT, allergens.

Mast cells have been found to interact with neurons from autonomic ganglia in the gut wall. They secrete tryptase, histamine and serotonin, which leads to increased organ sensitization and interference with their functions [26]. In both variety- and volume-limited patients, antral and duodenal mast cell densities were increased [13]. Increased mast cell density is associated with slower gastric emptying and increased gastric dysrhythmia in children with functional dyspepsia [25].

The aim of our study is to make a morphological analysis of the gastric mucosa in children with longitudinal enteral feeding through PEG with an emphasis on the inflammatory component.

Materials and Methods

The biopsy specimens from stomach of 37 children without GIT disease from the Clinic of Pediatrics and Medical Genetics MU - Plovdiv at age 0-18 years (20 of them are on oral feeding - controls and 17 on enteral feeding by precutaneous endoscopic gastrostomy (PEG) duration of 24–48 month were examined with light-microscopy and morphometric analysis. Written informed consent was obtained from the children's parents for the histological examination and the publication of the obtained data. The biopsy specimens were fixed in 10% neutral formalin and incorporated into formalin. Hematoxylin-eosin and Toluidine blue staining was performed on paraffin sections with a thickness of 5 μm. The observation and photo documentation of the microscope slides are performed with a digital photomicroscopic camera of a light microscope "Olympus BX51".

Using morphometric image analysis software ImageJ 1.8.0 we counted the number of parietal cells in the biopsy specimens (ImageJ, 2021). The statistical analysis of the results were carried out to the conventional standard statistical procedures using computer statistical analysis by SPSS, version 26.0 for Microsoft Windows XP.

Results

The morphological characteristics of gastric mucosa in children on longitudinal enteral feeding with PEG and that of the controls did not show significant differences in the morphological structure.

In the mucosa of children with oral feeding we observe areas with preserved covering columnar epithelium and transversely or longitudinally cut fundus glands. The parietal cells that secrete the hydrochloric acid of the gastric juice are rounded, eosinophilic, some of them binucleate. The chief cells synthesizing the enzyme pepsinogen have basophilic cytoplasm. In the controls, the parietal cells are mainly located in the body, and the chief cells occupy the base of the glands (**Fig. 1**).

In the mucosa of children with PEG we establish a small amount of loose connective tissue in the lamina propria. The glands are densely located next to each other, well supplied with blood with slightly hyperemic capillaries between them. Parietal cells are evenly distributed in the neck, body and bottom of the glands. The chief cells retain their localization at the bottom of the glands (**Fig. 2**).

No pronounced inflammatory lymphocytic infiltration was found in both groups, but in some cases with PEG with neurological disease (cerebral palsy) we established the significant presence of mast cells. The produced images in **Fig. 3** depict that the mast cells were localized in the connective tissue under the covering epithelium and near the fundic glands of the mucosa. Some of the mast cells were in a state of degranulation.

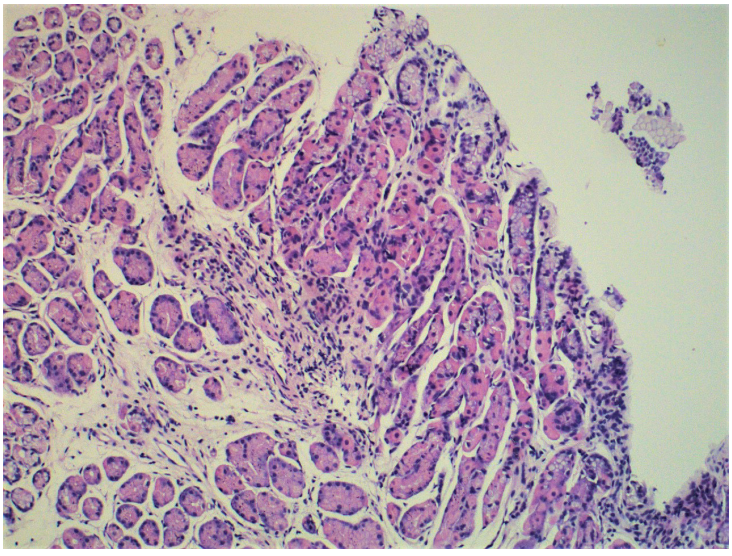

Fig. 1. Stomach controls. HE stain. x100.

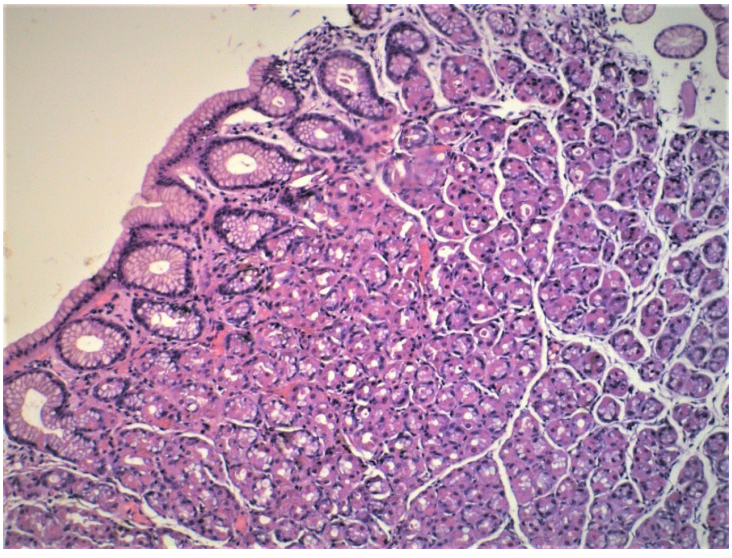

Fig. 2. Stomach PEG. HE stain. x100.

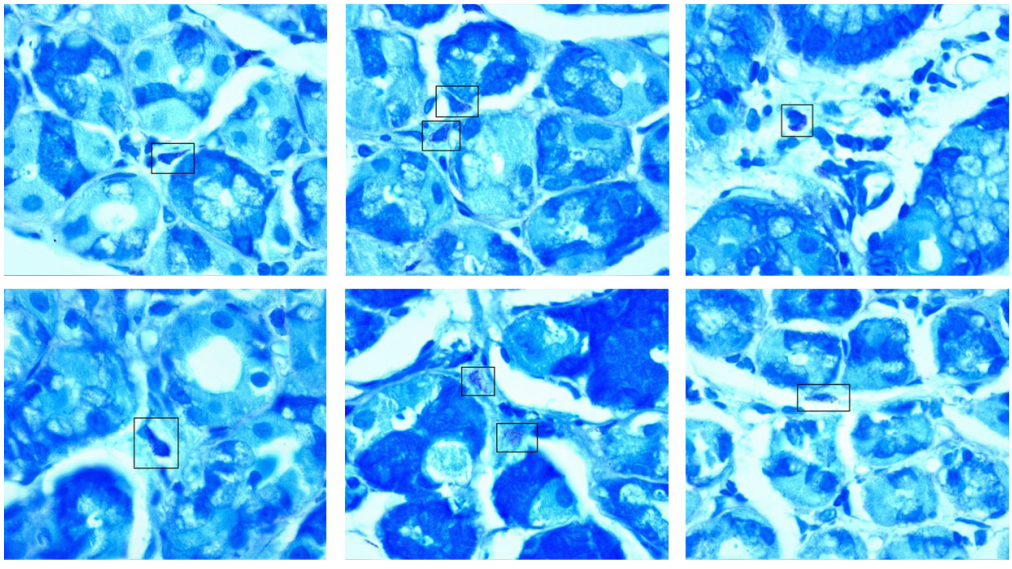

Fig. 3. Stomach PEG. Mast cells near the fundic glands. Toluidine blue stain. x 1000.

Morphometry

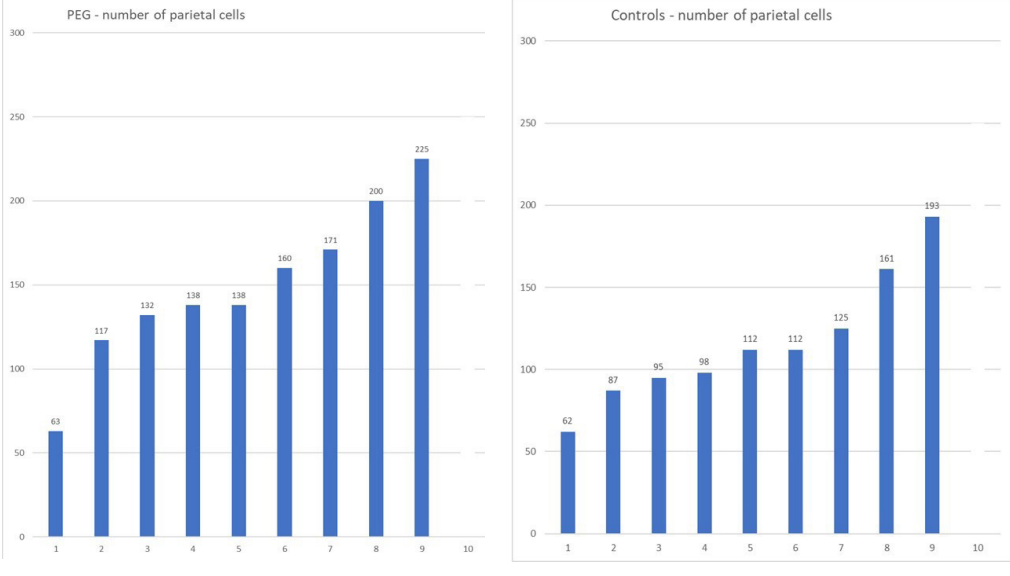

Fig. 4. Number of parietal cells.

The results in **Fig. 4** show that the number of parietal cells in the gasric glands of PEG patients was greater than in control patients. In each counting segment, more parietal cells were found in the PEG children than in the oral fed children.

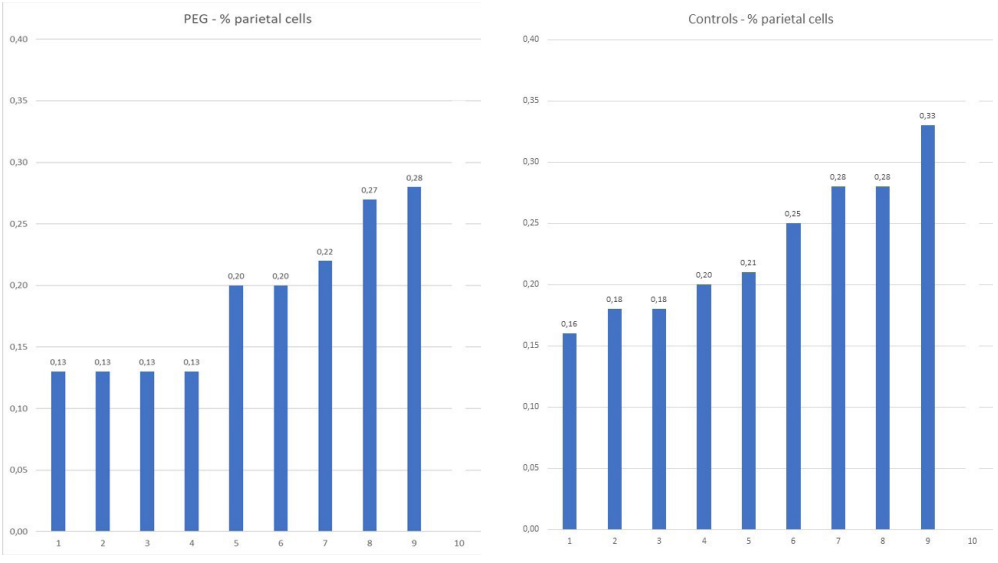

Fig. 5. Parietal cells %.

The results in **Fig. 5** show that the percentage of parietal cells in the gastric glands of patients with PEG is approximately equal to that of control patients, but in all segments we can see that it is decreased.

The greater number of parietal cells in the corpus mucosa in patients with percutaneous gastrostomy is associated with the greater number of closely spaced fundic glands, with tiny layer of connective tissue between them.

Discussion

An important characteristic of enteral feeding is the absence of physiological stimuli of the digestive process. Both visual, olfactory and gustatory stimuli, as well as complex neuro-humoral reflexes involving autonomic and sensory neuronal circuits, are involved. The synchrony in the hormonal activity of the enteroendocrine cells is also disturbed. All this affects the secretory functions of the GIT and in particular the secretion of hydrochloric acid from the parietal cells of the gastric glands.

Literature data on enteral nutrition and gastric acid secretion are mainly based on data from pH-metry of gastric contents. Clinical studies with pH-metry of gastric juice in enteral, parenteral and standard nutrition found that enteral nutrition stimulates acid secretion. Gastric content titration data, however, depend on the type of diet, as high protein administered in the stomach buffers hydrogen cations and gives a falsely elevated pH [4]. Gastric aspirate pH testing in infants on enteral nasogastric tube

feeding is used as a criterion for proper tube placement and is included in guidelines for gastric tube feeding [GUIDELINE. Gastric Tube Feeding in the NICU. Child and Adolescent Health Service. Government of Western Australia.]. A pH value ≤5.5 is considered predictive of proper gastric placement. The use of pH testing in infants, however, has limitations. It is unclear whether infants can produce adequate gastric acid to achieve a pH of 5, whether feeding frequency and medication use (proton pump inhibitor, histamine-2 receptor antagonist, etc.) affect reported pH results [14].

Percutaneous endoscopic gastrostomy has been a valuable tool in nutritional rehabilitation since its inception in 1980 [8]. The main and most common indication for PEG in children and adults are neurological disorders with inability to swallow or dysphagia [16, 19]. The majority of the children are suffering from cerebral palsy with inability to swallow. Some of these patients may also suffer from epilepsy, in which case they will need the tube for medication intake. Recurrent aspiration secondary to neurological disorder may result in failure to use the oral route safely and the insertion of a PEG tube should be undertaken [23]. Cerebral palsy (CP) is one of the main disabling disorders, characterized by permanent brain damage that affects motor and cognitive functions with different clinical symptoms in children [6]. The pathogenesis of CP is associated with increased systemic inflammatory response during intrauterine period or period before the age of 3.

The reason for PEG feeding in some of our patients is precisely CP. In the biopsy specimens of these patients we established the significant presence of mast cells under the covering epithelium and near the fundic glands of the mucosa.

Mast cells are the multifunctional immune cells that are one of the most important sources of proinflammatory cytokines. In a retrospective study of children with CP, the investigators detected higher levels of several perinatal circulating cytokines, including IL-9 [18]. It was found that in children with CP aged 3-18 years plasma levels of proinflammatory cytokines IL-1β, IL-6 and histamine levels were higher in individuals with CP compared to healthy controls [5]. The majority of mast cells are located in the gut wall. Here, they function as an important part of the immunological barrier between the internal milieu and luminal content [1]. Mast cells are present in all layers within the gastrointestinal tract. The close proximity of MCs and nerves is the emblem of the neuro-immune network and has indicated the existence of a bidirectional crosstalk between MCs and nerves acting in tandem with other neural and immune cells [2]. This dialog is crucial in the maintenance of intestinal homeostasis and it is responsible for diseases and in pain visceral perception [21].

The relationship between GIT and CNS disease is bidirectional. The role of the gut brain axis is to monitor and integrate gut functions, link affective and cognitive centers of the brain with peripheral intestinal functions and mechanisms such as immune activation, gut permeability, enteric reflex, and enteroendocrine signaling [7]. Neurological and neurodegenerative diseases are associated with complex pathologies including inflammation in both the central [3] and autonomic nervous system [27, 20, 10, 24]. These diseases are often characterized by poor gut health due to the loss of gut-barrier integrity [15, 17], which underscores the role of the brain-gut axis.

It has been established that mast cells play a role in multiple pediatric gastrointestinal disorders including eosinophilic esophagitis, functional dyspepsia, and irritable bowel syndrome [22]. A role for mast cells in feeding difficulties is biologically plausible and possibly related to increased gastric sensitivity. Mast cell infiltration and activation

has been shown to increase visceral sensitivity in both animal models and humans [12]. Mast cell infiltration and activation could account for hypersensitivity to stretch and possibly also for chemical sensitivity as has been demonstrated in adults with functional dyspepsia with enteral lipid infusion [9, 11].

Conclusion

Long term enteral nutrition via PEG does not cause significant morphological disorders in the structure of the stomach wall. The predominance of the glandular component over the connective tissue component in the gastric mucosa of children with PEG is probably an adaptation mechanism of the body for the secretion of a sufficient amount of gastric juice. Regarding increased mast cell activity in children with cerebral palsy further studies are needed to clarify whether this finding is related to the PEG or to the child‘s neurological disorder.

References

1. **Abraham, S. N., A. L. St John.** Mast cell-orchestrated immunity to pathogens. – *Nat. Rev. Immunol.,* **10(6)**, 2010, 440-452.
2. **Albert-Bayo, M., I. Paracuellos, A. M. González-Castro, A. Rodríguez-Urrutia, M. J. Rodriguez-Lagunas, C. Alonso-Cotoner, J. Santos, M. Vicario.** Intestinal mucosal mast cells: key modulators of barrier function and homeostasis. – *Cells*, **8(2)**, 2019, 135.
3. **Amor, S., F. Puentes, D. Baker, P. van der Valk**. Inflammation in neurodegenerative diseases. – *Immunology*, **129**(2), 2010, 154-169.
4. **Armstrong, D., F. Castiglione, C. Emde, T. Cilluffo, Ph. Duroux, J. Koerfer, E. Temler, C. Lamers, J. Jansens, A. Blum, J. Gonvers.** The effect of continuous enteral nutrition on gastric acidity in humans. – *Gastroenterol.,* **102(5)**, 1992, 1506-1515.
5. **Demir, C.** Increased systemic inflammatory response with mast cell activation in elder children with cerebral palsy. – *Clin. Exp. Health Sci.*, **12,** 2022, 294-301.
6. **Di, H., Q. He, Y. Liao, B. Kalionis, X. Tai.** The role of inflammatory cytokines in the pathogenesis of cerebral palsy. – *Gynecol. Obstet. (Sunnyvale)*, **6(2)**, 2016, 1-7.
7. **El-Hakim, Y., S. Bake, K.K. Mani, F. Sohrabji**. Impact of intestinal disorders on central and peripheral nervous system diseases. – *Neurobiol. Dis.,* **165,** 2022, 10562.
8. **El-Matary, W.** Percutaneous endoscopic gastrostomy in children. – *Can. J. Gastroenterol.,* **22(12),** 2008, 993-998.
9. **Feinle, C., O. Meier, B. Otto, M. D'Amato, M. Fried.** Role of duodenal lipid and cholecystokinin A receptors in the pathophysiology of functional dyspepsia. – *Gut,* **48(3),** 2001, 347-355.
10. **Femminella, G. D., G. Rengo, K. Komici, P. Iacotucci, L. Petraglia, G. Pagano, C. de Lucia, V. Canonico, D. Bonaduce, D. Leosco, N. Ferrara**. Autonomic dysfunction in Alzheimer's disease: tools for assessment and review of the literature. – *J. Alzheimers Dis.,* **42(2)**, 2014, 369-377.
11. **Fried, M., C. Feinle.** The role of fat and cholecystokinin in functional dyspepsia. – *Gut*, **51(1)**, 2002, 54-57.
12. **Hou, X. H., L. R. Zhu, Q. X. Li, J. D. Z Chen**. Alterations in mast cells and 5-HT positive cells in gastric mucosa in functional dyspepsia patients with hypersensitivity. – *Neurogastroenterol. Motil.,* **13**, 2001, 398-399.
13. **Issa, A., J. Edwards, M. Singh, C. Friesen, S. Edwards.** Presence of increased mast cells in infants and children with volume and variety limited intake. – *Nutrients,* **14(2)**, 2022, 365.

14. Kemper, C., L. Haney, A. Oschman, B. Lee, B. Lyman, L. Parker, D Brandon. Acidity of enteral feeding tube aspirate in neonates. - *Advances in Neonatal Care*, **19(4)**, 2019, 333-341.
15. Liddle, R. A. Parkinson's disease from the gut**.** - *Brain Res.*, **1693(Pt B),** 2018, 201-206.
16. Miller, R. E., B. Castlemain, F. J. Lacqua, D. P. Kotler. Percutaneous endoscopic gastrostomy. Results in 316 patients and review of literature. – *Surg. Endosc.*, **3(4)**, 1989, 186-190.
17. Morais, L. H., H. L. 4th Schreiber, S. K. Mazmanian. The gut microbiota-brain axis in behaviour and brain disorders. – *Nat. Rev. Microbiol*., **19**(4), 2021, 241-255.
18. Nelson, K. B., J. M. Dambrosia, J. K. Grether, T. M. Phillips. Neonatal cytokines and coagulation factors in children with cerebral palsy. – *Ann. Neurol*., **44(4)**, 1998, 665-675.
19. Nicholson, F. B., M. G. Korman, M. A. Richardson. Percutaneous endoscopic gastrostomy: a review of indications, complications and outcome. – *J. Gastroenterol. Hepatol.,* **15(1)**, 2000, 21-25.
20. Probst, A., A. Bloch, M. Tolnay. New insights into the pathology of Parkinson's disease: does the peripheral autonomic system become central? – *Eur. J. Neurol.,* **15(1)**, 2008, 1-4.
21. Quigley, E. M., O. F. Craig. Irritable bowel syndrome; update on pathophysiology and management. – *Turk. J. Gastroenterol*., **23(4)**, 2012, 313-322.
22. Ravanbakhsh, N., A, Kesavan. The role of mast cells in pediatric gastrointestinal disease. – *Ann. Gastroenterol.,* **32(4),** 2019, 338-345.
23. Safadi, B. Y., J. M. Marks, J. L. Ponsky. Percutaneous endoscopic gastrostomy. – *Gastrointest. Endosc. Clin. N. Am*., **8(3)**, 1998, 551-568.
24. Sirbu, C. A., R. M. Mezei, C. Falup-Pecurariu, O. G. Bratu, A. M. Sirbu, M. C. Ghinescu, F. I. Radu. Autonomic dysfunctions in multiple sclerosis: Challenges of clinical practice (Review). – *Exp. Ther. Med.*, **20(6)**, 2020, 196.
25. Song, S., Y. Song, H. Zhang, G. Li, X. Li, X. Wang, Z. Liu. Increased counts and degranulation of duodenal mast cells and eosinophils in functional dyspepsia - a clinical study. – *Med. Glas (Zenica)*, **12(1)**, 2015, 107.
26. Taylor, T. J., N. N. Youssef, R. Shankar, D. E. Kleiner, W. A. Henderson. The association of mast cells and serotonin in children with chronic abdominal pain of unknown etiology. – *BMC Res. Notes,* **21**, 2010, 3-265.
27. Zesiewicz, T. A., M. J. Baker, M. Wahba, R. A. Hauser. Autonomic nervous system dysfunction in parkinson's disease. – *Curr. Treat Options Neurol.*, **5(2),** 2003, 149-160.

Institute of Experimental Morphology, Pathology and Anthropology with Museum
Bulgarian Anatomical Society

Acta Morphologica et Anthropologica, 31 (1-2)
Sofia ● 2024

Mast Cells in Rat Pulmonary Pleura

Ivelina Ivanova[1], Ivaylo Stefanov[1,2], Vanesa Pilicheva[1]*

[1]Department of Anatomy, Medical Faculty, Trakia University, Stara Zagora, Bulgaria
[2]Department of Anatomy, Histology and Embryology, Pathology, Medical Faculty, Prof. Dr. Asen Zlatarov University, Burgas, Bulgaria

*Corresponding author e-mail: ivelina.ivanova@trakia-uni.bg

The aim of the present immunohistochemical study is to determine the metachromatic, tryptase and ghrelin positive mast cells in pulmonary pleura of male rats at different ages. The detection on serial sections of tryptase and ghrelin immunoreactivity with metachromasy allowed us to estimate the number of these three types of cells in lung pleura of different aged male rats. We revealed that the amount of toluidine blue positive mast cells (MCTB) in the lung pleura was significantly less than that of tryptase (MCTr) and ghrelin positive mast cells (GhrMC). The number of tryptase and ghrelin positive mast cells showed similar values. In the comparative study on serial sections, we observed that some MCTr and GhrMC did not show metachromasia. In pleura's subserous layer the percentage of MCTr and GhrMC with manifested metachromasia varies in the different age groups: 58-59% in 1-year-old, 42% in 3-month-old and 20% in 20-day-old animals.

Key words: mast cells, ghrelin, tryptase, pleura, rat

Introduction

Mast cells are tissue-resident cells, which take part in the secretion of a variety of biologically active mediators, cytokines, and chemokines [9]. Their mediators can influence the biological activities of neighboring cells and tissues [10]. These cells are multifunctional effector cells involved in inflamation processes, hypersensitivity and allergic disease [1]. There are two main immunohistochemical types of mast cells (MCs) according to the protease content: tryptase positive mast cells (MCTr) and chymase positive mast cells [15]. Ertuğrul et al. [2] found that ghrelin and tryptase-positive cells are morphologically similar to each other. Matos et al. [8] in their study reported that the MC tryptase induces eosinophil recruitment into the pleural cavity and this effect dependens on MC tryptase proteolytic activity. Recently Giannou et al., [4] described the discovery of MCs in human and mouse malignant pleural effusion formations and the elucidation of their fate and role.

Mature and immature Wistar rats have been widely used to study the role of metachromatic and tryptase positive mast cells in pathological conditions of the lung, particularly the lung pleura. However, the knowledge of age-related features in the distribution of different phenotypes of mast cells in the lung pleura of healthy rats is scarce. The aim of our work was to perform immunohistochemical study to determine the metachromatic (MCTB), tryptase (MCTr) and ghrelin positive (GhrMC) mast cells in pulmonary pleura of healthy male rats at different ages.

Materials and Methods

Experimental animals

In our study 18 male Wistar rats at age of 20 days, 3 months and 1 year were used. Animals were anesthetized with ketamine and xylazine and were transcardially perfused with 4% paraformaldehyde in phosphate buffer. The animals were received from Project No. 13 / 2017, Medical faculty, Trakia University. All procedures were performed in accordance with the Bulgarian legislation regarding animal care (Ordinance 20 of 01.11.2012 on the minimum requirements for the protection and welfare of experimental animals and the requirements for the sites for use, breeding and/or delivery) and in in accordance with Directive 2010/63 / EU of the European Parliament and of the Council of 22 September 2010 on the protection of animals used for scientific purposes.

Material

The lungs of each animal were immediately removed, leaving the left and right lung lobes in 4% paraformaldehyde for 24 hours, washed with phosphate-buffered saline (PBS), dehydrated in an alcoholic beaker, clarified in xylene and included in paraffin. Serial tissue sections of 5 μm thickness from each animal were prepared from the included material, mounted on gelatin coated slides, then deparaffinized twice in xylene and rehydrated by series of decreasing ethanol concentrations.

Histochemical method with toluidine blue for visualization of metachromatic mast cells

Tissue sections were mounted on gelatinized slides, twice placed in xylene and rehydrated by decreasing ethanol concentrations. The sections were immersed in a 0.1% solution of toluidine blue in McLivane's buffer, pH 3.

Immunohistochemical methods for visualization of tryptase- and ghrelin-positive mast cells

The tissue sections were washed in 0.1 M PBS and placed in 1.2% hydrogen peroxide in methanol for 30 minutes, following by antigen recovery in buffer (pH 9.0) for 20 minutes. Between these steps, sections were washed with an EnVision Flex Wash Buffer, then incubated in a humidified chamber overnight at 4°C with primary antibodies: mouse antihuman ghrelin (2F4) at 1:50 dilution (sc-293422 Santa Cruz Biotechnology), monoclonal mouse antihuman mast cell tryptase – ready for use (MBS9510697, DAKO). After triple washing with PBS, the sections were incubated with EnVision detection system (DAKO) for 24 hours at 4°C. The immune reaction

was visualized with diaminobenzidine. PBS replacing the primary antibody was used as a negative control. The slices were dehydrated, washed, coated with glass slides and photographed with a research microscope (LEICA DM1000) equipped with a digital camera (LEICA DFC 290).

Of the three serial sections used, two were stained with tryptase and ghrelin antibodies, and the third was stained with toluidine blue for metachromasia in the three different age groups.

Statistical methods

The number of mast cells in the study was determined on three microscopic fields (X 200) of sections of the left lung of each animal using a light research microscope (LEICA DM1000) equipped with a digital camera (LEICA DFC 290). Raw mast cell density data (number / field of view) were processed using GraphPadPrism 6 for Windows (GraphPad Software, Inc., USA) for analysis of variations (one-way ANOVA), followed by Tukey-Kramer test. Values of $P < 0.05$ were considered statistically significant. The data are presented as mean ± standard deviation (SD).

Results

We revealed that the amount of toluidine blue positive mast cells in the lung pleura was significantly less than that of tryptase and ghrelin positive mast cells (**Table 1**).

Table 1. Distribution (mast cell count (MC) "mean"/field of view ± standard deviation "SD") of toluidine blue (MCTB)-, tryptase (MCTr)-positive mast cells and ghrelin-positive cells (GhrC) in the visceral pleura in the caudal lobe of the left lung. **a** ($P<0.0001$) – statistically significant difference between the number of MCTB and that of MCTr and GhrMC. **%** – MCTr and GhrMC, also showed metachromasia.

Age, Parameter	**Pleura**
20 days, **Number of MC**: MCTB Min-max MCTr Min-max /**%** GhrMC Min-max /**%**	 3.2 5± 0.87 2-4 16.08±0.90**a** 15-17/**20** 16.0±0.85**a** 15-17 /**20**
3 months, **Number of MC**: MCTB Min-max MCTr Min-max /**%** GhrMC Min-max /**%**	 7.0±0.89 6-8 16.45± 0.69**a** 15-17 /**42** 16.82± 0.87**a** 16-18 /**42**

Table 1.

1 year, **Number of MC**: MCTB Min-max	 9.75± 0.96 8-11
MCTr Min-max /**%**	16.67± 0.49**a** 16-17 /**58**
GhrMC Min-max /**%**	16.58± 0.51**a** 16-17 /**59**

The number of triptase and ghrelin positive mast cells showed similar values. In the comparative study on serial sections, we observed that some MCTr and GhrMC did not show metachromasia. In the subserous layer of the pleura, the percentage of MCTr and GhrMC with manifested metachromasia varies in different age groups: 58-59% in 1-year-old, 42% in 3-month-old and 20% in 20-day-old animals. Comparing the number of mast cells in each lobe in rats of different ages, we found an age-dependent difference in the number of mast cells in the subserosal layer of the three lobes. In the cranial right lobe, the greatest number of the searched cells was found in the 1-year-old rats, followed by the 3-month-old and the 20-day-old. The same distribution of mast cells was observed in the left lung. In the right caudal lobe, the fewest mast cells were found in the 20-day-old rats, and the number was approximately equal and greater in the 3-month-old and 1-year-old rats **(Fig. 1)**. Comparing the number of mast cells in the different lobes for each age, we found that in all three lung lobes examined in the 20-day-old rats, the number of cells was the same. In the 3-month-old and 1-year-old rats, the number of mast cells in the caudal right lobe was the greatest, followed by the cranial right lobe and the left lung **(Fig. 1)**. The present study showed a different distribution of MCTB compared to MCTr and GhrMC **(Table 1)**. The amount of MCTB in the lung pleura was significantly less than that of MCTr and GhrMC **(Fig. 2A, D)**. In the comparative study on serial sections, we found that part of MCTr

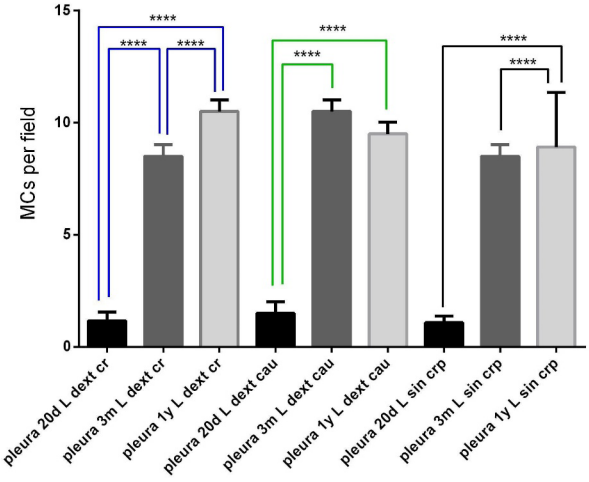

Fig. 1. Age-dependent difference in the number of mast cells in the subserosal layer of the three lobes of the lung- cranial lobe of the right lung, caudal lobe of the right lung and left lung.

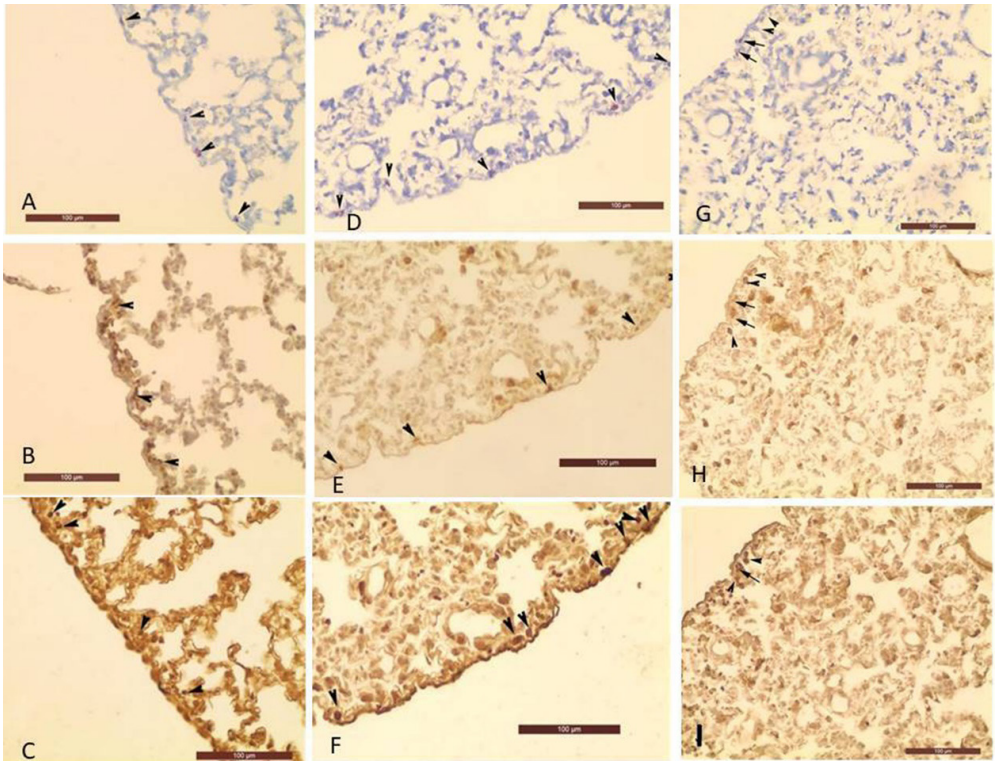

Fig. 2A. MCTB (arrowheads) in the subserosal layer of the visceral pleura in 20-day-old rats; **B.** MCTr (arrowheads) in the subserosal layer of the visceral pleura in 20-day-old rats; **C.** GhrMC (arrowheads) in the subserosal layer of the visceral pleura in 20-day-old rats; **D.** MCTB (arrowheads) in the subserosal layer of the pleura in 3-month-old rats; **E.** MCTr (arrowheads) in the subserosal layer of the pleura in 3-month-old rats; **F.** GhrMC (arrowheads) in the subserosal layer of the pleura in 3-month-old rats; **G.** MC (arrowheads) without metachromasia, but tryptase- and ghrelin-positive in the subserosal layer of the pleura. Arrows – MCTB. Age -1 year; **H.** MCTr (arrowheads) in the subserosal layer of the pleura without metachromasia but are ghrelin positive. Arrows – MCTr with metachromasia. Age -1 year; **I.** GhrMC (arrowheads) in the subserosal layer of the pleura without metachromasia, but are tryptase positive (arrow – GhrMC with metachromasia). Age -1 year. Bars = 100μm.

and GhrMC did not show metachromasia **(Figs. 2G, H, I)**. In the subserous layer of the pleura, the percentage of MCTr and GhrMC with manifested metachromasia varies in different age groups **(Table 1)**: it is the highest in 1-year-olds – 58-59%, followed by that in 3-month-olds – 42% and is the most -low in the 20-day-old animals – 20%. The number of GhrMC and MCTr in the pleura showed close values. At all three ages, no difference was found between the number of MCTr and GhrMC **(Figs. 2B, C, E, F).**

Discussion

This study presents original data regarding the normal density of the three types of mast cells: metachromatic, tryptase- and ghrelin positive mast cells in lung pleura of healthy

rats. The similar number of tryptase and ghrelin positive mast cells defines mast cells as a main source of ghrelin in pleura. The significance of our findings can be explained in several ways. Mast cell tryptase is a known smooth muscle mitogen participating in mast cell-mediated remodeling of the pleural vasculature but mast cell ghrelin may regulate contractility of vascular smooth muscle cells. In animal models was reported that ghrelin reduces the release of pro-inflammatory cytokines [7] and stimulates the release of the anti-inflammatory cytokine IL-10 by T lymphocytes and macrophages [16]. Gulubova et al., 2019, proved that ghrelin positive MCs number in the muscle layer of the stomach is significantly decreased in rats with metabolic disturbances which is related with lowered power of gastric muscle contraction [5]. It was found that that circulating ghrelin levels are deeply diminished in patients with gastric cancer related with the progression of gastric cancer [11]. On the other hand, it was shown that ghrelin is mitogenic having a promoting effect on neoplastic cell growth [14]. Mast cells as part of the innate immune system are involved in the pathogenesis of different tumors, exerting their pro- and antitumorigenic effects. Some studies have investigated the angiogenic role of MCs related to the increase of tumor growth and progression [6]. Mast cell mediators inducing angiogenesis are represented by basic fibroblast growth factor, tumor necrosis factor α and β, interleukin 4 (IL 4), interleukin 8 (IL 8) [13].

Other studies, however, reported the inhibitory role of MCs in tumor growth and progression, exerting a cytotoxic effect on tumor cells [3]. Both tryptase and chymase positive MCs have been detected in different solid tumors, including in lungs where tryptase positive MCs significantly predominated [6, 17]. In 2005, it has been reported that the frequency of the highly aggressive and relatively rare tumor malignant pleural mesothelioma (MPM) is increasing throughout the world [12]. Robinson et al., found that tryptase positive mast cells at tumor site were in higher number than chymase positive mast cells, even in some patients the chymase positive mast cells were absent [12]. Therefore, a high number of tryptase positive MCs can be assumed as independent favorable prognostic factor in pleural mesothelioma showing a correlation with a better prognosis. Robinson et al. revealed the importance of the immunologic analysis in the prognostic and therapeutic approach in patients with pleural mesothelioma [12].

Conclusions

It was found that immunohistochemical identification of mast cells by demonstration of tryptase in the rat lung is more reliable than toluidine blue staining. Mast cells are the main source of ghrelin in pleura. The knowledge of the distribution of different types of mast cells is of clinical importance for the development and prognosis of pathological processes of the pulmonary pleura.

Acknowledgments: The authors are thankful to the scientific project number 13/2017, Medical Faculty, Trakia University, Stara Zagora, for supporting and delivering of animals for this study.

References

1. **Da Silva, E. Z. M., M..C. Jamur, C. Oliver.** Mast cell function: a new vision of an old cell. – *J. Histochem. Cytochem.*, **62**(10), 2014, 698-738.
2. **Ertuğrul, T., G. Sevilgen.** An immunohistochemical investigation of the effect of sambucus nigra on chymase-, tryptase- and ghrelin- positive cells in rat lung. **–** *Kocatepe Vet. J.,* **15**(2), 2022, 209-216.
3. **Ghiara, P., D. Boraschi, L. Villa, G. Scapigliati, C. Taddei, A. Tagliabue.** In vitro generated mast cells express natural cytotoxicity against tumour cells. **–** *Immunology,* **55**(2), 1985, 317–324.
4. **Giannou, A. D.,** A. **Marazioti, M. Spella, N. I. Kanellakis, H. Apostolopoulou, I. Psallidas, Z.M. Prijovich, M. Vreka, D.E. Zazara, I. Lilis, V. Papaleonidopoulos, C. A. Kairi, A. L. Patmanidi, I. Giopanou, N. Spiropoulou, V. Harokopos, V. Aidinis, D. Spyratos, S. Teliousi, H. Papadaki, S. Taraviras, L.A. Snyder, O. Eickelberg, D. Kardamakis, Y. Iwakura, T. B. Feyerabend, H. R. Rodewald, I. Kalomenidis, T. S. Blackwell, T. Agalioti, G. T. Stathopoulos.** Mast cells mediate malignant pleural effusion formation. – *J. Clin. Invest.,* **125**(6), 2015, 2317-2334.
5. **Gulubova, M. V., A. N. Tolekova, K. Ivanova, S. Hamza, M. Hadzhi, D. Chonov, J. Ananiev.** Fructose-induced metabolic disturbances in rats and its impact on stomach endocrine cell number and smooth muscle contractility. – *Archives of Physiology and Biochemistry*, **126**(3), 2019, 1-9.
6. **Ibaraki, T., M. Muramatsu, S. Takai**, **D. Jin, H. Maruyama, T. Orino, T. Katsumata, M. Miyazaki.** The relationship of tryptase- and chymase-positive mast cells to angiogenesis in stage I non-small cell lung cancer. – *Eur. J. Cardiothorac. Surg*., **28**(4), 2005, 617-621.
7. **Işeri, S. O., G. Sener, B. Saglam, F. Ercan, N. Gedik, B. C. Yeğen.** Ghrelin alleviates biliary obstruction-induced chronic hepatic injury in rats. **–** *Regul. Pept.,* **146**(1-3), 2008, 73-79.
8. **Matos, N. A., J. F. Silva, C. M Tamires, K. A. Damasceno, I. D. G. Duarte, V. S. Lemos, G. D. Cassali, A. Klein.** Mast cell tryptase induces eosinophil recruitment in the pleural cavity of mice via proteinase-activated receptor. – *Inflammation,* **36**(6), 2013, 1260-1267.
9. **Metcalfe, D., D. Baram, Y. A. Mekori.** Mast cells. **–** *Physiol. Rev*., **77**(4), 1997, 1033-1079.
10. **Mukai, K., M. Tsai, H. Saito, S. J. Galli.** Mast cells as sources of cytokines, chemokines, and growth factors. – *Immunol Rev.*, **282**(1), 2018, 121-150.
11. **Murphy, G., F. Kamangar, S.M. Dawsey, F. Z. Stanczyk, S. J. Weinstein, P. R. Taylor, J. Virtamo, C.C. Abnet, D. Albanes, N.D. Freedman.** The relationship between serum ghrelin and the risk of gastric and esophagogastric junctional adenocarcinomas. **–** *J. Natl. Cancer Inst.,***103**(14), 2011, 1123-1129.
12. **Robinson, B.W., A.W. Musk, R. A. Lake.** Malignant mesothelioma. – *Lancet*, **366**(9483), 2005, 397-408.
13. **Tharp, M. D.** The interaction between mast cells and endothelial cells. **–** *J. Invest. Dermatol.,* **93**(2), 1989, 107-112.
14. **Tian, P.Y., X. M. Fan.** The proliferative effects of ghrelin on human gastric cancer AGS cells. **–** *J. Dig. Dis.,* **13**(9), 2012, 453-458.
15. **Tütüncü, Ş., A.Ç. Torun, T. Ertuğrul**. The role of resveratrol on mast cell and chymase and tryptase expression in blunt – chesttrauma-induced acute lung injury in rats. – *Turk. J. Vet. Anim. Sci.*, **44**, 2020, 1260-1268.
16. **Warzecha, Z., P. Ceranowicz, A. Dembinski, J. Cieszkowski, B. Kusnierz-Cabala, R. Tomaszewska, A. Kuwahara, I. Kato.** Therapeutic effect of ghrelin in the course of cerulein induced acute pancreatitis in rats. **–** *J. Physiol. Pharmacol.,* **61**(4), 2010, 419-427.
17. **Welsh, T.J., R. H. Green, D. Richardson, D. A. Waller, J.K. O'Byrne, P. Bradding.** Macrophage and mast-cell invasion of tumor cell islets confers a marked survival advantage in non-small-cell lung cancer. **–** *J. Clin. Oncol*., **23**(35), 2005, 8959-8967.

Institute of Experimental Morphology, Pathology and Anthropology with Museum
Bulgarian Anatomical Society

Acta Morphologica et Anthropologica, 31 (1-2)
Sofia ● 2024

Morphological Study of the Tongue during Acupuncture

Nikola Pirovski[1], Dimitrinka Atanasova[1,2], Ivelina Ivanova[1], Sevinch Hamza[1], Nikolay Dimitrov[1]*

[1] *Department of Anatomy, Faculty of Medicine, Trakia University, Stara Zagora, Bulgaria*
[2] *Institute of Neurobiology, Bulgarian Academy of Sciences, Acad. G. Bonchev Str., Bl. 23, 1113 Sofia, Bulgaria*

**Corresponding author e-mail: nikola.pirovski@trakia-uni.bg*

The aim was to investigate the morphological changes occurring in the tissues of the rat tongue during acupuncture. Acupuncture needles on the rat's tongue were placed at an acupuncture point corresponding to the human acupuncture point Ex-HN-10 (Juquan). We used a methodology developed by us. In the needle tract formed after acupuncture, we observed a violation of the integrity of the epithelium, the lamina propria, the deep muscles and nerve fibers of the tongue. We scrutinized nerve fibers in the vicinity of the needle tract, some of them were unaffected by the needle and others were destroyed. We detected mast cells (MCs) in the tissues near the blood vessels and nerve fibers as well as in the nerve fibers themselves. Some of the MCs in the vicinity of the needle showed signs of degranulation with released granules found a considerable distance from the cell.

Key words: acupuncture, acupoint, tongue, needle, mast cells

Introduction

Acupuncture is one of the main areas of Traditional Chinese Medicine (TCM). This is a method for beneficial effects on health, in which acupuncture needles are placed in acupuncture points on the body. Tongue acupuncture is part of (TCM) and is becoming increasingly popular as a method of treatment. The doctor who is scientifically researching this area in the present time is Prof. Sun, practicing mainly in Hong Kong. Autism is one of the diseases in which the effectiveness of tongue acupuncture is studied [19]. Depression is another disease affected by acupuncture on the tongue. Most studies have shown a positive effect of these procedures, with difficulties in the methodology and selection of homogeneous groups [7]. The clinical effect and application of electroacupuncture on the tongue in the treatment of patients with lingual hemangiomas have been studied, and the results of this method of treatment have been

reported [9]. According to some authors, due to the close relation of the tongue to the brainstem and cerebellum, its stimulation can increase the associated nerve pathways to the motor/somatosensory cortex, leading to an improvement in motor function, even with a short course of acupuncture treatment on the tongue [15].

The human tongue assists in a variety of functions; the anterior tongue plays a prominent role in speaking and mastication, while the posterior tongue performs a role in upper airway maintenance [20]. The tongue is innervated by hypoglossal nerve (CN XII), trigeminal (CN V3) and glossopharyngeal (CNIX) nerves; autonomic nerve fibers which stem from the intermedio-facial nerve (CN VII), the glossopharyngeal nerve, and the vagus nerve (CN X); and sensory nerve fibers. Characteristic features of the tongue in rodents are the elongated body of the tongue and the presence of a prominence known as the "intermolar" prominence. The dorsal surface of the mucosa of the tongue is covered by lingual papillae. The tongue papillae with its taste buds in humans and mammals are the receptors for the sensation of taste [18].

The dorsal surface of the tongue in rats is covered by partially keratinized stratified squamous epithelium. The lamina propria is located under the epithelial layer and is represented by the loose connective tissue that includes the blood vessels and nerves. The lamina propria is fused with the underlying connective tissue of the tongue muscles without a sharp boundary. The large number of papillae, which are different in size, shape, and localization on the dorsal surface of the tongue. The connective tissue of the tongue includes a large number of vessels and nerves [2].

Mast cells (MCs) are found in surfaces in contact with the external environment, in all tissues of the body, but are widespread near blood vessels and nerves. Their function is related to immunity, protection against parasitic infections, immunomodulation, tissue repair and angiogenesis [11]. Specific connective tissue cells called mast cells, which are missing in the brain, are found in the skin and mucous membranes [14]. In mammals, they are associated mainly with blood vessels and nerve fibers, and with the boundaries between the organism and the external environment. Mast cells (MCs) are also found in the tongue of rats. The authors describe in rat tongue a number of MCs scattered in the submucosal area adjacent to nerve bundles, blood vessels, and skeletal muscle of the tongue. MCs are found in bundles containing both myelinated and unmyelinated nerves in the tongue of rats [1]. Studies of the distribution of MCs in healthy rats were performed. MCs were found in rat tongue. MCs have also been observed in other internal organs in rats, with increased numbers of MCs in inflammatory lesions. The role of MCs and the changes that occur in them as a result of acupuncture at certain points on the body have been studied by many authors [3, 4, 5]. The results described in the literature by some authors in combining classical acupuncture with electroacupuncture suggest that peripheral nerves play an important role in the convergence and degranulation of MCs [8]. There is still insufficient research on the effects of acupuncture on the tissues, MCs and nerves of the tongue. The aim of our study was to investigate the morphological changes occurring in the tissues of the tongue during acupuncture.

Materials and Methods

Wistar rats were used for experimental animals in the present study. The tongues of a total of 25 Wistar rats of both sexes weighing between 220-350g and 3 months of age

were studied. The rats were provided by project 13/2017 at the Medical Faculty of the Trakia University. All studies were conducted in accordance with the regulations for work with experimental animals in the Republic of Bulgaria and are in accordance with the ethical standards specified in the rules of the Department of Anatomy at the Medical Faculty of the Trakia University and comply with the European Animal Welfare Directive, with the Commission on Ethical Treatment of Humans and Animals.

Animals were initially premedicated with ether for 5 minutes, followed by intraperitoneal injection of xylazine and ketamine (40-80 mg/kg, i.p). After maximal extension of the tongue the experimental animals were pierced with an acupuncture needle (acupuncture needles were inserted into the acupuncture point) 0.22×13-mm stainless steel needle, (Beijing Zohongyan Taihe Medical Instrument Co., Ltd., China) at point Ex-HN-10 (Juquan). The location is in the center of the tongue body and the needle was kept for 10 minutes. The depth differ form a few millimeters, up to pierce the entire tongue. Due to its elasticity, the tissues quickly regain their integrity after removing the acupuncture needle. The defect that occurs in the tissues is minimal in diameter and the needle tract is difficult to distinguish. In order to trace more precisely the depth of its penetration and to demonstrate the needle tract and the surrounding tissues, in a state as close as possible to the in vivo state, we altered the method by leaving the needle in the tissues during the processing of the taken material until the stage of "cutting". In this case, the observed needle tract shows the exact path of the needle and the deformation of the surrounding tissues at the time of insertion of the needle. The methodology developed by us allows visualization of the needle tract formed after acupuncture and the tissues located near the needle tract and the MCs contained in them [4, 5]. This technique was also used to study the effect of acupuncture in rat tongue. Together with the needle inserted at the test point (EX-HN-10), the rats were perfused through the ascending aorta with 4% paraformaldehyde in 0.1 M phosphate buffer (pH 7.36). The tongue was cut near its root and a piece of tongue material together with the needle inserted into it was taken and placed for fixation in 10% formalin for 48 hours. The 10 × 10 × 10 mm tissue blocks were then placed under running water to wash away excess fixative, dehydrated through an ascending row of alcohols, and placed in Cedarwood oil until amber in color. In some of the experimental animals, material from point EX-HN-10 was taken without inserting a needle into the point in order to establish the normal morphological structure in it. The tissue blocks were embedded in paraffin and cut to a thickness of 7 μm. Classical histological staining such as Orcein, Van Gieson, Azan, Toluidine blue, Bismarck brown and immunohistochemical techniques to detect tryptase in mast cells have been applied.

The paraffin sections were washed in 0.1M PBS and placed in 1.2% hydrogen peroxide and methanol for 30 minutes. Antigen recovery was performed in buffer (pH 9.0) for 20 minutes. After washing with an EnVisionFlexWash Buffer, the sections were incubated in a humidified chamber overnight at 4°C with primary antibody: Monoclonal Mouse antihuman mast cell tryptase (Dako, Danmark) – ready to use. Then sections were washed with PBS and incubated with EnVision detection system (DAKO) for 24 hours at 4°C. The reaction was demonstrated with diaminobenzidine. The negative control was done by PBS instead of primary antibody. The samples were photographed with a research microscope (Leica DM1000) equipped with a digital camera (Leica DFC 290)

Results

Holding the needles in the tongue for 10 min in the anesthetized rats allows to track the changes occurring over time in the tissues and cells. This is especially important for the reaction of mast cells with their accumulation around the area of the needle tract and their degranulation. After removal of the acupuncture needle, rapid closure of the adjacent tissues in the vicinity of the needle tract is observed. The tissues quickly fill the defect caused by the acupuncture needle and the needle tract becomes difficult to detect after removing the needle without using the methodology developed by us. The long retention of the acupuncture needle in the tissues with our technique allowed for a good visualization of the needle tract during processing of the tongue samples. The stains we use visualize well the needle tract, MCs, epithelium, blood vessels, nerves and muscles of the tongue.

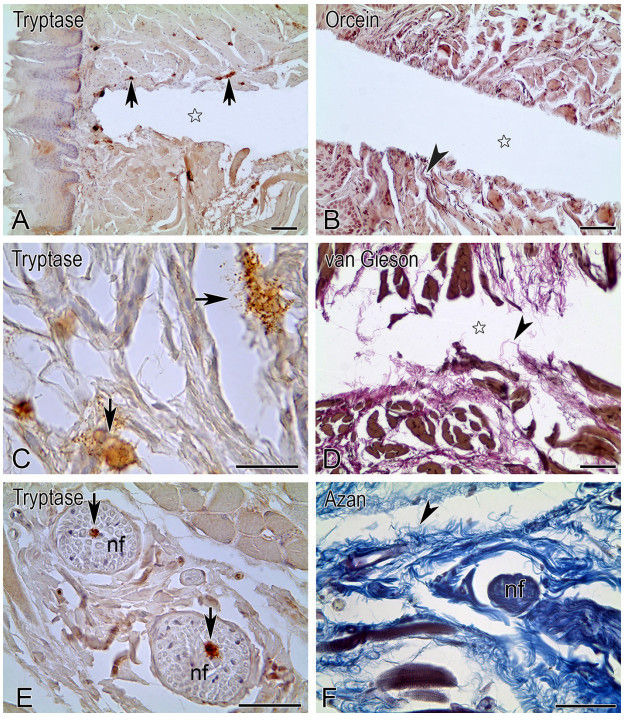

Fig. 1. (A, C, E) Triptase positive MCs in the vicinity of the needle tract. Photomicrographs stained with Orcein (B), van Gieson (D) and Azan (F) showing the tissue reaction in the vicinity of the needle tract formed after acupuncture. Needle tract (star), elastic fibers (arrowheads), collagen fibers (arrowheads), nerve fibers (nf). Scale bar = 50 μm.

After experimental acupuncture at point Ex-HN-10 in a rat on a sagittal incision, the course of the needle tract formed after acupuncture is observed, which passes through the epithelium, lamina propria, fascia, epimysium of the muscles of the tongue and after this goes deep, and in some cases, there is a breakthrough on the other side of the tongue. The tissue folds in the direction of the needle tract. We observe that large, deep-lying structures near the point, such as vessels and nerves, are not affected. This showed that the acupuncture needle placed at this research point did not cause severe damage to the surrounding tissues and did not affect large vessels and nerves in the depth of the tongue.

Histological examination of the tissues in the vicinity of the acupuncture needle tract reveals a violation of the integrity of the epithelium, the subcutaneous loose connective tissue with the elastic and collagen fibers located in it, the fascia and the muscles or their deformation (**Figs. 1B, D, F**). The integrity of the epithelium was disrupted and it folds in the direction of the needle tract. We observed compaction and displacement of the connective tissue and the cells contained in it near the needle

tract (**Fig. 1**). The canal formed by the acupuncture needle (the needle tract) is very clearly visualized in the muscles. There is a partial destruction of the transverse striated muscle fibers in the needle tract, in the depth of the tongue. Detached pieces of skeletal muscle fall into the needle tract formed after acupuncture (**Fig. 1D**). Collagen and elastic fibers are deformed, and some of them are torn. Parts of the collagen and elastic fibers that are entrained by the acupuncture needle fall among the transversely striated skeletal muscles. (**Figs. 1B, D, F**).

We observed nerve fibers in the vicinity of the needle tract formed after acupuncture. Some of these nerve fibers were unaffected by the needle (**Fig. 1E, F**).

Compression and displacement of the tissue near the needle tract is observed, together with the mast cells (MCs) contained in it. In the field of the needle, some of the MCs showed signs of degranulation with released granules found a considerable distance from the cell (**Fig. 1C, Figs. 2C, 2D**). Acupuncture causes a reaction in the mast cells in the tissues surrounding the needle tract. This reaction is expressed in their clustering near the needle tract and their degranulation.

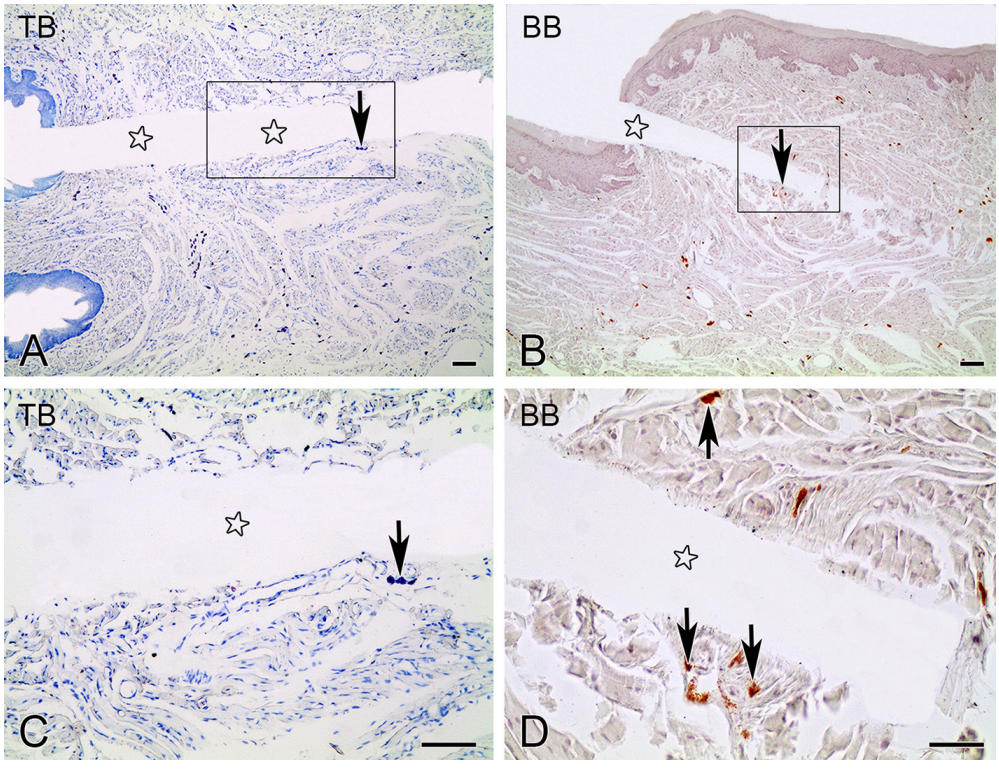

Fig. 2. Toluidine blue (A, C) and Bismarck Brown (B, D) stained micrographs visualizing mast cells in the vicinity of the needle tract formed after acupuncture. Needle tract (star), mast cells (arrows). (C, D) Mast cells showed signs of degranulation with released granules found at a considerable distance from the cells. Scale bar = 50 μm.

Discussion

The results obtained should be considered in the light of the importance of tongue acupuncture in the treatment of diseases in humans and animals. These rat studies will expand our understanding of tongue acupuncture in humans. From the incisions made in the frontal, horizontal, and sagittal planes of the tongue, sagittal sections provided the largest area for single-section study and were, in our opinion, more suitable than other sections for tracing the needle tract formed after acupuncture of the tongue. Longitudinal (sagittal) sections of the needle tract give a better idea of the changes that occur in the tongue as a result of experimental acupuncture because we can examine the epithelium, underlying connective tissue, and musculature in a single section. In control transverse (horizontal) sections, only the changes occurring in the relevant tissue and in particular in the musculature could be examined. The tract of the needles is very well visualized on the sagittal section, as well as the surrounding structures. To study the normal structure of the tongue in rats, other authors have preferred sagittal sections of the tongue [2]. Due to the innovation of our research, we were unable to find data on morphological studies of the tongue by other authors before us. Therefore, we compare our results with the described changes in acupuncture points located on the body. Although there is a difference in the structures, the principles of influence of the acupuncture needle are similar. Some authors have described the changes caused by acupuncture in acupuncture points located on the body. Acupuncture in acupuncture points located on the body causes destruction in the vicinity of the needle tract formed after acupuncture caused by the needle and deformation in the structures adjacent to the needle tract [3]. Structures such as sebaceous glands, hair follicles, blood and lymph vessels are deformed and flattened, and intercellular distances are reduced. Local irritation and release of neuropeptides from sensory nerves as a result of acupuncture has been described [10]. In the immediate vicinity of the needle tract formed after acupuncture, partial destruction has been observed and described by us in research on acupuncture points located on the body, and deformation of the collagen and elastic fibers and folding of the epithelium in the direction of the needle tract [3]. The acupuncture needle displaces the tissues in its course and the deep blood vessels and nerves near the needle tract are not affected [3]. This showed that tongue acupuncture at point Ex-HN-10 is a relatively safe treatment method that does not cause severe damage to deep vessels and nerves. This determines the possibility of its safe useage for treatment in humans and animals. Acupuncture has a strong mechanical effect. We observe destruction of collagen fibers in the connective tissue by the acupuncture needle, which also affects the mast cells located there and MCs in connective tissue have a role in transmitting the mechanical signal from the acupuncture stimulation. The results obtained in this study confirm our previous studies. The observed accumulation of MCs around nerve bundles and blood vessels coincides with the described normal distribution of MCs for the respective age. In 3-month-old rats, more MCs were observed in the deep muscle layer of the tongue than the lamina propria [12]. Feng and Jinglan [6] believe that the reactivity of MCs in rat skin to serotonin is high. The role of MCs in analgesia in acupuncture and increased degranulation of MCs after acupuncture has been described by many authors [5, 16]. Accumulation of histamine and serotonin positive MCs near the needle tract formed after acupuncture has been observed after acupuncture into the body‘s acupuncture points in our previous studies

[4, 5]. Serotonin secretion from MCs was observed as a result of corporal acupuncture in rats [5]. We assume that serotonin and histamine are released by mast cells during tongue acupuncture, and this could be a subject of additional immunohistochemical studies. But there are also authors who believe that the number and degranulation of MCs are not affected by acupuncture [17]. Our previous research confirms the thesis of the influence of acupuncture on MCs of the tongue [13]. Studies have shown that the acupuncture needle affects certain structures in the tissues or passes close to them without directly affecting them [3]. These results are consistent with the results obtained in this study

In conclusion, acupuncture causes morphological changes in the tissues of the tongue and degranulation of MCs.

References

1. **Chapman, G. B.** Occurrence of mast cells within bundles of myelinated and unmyelinated nerves in the rat tongue. – *Anat. Rec*., **256(4)**, 1999, 347-353.
2. **Davydova, L., G. Tkach, A. Tymoshenko, A. Moskalenko, V. Sikora, L. Kyptenko, M. Lyndin, D. Muravskyi, O. Maksymova, O. Suchonos**. Anatomical and morphological aspects of papillae, epithelium, muscles, and glands of rats' tongue: Light, scanning, and transmission electron microscopic study. – *Interv. Med. Appl. Sci.,* **9(3)**, 2017, 168-177.
3. **Dimitrov, N.** Morphological changes in biologically active Point /BAP/ ST36 after acupuncture in rat. - *Acta Morphol. et Anthropol*., **19**, 2012, 30-33.
4. **Dimitrov, N., D. Atanasova, N. Tomov, I. Ivanova, Y. Staykova, K. Dinkova, I. Ganeva, D. Sivrev.** Distribution of histamine positive mast cells in the vicinity of the needle tract following acupuncture in "Zusanli" (ST36) acupoint in rats. – *Acta Morphol. Anthropol*., **23**, 2016, 26-31.
5. **Dimitrov, N., D. Atanasova, N. Tomov, D. Sivrev, N. Lazarov**. Acupuncture causes serotonin release by mast cells. – *Rom. J. Morphol. Embryol*., **58(3)**, 2017, 961-968.
6. **Feng, Y., W. Jinglan**. Histochemical and immunohistochemical observations on heterogenety in mast cells of rat. – *Acta Anat. Sinica*, **1**, 1989, 90-94.
7. **Lee, M. S., T. Choi, B. Shin, E Ernst.** Acupuncture for children with autism spectrum disorders: A systematic review of randomized clinical trials. – *J. Autism Dev. Disord*., **42(8)**, 2012, 1671-1683.
8. **Li M., J. Shi, X. Liu, L. N. Wang, J. Zhang, L. L. Li, X. M. Guan.** Effects of electroacupuncture on the number of subcutaneous mast cells in and beside the acupoint and the inflammatory pain focus in the rat. – *Zhongguo Zhen Jiu*, **23**, 2003, 597-601.
9. **Li, J. H., Y. L. Xin, W. Zhang, Z. Wei, L. Jiang-tao, Q. Kuan-hong.** Effect of electro-acupuncture in treating patients with lingual hemangioma. – *Chin. J. Integr. Med*., **12(2)**, 2006, 146-149.
10. **Lundeberg, T.** Effect of Sensory Stimulation (Acupuncture) on Circulatory and Immune Systems. *In: Acupuncture: A Scientific Appraisal* (Eds E. Ernst and A. White), Oxford, Butterworth-Heinemann, 1999, 93-106.
11. **Metcalfe, D., D. Baram, Y. A. Mekori**. Mast cells. – *Physiol. Rev*., **77(4)**, 1997, 1033-1079.
12. **Pirovski, N., N. Tomov, D. Atanasova, N. Dimitrov.** Mast cells in the rat tongue. – *Acta Morphol. Anthropol*. **25**(3-4), 2018, 84-89.
13. **Pirovski, N., Y. Staykova-Pirovska, D. Atanasova, N. Dimitrov.** Mast cell reaction to acupuncture on tongue – *TJS*, **3**, 2019, 199-202.

14. **Ross, M., W. Pawlina**. *Histology: a text and atlas: with correlated cell and molecular biology. 6th edition.*, Philadelphia, Wolters Kluwer/Lippincott Williams&Wilkins Health, 2011, 110-458.
15. **Sun, J. G., C. H. Ko, V. Wong, X. R. Sun**. Randomised control trial of tongue acupuncture versus sham acupuncture in improving functional outcome in cerebral Palsy. – *J. Neurol. Neurosurg. Psychiatry*, **75(7)**, 2004, 1054-1057.
16. **Zhang, D., G. Ding, X. Shen, W. Yao, Z. Y. Zhang, Y. Q. Zhang, J. Y. Lin**. Influence of mast cell function on the analgesic effect of acupuncture of „Zusanli“ (ST 36) in rats. – *Acupunct. Res.,* **32(3)**, 2007, 147-152.
17. **Zong, A., X. Shi, F. Zhang**. Effects of electro-acupuncture on fascial mast cells in „Zusanli“ acupoint area of rabbits. – *J. Zhengzhou Univ.* (Sci. Med.), **27**, 1992, 226-229.
18. **Witt, M., K. Reutter**. Anatomy of the tongue and taste buds. In: *Handbook of olfaction and gustation* (Ed R. Doty), Hoboken, John Wiley&Sons, 2015, 637-664.
19. **Wong, V., J. Sun, D. Yeung.** Randomized control trial of using tongue acupuncture in autism spectrum disorder. – *J. Tradit. Chin. Med. Sci.*, **1(1)**, 2014, 62-72.
20. **Zaidi, F. N., P. Meadows, O. Jacobowitz, T.M. Davidson**. Tongue anatomy and physiology, the scientific basis for a novel targeted neurostimulation system designed for the treatment of obstructive sleep apnea. – *Neuromodulation*, **16(4)**, 2013 376-386.

Institute of Experimental Morphology, Pathology and Anthropology with Museum
Bulgarian Anatomical Society

Acta Morphologica et Anthropologica, 31 (1-2)
Sofia ● 2024

Morphometric and Histological Structure of Bulbus Oculi in Goats

Semine Dalga[1], Kadir Aslan[1], Serap Koral Taşçı[2], Dilem Ermutlu[2], Serap İlhan Aksu[2]*

[1] *Department of Anatomy, Veterinary Faculty, Kafkas University, Kars, Turkey*
[2] *Department of Histology, Veterinary Faculty, Kafkas University, Kars, Turkey*

*Corresponding author e-mail: sdalga91@gmail.com

This study aimed to identify the morphometrical and histological structure of eyeball (*bulbus oculi)* in Abaza and Gurcu goats. The study analyzed ten pairs of *bulbus oculi* from Abaza and Gurcu goats (5F/5M), taking several morphometric measurements over the eyes using a digital caliper. The eyes observably possessed all recognized anatomical formations in both goat breeds. However, the lens was different in Gurcu goats. Analyses revealed that the *pupilla* dorso ventral diameter (P<0.001***), lens dorso ventral diameter (P<0.005**), and lens medio lateral diameter (P<0.05*) parameters were all statistically significant in Abaza and Gurcu goats. Histologically, Abaza goats had narrow iris structures and dense muscle fibers, whereas Gurcu goats displayed wider and mostly connective tissue formation. Similarly, the choroid of Abaza goats had more dense connective tissue and a narrow structure, whereas the choroid of Gurcu goats retained less connective tissue and a larger layout.

Key words: eye anatomy, bulbus oculi, lens, goat

Introduction

A typical eye is a lens-containing specialized sensory organ [5]. The eye is also one of the complex sense organs, with an extreme sensitivity to external factors, light, and diseases [2, 28, 49], consisting of the optic nerve, eyeball *(bulbus oculi)*, and accessory organs of the eye *(organa oculi accessoria)* [46]. The bulbus oculi develops from the optic vesicle, a protrusion of the brain, and the lens develops from the ectoderm adjacent to the optic vesicles. Cornea, however, forms through the induction of the lens sac [19, 53]. The macroanatomical and morphometric features of the eyeball differ between species and races. Cats have the largest eyeball compared to the body sizes of domestic mammals, followed by dogs, horses, and cattle [24]. The embowed anterior

and the posterior parts of the eyeball are called the *polus anterior* and *polus posterior*, respectively. The axis uniting these two parts from the outside from frontally to the back is called the axis bulbi externus (axis opticus), and the axis joining them from the inside is called the axis bulbi internus [24, 46].

From the past to the present, mainly anatomical, histological, and pathological studies have been conducted on eye tissues through modeling various animals. Some of these studies were performed in humans [18, 52], pigs [11, 26, 31], buffaloes [4], horses [43, 45], dogs [6, 40], sheep [12, 41], and bears [20, 36]. Only the eye is a specific sensory organ that pathologists routinely assess during pre-clinical general studies for the development of novel medicine. Therefore, it is crucial to ascertain and understand the typical histology of the eye tissue in all animal species [7, 51].

Materials and Methods

Ethical approval

This study was approved by the Kafkas University Animal Experiments Local Ethics Committee (Approval no: 2022/067).

Animals

Accordingly, the study analyzed ten pairs of *bulbus oculi* from mature five Abaza and five Gurcu goats.

Anatomical findings

The eyeball from the skulls were removed from orbital cupping and isolated, taking several morphometric measurements over the dissected *bulbus oculi* using a digital caliper **(Figs. 1, 2)**. After macro-anatomical and morphometric measurements, Abaza and Gurcu goat eyes were kept in a 10% formaldehyde solution for histological analyses.

Histological examination

Then, the tissues were paraffin blocked by processing tissues through the subsequent (standard) customary histological tissue solutions. By cutting 5 µm thick sections from the prepared blocks, Triple staining (Crossman's Modified Triple Staining) technique was used to analyze the tissues histologically.

Statistical analysis

Using the SPSS 20 program, the mean values and standard deviations of the obtained data and the correlation coefficients between these features were assessed. Taking the terms of Nomina Anatomica Veterinaria [30] as a basis, the study also utilized to photograph the images of bulbus oculi using the Nikon D700 digital camera.

Results

Morphometric Results

Figure 1 and **Figure 2** display the reference points taken from bulbus oculi and lens analyzed in Abaza and Gurcu goats. Correspondingly, **Table 1** and **Table 2** provide the mean and standard deviation values of the morphometric findings of the bulbus oculi and correlation analyses of these values, respectively. However, **Table 3** lists the comparative results of the morphometric measurements taken from *bulbus oculi* with other studies. Macro-anatomical analysis revealed that the bulbus oculi from Abaza goats demonstrated typical anatomical characteristics **(Fig. 1A, Fig. 2A)**. However, the lens in Gurcu goats consisted of two nodes, although it visually displayed a typically similar structure **(Fig. 2B).** Analyses revealed that the pupilla dorso ventral (DV) diameter (P<0.001***), lens DV diameter (P<0.005**), and lens medio-lateral (ML) diameter (P<0.05*) parameters were all statistically significant in Abaza and Gurcu goats.

Table 1. Mean values of morphometric measurements taken from *bulbus oculi* in Abaza and Gurcu goats (right/left)

Parameters (in mm)	Abaza right	Abaza left	Gurcu right	Gurcu left
BDV diameter	23,50±4,07	23,27±3,55	25,82±2,14	26,06±2,13
BML diameter	26,40±1,65	25,63±3,25	27,47±1,61	27,41±2,33
Axial diameter	27,21±1,79	25,77±2,43	27,39±3,86	27,98±1,73
Cornea DV diameter	10,30±2,01	10,55±2,04	11,13±1,03	11,55±1,62
Cornea ML diameter	17,42±1,64	17,30±3,68	16,85±1,17	16,96±1,10
Pupillary DV diameter	5,45±0,2	5,54±0,1	8,37±1,24	8,38±1,26
Pupillary ML	9,13±0,7	9,47±0,7	9,42±1,54	9,45±1,51
Lens DV diameter	10,31±0,3	10,33±0,4	11,92±1,28	11,44±0,99
Lens ML diameter	11,08±0,3	11,24±0,3	11,61±0,36	11,89±0,64
Lens Thickness	7,24±0,4	7,25±0,4	7,69±0,95	7,67±1,08

Table 2. Correlation analysis of parameters taken from *bulbus oculi*

Abaza→ Gurcu↓	**DV diameter**	**ML diameter**	**Axial diameter**	**corDV**	**corML**	**PupiiDV**	**pupiiML**	**LensDV**	**lensML**	**Lens thickness**
DVdiameter		,604	,207	,158	-,249	-,136	-,385	,759*	,162	,659*
MLdiameter	,720*		-,318	,207	,585	-,098	-,048	,662*	,398	,702*
Axial diameter	,758*	,711*		-,161	-,547	-,433	-,612	,143	-,596	,135
corDV	-,265	-,281	-,094		,221	,734*	,434	-,214	,280	-,176
corML	-,298	-,138	-,141	,556		,110	,406	,017	,377	,167
PupiiDV	,864**	,477	,556	-,583	-,336		,488	-,385	,449	-,551
pupiiML	-,559	-,370	-,312	,893**	,650*	-,814**		-,526	,642*	-,417
LensDV	-,243	,047	-,222	,331	,065	-,541	,562		,197	,919**
lensML	,456	-,080	-,015	,130	,012	,444	-,085	,009		,090
Lens thickness	,980**	,808**	,802**	-,313	-,297	,826**	-,549	-,148	,353	

Table 3. Statistical data of similar parameters in other studied species, * M and F stand for 'Male' and 'Female,' respectively

Parameters (in mm)	BML	BDV	CML	CDV	PDV	PML	Lens Thickness
Buffalo (12)	35,10±0,38	34,3±0,42					8,67±0,15
Camel					right 2,04±0,21 left 2,08±0,23		
Sahel Goat M*/right	8,12±0,53	7,17±0,46					
M/left	8,14±0,34	7,09±0,37					
F*/right	8,34±0,36	7,21±0,49					
F/left	8,20±0,44	7,13±0,52					
Wad M/right	8,16±0,74	6,82±0,70					
Wad M/left	7,70±0,67	6,88±0,87					
Wad F/right	8,50	7,43±0,35					
Wad F/left	8,47±0,39	7,39±0,27					
Red skoto M/right	8,07±0,15	6,97±0,19					
Red skoto M/left	7,87±0,29	7,17±0,03					
F/right	8,83±0,34	7,70±0,34					
F/left	8,70±0,31	7,53±0,21					
Barbary Sheep			25,05±2,18	17,95±1,68			9,44±0,33
Awassi sheep M/right		25,95±0,49	21,99±0,30	17,08±0,26	6,75±0,28	11,88±0,29	8,87±0,21
M/left		26,56±0,53	21,98±0,32	16,87±0,38	7,38±0,33	11,83±0,35	19,28±0,16
F/right		29,33±0,44	24,09±0,38	17,88±0,43	7,49±0,28	13,58±0,24	10,08±0,14
F/left		28,38±0,46	24,39±0,40	18,66±0,40	7,69±0,24	13,71±0,74	10,36±0,16

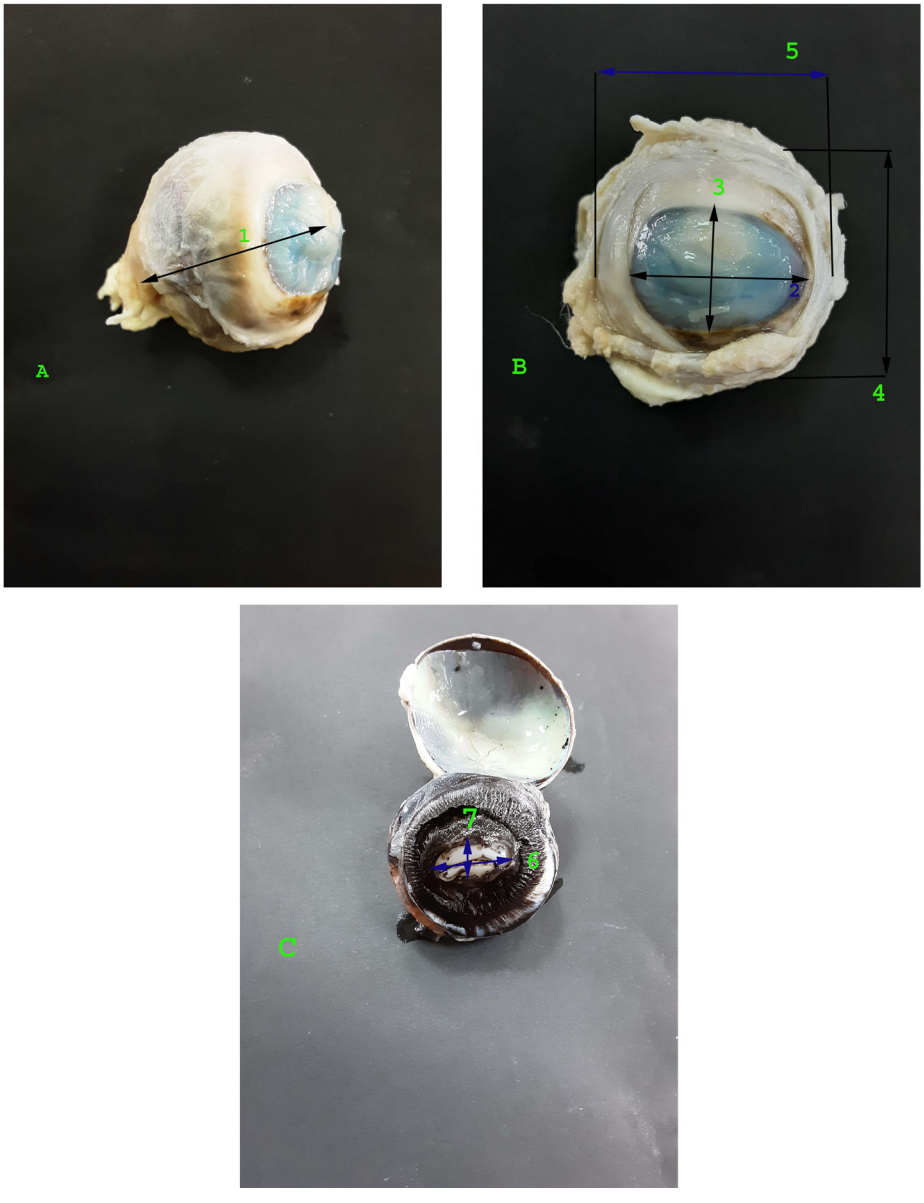

Fig. 1. Measuring points of samples taken over Bulbus oculi, (A, B, C): A: Axial length/ diameter: Distance between Polus anterior and pole posterior **(1)**, B: Medio-lateral (CML) diameter: Distance between temporal and nasal endpoints of the cornea **(2),** Dorso-ventral (CDV) diameter: Distance between the dorsal end of the cornea and endpoints in the ventral direction **(3)**, Dorso-ventral (BDV) diameter: Distance between the endpoint of the bulbus oculi in the dorsal direction and its ventral endpoints **(4)**, Medio- lateral (BML) diameter: Distance between temporal and nasal endpoints of bulbus oculi **(5)**, C: Medio-lateral (PML) diameter: Distance between temporal and nasal endpoints of *pupilla* **(6)**, Dorso-ventral (PDV) diameter: Distance between the endpoint of the *pupilla* in the dorsal direction and the endpoints in the ventral direction **(7)**.

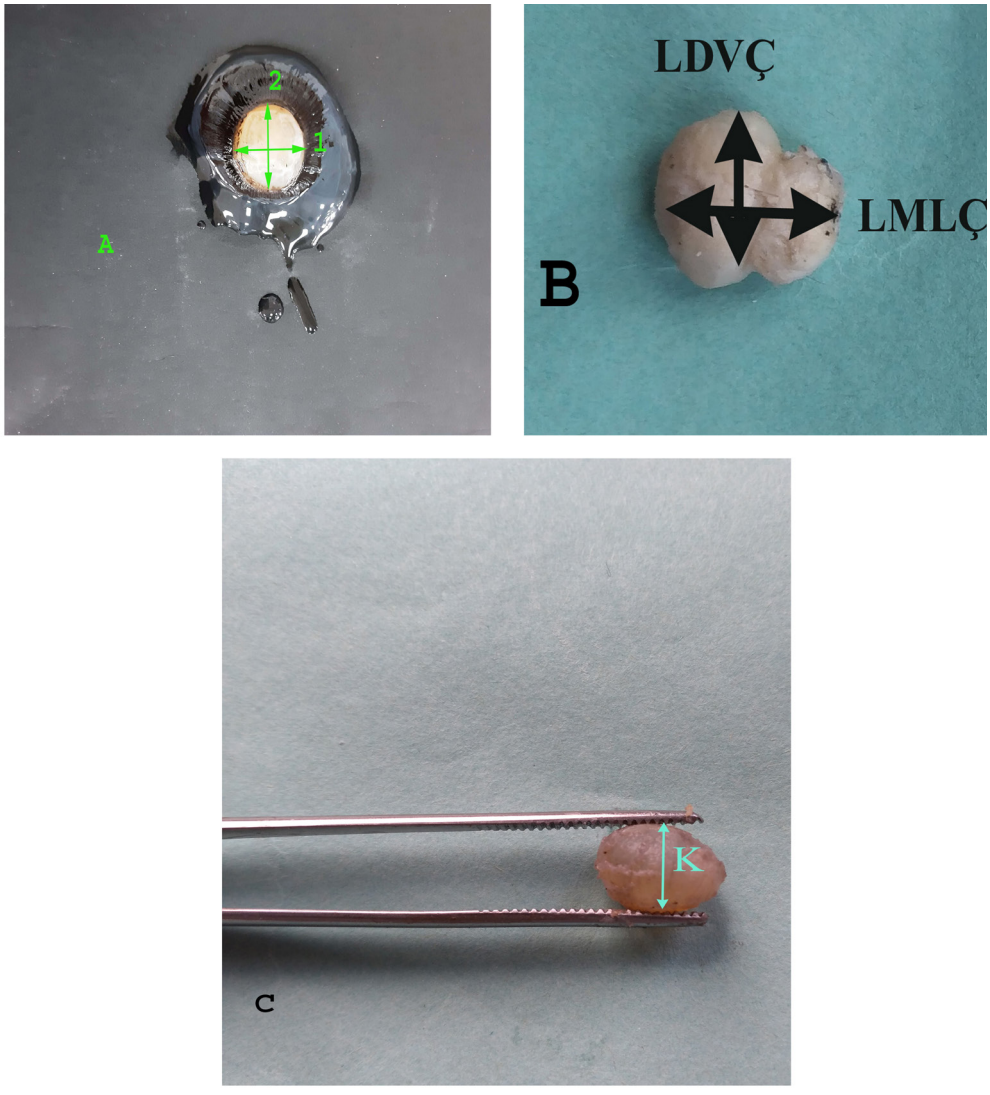

Fig. 2. (A, B, C): Lens measurement points **A:** Lens from Abaza goat**,** Dorso-ventral (LDV) diameter: Distance between the lens endpoint in the dorsal direction and the ventral direction **(1),** Medio-lateral (LML) diameter: Distance between the temporal and nasal endpoints of the lens **(2), B:** The same measurement points of the lens in Gurcu goats, **C:** Thickness: The distance from the middle point to the anterior and posterior endpoints of the lens.

Histological Results

Three main layers of the eyeball, the cornea and sclera (*from tunica fibrosa bulbi*), choroid, iris, *corpus ciliare* (from *tunica vasculosa bulbi*), and from *tunica interna* bulbi retina were studied histologically during the analysis of Abaza and Gurcu goats ocular structures.

Corneoscleral tegmental, sclera, and corneal structures the outer or fibrous layer were scrutinized. The sclera notably consisted of episcleral, *substantia propria*, and *lamina fusca* layers in both species. The propria of the sclera was explicitly composed of thick collagen fibers, and there were neural structures and blood vessels between the collagen fibers. The *lamina fusca* region on the opposite side of the choroid was composed of thinner collagen fibers than the substantia propria, and there were melanocytes between these fibers (**Fig. 3A**). Additionally, the distance between the *substantia propria* and episcleral layers of the sclera, known as Tenon's space

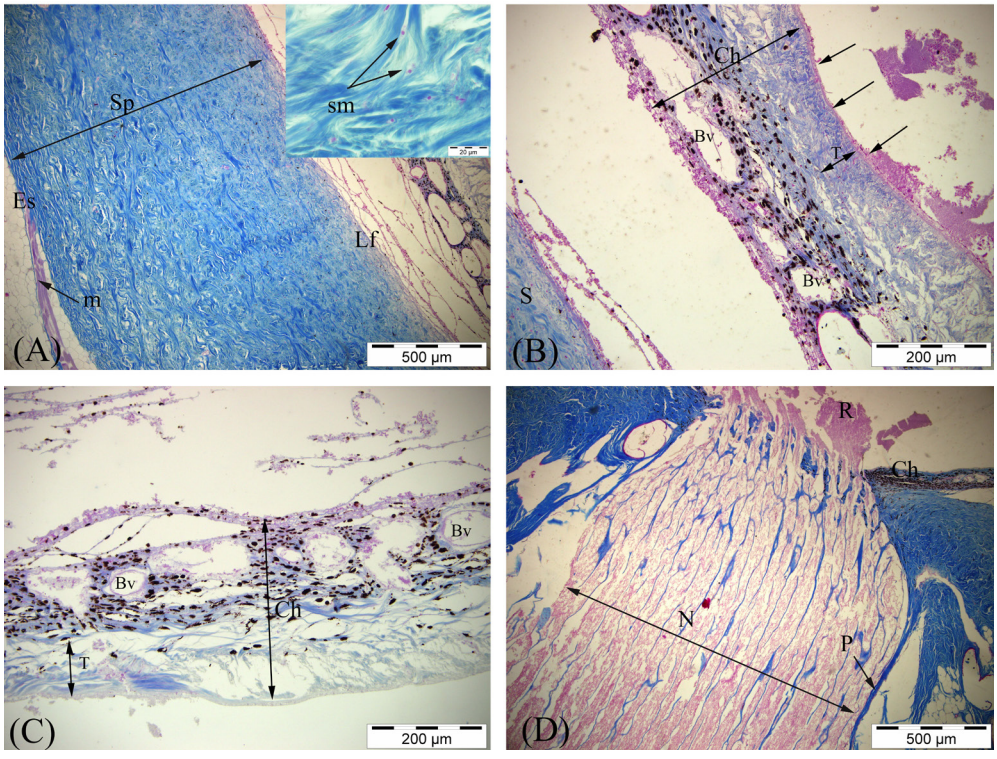

Fig. 3. Crossman's Modified Triple Staining of cross section of *bulbus oculi* A) Abaza goat sclera and choroid view, Ch: Choroid, Es: Episclera, Lf: Lamina fusca, m: muscle bundle in episclera, sm: smooth muscle, Sp: Substantia propria, S: Sclera, B) Abaza goat choroid, Bv: Blood vessel, Ch: Choroid, T: Tapetum fibrosum, Arrows: Retinal pigment epithelium, C) Gurcu goat choroid, Bv: Blood vessel, Ch: Choroid, T: Tapetum fibrosum, D) Ch: Choroid, R: Retina, S: Sclera, N: Optic nerve, P: Piameter, Triple stain.

(episcleral space), was identified. The cornea, the anterior segments of the eye, was identified to have a posterior surface consisting of a single-layered squamous epithelium, an anterior surface with stratified squamous non-keratinized epithelium, and a stroma in the middle. The stroma observably consisted of lamellar collagen fibers. Fontana clefts (the trabecular meshwork) and Schlemm's canal were explicitly definable in the corneascleral region (**Fig. 4A, B**). In both Abaza and Gurcu goats, the choroid appeared to contain five layers: from the bottom *lamina basalis* (Bruch's

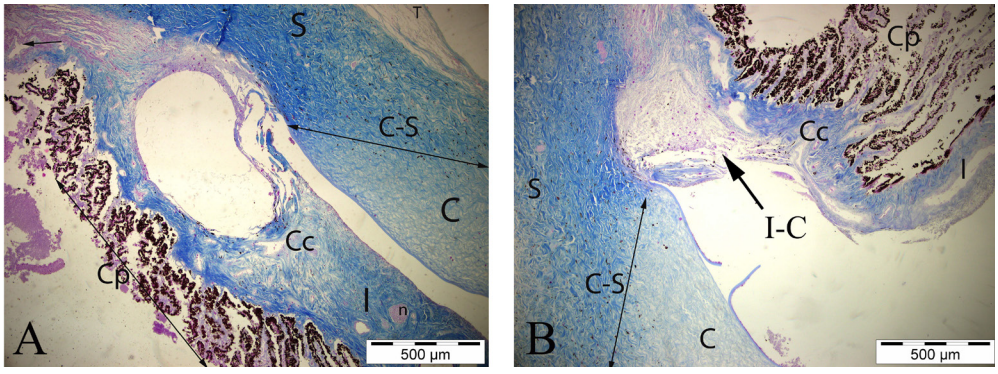

Fig. 4. Crossman's Modified Triple Staining of cross section of *bulbus oculi* A) Abaza Goat Corneoscleral Image, B) Gurcu Goat Corneoscleral Image, C: Cornea, Cc: Corpus ciliare, Cp: Ciliary processus, I: Iris, I-C: Iridocorneal region, n: Neural degradation, C-S: Corneoscleral cross, S: Sclera, T: Trabecular network, Triple stain.

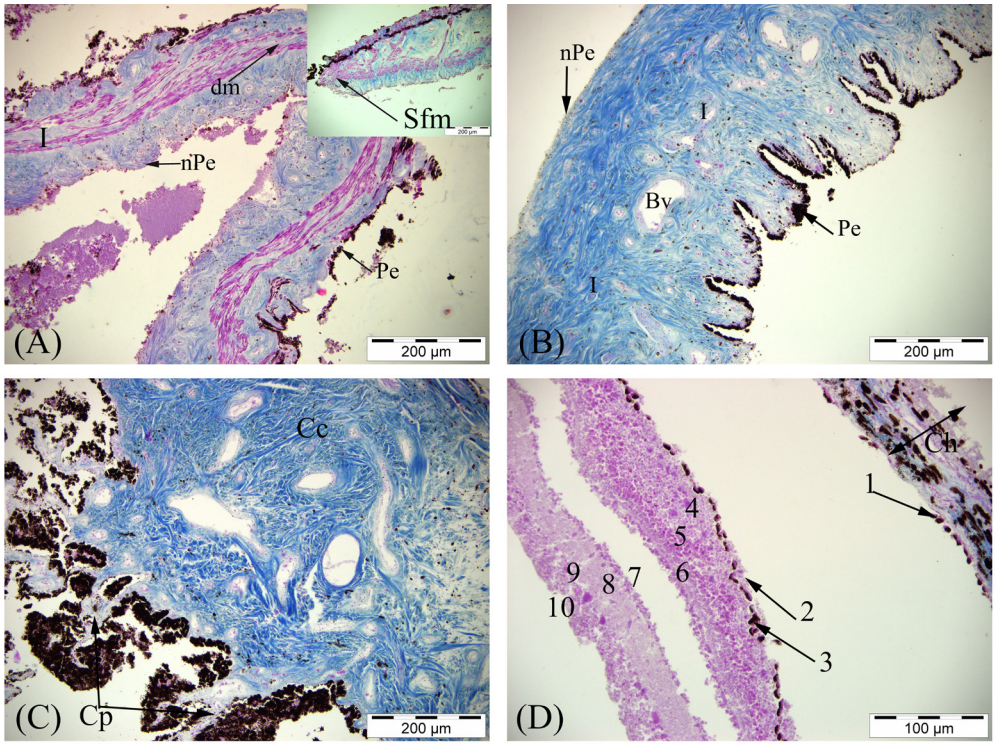

Fig. 5. Crossman's Modified Triple Staining of cross section of *bulbus oculi***.** A) Abaza Goat Iris view, B) Gurcu Goat Iris view C) Gurcu Goat Corpus ciliary view, Bv: Blood vessel, Co: Cornea, I: Iris, Cc: Corpus ciliare, Cp: Ciliary processus, dm: dilator muscle, nPe: Non-pigmented epithelium, Pe: Pigmented-epithelium, Sfm: Sphincter muscle, D) Retina, Ch: Choroid, 1: the pigmented layer of the iris, 2: rod and cone receptors layer, 3: *membrana limitans externa*, 4: outer nuclei layer, 5: outer plexiform, 6: inner nuclei layer, 7: inner plexiform, 8: ganglion cells layer, 9: neural fibers layer, 10: *membrana limitans interna*, Triple staining.

membrane), *lamina capillarum, tapetum fibrosum, lamina vasculosa* and the *lamina suprachoroidea* (**Fig. 3B, C**). The *tapetum fibrosum*, nevertheless, observably consisted of wider collagen fibers and contained fibroblasts. The tapetum of the choroid in Abaza goats (**Fig. 3B**) was more orderly and firmer when compared to Gurcu goats (**Fig. 3C**). However, it might display vary depending on the age or gender. In both species, the choroid structure had explicitly dense pigment cells. The *processus ciliaris* and *corpus ciliare* structures rimmed by a bilayer epithelium (cubic) were observed between the choroid and iris layers of the *tunica vasculosa bulbi* region (**Fig. 5C**). There were also several distinctly identified tissues, including pigmented iris epithelium tissue the subsequent section of the corpus ciliare, neural plexuses in the dense collagen fibers of the stroma, numerous melanocytes, blood vessels, dilator, and sphincter muscle structures (**Fig. 5A, B**). The retinal structure of the *tunica interna bulbi* section from outside-in retained ten observable layers (**Fig. 5D**). In addition, the *nervus opticus* rimmed by the perineurium and epineurium was identified (**Fig. 3D**).

Discussion

In Sahel goats, the right medio-lateral (ML) diameter of bulbus oculi was reportedly 8.12±0.53 mm and 8.34±0.36 mm, in males and in females respectively, whereas the left ML diameter was 8.14±0.34 mm in males and 8.20±0.44 mm in females [33], The same study reported the medio-lateral diameter of eyeball in two other goat breeds as follows in West African dwarf goats [33], the right and left diameters of mediolateral was 8.16±0.74 mm, and 7.70±0.67 mm in males, respectively; however, it was 8.50±0.00 mm and 8.47±0.39 mm for the right and left mediolateral diameters in females. In Red Sokoto goats [33], correspondingly, the right diameter of mediolateral was 8.07±0.15 mm, in males and 8.83±0.34 mm in females, whereas the left diameter of mediolateral was 7.87±0.29 mm in males and 8.70 ± 0.31 mm, in females.

Considering the mentioned goat breeds above, the DV diameter of the both side (Right/Left) *bulbus oculi* for Sahel goats [33], were 7.17±0.46 mm and 7.09±0.37 mm, in males, whereas it was 7.21±0.49 mm and 7.13±0.52 mm, for the right and left *bulbus oculi* in females, respectively. Similarly, the right and left diameters of dorsoventral of the *bulbus oculi* in West African dwarf goats [33] were (6.82±0.70) mm, and (6.88±0.87) mm, in males; however, it was (7.43±0.35) mm, and (7.39±0.27) mm, in females, respectively. The right and left DV diameters, on the other hand, were measured as 6.97±0.19 mm and 7.17±0.03 mm among Red Sokoto male goats [33], whereas it was (7.70±0.34) and (7.53±0.21) mm, for the right and left *bulbus oculi* in females, respectively. Another study focusing on Awassi sheep [13] reportedly measured the dorsoventral diameter of the right and left eyeball as (25.95±0.49) mm, and (26.56±0.53) mm, in males, whereas it was (29.33±0.44) mm and (28.38±0.46), mm in females, respectively. Medio lateral diameter of the Awassi sheep [13], however, was (28.11±0.42) mm and (27.50±0.39) mm, for the right and left eyes in males, respectively [13]. A study on *Bubalus bubalus* also reported the medio-lateral diameter of the bulbus oculi as (35.10±0.38) mm and the dorsoventral diameter as (34.3±042) mm [50]. The current study, on the other hand, measured the DV diameter of *bulbus oculi* in Abaza goats as 23.50±4.07 mm and 23.27±3.55 mm on the right and left, whereas it was 25.82±2.14 mm and 26.06±2.13 mm for the right and left in Gurcu goats.

The mediolateral diameter of the cornea was 25.05±2.18 mm, and the DV diameter was 17.95±1.68 mm in Barbary sheep (Ammotragus lervia) [17]. The study on Awassi sheep [13], however, the medio-lateral diameter of the cornea was (21.99±0.30) mm on the right side and, (21.98±0.32) mm on the left side in males, whereas it was (24.09±0.38) mm on the right and (24.09±0.40) mm, on the left side in females. The same study documented that the dorso-ventral diameter of the cornea was (17.08±0.26) mm, on the right and (16.87±0.38) mm, on the left side in females; however, these measurements were 17.88±0.43 mm, on the right and 18.66±0.40 mm, on the left in females. Considering the Barbary sheep (Ammotragus lervia), Fornazari et al. [17], reported the lens thickness as (9.4±0.33) mm. Verma et al., [50], measured a lens thickness of (8.67 ± 0.15) mm in buffalo (*Bubalus bubalus*). Similarly, the study on Awassi sheep reported that [13], mean lens thickness, was (8.87±0.21) mm and (19.28±0.16) mm, on the right and left side in males, whereas it was (10.08±0.14) mm, and (10.36±0.16) mm, on the right and left in females, respectively. The current study also measured the mean lens thickness in Abaza goats as 7.24±0.4 on the right and 7.25±0.4 mm, on the left. These measurements were comparable in Gurcu goats as the lens thickness on the right and left was 7.69±0.95 and 7.67±1.08 mm, respectively. The *pupilla* dorso ventral diameter ($P<0.001$***), lens dorso-ventral diameter ($P<0.005$**), and lens medio-lateral diameter ($P<0.05$*) parameters were all statistically significant in Abaza and Gurcu goats. However, the difference in lens thickness between the males and females in Awassi sheep [13], was statistically significant ($P<0.001$).

Abuagla et al., [1], reported the *pupilla* diameter among camels as 2.04±0.21 cm, and 2.08±0.23 cm, on the right and left, respectively. The same literature documented that the DV diameter of the pupil in Awassi sheep [13], was 6.75±0.28 mm, on the right and 7.38±0.33 mm, on the left in males, whereas it was 7.49±0.28 mm, on the right and 7.69 ± 0.24 mm, on the left in females. Additionally, they measured the ml diameter of the *pupilla* in Awassi sheep [13], as 11.88±0.29 mm, on the right and 11.83±0.35 mm, on the left in males; correspondingly, it was 13.58±0.24 mm, on the right and 13.71±0.24 mm, on the left in females. In Abaza goats, however, this study measured the DV and ML diameters of the pupilla as 5.45±0.2 mm, and 9.13±0.7 mm, on the right and 5.54±0.1 mm, and 9.47±0.7 mm, on the left, respectively. Similarly, the measurements for the same parameters in the Gurcu goats were 8.37±1.24 mm, and 9.42±1.54 mm, on the right and 8.38±1.26 mm, and 9.45±1.51 mm, on the left, respectively.

Tunica fibrosa bulbi (Sclera and cornea) is an outer section (Ross and Pawlina). Studies indicated that the sclera is composed of tightly packed collagen tissue in mammals, whereas some other vertebrates (such as geese and ducks) might additionally contain sclera structures such as cartilage or bone tissue [15, 34]. As in other mammalian creatures, the eye sclera of Abaza and Gurcu goats is histologically composed of three segments: Lamina fusca, stroma and episclera [21, 31], and these layers also contain collagen fibrils, with locally visible melanocytes and neural endings. Alternatively, the sclera part of the eyes in goats, buffalo, donkeys and cattle reportedly possessed bundles of smooth muscle cells [37]. In line with the literature, the current study also identified muscle cell bundles in the episclera of the goat's eye sclera.

The cornea is a transparent, densely innervated membrane that keep safe the eye from external traumas and foreign objects but contains no blood or lymphatic vessels. The structure of the corneas in several animals (donkeys, horses, wild and domesticated

ruminants, rodents, marine mammals, herbivores, pigs, bears, and primates) have reportedly been well-identified. In mammals, the cornea be composed of a non-keratinized stratified squamous epithelium in the upper section, Bowman's layers below the epithelium, stroma in the middle, Descemet's membrane and endothelium at the bottom [8, 20, 21, 23, 29, 31, 37]. The previous studies on the cornea of laboratory (experimental objects) and domestic animals reported no Bowman's layer in all species, albeit only primates might possess it [9]. The following studies, however, indicated that various mammalian species, including pigs [10], oxen [27], deer [38], bears [20], sheep [39], and dogs [35], reportedly possessed the Bowman layer. In line with the relevant literature, the current study also identified that the cornea of Abaza and Gurcu goats consisted of a well-located epithelial layer, a thin **Bowman's** swap, a stroma formed of wider collagen filaments, Descemet's membrane, and endothelium, as in other mammalian species. The current study additionally identified trabecular meshwork (Fontana slits) and Schlemm's canal structures in the corneascleral region.

In most domesticated mammalian animals, the choroid is composed of 5 layers: basal layer (Bruch's membrane), capillary layer, tapetal regionand, vascular layer and the suprachoroidal [5, 47, 25]. Both invertebrates and vertebrates possess tapeta. In vertebrates, the deep retina or choroid contains the tapeta. Considering the choroidal tapeta structures, there are two classes: tapetum cellulosum and tapetum fibrosum. The tapetum fibrosum contains no cells and consists of tightly packed collagen fibrils [44]. Ollivier et al. [32], reported that tapetum lucidum is absent in red kangaroos, pigs, primates, squirrels and birds, whereas it is present in reptiles, fish, dogs, bats, cows, cats, sheep, crocodiles, goats, lemurs, and weasels. In Abaza and Gurcu goats, the tapetum fibrosum layer in the choroid, which retains numerous melanocytes and blood vessels, observably consists of collagen fibril bundles arranged regularly. Furthermore, it was devoid of melanocytes.

In Abaza and Gurcu goats, the epithelial layer of the *corpus ciliare* and *processeus ciliaris* is internally pigmented and resembles that of camels [22], bears [20, 36] and sheep [12]. Both goat species observably contained two epithelial layers, albeit the upper one is non-pigmented. Like other mammals, the current study also identified extensive blood vessels, dilator and sphincter muscle structures, a wide collagen tissue, and neural endings locally in the iris stroma of Abaza and Gurcu goats. Surprisingly, the iris of Abaza goats has well-developed dilator and sphincter muscles. Histologically, however, the retina consisted of ten layers, much like in other mammalian species [3, 12, 14, 16, 20, 42, 48].

Conclusion

The literature reviews revealed that studies referenced the *bulbus oculi* in some domestic and wild animals. Contrary to the current study, however, no study in the literature reported comparative anatomical and histological analyses. It is essential for clinical research to identify the species-specific traits of this anatomical, morphometric, and histological study on Abaza and Gurcu goats. Therefore, it is anticipated that the findings of this study will contribute significantly to the scientific fields where animal, human and three-dimensional experimental models can be used in the field of ophthalmology.

References

1. **Abuagla, I. A., H. A. Ali, Z. H. Ibrahim.** An anatomical study on the eye of the one-humped camel (*Camelus Dromedarius*). – Int. J. Vet. Sci., **5 (3)**, 2016, 137-141.
2. **Akın, F., E. Samsar.** *Goz hastaliklari*, Ankara, Medipres, 2005. [in Turkish]
3. **Altunay, H**. Fine structure of the retinal pigment epithelium, bruch's aembrane and choriocapillaris in the ostrich (*Struthio camelus*). – *Anat. Histol. Embryol.,* **33**, 2004, 38-41.
4. **Babu, A. P., P. J. Ramayya, Y. Nagamalleswari, M. Sreenu, K. L. Kavitha.** Histological studies on ageing changes in the retina of buffaloes (*Bubalus bubalis*). - *Indian J. Anim. Res.*, 2022.
5. **Bacha, J. W., M. L. Bacha.** *Color atlas of veterinary histology*, 2nd Edition, Philadelphia, Lippincott Williams & Wilkins, 2000.
6. **Bedford, P, G., I. Grierson.** Aqueous drainage in the dog. – *Res. Vet. Sci*., **41(2)**, 1986, 172–186.
7. **Bolon, B., R. H. Garman, I. D. Pardo, K. Jensen, R. C. Sills, A. Roulois, A. Radovsky, A. Bradley, L. Andrews-Jones, M. Butt, L. Gumprecht**. STP position paper: Recommended practices for sampling and processing the nervous system (brain, spinal cord, nerve, and eye) during nonclinical general toxicity studies. – *Toxicol. Pathol*., **41(7)**, 2013, 1028–1048
8. **Cafaro, T. A., M. F. Suarez, C. Maldonado, J. O. Croxatto, C. Insfran, J. A. Urrets-Zavalia, H. M. Serra.** On the cornea of healthy Merino sheep: A detailed ex vivo confocal, histological and ultrastructural study. – *Anat. Histol. Embryol.*, **44**, 2015, 247– 254.
9. **Calmettes, L., F. Deodati, H. Planel, P. Bee.** Etude histologique et histochimique de L'epithelium anterieur. – *Arch. Ophthalmol*., **16**, 1956, 481–506. [in French]
10. **Camber, O., C. Rehbinder, T. Nikkila, P. Edman.** Morphology of the pig cornea in normal conditions and after incubation in a perfusion apparatus. – *Acta Vet. Scand.*, **28 (2)**, 1987, 127-134.
11. **Crespo-Moral, M., L. Garcia-Posadas, A. Lopez-Garcia, Y. Diebold.** Histological and immunohistochemical characterization of the porcine ocular surface. – *PloS ONE,* **15(1)**, 2020.
12. **Dalga, S., İ. S. Aksu, K. Aslan, T. Deprem, R. Uğran.** Anatomical and histological structures of eye and lacrimal gland in Norduz and Morkaraman sheep. – *Turk. J. Vet. Anim. Sci*., **46(2), 18**, 2022.
13. **Demircioğlu, İ., B. Yılmaz.** Morphometric investigation of bulbus oculi of Awassi Sheep (*Ovis aries*). – *Dicle Üniversitesi Veteriner Fakültesi Dergisi*., **12 (2)**, 2019, 108-111. [in Turkish]
14. **Derbalah, A, E, M.** Light & Electron microscopical studies on the eye of one – humped camel (*Camelus dromedaries*). *M.V.Sc. Thesis*, Alexandria University, 2002. [in Turkish]
15. **Dursun, N.** *Anatomy of domestic birds*. Ankara, Medisan Publishing House, 2008. [in Turkish]
16. **Ehrenhofer, M. C. A., C. A. Deeg, S. Resse, H. G. Liebich, M. Stangassinger, B. Kaspers.** Normal structure and age related changes of the equine retina. – *Vet. Ophthal*., **5(1)**, 2002, 39-47.
17. **Fornazari, G. A., F. Montiani-Ferreira, F. I. R. Barros, A. T. Somma, B. Somna.** The Eye of the Barbary Sheep or Aoudad (*Ammotragus lervia*): Reference values for selected ophthalmic diagnostic tests, morphologic and biometric observations. – *Open Vet. J*., **6(2)**, 2016, 102-113.
18. **Gierek, A., M. Sosniez, B. Bialas, A. Szymanski**. Morphological picture of the iridocorneal angle of the human eyeball viewed under a scanning electron microscope. – *Ophthalmologia*, **169**, 1974, 371-376.

19. **Hassa, O., R. N. Aştı**. *Embriyoloji.* Ankara, Yorum Basın Yayın Sanayi LTD ŞTİ, 2003. [in Turkish]
20. **Kirbaş D. G., T. S. Koral, S. Dalga, A. S. İlhan.** Anatomical and histological studies on the eyes of brown bear (*Ursus arctos horribilis*). – *Turk. J. Vet. Anim. Sci*., **44**, 2020, 871–878.
21. **Klećkowska-Nawrot, J. E., K. Goździewska-Harłajczuk, M. Darska, K. Barszcz, M. Janeczek.** Microstructure of the eye tunics, eyelids and ocular glands of the Sulawesi bear cuscus (*Ailurops ursinus* Temminck, 1824) (*Phalangeridae: Marsupialia*) based on anatomical, histological and histochemical studies. – *Acta Zool*., **100(2)**, 2019, 183-208.
22. **Kotb, A. M.** Comparative morphological studies on the vascular tunic of the eyeball in some domestic mammals. *M.V.Sc. Thesis*, Assiut University, 2006.
23. **König, H. E., H. G. Liebich.** *Anatomia zwierzat domowych***.** Łódź, Galaktyka, 2006. [in Polish]
24. **König, H. E., H. G. Liebich.** *Veterinerinary anatomy of domestic animals*, 6th Edition, Schattauer GmbH, 2014.
25. **Malsawmkima, B. R. K., Y. L. Vyas, D. M. Bhayani**. Histomorphological study on vascular tunics of the adult Surti buffalo (*Bubalus bubalis*). – *Int. J. Interdiscip. Multidiscip. Stud.*, **2**, 2014, 24-28.
26. **McMenamin, P. G., R. J. Steptoe.** Normal anatomy of the aqueous outflow system in the domestic pig eye. – *J. Anat*., **178**, 1991, 65-77.
27. **Merindano, M. D., J. Costa, M. Canals, J. Potau, D. Ruano.** A comparative study of Bowman's layer in some mammals: relationships with other constituent corneal structures. – *Eur. J. Anat.,* **6**, 2002, 133-40.
28. **Miller, K. A**. Ocular motility and binocular vision (Sights and sounds in ophthalmology), St. Louis, Mosby Co, 1989.
29. **Nautscher, N., A. Bauer, M. Steffl, W. M. Amselgruber.** Comparative morphological evaluation of domestic animal cornea. – *Vet. Ophthal.,* **19(4)**, 2016, 297-304.
30. **Nomina Anatomica Veterinaria (NAV)** 6th Edition, World Association of Veterinary Anatomists, Hanover (Germany), Ghent (Belgium), Columbia, MO (U.S.A.), Rio de Janeiro (Brazil), 2017.
31. **Nickel, R., A. Schummer, E. Seiferle.** The anatomy of the domestica nimals. Berlin, Springer, 2004.
32. **Ollivier, F. J., D. A. Samuelson, D. E. Brooks, P. A. Lewis, M. E. Kallberg, A. M. Komáromy.** Comparative morphology of the *tapetum lucidum* (among selected species). – *Vet. Ophthal.*, **7(1)**, 2004, 11-22.
33. **Olopade, J. O., H. D. Kwari., I. O. Agbashe, S. K. Onwuka.** Morphometric study of the eyeball of three breeds of goats. – *Int. J. Morphol.,* **23(4)**, 2005, 377-380.
34. **Öktay, M.** *Comparative anatomy of vertebrate animals*. Istanbul, İstanbul Üniversitesi Fen Fakültesi, 1998, 340-353. [in Turkish]
35. **Paszta, W., J. E. Klećkowska-Nawrot, K. Goździewska-Harłajczuk.** Anatomical and morphometric evaluation of the orbit, eye tunics, eyelids and orbital glands of the captive females of the South African painted dog (*Lycaon pictus pictus* Temminck, 1820) (*Caniformia: Canidae*). – *PloS ONE*, **16(4)**, 2021.
36. **Paszta, W., K. Gozdziewska-Harłajczuk, J. Kleckowska-Nawrot.** Morphology and histology of the orbital region and eye of the asiatic black bear (*Ursus thibetanus*) similarities and differences within the *Caniformia* suborder. – *Animals*, **12**, 2022, 801.
37. **Prince, J. H., C. D. Diesem, I. Eglitis, G. L. Ruskall.** *Anatomy and histology of the eye and orbit in domestic animals*. Springfield, Charles C. Thomas Blackwell Scientific Publications, 1960.
38. **Rehbinder, C., G. Winqvist, C. Roos.** Structure of the cornea in some *Cervidae*. – *Acta Vet. Scand.*, **18**, 1977, 152-158.

39. **Reichard, M., M. Hovakimyan, A.Wree, A. Meyer-Lindenberg, I. Nolte, C. Junghans, R. Guthoff, O. Stachs.** Comparative in vivo confocal microscopical study of the cornea anatomy of different laboratory animals. – *Cur. Eye Res.,* **35(12)**, 2010, 1072-1080.
40. **Ripolles-Garcia, A., G. Ruthel, G. S. Ying, Y. Chen, N. Cuenca, G. D. Aguirre, W. A. Beltran**. Characterization of the canine retinal vasculature with optical coherence tomography angiography: Comparisons with histology and fluorescein angiography. – *Front. Neuroanat*., **15**, 2021.
41. **Saadatlou, M. A. E.** Histoanatomical studies of the fibrous tunic of eye in Dromedary camel. – *Kafkas Universitesi Veteriner Fakültesi Dergisi*, **23(6)**, 2017, 911-915.
42. **Samuelson, D. A.** *A textbook of veterinary histology***.** Philadelphia, Saunders (Elsevier), 2007.
43. **Samuelson, D., P. Smith, D. Brooks.** Morphologic features of the aqueous humor drainage pathways in horses. – *Am. J. Vet. Res.,* **50(5)**, 1989, 720–727.
44. **Schwab, I. R., C. K. Yuen, N. C. Buyukmihci, T. N. Blankenship, P. G. Fitzgerald**. Evolution of the tapetum. – *Trans. Am. Ophthalmol. Soc.,* **100**, 2002, 187-99.
45. **Schwieder, A., C. Pfarrer, B. Ohnesorge, C. Staszyk, A. Bienert-Zeit.** Comparative studies on the histological characteristics of equine nasomaxillary aperture and paranasal sinus mucosa considering topographic and age-related differences. – *Acta Vet. Scand*., **62(1)**, 2020, 34.
46. **Serbest, A.** Sensory organs. In: *Anatomy of domestic mammals and poultry,* Bursa, Uludağ Üniversitesi Veteriner Fakültesi, 2010. [in Turkish]
47. **Slatter, D. H.** *Fundamento de oftalmologia veterinaria*. 3rd Edition. Sao Paulo, Roca, 2005. [in Spanish]
48. **Soliman, S. M., S. M. Adam, U. K. M. Abd allah.** Light and electron microscopic structure of goat's retina. – *J. Vet. Med. Res.*, **20(1)**, 2010, 52-62.
49. **Tekelioğlu, M. Özel** *histoloji, ince yapı ve Gelişme.* Ankara, Antıp Yayınları, 2002. [in Turkish]
50. **Verma, A., A.Pathak, M. M. Farooqui, A. Prakash, K. Prabhakar.** Gross and morphometrical observations of eyeball in buffalo calf (*Bubalus bubalus*). – *Rum. Sci.*, **5(2)**, 2016, 169-172.
51. **Vrolyk, V., M J. Desmarais, D. Lambert, J. Haruna, M. O. Benoit-Biancamano**. Neonatal and juvenile ocular development in göttingen minipigs and domestic pigs: a histomorphological and immunohistochemical study. – *Vet. Pathol*., **57(6)**, 2020, 889-914.
52. **Wang, J., Z. Hongpeng, J. Jing, W. Lixuan, L. Wenxin, H. Yuan, L. Xuan, F. Guangyu, C. Kinon.** A histological study of atherosclerotic characteristics in age-related macular degeneration. – *Heliyon*., **8(3)**, 2022.
53. **Yıldırım, M., I. Okar, H. Dalkıç.** İnsan *embriyolojisi klinik yönleri***,** Istanbul, Nobel Tıp Kitabevleri, 2002. [in Turkish]

Institute of Experimental Morphology, Pathology and Anthropology with Museum
Bulgarian Anatomical Society

Acta Morphologica et Anthropologica, 31 (1-2)
Sofia ● 2024

Survey on Virtual Microscopy versus Light Microscopy in Histological Education among Students in Medicine and Dental Medicine

Zdravka Harizanova[*], *Ferihan Popova, Pepa Atanassova, Stoyan Novakov, Yvetta Koeva, Nadya Penkova*

Department of Anatomy, Histology and Embryology, Faculty of Medicine, Medical University – Plovdiv, Bulgaria

*Corresponding author e-mail: zdravka.harizanova@mu-plovdiv.bg

Virtual microscopy (VM) involves digitally photographing tissue sections on microscope slides and provides a physically distant opportunity for histology education. This method was particularly important during the Covid-19 pandemic. The aim of the present study was to verify the students' opinion on this innovative method and its implementation in histological education. 152 UK and 50 Bulgarian students at Medical University of Plovdiv participated. We performed a survey using Google Forms test among the students. The students think that virtual microscopy will increase the understanding of the microscopic structures but cannot replace the conventional light microscopy and teacher guidance. 147 of them prefer studying histological sections via both methods. Virtual microscopy represents a modern tool with increased quality and utility in microscopy education. However, the role of the teacher and the light microscopy are also very significant and using both methods will provide the most beneficial training in histology.

Key words: histology, light microscopy, medical education**,** virtual microscopy

Introduction

Medical histology has been a basic science course in the medical school curriculum worldwide [3]. A sound knowledge of microscopic anatomy and histology is of fundamental importance in medical training and education. Since the middle of the 19th century, light microscopes and histological specimens have been used. In Heidelberg, in 1846, Jacob Henle became the first anatomist (and pathologist) to introduce a microscopy course where every student worked at an individual microscope. At the beginning of the 20th century, projectors were introduced to the market with the aid of which the microscopic specimens could be projected onto a screen. This method has been used for a long time [13]. During the late 20th century electron photomicrographs

were introduced. Such methods depend on the availability of suitable classroom space (microscopy lab) with rigid opening hours and a teacher [14]. Since the beginning of the 21st century there has been a huge technological development allowing histological specimens to be scanned. Afterwards these images are compressed and stored on the Web or disks. The Covid-19 pandemic led to the cancelation of face-to-face teaching [5]. The academics sought to create an environment that balanced student independence with teacher guidance. Research has shown that an active learning approach to histology teaching that incorporates Virtual microscopy leads to a beneficial outcome on student success [4, 12, 15]. Virtual microscopy is an emerging technology which provides a physically distant opportunity for histology and histopathology education. It involves digitally photographing tissue sections on microscope slides using one or more microscope objectives at one or more focal planes. Furthermore, Virtual microscopy software reproduces a high-quality image with meticulous clarity and added features that allow students and teachers to highlight, annotate, and zoom. Using computer software these images can be viewed on a monitor. Magnification and focus can be adjusted by clicking the mouse button [10].

In the Department of Anatomy, Histology and Embryology of Medical University-Plovdiv students in Medicine and Dental medicine study Cytology, General histology and Embryology and Organ Histology using conventional light microscopy plus a histological database of digital microscopic slides on CDs and USB flashes and stored in SharePoint (Microsoft). Our team participates with specialists from Romania, Spain, and Poland in an international Erasmus project which aims to scan microscopic slides using Leica Aperio AT2 scanner and upload them in a shared virtual platform to upgrade our existing slides collection.

Aim

Based on the long experience of our department with the use of a histological database of digital microscopic slides, the aim of the present study was to verify the opinion of the Medical University-Plovdiv students on this innovative method – virtual microscopy and their attitude to its implementation in anatomical and histological education, especially if distant learning is required.

Subjects and Methods

152 UK students at Medical University of Plovdiv participated (61 males and 91 females). 122 of them were students in medicine and 30 were in dental medicine, 127 of them were in first year and 25 were in second year. 50 Bulgarian students also took part in the survey (26 males and 24 females), 41 of them were students in medicine, 9 in dental medicine, 25 of them were first year and 25- second year.

We performed a survey via Google Forms test which included 10 yes-and-no questions as well as multiple choice questions on the students' opinion based on media and internet.

Our histological database contains slide collection images taken on Leica microscope model DM3000LED equipped with a digital camera model Leica FLEXACAM C3. The used microscopic magnifications are x100 and x400. The average size of the image files is 1.2 MB, and the type of the image is JPEG.

Results

Statement 1. Virtual microscopy will increase students' level of understanding for the microscopic structures.

Ninety four (68.8%) of the UK students think that Virtual microscopy will increase their level of understanding of the microscopic structures, 9 (5.9%) of them disagree with that and 49 (32.2%) are not sure about the statement. At the same time 22 (44%) of the Bulgarian students agree with the statement, 13 (26%) do not and 15 (30%) are not sure (**Fig. 1**).

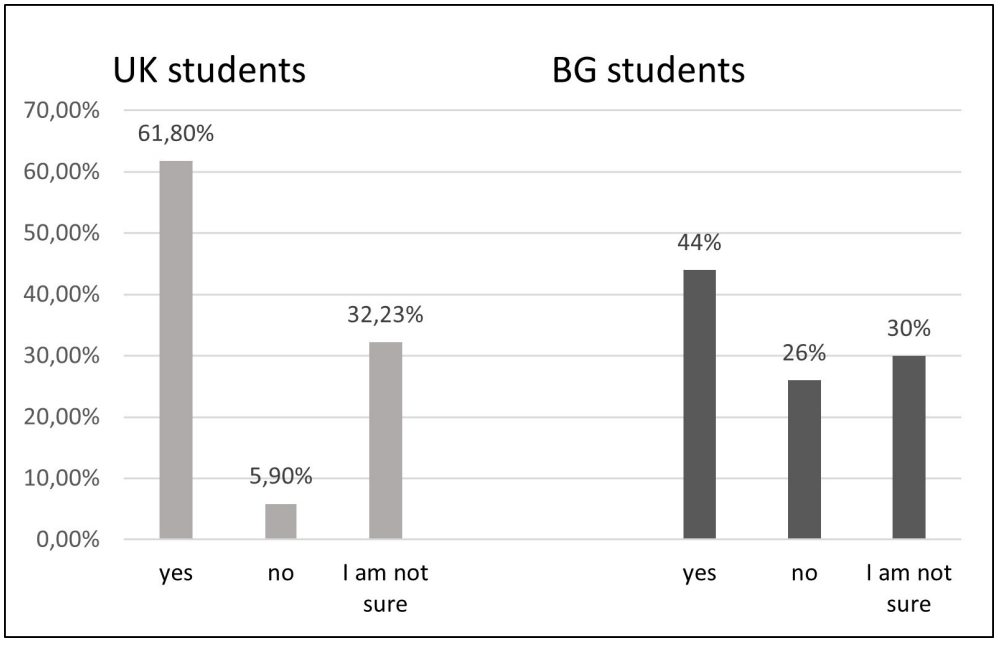

Fig. 1. Do you think that VM will increase your level of understanding the microscopic structures?

Statement 2. Limitations for using Virtual microscopy.

When asked what limitations they think Virtual microscopy might have 9 (5.9%) of the UK students answer hardware limitations, 15 (9.9%) say software limitations, 22 (14.5%) state internet connection, 41 (27%) give lack of experience as an answer and most of them - 65 (42.8%) think that all these reasons will limit them. 2 (4%) of the BG students answer hardware limitations, 3 (6%) say software limitations, 3 (6%) state internet connection, 20 (40%) give lack of experience as an answer and again most of them – 22 (44%) think that all these reasons will limit the usage of VM (**Fig. 2**).

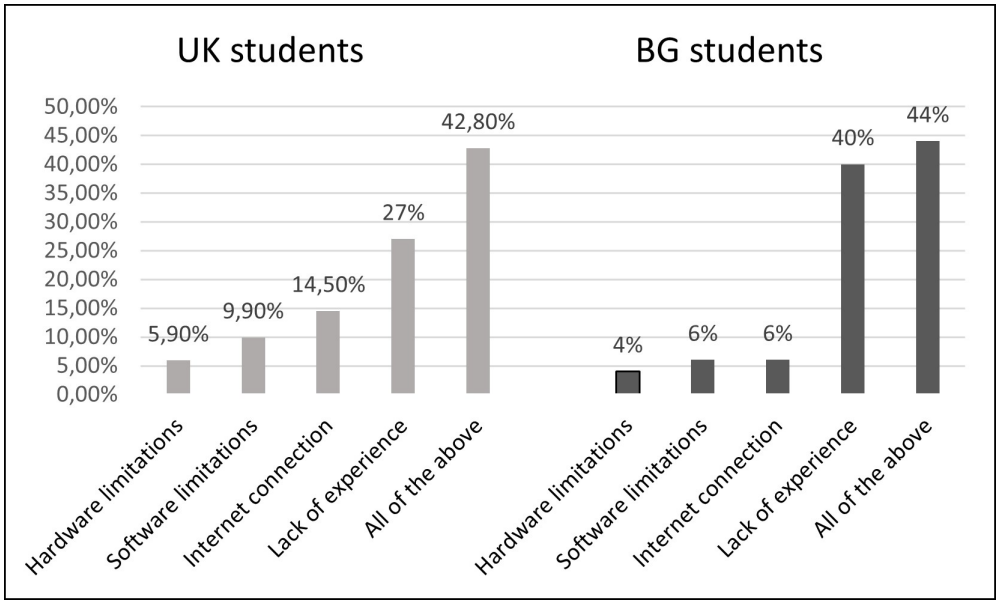

Fig. 2. What limitations do you think VM might have?

Statement 3. Virtual microscopy can replace the teacher's role.

Thirty one (20.4%) of the UK students agree with the statement that Virtual microscopy can replace the teacher in studying microscopic structures, 23 (15.1%) are not sure, but most of them – 98 (64.5%) disagree with the statement. At the same time 4 (8%) of the BG students agree, 3 (6%) are not sure and again most of them – 43 (86%) disagree (**Fig. 3**).

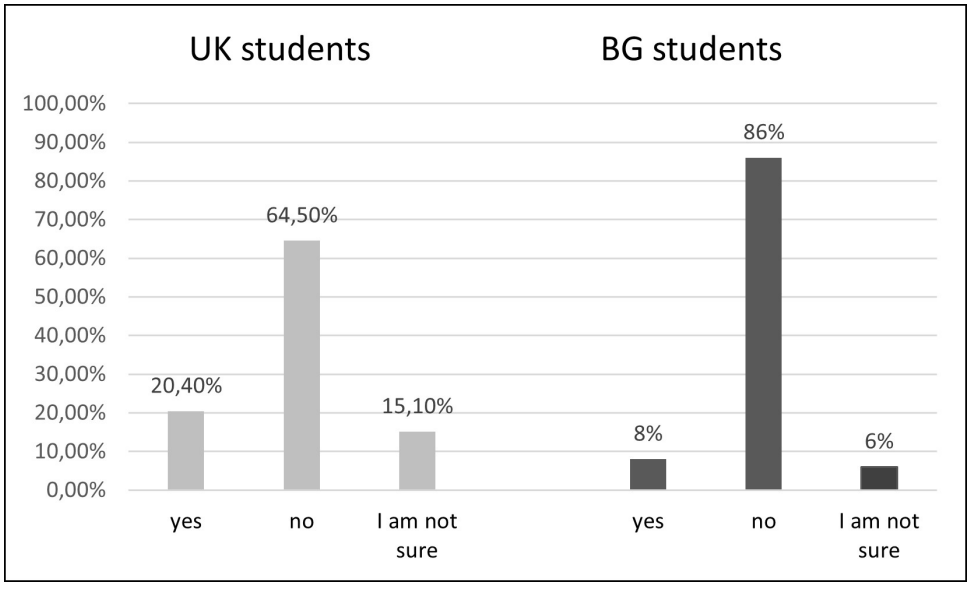

Fig. 3. Do you think that VM can replace the teacher in studying microscopic structures?

Statement 4. Virtual microscopy will make studying easier.

Ninety five (62.5%) of the UK students think that Virtual microscopy will make their studying easier, 8 (5.3%) do not share this opinion and 49 (32.2%) are not sure. 25 (50%) of the BG students also agree with the statement, 13 (26%) disagree and 12 (24%) are not sure (**Fig. 4**).

Statement 5. Which method do students prefer?

When asked which method they prefer to study microscopic structures, 21 (13.8%) of the UK students answer conventional microscopy, 19 (12.5%) say virtual microscopy, but most of them - 122 (80.3%) state they prefer combined method. 14 (28%) of the BG students say they prefer conventional microscopy, only one answers virtual microscopy and again most of them - 35 (70%) respond they prefer combined method (**Fig. 5**).

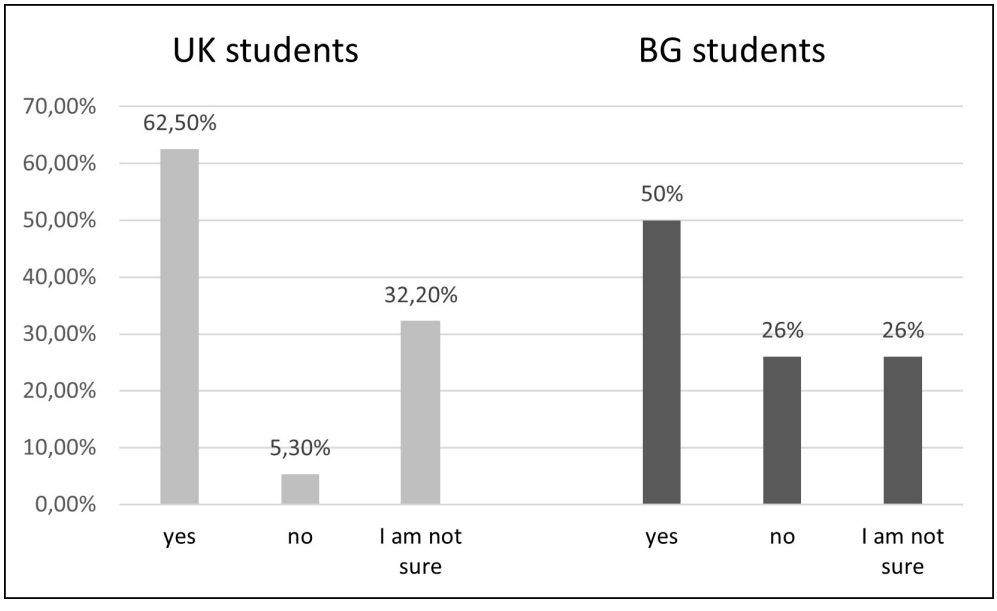

Fig. 4. Do you think that VM will make your studying easier?

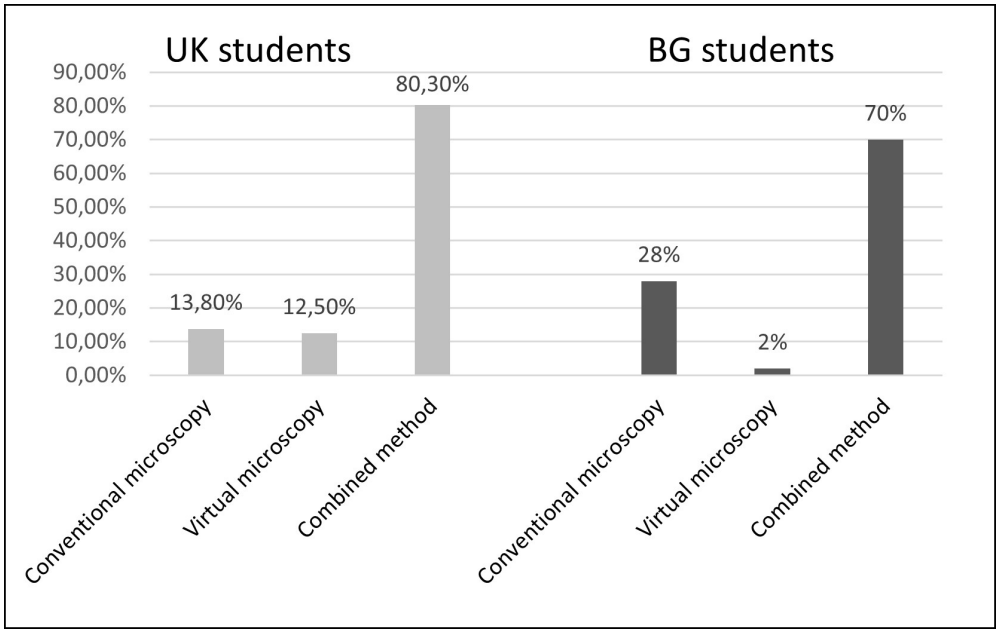

Fig. 5. You prefer studying microscopic structures by:

Discussion

The course in "Cytology, Histology and Embryology" in medical studies in the Medical University of Plovdiv is a mandatory propaedeutic step in teaching the fundamental discipline Human Anatomy. Students acquire knowledge of the basic structural elements in the human body: cells, tissues. The aim of the histology course in medical studies in the Department of Anatomy, Histology and Embryology is to give students knowledge of the normal microscopic structure of the human eukaryotic cells, tissues, and organs. Thus, they can apply this knowledge in the distinction of histopathology structures. This is of main importance later in the differential diagnosis of various non-tumor and tumor diseases. Considering the latter, the practical in-person classes aim to train students in using conventional light microscopes during their first two years of education, while the online usage of JPEG files of the microscopic slides in USB drive helps the students with detailed learning and knowledge validation of the histological structures of human tissues and organs. Similar training approach is used in the histopathology studies in medical universities in Bulgaria. The histology and histopathology studies in Medical University - Plovdiv are conducted in microscopic rooms equipped with conventional microscopes for each student in the presence of an assistant professor. Some of the microscopic rooms are equipped with a microscopic system connected to the teacher's screen allowing control of the observing slides. A teacher's screen is connected to a TV monitor and a white board is available for discussions and to focus on certain histological and histopathological structures.

This course is considered highly challenging by the students, so histology academics committed to improve student learning by incorporating Virtual microscopy in teaching especially with the rapid acceleration in the use of computers and the Web [5]. Universities such as the University of Copenhagen [16], the University of South Carolina School of Medicine [5], the University of Iowa [8], the University of Los Angeles, CA [16] have been using virtual slides and microscopes since year 2000. According to surveys among the students at these universities they prefer the accessibility and efficiency of the Virtual Microscope Laboratory versus the regular microscope laboratory. Regular microscope laboratories were opened during the day, while Virtual Microscope Laboratory could be used without limitations. This was very useful for the students especially before practical examinations. In addition, students rated the quality of images and navigation of the virtual microscope equal to or better than a real microscope. Virtual slides are always in focus with ideal condenser and light adjustment, thus decreasing the student time and some of the frustration in operating a real microscope [9, 2, 11]. All students have identical slides. This reduces student complaints that the slides in their individual collection were not as good as those of a fellow student. Furthermore, Virtual Microscopy incorporated in a virtual platform on the Web allows sharing information between different universities which is not possible with glass slide collection.

As in other universities Covid-19 pandemic led to cancelation of face-to-face teaching for a few months. This has provoked our team at the Department of Anatomy, Histology and Embryology in Medical University- Plovdiv to create an environment that combines student independence with teacher guidance. In this relation, we decided to validate our students' opinion upon Virtual Microscopy and its implementation in histology teaching. 68.8 % of the UK students and 44 % of the Bulgarian ones state that Virtual Microscopy will increase their level of understanding the microscopic structures while 32.2 % of the UK students and 30 % of the Bulgarian ones are not sure. 62.5 % of the UK students and 50 % believe that Virtual Microscopy will make their studying in histology easier by reducing the time and accessing the specimens wherever and whenever they choose. Over two thirds of the students that participated in a similar survey at the University of South Carolina also found using virtual slides easier than light microscope and glass slides. They agreed that using this method saved them time [3].

However, we believe that student-teacher communication is of great importance for the most beneficial outcome from learning histology. This totally corresponds to our students' opinion. When asked if they think that Virtual Microscopy can replace the role of the teacher 64.5 % of the UK students and 86 % of the Bulgarian ones disagree with the statement. Anatomical and histological sciences should not be delivered predominantly online, particularly programs that are designed to equip students with practical skills in medical laboratories. This opinion refers to other universities also [6, 15, 1]. In our university, most anatomical and histological work is performed using a microscope, which is a vital skill for medical students, therefore development of skills face to face in the laboratory is the golden standard for teaching. The situation is the same in University of South Australia [4] and other universities [7]. This is in total agreement with our students' opinion. 80.3 % of the UK students and 70 % of the Bulgarian ones state that they prefer studying the microscopic structures using combined method, both conventional and virtual microscopy.

Conclusion

The results of the current survey revealed that the medical students in our university prefer studying the microscopic structures using combined methods, both conventional and virtual microscopy. According to our students‘ opinion Virtual microscopy represents a modern tool that will increase their level of understanding of the microscopic structures. However, for our students the role of the teacher and the light microscopy are also very significant and using both methods will provide the most beneficial training in histology.

Acknowledgements: This work is part of international project, co-funded by the European Union and Erasmus+ program, with the participation of Medical University of Plovdiv, titled "Digital transformation of Histology and Histopathology by Virtual Microscopy (VM) for an innovative medical school curriculum" with Ref. no.: 2022-1-RO01-KA220-HED-000089017.

R e f e r e n c e s

1. Attardi, S. M., S. Choi, J. Barnett, K. A. Rogers. Mixed methods student evaluation of an online systemic human anatomy course with laboratory. – *American Association of Anatomists*, **9**, 2016, 272-285.

2. Barbeau, M. L., M. Johnson, C. Gibson, K. A. Rogers. The development and assessment of an online microscopic anatomy laboratory course. – *American Association of Anatomists*, **6**, 2013, 246-256.

3. Blake, Ch. A., H. A. Lavoie, C. F. Millete. Teaching medical histology at the University of South Carolina, School of Medicine: Transition to virtual slides and virtual microscopes. – *Anatomical record. Part B, New anatomist*, **275(1)**, 2003, 196-206.

4. Bloodgood, R. A. Active learning: A small group histology laboratory exercise in a whole class setting utilizing virtual slides and peer education. – *Anat. Sci. Education,* **5,(6)**, 2012, 367-73.

5. Caruso, M. C. Virtual microscopy and other technologies for teaching histology during Covid-19. – *Anat. Sci. Education*, **14(1)**, 2021, 19-21.

6. Evans, D. J. R., B. H. Bay, T. D. Wilson, C. F. Smith, N. Lachman, W. Pawlina. Going virtual to support anatomy education: A STOPGAP in the midst of the Covid-19 pandemic. – *Anat. Sci. Educ.*, **13**, 2020, 279-283.

7. Franchi, T. The impact of the Covid-19 pandemic on current anatomy education and future careers: A student's perspective. – *Anat. Sci. Educ*., **13**, 2020, 312-315

8. Harris, T., T. Leaven, P. Heidger, C. Kreiter, J. Duncan, F. Dick. Comparison of a virtual microscope laboratory to a regular microscope laboratory for teaching histology. – *Anat. Record,* **265**, 2001, 10-14.

9. Heidger, Jr. PM, F. Dee, D. Consoer, T. Leaven, J. Duncan, C. Kreiter. Integrated approach to teaching and testing in histology with real and virtual imaging. *Anat. Record*, **269(2**), 2002, 107-12.

10. Krippendorf, B. B., L. John. Complete and rapid switch from light microscopy to virtual microscopy for teaching medical histology. – *Anatomical Record. Part B, New anatomist*, **285(1),** 2005, 19-25.

11. Lee, B. C., S. T. Hsieh, Y. L. Chang, F. Y. Tseng, Y. J. Lin, Y. L. Chen, S. H. Wang, Y. F. Chang, Y. L. Ho, Y. H. Ni, S. C. Chang. A web-based virtual microscopy platform for improving academic performance in histology and pathology laboratory courses: A pilot study. – *Anat. Sci. Educ.,* **13**, 2020, 743-758.

12. **Nauhria, S., P. Ramdass**. Randomized cross-over study and a qualitative analysis comparing virtual microscopy and light microscopy for learning undergraduate histopathology. – *Indian J. Pathol. Microbiol.,* **62(1**), 2019, 84-90.
13. **Paulsen, F., M. Eichhorn, L. Bräuer**. Virtual microscopy-The future of teaching histology in the medical curriculum? - *Ann. Anat.,* **192(6**), 2010, 378-82.
14. **Tian, Y., W. Xiao, Ch. Li, Y. L. Liu, M. Qin, Y. Wu, L. Xiao, H. Li**. Virtual microscopy system at Chinese medical university: an assisted teaching platform for promoting active learning and problem-solving skills. – *BMC Medical Education*, **14(1)**, 2014, 74.
15. **Vainer, B., N. W. Mortensen, S. S. Poulsen, A. H. Sørensen, J. Olsen, H. H. Saxild, F. F. Johansen.** Turning microscopy in the medical curriculum digital: Experiences from the faculty of health and medical sciences at University of Copenhagen. – *J. Pathol. Inform*., **8**, 2017, 11
16. **Wong, M., J. Frye, S. Kim, A. M. Marchevsky**. The use of screencasts with embedded whole-slide scans and hyperlinks to teach anatomic pathology in a supervised digital environment. – *J. Pathol. Inform* , **9(1)**, 2018, 39.

Institute of Experimental Morphology, Pathology and Anthropology with Museum
Bulgarian Anatomical Society

Acta Morphologica et Anthropologica, 31 (1-2)
Sofia ● 2024

Review Articles

History of the Red Nucleus, its Tracts and Species Evolutionary Choice

Enrico Marani

Tiboel Siegenbeekstraat 15, 2313HA Leiden, The Netherlands;

Corresponding author e-mail: enrico.marani@outlook.com

The red nucleus is a constant in the vertebrate brain. A general pattern of its tracts can be discerned, which is differently applied in human's, mammalian's and bird's brains. At the base of the difference is the magnocellular and parvocellular parts. The magnocellular part axons travel to the contralateral spinal cord, while the parvocellular part projects to the ipsilateral inferior olive. This olivary projection, part of the dentate-rubro-olivary pathway, is associated with olivary hypertrophy. In rodents both red nucleus parts can contribute to the rubro-spinal tract and its development is described. The history of the separation of both human tracts is explained. In birds the crossed tract is solely present and magnocellular and parvocellular areas are debated. The spino-rubral connection is described in relation to perturbation of movements. Special scientific advances discussed concern: asymmetry of the red nucleus, ruber and migraine, mutation and olivary hypertrophy, the red nucleus and POU domain and ruber involvement in restless legs syndrome.

Key words: immuno(cyto)chemistry, rubrospinal, rubro-olivary, tegmental tracts

Introduction

Recently two review articles that concern the red nucleus have been published [1,42]. The general tendency of these articles is that our current knowledge of the anatomy of the red nucleus and its functions are underestimated in research. These overviews of red nucleus research are produced with some important topics unaccounted for that mainly are related to its history. This article starts with highlighting some historic points and pays attention to recent discoveries in the light of previous research.

Architectural stamped (neuro)anatomists

The fundamentals of our knowledge of the brain macroscopy have their origin in the baroque period, starting with the contra-reformation after the Council of Trent

(1545–1563), hence around 1600. It ended towards the French revolution (1750/1780). The Rococo style started in France around 1720, but the baroque kept its influence in architecture after 1720. The baroque seventeenth century was an age of high monarchy. Royal absolutism was the governmental system in France, which was taken over from Renaissance Italy. Protection of arts, stimulation of science and of architecture are the main characteristics of this princely atmosphere in Europe. Architecture elaborated into city planning Versailles, construction of Schönbrunn outside Vienna and creating Sans Souci at Potsdam. The start towards it, the baroque period and its slow ending at the end of the eighteen century all contributed to the interest in the other architecture, that of the brain [29].

These ancient, architectural stamped, (neuro)anatomists studied and named the brain structures from their own daily experience: best known is the naming of "mammillary bodies" mirroring the view on the female breasts in a Bavarian "dirndel" (tavern wench) dress. The cerebellar tonsils resemble the inside of the throat with two inflamed tonsils and the colliculus superior and inferior were compared to the buttocks or nates with its hanging testes below it. This naming habit started far earlier. For example, the Latin nautical term "puppi," referring to the stern of a ship, was applied to the cerebellum in the eleventh century [67]. Niels Stensen (1638-1686) already remarked that using these "household" terms for neuroanatomical structures indicates that the user presumably does not know the real meaning of these brain areas [22]. Description of the brain structure through the ages gives: Varolio (1543-1575) in 1573 discerned cerebrum, spinal marrow and cerebellum, Willis (1621-1675), in 1664, adds striate body, optic thalamus and tectum and its full subdivision is not earlier than by Meynert (1833-1892) in 1872 (**Fig. 1**, [58]).

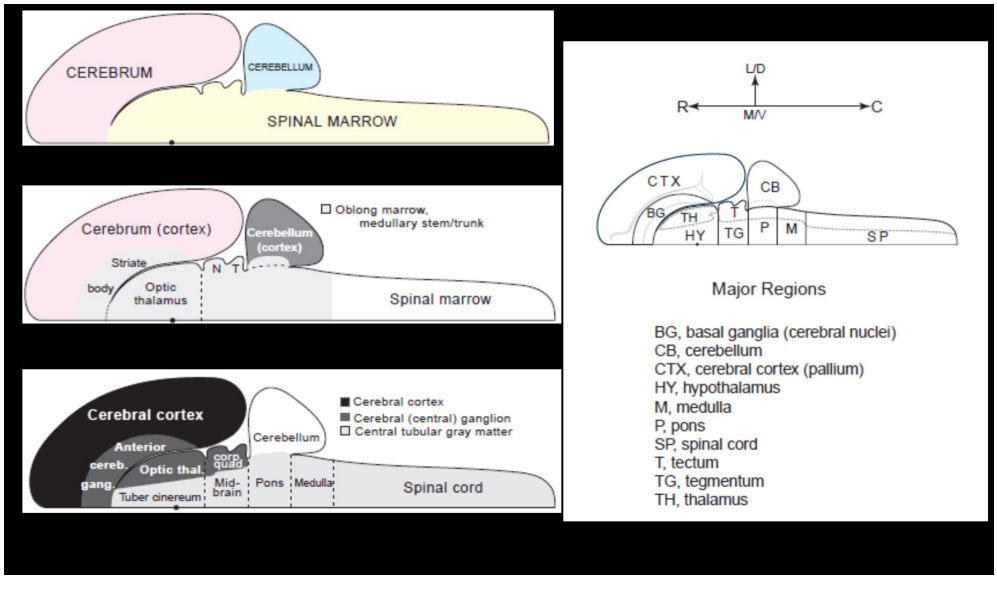

Fig. 1. Segmental subdivision of the brain by Varolio, Willis and Meynert leading to the nowadays accepted brain partition in ten parts ([58]; fig. [33])

Red nuclei and its tracts

The red nucleus is a group of neurons located high in the brainstem, containing small and large neurons that shows a light red glow in non-fixed sections by which it was detected by these early (neuro) anatomists (**Fig. 2**). Note that some scientists name it a small mesencephalic grey matter structure [18], while others termed it a large subcortical structure [1].

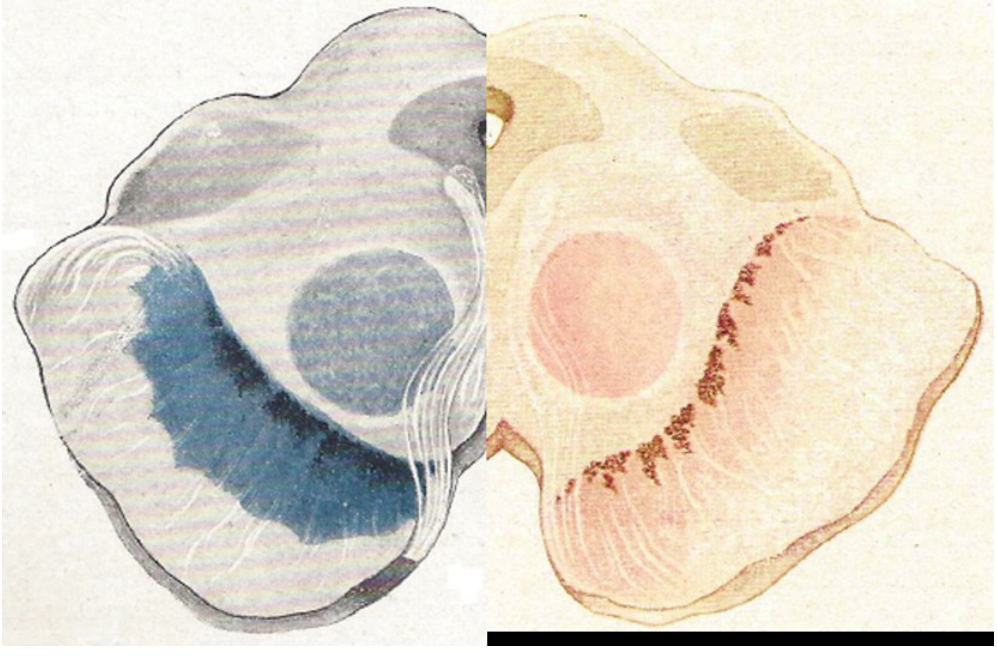

Fig. 2. The human nucleus ruber (red nucleus) stained for iron (left, Berlin blue reaction) and its natural appearance in a mesencephalic section (right). Note that the substantia nigra, in the foot of the brain section, shows the same phenomena (Burdach, 1822,"rother Kern" [7]).

Thus, red nucleus is not a "household" name, but it is based on its visual reality. It is also believed that the red nucleus looks pale pink due to the presence of iron in it. The cause of the pinkish appearance is the presence of a higher concentration of capillaries than the direct environment of the nucleus ("sehr gefässreiches", [39]), which is confirmed by the high amount of blood vessel alkaline phosphatase in this nucleus. Massion [37] denies this, but his figure demonstrates high vessel content. It is also characterized by the presence of a large amount of iron (**Fig. 2**) and high concentrations of vitamin B2 [14]. One should also note that this nucleus is one of the few that contains even higher concentrations of iron in Parkinson's dyskinesia [28] and of Parkin, a Parkinson's disease related protein [71]). As a result, this nucleus can also be noted microscopically and biochemically, which is used for colouration of the tissue, and as such it has intrigued these ancient neuroanatomists, also by its size and connections (see [39]). Microscopy brought the solution and it is now an ordinary mesencephalic large nucleus involved in cerebellar circuits (**Fig. 3**) and in spinal cord steering. The rubrospinal tract shows activity during automated, already

learnt, movements [23]. The red nucleus has been subdivided into a parvocellular part that derives the central tegmental tract (orange in **Fig. 3A**) and a magnocellular part, the origin of the rubro-spinal tract. Its rubro-spinal tract was for the first time described by von Monakow in 1883 [40]. Counterpart is the medial tegmental tract by which the nucleus of Darkschewitsch (**Fig. 3B**) is the most important contributor with the interstitial nucleus of Cajal and the nucleus of the fields of Forel [41].

The red nucleus is present in humans, all other mammals [20] and in birds. Amphibians, reptiles, and various fish do have a red nucleus. This review centres on comparing likeness in structure between nuclei of different organisms. Similarity between nuclei of different species has to be based on three arguments: likeness in localisation (topography), likeness in cell architecture and a likeness in connections of the nucleus. Nevertheless, such a similarity will not be absolute. We start with the rat and cat as mammal exponents, describe the human red nucleus to end with the pigeon. Note that reptiles and amphibians do have a "red nucleus", but it is considered a small and differently built nucleus. The primitive red nucleus is difficult to border in the ventral mesencephalon, but still does serve the connections between cerebellum via cerebellar nuclei and the spinal cord. It is omitted in this overview due to its cytological difference in similarity to other vertebrates, by its absence of olivary projections (anurans: frogs, toads, tree frogs) and the non-existence of cortical connections (quadrupedal reptiles). In lower vertebrates the presence of a red nucleus and its rubrospinal tract is linked to the presence of limbs or limb-like structures [12, 61].

The nuclei in the brainstem, including the red nucleus, have been classified as open and closed nuclei by their dendritic extensions towards other nuclei [30]. The magnocellular part of the red nucleus is considered a closed part, while the parvocellular red nucleus neurons are heavily involved in dendritic spread within the neighbouring reticular formation neurons. Borders of the capillary rich red nucleus can be established despite the parvocellular open structure (**Fig. 2**). The red nucleus produces, in origin, two output connections that derive from its parts: a series of connections that are grouped into a tract, which stays at the same side as the nucleus is placed and a series of connections that are fasciculated at the other side of the nucleus, its contralateral tract. Since the brainstem is bilaterally symmetric we do have four tracts, two crossed and two uncrossed. One side "should" contain a crossed and uncrossed tract.

The rat rubrospinal tract during development

Lakke's study in the *rat* [26] included also the development of the connections of the red nucleus [27]. The red nucleus in rat receives cortical information and is involved in the cerebellar and spinal systems. By its bulbospinal and rubrospinal tracts the red nucleus projects contralaterally to: the nucleus reticularis lateralis, the nucleus facialis, the nucleus interpositus, the nucleus vestibularis descendens, the nucleus cuneatus, and the spinal cord; ipsilaterally to the nucleus ventralis lateralis thalami (see [27] for references). The connection of the red nucleus to the nucleus olivaris inferior has been denied in the rat [55]. However, the parafascicular prerubral area, a diffuse nucleus directly above and partially aside of the nucleus ruber, around the fasciculus retroflexus and near the ventricle, does project to the olivary nucleus [54]. This parafascicular prerubral area is in the same position and contains the same function as a parvocellular red nucleus [53]. The rat's red nucleus tracts contain a crossed one for the spinal cord that reaches high (cervical) and low (lumbosacral) parts of the spinal cord [8].

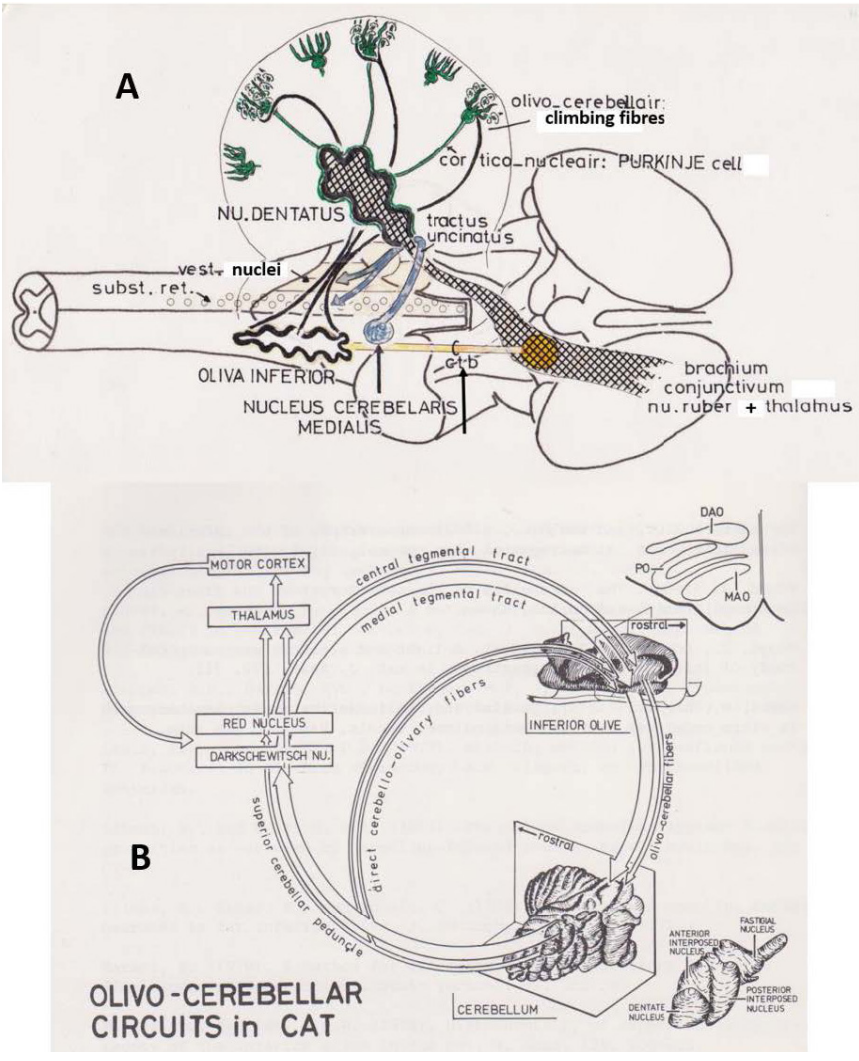

Fig. 3A. Overview of cerebellar connections with the tractus uncinatus in blue, brachium conjunctivum black-crossed and the central tegmental tract in orange (ctb arrow; fig. from exposition "cerebellum" Gesellschaft für Histochemie, 1983, Gargellen). **B**: The neural connections involved in the red nucleus by its participation in the olivo-cerebellar circuits, Darkschewitsch nucleus and inferior olivary complex of the cat. The inferior olive (top right) can be subdivided into three main parts: the dorsal accessory olive (DAO) the principal olive (PO) and medial accessory olive (MAO). Cells of the inferior olive project to the cerebellar cortex as climbing fibres. These fibres constitute the olivo-cerebellar tract. Within the cerebellar cortex the intrinsic connections relay the information towards the cerebellar nuclei (bottom right). The output system of the cerebellar nuclei is the superior cerebellar peduncle, which terminates in the contralateral red nucleus and the nucleus of Darkschewitsch. The cerebellar nuclei also project back to the inferior olive. A closed loop exists because both the red nucleus and the Darkschewitsch nucleus project back to the inferior olive by the central and medial tegmental tract respectively. The output of this closed loop is through axons of the cerebellar nuclei that project on the thalamus (fig. [31], courtesy J.Voogd).

Following injections of horseradish peroxidase or wheat germ agglutinin-horseradish peroxidase conjugate into the spinal cord, at different levels and at different gestational ages the rubrospinal tract development could be followed (**Fig. 4**). By embryonic day 17 (E17) fibers from all subdivisions of the nucleus ruber have started their descent towards the spinal cord. On E18 fibers from the ventrolateral red nucleus arrived into the lower cervical spinal cord, while those from the caudal nuclear area terminate into the lower thoracic spinal cord. At E19 fibers from the dorsomedial red nucleus and from the parvicellular area have just reached the cervical spinal cord, while fibers from the ventrolateral and caudal areas have appeared into lower thoracic levels. At E21 fibers from the dorsomedial red nucleus have turned up into the lower cervical spinal cord. Fibers from the ventrolateral and caudal nucleus finished their descent through the lumbosacral spinal cord during the first three postnatal days. During their descent the rubrospinal fibers are limited to the white matter of the spinal cord (**Fig. 4**). In general, early descending fibers originate from neurons located caudally and ventrolaterally, and later descending fibers from neurons located more rostrally and dorsomedially in the magnocellular red nucleus. The sharp distinction of the connections between magnocellular and parvocellular parts of the red nucleus as kept by the overviews [1, 42]), is less present in the rat in the course of its development and during its maturity [23].

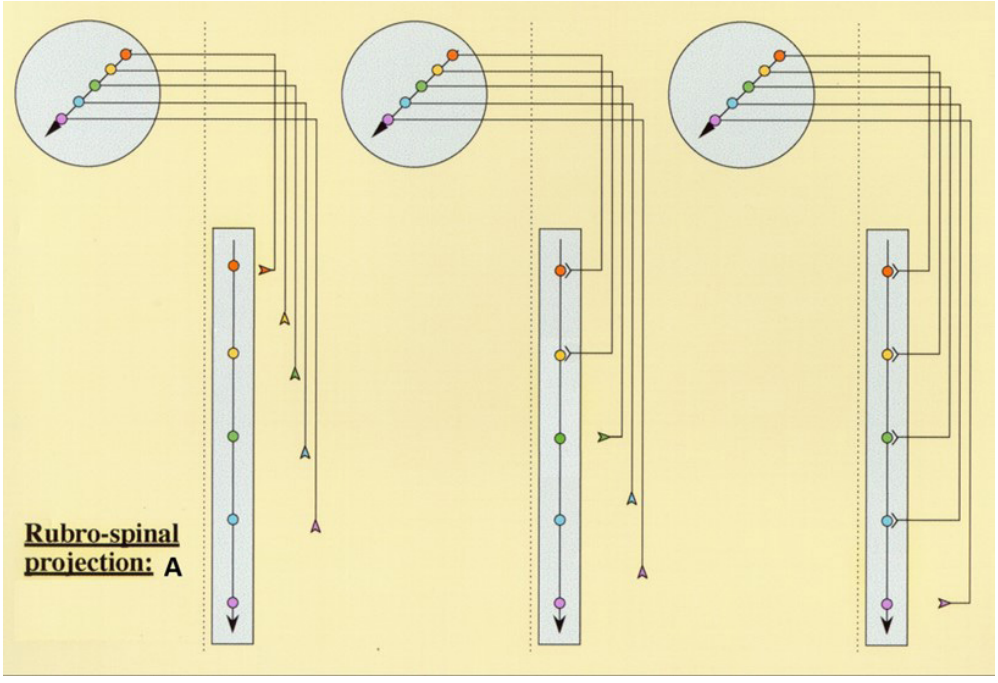

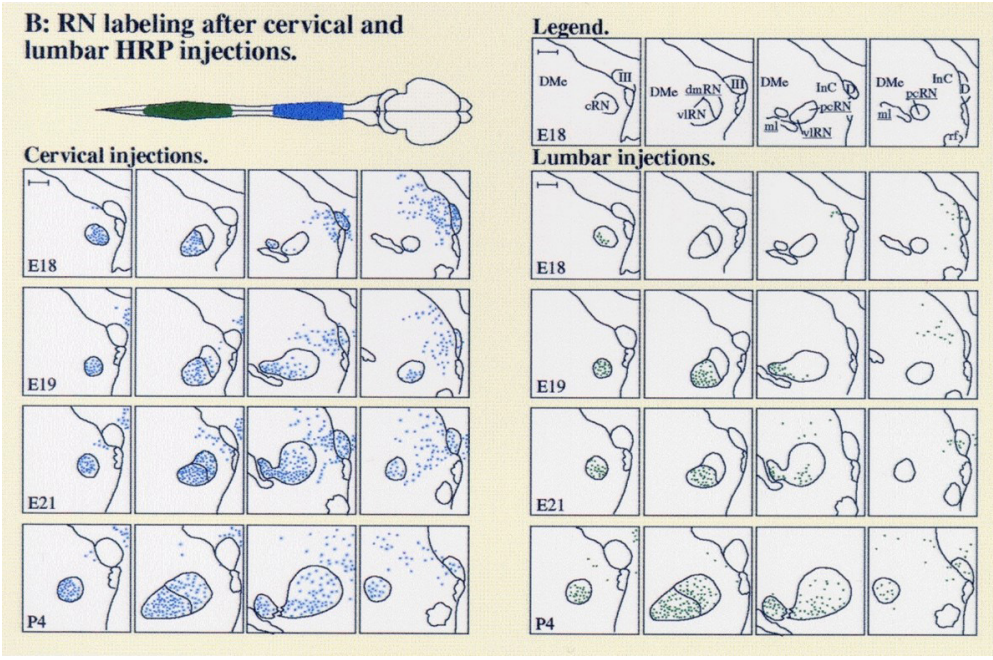

Fig. 4. In **A** the descending spinal fibres of the red nucleus are shown at their topography in the rubro-spinal tract during descent. **B**, shows the labelling of the red nucleus after HRP injections at cervical and lumbar levels (courtesy E. Lakke; Legend: III, oculomotor nucleus; DMe, nucleus reticularis mesencephalicus profundus; InC, nucleus interstitialis Cajal; D, nucleus Darkschewitsch;, ml lemniscus medialis; rf, fasciculus retroflexus).

Red nucleus and tracts in humans as well as olivary hypertrophy

In humans the steering of motor activities had been subdivided in pyramidal and extrapyramidal guiding or differently said a direct cortical influence (pyramidal) and an indirect one (extrapyramidal). The indirect cortical steering (Bechterew, 1885 [2]) should go over the red nucleus as was deduced from animal and clinical research as described by Probst [49] for the central tegmental connection. The human nucleus contains also large and small cells. It was Verhaart (1889-1983; for cv see [66]), who unravelled the human nucleus ruber connections due to his comparative neuroanatomical approach. Verhaart [62, 63] finalized his results on the red nucleus in "The central tegmental tract" in 1949 [64]. This uncrossed tract was exclusively related to the red nucleus. The crossed rubrospinal tract in humans was found inconstant and of "slight dimension", and "through the development of the frontal part of the red nucleus and the regression of the caudal part, this nucleus has changed its character from a pre-eminently motor nucleus to a nucleus connected to the olivocerebellar system" (Verhaart, [63]). Simply said, part of the nucleus was reduced compared to other mammalian red nuclei. Its crossed spinal projecting part was minimally present and hardly reached the start of the cervical spinal cord. Sie Pek Giuk [56], working at Verhaart's department, showed that 20% of the myelinated red nucleus fibres originated in the magnocellular part. "In the bipedal human, the magnocellular red nucleus is rudimentary" [43]. This overstated

claim has been contradicted by tractography studies on 100 persons in the Human Connectome Project, in which a clear localisation of the human magnocellular part was encountered: “note that the magnocellular regions appear well delineated in the upper slices located dorsally” [9].

Several publications have been considering the cooperation between the corticospinal and rubrospinal tracts. These studies use corticospinal tract damage also in humans (for overview see [44]). Lesions in the animal red nucleus are compensated by the corticospinal tract and by damage of the corticospinal tract recompense has been noticed in the cortico-rubro-spinal connections. In upper limb steering the red nucleus is responsible for pronation, while the cortico-spinal tract relates to arm reach and hand grip. Since in humans the rubro-spinal tract does not reach (below) cervical levels, it is puzzling that the red nucleus is still involved in improvement of the mobility of patients with cortico-spinal tract and spinal cord damage [42].

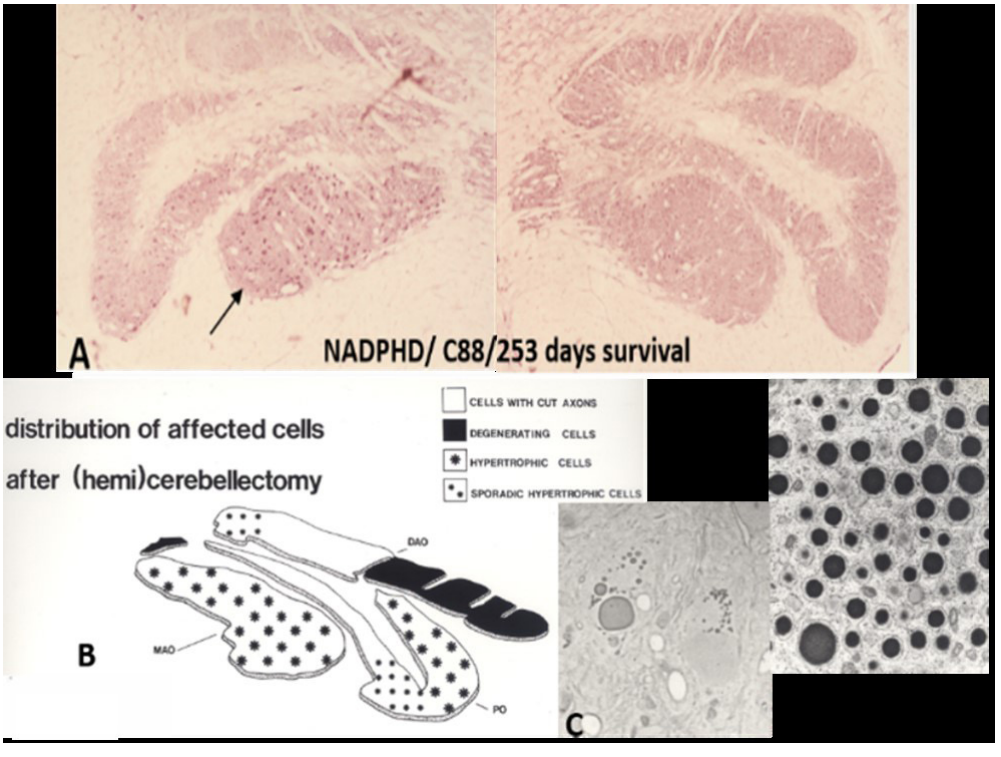

Fig. 5. Experimentally induced olivary hypertrophy in the cat. **A**: Increased enzymatic activity of NADPHD after a survival time of 253 days is shown after a hemicerebellectomy. Present in the cat rostro-lateral medial accessory olivary (MAO) are hypertrophic neurons, arrow. **B**: overview of the areas containing hypertrophic olivary neurons together with sporadic hypertrophic areas in the inferior olive. **C**: Light microscopic section treated for the anhydride technique. Positive dense globular inclusions are noted within the hypertrophic neurons indicating that accumulation of protein-bound carboxyls could occur within the hypertrophic cells in the cat [32]. **D**: The electron micrograph shows the osmiophilic globular inclusions within the cat extended granular endoplasmic reticulum (courtesy AJP Boesten, see [5]; adapted fig., courtesey [33]).

Olivary hypertrophy. Sometimes luck is at your side. Cleaning the loft of the Leiden Neurology Department brought out the series of sections of the cats studied by Rademaker. Verhaart found the olivary hypertrophy in these series, e.g. in the cat Marie-Antoinette (Rademaker [50] studied cerebellar posture and named all his experimental cats). Within Verhaart's group, the cerebello-rubro-olivary hypertrophy was established as caused by cerebellar and cerebellar nuclei deficits and it was the basis for Verhaart and Voogd's [65] experimental results [5]. Olivary hypertrophy is judged a combined retrograde and antegrade transneuronal reaction, because the direct cerebello-olivary projections, the dentate-rubral projections and the Darkschewitsch-olivary projections (**Fig. 3**) coincide in the hypertrophic olivary areas as studied in cats (**Fig. 5**). Palate myoclonus has been regularly related to olivary hypertrophy (for overviews, see [13, 16]). In short, lesions or haemorrhages of the brainstem or cerebellum are nearly always related to olivary hypertrophy, which is generally considered a "degeneration" of the inferior olive, but it is in fact hyperactivity of the olivary neurons. The discovery of the reduction of serotonin in the hypertrophic inferior olive supports its hyperactivity (see [33] for more (enzyme)histochemistry and references). The detection of this serotoninergic effect opened a new medical approach for myoclonus using the serotonin precursor 5-hydroxytryptophan. The detection of the relation between typical lesions and olive hypertrophy was already described in 1882 by Meyer [38]. At first publications restricted the lesions to damage of the tegmentum pontis with homolateral inferior olive hypertrophy, later on to cerebellar lesions, always involving the dentate nucleus, producing contralateral inferior olive hypertrophy. Bilateral inferior olivary hypertrophy was described after a shot wound involving lesions of the right-sided dentate nucleus and right-sided tegmentum pontis [61] supporting the earlier cerebellar findings. The correlation between palate myoclonus and these types of lesions and inferior olive hypertrophy came late. From around 1930 on several tens of articles have been published relating palate myoclonus to inferior olivary hypertrophy (see [33]).

In 1967 Jean Massion [36] published an overview of the mammalian red nucleus. The article had two main parts: an anatomical and a physiological one. Its anatomical description was mainly based on the results of early chromatolysis or the late neuronal changes, consisting of atrophy and loss of cells or silver degeneration studies carried out by several researchers. The anatomical results noticed a series of uncertainties that asked for more research and most research concerned the magnocellular part and clearly less the parvocellular part. His summary of the anatomical connections had been generally accepted (**Fig. 6**).

Its physiological part concludes that "the rubrospinal tract exerts a multiple action on the spinal cord. Through the intermediary of interneurons, it excites alpha moto-neurons and also gamma motoneurons (to the static fusimotor fibers) of the contralateral flexor muscles. At the same time, it inhibits the alpha fibers and the static fusimotor fibers of the contralateral extensor muscles. Moreover, it facilitates a whole set of inhibitory and excitatory spinal reflexes by acting directly on interneurons involved in these reflexes. Furthermore, the rubrospinal tract is responsible for the facilitation of the cells of origin of the ventral spinocerebellar tract. It also controls activity in the primary afferents as these enter the spinal cord by means of presynaptic inhibition" [36]. The ruber electrophysiological results in those days belonged to the high-quality research. Thus, rubrospinal effects are activation of contralateral flexion and inhibition of contralateral extension.

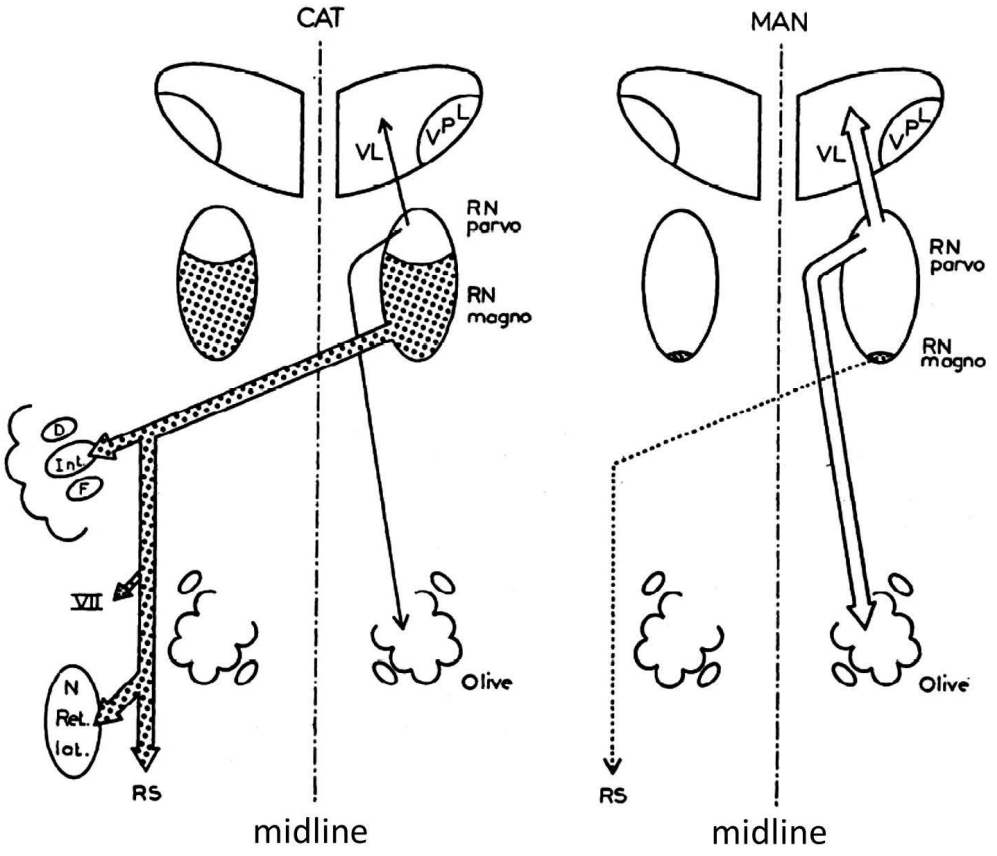

Fig. 6. Comparison of efferent connections of the red nucleus in cat and in man. RN Parvo, red nucleus, parvocellular part; RN magno, red nucleus, magnocellular part; RS, rubrospinal tract; VL, ventrolateral nucleus of the thalamus; VPL, ventroposterolateral nucleus; D, dentate nucleus; Int, nucleus interpositus; F, fastigial nucleus; N Ret. Lat, lateral reticular nucleus (adapted fig.2, [36])

Red nucleus and tracts in birds

The capillary rich red nucleus in the *pigeon* [68, 72] has to a certain degree a different cytoarchitecture that is though linked to that of mammals. Large cells (58 μm; 40-50 according to [69] pigeon; 70-100 mu in the chicken, [45]), medium cells (39 mu) and small cells (25 mu) are counted by Johnston [21] in the pigeon that compare to the red nucleus counts of Ramon y Cajal (1909-1911, [10]). "Large, medium and small-sized cells appeared to be equally distributed throughout each level of the nucleus. No noticeable sub grouping of cells, such as to constitute the sub groupings delineated in some mammals, was observed" [21]. Nevertheless a weaker subdivision of a magnocellular area (apex and ventrolateral part) has also been discerned. The rest of the nucleus has been dominated by medium and small cells, called a parvocellular area [69]. In the chicken a clear magnocellular and parvocellular area can be discerned [45]. The guinea pig study of Robak et al. [52] supports that the smaller cell group belongs to spiny and a-spiny interneurons, as interneurons are also known from the

rat [51]. Such a clear statement is to the best of my knowledge not found for the avian red nucleus. Although histochemistry of the metabolism of the different types of neurons can discern between large and medium chicken red nucleus neurons, such is not viable for the small cells [45]. Often interneurons are inhibitory, but GABA-like immunoreactivity is absent in the red nucleus of the pigeon [11]. Therefore, no arguments for avian interneurons can be taken from literature.

The avian rubrospinal tract crosses the midline and descends in the brainstem before shifting to the lateral part to reside in the dorso-lateral funiculus of the spinal cord. It arises from all cell sizes of the red nucleus. The avian rubrospinal tract reaches all levels of the spinal cord. Within the spinal grey this tract terminates in the layers 4 and 5, low in the dorsal horn and its intermediate area. An uncrossed rubrospinal tract has not been found in birds. The red nucleus receives contralateral lateral-cerebellar nucleus fibres and from the contralateral dorsal column nuclei [68, 69]. A restricted projection to the red nucleus relays from the hyperstriatum accessorium of the anterior Wulst. Thus a cortical/pallial projection is present. A much denser projection arises from the caudal part of the nucleus principalis precommissuralis and the medial part of the medial spiriform nucleus, organizing the thalamic connection. The red nucleus projects directly to the contralateral cerebellar cortex as mossy fibres. A direct olivary connection is not present, but should pass over the thalamic area [69]. The red nucleus in birds facilitates contralateral flexor and inhibits contralateral extensor activity like in mammals and it is involved in execution of learned motor behaviour [21].

The mallard superspinal nucleus is localized at the transition of spinal cord and brainstem. It innervates part of the craniocervical muscles, involved in head posture during its movements. Upward tilting muscles like the m splenius capitis and m. complexus and muscles for bending, e.g. m. rectus capitis ventralis, are steered by the superspinal nucleus. The ruber projects bilaterally to this superspinal nucleus. This rubro-"cervical" connection is somewhat restricted, but undeniable [59]. Not only the nucleus ruber, but also the reticular mesencephalic formation dorsal to the red nucleus and around the oculomotorius nucleus participate in this connection [60].

The direct spinal-rubral loop

The detection of a direct spinal influence on the magnocellular red nucleus was for the first time supposed by Kerr [24]. Its confirmation was obtained by the physiological cat studies of Padel and Jeneskog ([46, 47]; see also [48]). Spinal information will reach the magnocellular part of the red nucleus using fibres present in the cat's lemniscus medialis to ascent. Stimulation of these lemniscal fibres produces powerful monosynaptic EPSP's and disynaptic IPSP's on nearly all magnocellular red neurons. The magnocellular red nucleus is involved in several loops: direct spino-rubro-spinal loop, spino-cerebello-rubro-spinal loop and the spino-cortico-rubro-spinal loop. The rubro-spinal connection is involved in activating flexor motor activity and inhibition of extensor activity, but its spino-rubral part mainly in the sending of information on the perturbation of ongoing movements [48].

Note that sparse rubral ascending degeneration is found in the human red nucleus in Wallenberg syndrome related to lemnicus medialis degeneration (central tegmental tract was degeneration free), but not after C1 transverse lesion ([34] its **Figs. 4** and **5**).

Special scientific advances

The red nucleus and association cortex.

Critical checking of 20 patients with head and neck cancer from a far larger group using ^{18}F-FDG (radioactive fluordeoxyglucose) in a PET (positron emission tomography) study showed a difference in the metabolic activity of the left and the right red nucleus in humans. The results demonstrated that the right red nucleus is more intensely related to cortical association network areas or hubs [17] compared to the left red nucleus. The left red nucleus in its turn has a more intense relation with the cerebellum compared to the right one (**Fig. 7**). This functional asymmetry could only be detected due to a newly developed high-resolution semiconductor PET [18].

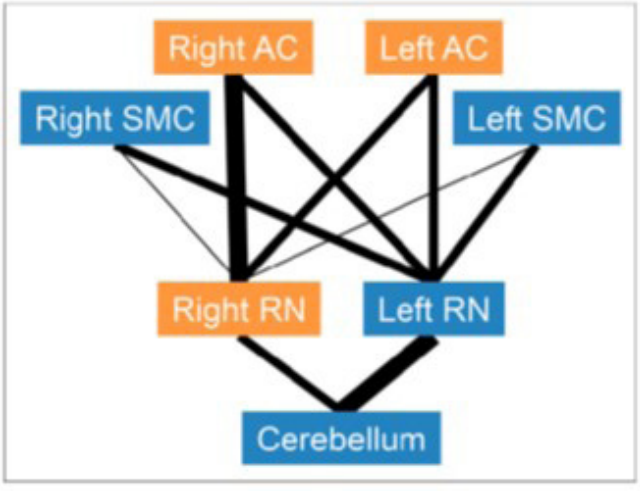

Fig. 7. Width of lines represents degree of association between 2 regions. AC, association cortex; RN, red nucleus; SMC, sensimotor cortex [18].

The red nucleus and migraine.

Migraine has also been coupled to brainstem malfunctions. Migraine without aura has been related to the red nucleus and the substantia nigra using resting-state functional magnetic resonance imaging (fMRI). The functional connectivity of the red nucleus showed reduced left red nucleus-based functional connectivity with the left middle frontal gyrus, reduced right red nucleus-based functional connectivity with the ipsilateral superior parietal lobe, and left increased functional connectivity with the ipsilateral cerebellum. The results also demonstrated significantly decreased right substantia nigra-based functional connectivity with the right postcentral gyrus, left parietal lobule, and left superior frontal gyrus [19]. It should be noted that this article also describes functional asymmetry of the red nuclei.

Leigh syndrome, SURF1 mutations and olivary hypertrophy.

Leigh mitochondrial syndrome can be related to cytochrome c oxidase deficiency. This enzyme is functional in mitochondria and is a complex of several units. The mitochondrial genome and the nuclear genome produce 3 and 10 units respectively. The assembly is done by *SURF1* COX genes. Mutations of the *SURF1* produces the Leigh syndrome in children and sometimes in adults. In children it is lethal. Magnetic resonance studies show in most cases olivary hypertrophy and often subthalamic nucleus disturbances

[57]. Bilateral olivary hypertrophy is also reported in children with Leigh syndrome [4]. Several other diseases also produce olivary hypertrophy. Cerebrovascular diseases including haemorrhage, infarction, and vascular malformations are the most frequently reported cases in both types of olivary hypertrophy, 62% unilateral and 30% bilateral hypertrophy [25].

The red nucleus and Pou4f1.

The mouse red nucleus contains a strong presence of *Pou4f1* that is responsible for a precise differentiation pathway. This transcription factor with a DNA binding of the POU domain is related to its specification. In *POU4f1*$^{-/-}$ mice red nucleus cells do not survive and fail to correctly contact its peripheral aims [70]. Despite the loss of function in the transgenic mice Pou4f1$^{TauLacZ/+}$ embryos compared to Pou4f1$^{TauLacZ/TauLacZ}$ embryos, it was shown that the red nucleus was still present. However, its cellular organisation was disturbed, the nucleus worse bordered and a delay in radial migration occurred (**Fig. 8**). Moreover, the axons did descent in the spinal cord but were defasciculated. *POU4f1* is not necessary for the generation of the red nucleus, but co-determines its development, connections and maintenance [35].

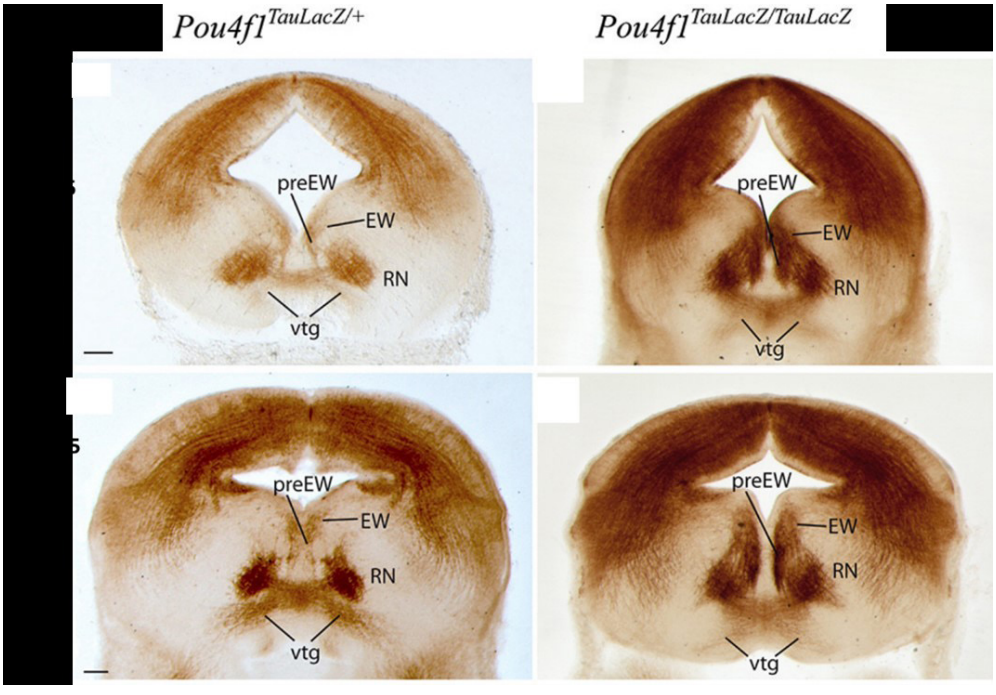

Fig. 8 . Coronal mesencephalic sections in Pou4fTauLacZ/+ and Pou4fTauLacZ/TauLacZ embryos processed by immunohistochemistry. The figure contains the embryonic stages: E14.5 and E15.5, earlier stages are not shown here. The normal generation of the RN and its projections in the control embryos is presented at the right. Left, the RN development in the mutant embryos showed a clear delay in radial migration. The RN displayed a certain spatial disorganization. Abbreviations: EW, Edinger-Westphal nucleus; RN, red nucleus; preEW, pre-Edinger-Westphal; vtg, ventral tegmental decussation. Scale bars=150 mm. (Fig. adapted from [35], part of their fig. 1).

The red nucleus and restless legs syndrome.

The red nucleus has been related to restless legs syndrome in various articles. A magnetic resonance study accompanied by a meta-analysis shows that in these patients high iron concentrations have been detected in caudate, putamen and red nucleus [3]. During a combined limb movement and sensory leg discomfort period, patients showed activity in the cerebellum and thalamus. Additional activation in the red nuclei and brainstem close to the reticular formation was noticed. If only sensory leg discomfort was present bilateral activation of the cerebellum and the contralateral thalamus, but no involvement of the red nucleus was observed [6]. Seemingly the restless legs syndrome is coupled to the dentate-ruber-olivary-cerebellum loop in humans. In rat lesions, the role of the cerebello-rubral-spinal loop is supported in restless legs syndrome [15].

Conclusion

Historical overviews show that in humans the uncrossed rubral connections are robustly developed. Mutually in rats, due to the area parafascicularis prerubralis, and in cats both uncrossed and crossed tracts are present, while in birds the crossed rubro-spinal tract is exclusively utilized, demonstrating the different species evolutionary choice. Localization and partly the cellular sizes of the red nuclei are comparable in mammals and birds. The presence of red nucleus interneurons in birds needs further research. Functional activities concern contralateral flexor activation and contralateral extensor inhibition. Moreover, the rubro-spinal tract is active when automated, already learnt, movements have to be performed and spino-rubral effects concern perturbation of ongoing movements. The occurrence of asymmetry between left and right red nuclei has been established by fMRI and PET studies. Olivary hypertrophy not only occurs due to brainstem/cerebellar deficits and vascular infarctions, but also because of mitochondrial genetic mutations. The red nucleus is involved in migraine and in restless legs syndrome. Human red nucleus activity after spinal cord damage to improve mobility of these patients surprises.

References

1. **Basile, G. A, M. Quartu, S. Bertino, M. P. Serra, M. Boi, A. Bramanti, G. P. Anastasi, D. Milardi, A. Cacciola.** Red nucleus structure and function: from anatomy to clinical neurosciences. – *Brain Struct. Funct.,* **226**, 2021, 69-91.
2. **Bechterew, W.** Ueber eine bisher unbekannte Verbindung der grossen Oliven mit dem Grosshirn. – *Neurol. Zentr*., **4** ,1885, 194-196 [in German]
3. **Beliveau, V., A. Stefani, C. Birkel, C. Kremser, E. R. Gizewski, B. Högl, C. Scherfler.** Revisiting brain iron deficiency in restless legs syndrome using magnetic resonance imaging. – *Neuroimage,* **34**, 2022, 103024.
4. **Bindu, P. S., A.B. Taly, K. Sonam, C. Govindaraju, H. R. Arvinda, R. Vinda, N. Gayatheri, M. M. Srinivas Bharath, D. Ranjith, N. Nagappa, S. Sinha, N. A. Khan, K. Thangaraj.** Bilateral hypertrophic olivary nucleus degeneration on magnetic resonance imaging in children with Leigh and Leigh-like syndrome. – *Br. J. Radiol.,* **87**, 2014, 20130478.
5. **Boesten, A. J. P., J. Voogd.** Hypertrophy of neurons in the inferior olive after cerebellar ablations of the cat. – *Neurosci. Lett.,* **61**, 1985, 49-54.
6. **Bucher, S. F., K. C. Seelos, W. H. Oertel, M. Reiser, C. Trenkwalder.** Cerebral generators involved in the pathogenesis of the restless legs syndrome. – *Ann. Neurol*., **41**, 1997, 639-645.

7. Burdach, K. F. *Vom Baue und Leben des Gehirns*, vol 2, Leipzig, Dyk'sche Buchhandlung, 1822 [in German]
8. Cabot, J. B., A. Reiner, N. Bogan. (1982) Avian bulbospinal pathways: Anterograde and retrograde studies of cells of origin, funicular trajectories and laminar terminations. – *Prog. Brain Res*., **57**, 1982, 79-108.
9. Cacciola A., D. Milardi, G.A. Basile, S. Bertino, A. Calamuneri, G. Chillemi, G. Paladina, F. Impellizzeri, F. Trimarchi, G. Anastasi, A. Bramanti, G. Rizzo. The cortico-rubral and cerebello-rubral pathways are topographically organized within the human red nucleus. – *Sci. Reports* **9**, 2019, 12117.
10. Cajal, S, Ramon. *Histologie du systéme nerveux de I'homme et des vertébrés*, vols 1 et 2. Maloine, Paris,1909-1911. [in French]
11. Dominici, L., H. J. Waldvogel, C. Matute, P. Streit. Distribution of GABA-like immunoreactivity in the pigeon brain. – *Neurosci*, **25**, 1988, 931-950.
12. Donkelaarten, H. J. Evolution of the red nucleus and rubrospinal tract. – *Behav. Brain. Res.* **28**, 1988, 9-20.
13. Frenken, C. W. G. M. *The myocloni of the non-epilectic form*. PhD Thesis Nijmegen University, The Netherlands, 1977 [in Dutch]
14. Friede, R. L. *Topographic brain chemistry*. Academic Press, NY, London 1966.
15. Guo, C. N, W. J. Yang, S. Q. Zhan, C. Han, L. Li, X. Xu, G. Zhang, Z. Lin, N. Xiong, T. Wang. Targeted disruption of supraspinal motor circuitry reveals a distributed network underlying Restless Legs Syndrome (RLS)-like movements in the rat. – *Sci. Reports*, **7**, 2017, 9905.
16. Hagen, C. J. *On olivary hypertrophic degeneration.* PhD Thesis, University of Amsterdam, 1969[in Dutch]
17. Heuvel, M. P. van den, O. Sporns. Network hubs in the human brain. – *Trends Cognitive Sci*., **17**, 2013, 683-696
18. Hirata, K., N. Hattori, W. Takeuchi, T. Shiga, Y. Morimoto, K. Umegaki, K. Kobayashi, O. Manabe, S. Okamoto, N. Tamaki. Metabolic activity of red nucleus and its correlation with cerebral cortex and cerebellum: A study using high-resolution semiconductor PET system. – *J. Nuclear Med*., **56**, 2015, 1206-1211.
19. Huang, X., D. Zhang, Y. Chen, P. Wang, C. Mao, Z. Miao, C. Liu, C. Xu, X. Wu, X. Yin. Altered functional connectivity of the red nucleus and substantia nigra in migraine without aura. – *J. Headache Pain,* **20**, 2019, 104.
20. Huisman, A. M. *Collateralization of descending spinal pathways from red nucleus and other brainstem cell groups in rat, cat and monkey*. PhD Thesis, Erasmus University, Rotterdam, The Netherlands, 1983.
21. Johnston, A. *The avian red nucleus: a comparative physiological and behavioural study on Columba livia*, PhD theses, Durham University, 1975
22. Kardel, T., H. Jacobeaus. Steno: Life-science-philosophy. – *Acta Histol. Sci. Nat. Med.,* **42**, 1994
23. Kennedy, P. R. Corticospinal, rubrospinal and rubro-olivary projections: a unifying hypothesis. – *TINS* **13**, 1990, 474-479.
24. Kerr, F. W. L. The ventral spinothalamic tract and other ascending systems of the ventral funiculus of the spinal cord. – *J. Comp. Neurol.,* **159**, 1975, 335-356.
25. Konno, T., D. F. Broderick, P. Tacik, J. N. Caviness, Z. K. Wszolek. Hypertrophic olivary degeneration. A clinico-radiologic study. – *Parkinson Rel. Disord.,* **28**, 2016, 36e40.
26. Lakke, E. A. J. F. The projections to the spinal cord of the rat during development; a time-table of descent. – *Adv. Anat. Embryol. Celbiol.* **135**, 1997, 1-143.
27. Lakke, E. A. J. F., E. Marani. Prenatal descent of rubrospinal fibers through the spinal cord of the rat. – *J. Comp. Neurol.,* **314**, 1991, 67-78.
28. Lewis, M. M., G. Du, M. Kidacki, N. Patel, M. L. Shaffer, R. B. Mailman, X. Huang. Higher iron in the red nucleus marks Parkinson's dyskinesia. – *Neurobiol. Aging*, **34**, 2014, 1497–1503.

29. Luyendijk-Elshout, A. Of masks and mills: the enlightened doctor and his frightened patient. In: *The Languages of psyche. mind and body in enlightenment thought.* (Ed. G. S. Rousseau), University California Press, pp 186-230, 1990.
30. Mannen, H., T. Mannen, N. Mannen, N. Ishizuka. *A dendro-cyto-myeloarchitectonic atlas of cat's brain*. Tokyo, Iwanami Shoten, 1988.
31. Marani, E. *Topographic enzyme histochemistry of the mammalian cerebellum. 5'Nucleotidase and acetylcholinesterase*. PhD Thesis, Leiden University, 1982.
32. Marani, E. Topographic histochemistry of the cerebellum. – *Progress in Histochemistry & Cytochemistry* **16(4)**, 1986, 1-169.
33. Marani, E., C. Heida. *Head and Neck. Morphology, models and function.* Springer Nature, Cham, Switzerland, 2018.
34. Marani, E., J. H. R. Schoen. A reappraisal of the ascending systems in man, with emphasis on the medial lemniscus. – *Adv. Anat. Embryol Cell Biol.,* 179, 2005, 1-76.
35. Martinez-Lopez, J. E., J. A. Moreno-Bravo, M. P. Madrigal, S. Martinez, E. Puelles. Red nucleus and rubrospinal tract disorganization in the absence of *Pou4f1*. – *Front Neuroanat* **9**, 2015, 8.
36. Massion , J. The mammalian red nucleus. – *Physiol. Rev.,* **47**, 1967, 383-436.
37. Massion, J. Red nucleus: past and future. – *Behav. Brain Res.,* **28**, 1988, 1-8.
38. Meyer, P. Ueber ein fall von ponshaemorraghie mit secundären degenerationen der schleife. – *Arch. Psych. u Nervenkrankh*, **13**, 1882, 63. [in German]
39. Monakow, von C. Der rote kern, die haube und die regio hypothalamica bei einigen säugetieren und beim mensch. – *Arb. Hirnanat. Inst. Zűrich*, Heft III, 1909, 49-267[in German]
40. Monakow, von C. Experimenteller beitrag zur kenntnis des corpus restiforme, des 'äusseren acusticuskerns' und deren beziehungen zum rückenmark. – *Arch. Psychiat. Nerven.* **14**, 1883, 1-16 [in German]
41. Ogawa, T. The tractus tegmenti medialis and its connection with the inferior olive in the cat. – *J. Comp. Neurol.,* **70**, 1939, 19-36.
42. Olivares-Moreno, R., P. Rodriquez-Moreno, V. Lopez-Virgin, M. Macias, M. Altamira-Camacho, G. Rojas-Piloni. Corticospinal vs rubrospinal revisited: An evolutionary perspective for sensorimotor integration. – *Front. Neurosci., Sec. Neuroprosthetics,* **15**, 2021.
43. Onodera, S., T.P Hicks. A comparative neuroanatomical study of the red nucleus of the cat, macaque and human. – *Plos One*, **4**, 2009, 8, e6623.
44. Oudega, M., M. A. Perez. Corticospinal reorganization after spinal cord injury. – *J. Physiol.,* **590**, 2012, 3647-3663.
45. Ovtscharoff, W, R. Gossrau. Histochemie und elektronenmicroscopie des nucleus ruber des huhnes (*Gallus domesticus*). – *Histochemie,* **30**, 1972, 73-81. [in German]
46. Padel, Y., T. Jeneskog. Inhibition of rubro-spinal cells by somaesthetic afferent activity. – *Neurosci. Lett.,* **21**, 1981, 177-182.
47. Padel, Y., T. Jeneskog. A fast feed-back pathway transmitting sensory information to rubrospinal cells in the cat. – *Behav. Brain Res.,* **8**, 1983, 263-264.
48. Padel, Y., J.-A. Rathelot, L. Vinay. Analysis of potentials induced in red nucleus neurons from the somaesthetic pathway stimulated at bulbar levels. –*Exp. Brain Res*., **106**, 1995, 377-390
49. Probst, M. Zur Kenntnis der Hirnes und fiber zwischenhirn-olivenbahn. – *Jahrb. Psychatr. Neural.,* **23**, 1903, 350-381. [in German]
50. Rademaker, G. G. J. Das stehen. Statische reaktionen. Gleichgewichtsreaktionen und muskeltonus. Unter besonderer berücksichtigung ihres verhaltens bei kleinhirnlosen tieren. – *Monogr. Gesamtgeb. Neurol. Psychiatr.*. **5,** 1931.
51. Reid, J. M., D. G. Gwyn, B. A. Flumerfelt. A cytoarchitectonic and Golgi study of the red nucleus in the rat. – *J. Comp. Neurol.,* **162**, 1975, 337-362.
52. Robak, A., S. Szteyn, K. Bogus-Nowakowska, T. Doboszynska, M. Rowniak. The cytoarchitectonic and neuronal structure of the red nucleus in guinea pig: Nissl and Golgi studies. – *Folia Morphol.,* **58**, 2000, 333-342.

53. Ruigrok, T. J. H., F. Cella. Precerebellar nuclei and red nucleus. In : *The rat nervous system,* 2nd ed. (Ed. G. Paxinos), San Diego, CA, Academic Press,
54. Ruigrok, T. J. H., X. Wang, E. Sabel-Goedknegt, P. Coulon, Z. Gao. A disynaptic basal ganglia connection to the inferior olive: potential for basal ganglia influence on cerebellar learning. – *Front. Syst. Neurosci.,* **17**, 2023.
55. Rutherford, J. G., W. A. Anderson, D. G. Gwyn. A reevaluation of midbrain and diencephalic projections to the inferior olive in rat with particular reference to the rubro-olivary pathway. – *J. Comp. Neurol.,* **229**, 1984, 285-300.
56. Sie Pek Giok. *Localisation of fibre systems within the white matter of the medulla oblongata and the cervical cord in Man.* PhD Thesis, Leiden University, E. IJdo, 218 pp, 1956
57. Sonam, K., N. Akthar Khan, P. Sankaran Bindu, A. B. Taly, N. Gayathri, M. M. Srinivas Bharath, C. Govindaraju, H. R. Arvinda, M. Nagappa, S. Sinha, K. Thangaraj. Clinical and magnetic resonance imaging findings in patients with Leigh syndrome and SURF1 mutations. – *Brain Develop.,* **36**, 2014, 807-812.
58. Swanson, L. W. What is the brain. – *TINS.,* **23**, 519-527, 2000.
59. Tellegen, A. J., J. L. Dubbeldam. Location of reticular premotor areas of a motor centre innervating craniocervical muscles in the mallard (*Anas platyrhychos* L.). – *J. Comp. Neurol.,* **405**, 1999, 281-98.
60. Tellegen, A. J., J. L. Dubbeldam. Do craniocervical and jaw motor nuclei receive input from the same population of reticular premotor neurons? A double labelling tracing study in the mallard (*Anas platyrhynchos*). – *Neurosci. Lett., 209*, 1996, 77-80.
61. Uemura, H. Pathologisch-anatomische untersuchungen ueber die verbindingsbahnen zwischen dem kleinhirn und den hirnstam. – *Schweiz. Arch. Neurol. Psychiatr.,* **1**, 1917, 151. [in German]
62. Verhaart, W. J. C. Die zentralen haubenbahn bei affen und menschen. – *Schw. Arch. Neur. u Psych.,* **38**, 1936, 270–283. [in German]
63. Verhaart, W. J. C. The rubrospinal system with monkey's and man. – *Psych. Neurol.,* **42**, 1938, 335– 343.
64. Verhaart, W. J C. The central tegmental tract. – *J. Comp. Neurol*., **90**, 1949, 173–192.
65. Verhaart, W. J. C., J. Voogd. Hypertrophy of the inferior olives in the cat. – *J. Neuropathol. Exp. Neurol.,* **21**, 1962, 92-104.
66. Voogd, J., E. Marani. Verhaart 1889-1983. In: *History of Neurology* (Eds. G. W. Bruyn P. Koehler P), 2002, pp 377-386.
67. Voogd, J., C. I. De Zeeuw. Cerebellum: What is in a name. Historical origin and first use of this anatomical term. – *Cerebellum,* **19***,* 2020, 550-561
68. Wild, J. M, J. B. Cabot, D. H. Cohen, H. J. Karten. Origin, course and terminations of the rubrospinal tract in the pigeon *(Columba livia). – J. Comp. Neurol*., **187**, 1979, 639-654.
69. Wild, J. M. Direct and indirect "cortico"-rubral and rubro-cerebellar cortical projections in the pigeon. – *J. Comp. Neurol.,* **326**, 1992, 623-636.
70. Xiang, M., G. Lin, L. Zhou, W. H. Klein, J. Nathans. Targeted deletion of the mouse POU-domain gene Brn-3a causes a selective loss of neurons in the brainstem and trigeminal ganglion, uncoordinated limb movement and impaired suckling. – *Proc. Natl. Acad. Sci. U S A*, **93**, 1996, 11950–11955.
71. Zarate-Lagunes, M., W. J. Gu, V. Blanchard, C. Francois, M. P. Muriel, A. Mouatt-Prigent, B. Bonici, A. Parent, A. Hartmann, J. Yelnik, G. A. Boehme, L. Pradier, S. Moussaoui, B. Faucheux, R. Raisman-Vozari, Y. Agid, A. Brice, E. C. Hirsch. Parkin immunoreactivity in the brain of human and non-human primates: an immunohistochemical analysis in normal conditions and in Parkinsonian syndromes. – *J. Comp. Neurol.,* **432**, 2001,184-96.
72. Zecha, A. Does a bird possess a rubro-bulbo-spinal fascicle? – *Ned Tijdschr Geneesk*, **105**, 1961. [in Dutch]

Institute of Experimental Morphology, Pathology and Anthropology with Museum
Bulgarian Anatomical Society

Acta Morphologica et Anthropologica, 31 (1-2)
Sofia ● 2024

ANTHROPOLOGY AND ANATOMY 31 (2)

Original Articles

Abnormal Hemispheric Lateralization as a Marker for the Neurodevelopmental Origin of Schizophrenia. Gender Impact Insights

*Katerina Akabalieva[1], Asen Beshkov[2], Vasil Kotetarov[3], Valentin Akabaliev[2], Stefan Sivkov[4,]**

[1]Department of Psychiatry, Medical University, Sofia, Bulgaria
[2]Department of Psychiatry and Medical Psychology, Medical University, Plovdiv, Bulgaria
[3]State Psychiatric Hospital, Pazardzhik, Bulgaria
[4]Department of Anatomy, Histology and Cytology, Medical University, Pleven, Bulgaria

*Corresponding author: st.sivkov@yahoo.com

The gender differences in left-eyedness between schizophrenic and control subjects and the correlations with MPAs as an index of maldevelopment were studied.

The study included 98 schizophrenic patients meeting DSM-V criteria for schizophrenia and 82 control subjects without records of psychiatric disorder. Subjects with a history of drug/alcohol abuse, neurological disorder, mental disability, and ocular pathology were excluded. Three eye dominance tests and seven MPAs on the Waldrop scale were used.

Schizophrenic patients were more left-eyed than the control subjects. In males, the difference did not reach statistical significance. Female patients scored significantly higher on the eye tests. MPAs showed higher frequencies in schizophrenic vs. control subjects. Statistically significant positive correlations were found between left-eyedness and MPAs.

Left-eyedness is a useful biomarker of altered hemispheric lateralization. The cooccurrence of left-eyedness and MPAs, in one subject, appears to be a more reliable index of underlying neurodevelopment disorder.

Key words: schizophrenia, laterality, eye dominance, minor physical anomalies, sexual dimorphism

Introduction

Lateralization is the functional dominance of one of the dual organs of the body: hands, feet, eyes, and even ears, during spontaneous or purposeful actions. Lateralization is the process that organizes this asymmetry, leading to the choice of one side over the other.

The neuro-ontogenetic theory of the development of schizophrenia postulates that the disease is a consequence of aberrant brain development during the fetal or neonatal period [11, 18]. Lateralization of brain functions (including eye dominance) takes place in the early fetal stages of individual development, which suggests that cerebral asymmetry is a key dimension of neurodevelopment.

The most often used assessment for functional lateralization is hand dominance [2, 3, 10, 14]. Handedness, however, is influenced by many factors like geographic region, genetic and cultural factors, and gender. The choice of a dominant eye for vision is not a result of external influence, which makes it a strong predictor of brain lateralization. The concept of eye dominance relates to the tendency to prefer visual information coming through one of the eyes and the objects being thus more clearly and exactly reproduced, more stable, and even larger [14, 15].

However, there is a small number of studies, in which higher left eye dominance was found in schizophrenic patients than in control subjects [1, 5, 6, 7, 8, 16]. The reported percentages of left-eyedness in schizophrenic patients are extremely variable. Some authors found as high as 73% left-eyedness (male schizophrenics) [15], while others did not find a difference in eye dominance between schizophrenic and control subjects [13] A few studies considered eye dominance in relation to gender differences and the results are contradictory. Dane (2009) found left eye dominance prevalence only in male schizophrenics compared to controls but did not find such prevalence in schizophrenic females [4]. Yan et al., 1985 found just the opposite – left eye dominance in female schizophrenics was more frequent than in male schizophrenics [19]. Another author did not find any significant sex difference in eye dominance between schizophrenic patients and controls [15].

In this context, the aim of the study is to investigate sexual differences in left eye dominance as a biological marker of neuronal dysontogenesis in schizophrenic patients and control subjects. This study is part of a larger investigation project on the intriguing relations between six groups of markers of neuronal dysontogenesis - left-handedness, left-footedness, left-eyedness, minor physical anomalies, digit ratio, and cognitive (attention and memory) deficit.

Material and Methods

Subjects

The study was conducted in the Clinic of Psychiatry at the University Hospital in Sofia and the State Psychiatric Hospital in Radnevo. The sample included 98 (56 men, 42 women) consecutively admitted schizophrenic inpatients with a mean age of 34.45 years (SD=15.67, range 23-79) for men and 42.20 years (SD=11.38, range 21-63) for women.

The patients satisfied the Diagnostic and Statistical Manual of Mental Disorders-V (DSM-V) criteria for a diagnosis of schizophrenia based on case records review,

DSM-V-based semi-structured interview and information obtained from relatives for stronger validation of the diagnosis. To enhance the homogeneity of the schizophrenic group, potential subjects were excluded if they had a history of drug or alcohol abuse, identifiable neurological disorder (seizure disorder, head injury, multiple sclerosis, etc.), or any signs of intellectual disability or somatic disorder with neurological components.

For the eye tests exclusion criteria were any previous or present eye and upper limb disorders hampering the performance of the eye tasks. Impaired visual acuity, higher than +/-2 dioptres, and more than +/-1 dioptre difference between the two eyes were exclusion criteria, as these have been proven to confound the performance of eye tasks.

The control group consisted of 82 subjects (30 men, 52 women) with a mean age 34.70 years (SD=16,82, range 18-79) for men and 44.50 years (SD=10.73, range 23-67) for women. Normality was defined as the absence of a previous or present psychiatric disorder, according to DSM-V. Controls satisfied exclusion criteria like those applied to schizophrenic patients. In addition, for better separation between the control and the schizophrenic group, we implemented another exclusion criterion for controls - having a first-degree relative with a history of a psychotic disorder, major affective disorder, or suicide.

To avoid eventual confound due to ethnic and racial differences related to lateralization, both schizophrenic patients and controls were of Bulgarian origin. Individuals were excluded if their parental or grandparental ethnic group was other than Bulgarian.

The refusal rate of potential participants was insignificant [below 5%], excluding selectivity bias.

The study was approved by the Local Ethics Committee and all subjects gave written informed consent prior to participation.

Instruments

Eye Dominance Scale

Eye dominance (ocular sighting dominance) was measured by a set of three eye dominance tests, administered as performance assessments, not as preference questionnaires.

Each test was performed twice and the subject was asked to perform the test again if there was any inconsistency in the preference.

1. Looking through a monocle test – the participant is asked to take with both hands a monocle and look through it.

2. Hole-in-card test - the participant is asked to hold the card with both hands at arm's length and look with both eyes through the hole at an object. While continuing to focus on the object and keeping the object centered in the hole with both eyes open, the participant must slowly bring the card towards the face until it touches his nose. The card is positioned over one of the subject eyes.

3. Porta test (modified Miles test) - the participant is asked to extend one arm and to align a forefinger with a distant object with both eyes open, then to close his left eye and then the right eye consequently. The object is still aligned with the index finger when seen with the dominant eye. A potential limitation of the test is the impact of the arm that the patient uses according to his hand dominance.

Each eye test is rated: 0 – Preference for right eye; 1 – No preference (both eyes equally); 2 – Preference for left eye. Each test score ranges from 0 to 2; the eye set total score ranges from 0 to 6.

All assessments were performed by the same examiner.

Statistical analysis

As our data is not continuous and lacks normal distribution, the non-parametric Mann-Whitney test for means difference between two independent groups was used. For comparing categorical data χ^2-test (in 2x2 table with Yates' correction for continuity) was used for comparing categorical data, χ^2-test (in 2x2 table with Yates' correction for continuity) was used for comparing categorical data.

The categories of the eye tests can be treated as ordinal data – graded, in ascending order of leftedness: 0 - Preference of right eye; 1– No preference -both eyes equally; 2 – Preference of left eye. Ordinal data allows for calculating the mean left-eyedness for every single eye test. A variable mean is usually more sensitive than its categories in detecting a difference between groups. Besides, it enables comparing the important differences between the mean sum of left-eyedness of the Eye Dominance Subscale and the mean sum of the Eye Dominance Scale (3 eye tests) between schizophrenic and control subjects.

Statistical significance was defined as $p < 0.05$; two-tailed. Data was analyzed with SPSS 25.0.

Results

Comparison of eye dominance between schizophrenic and control subjects

The frequency of left eye dominance is significantly higher in schizophrenic than in control subjects in the three eye tests – Looking through a monocle (40.0% vs. 19.5%, $p<0.004$), Hole test (42.1% vs. 19.5 %, $p< 0.03$) and Porta test (42.4% vs. 20.7%, $p<0.06$). But this general comparison of left eye dominance between schizophrenic and control subjects, when examined by gender demonstrate marked difference in men and women. *Comparison of eye dominance between schizophrenic and control subjects by gender.*

Intra-gender comparisons

Schizophrenic men versus control men

Male schizophrenic patients show higher left eye dominance than the same-sex controls for the 3 eye tests and Sum 3 eye tests. The frequency of left eye preference is higher in male schizophrenics than the same-sex control subjects in the three tests - Looking through monocle (35.8% vs.16.7%), Hole test (35.8% vs. 23.3%) and Porta test (41.7% vs. 23.3%).

However, none of these differences is statistically significant at $p<.05$ - Hole test ($p=.348$), while Looking through monocle ($p=.080$), Porta test ($p=.164$) and Sum 3 eye tests ($p=.089$) merely approach statistically significant difference.

Schizophrenic women versus control women

Female schizophrenic patients show markedly higher left eye dominance than the same-sex controls for the 3 eye tests and Sum 3 eye tests. The frequency of left eye

Table 1. Comparison of eye dominance between schizophrenic and control subjects by gender

	Men (N=83)						Women (N=94)					
	Schizophrenia (N=53)*		Controls (N=30)*		Statistical Significance**		Schizophrenia (N=42)*		Controls (N=52)*		Statistical Significance**	
EYE TESTS	n	%	n	%	χ^2	p	n	%	n	%	χ^2	p
Looking through monocle					5.040	.080					6.202	**.013**
Right	32	60.4%	25	83.3%			23	54.8%	41	78.8%		
Both	2	3.8%	0	0.0%			0	0.0%	0	0.0%		
Left	19	35.8%	5	16.7%			19	45.2%	11	21.2%		
Hole test					2.113	.348					11.428	**.001**
Right	33	62.3%	23	76.7%			21	50.0%	43	82.7%		
Both	1	1.9%	0	.0%			0	0.0%	0	.0%		
Left	19	35.8%	7	23.3%			21	50.0%	9	17.3%		
Porta test					3.618	.164					6.028	**.014**
Right	27	56.3%	23	76.7%			21	56.8%	42	80.8%		
Both	1	2.1%	0	0.0%			0	0.0%	0	0.0%		
Left	20	41.7%	7	23.3%			16	43.2%	10	19.2%		
Sum 3 eye tests					9.546	.089					8.504	**.037**
0	18	37.5%	19	63.3%			15	40.5%	36	69.2%		
2	13	27.1%	4	13.3%			6	16.2%	7	13.5%		
3	1	2.1%	0	0.0%			0	0.0%	0	0.0%		
4	6	12.5%	6	20.0%			6	16.2%	4	7.7%		
5	1	2.1%	0	0.0%			0	0.0%	0	0.0%		
6	9	18.8%	1	3.3%			10	27.0%	5	9.6%		

* Valid cases - the sum of the Right, Both and Left categories does not always add up to the total number, due to missing data for some cases
**Pearson Chi-Square

preference is higher in female schizophrenics than the same-sex controls in the three tests – Looking through monocle (45.2% vs. 21.2%), Hole test (50.0% vs. 17.3%) and Porta test (43.2% vs. 19.2%). In contrast to the male intra-gender comparison, all the differences in women are statistically significant - Looking through monocle ($p=.013$), Porta test ($p=.014$) and Sum 3 eyes tests ($p=.037$) have statistical significance at $p<.05$, while Hole test reach a very strong statistically significant difference at $p<.001$.

Difference between the two intra-gender comparisons of left eye dominance

The two intra-gender comparisons show that schizophrenic patients are more left eye dominant than controls in both sexes, but this difference is much more pronounced in women than in men for all three eye tests. Thus, women contribute the bigger part to this strong overall difference in left eye preference between schizophrenic and control subjects.

It is noteworthy that the small number of subjects with no eye preference (category Both) is entirely in the male schizophrenic group**.** Intermediate degrees of left eye dominance are those between grade 0, which indicates the exclusive right eye dominance, and grade 6, which shows the maximum leftward shift for left eye dominance i.e., subjects with grades 2,3,4, and 5 of Sum 3 eye tests. Importantly, the number of such "intermediate" men are almost twofold the corresponding number of "intermediate" woman (21 vs. 12).

Correlations between minor physical anomalies and left eye dominance

All seven MPAs show higher frequencies in schizophrenic vs. control subjects. The greatest differences are found for single transverse palmar crease of the left hand ($p<.002$), transversally furrowed tongue ($p<.006$), single transverse palmar crease of the right hand ($p<.054$). Importantly, the sum of the seven MPAs is significantly higher ($p<.003$) in schizophrenic vs. control subjects.

To address the low internal consistency of the MPAs of the Waldrop Physical Anomaly Scale (40) and to capture more subtly and diversely the multiple correlations between left-eyedness and MPAs, the 7 MPAs were divided into 3 groups in descending order of their differentiating strength between schizophrenic and control subjects.

1. Sum 3 MPAs = Single transverse palmar crease of the left hand, transversely furrowed tongue, and Single transverse palmar crease of the right hand
2. Sum 5 MPAs = Sum 3 MPAs + left/right adherent earlobes
3. Sum 7 MPAs = Sum 5 MPAs + left/right curved fifth finger

Correlation matrix between the 3 eye tests and MPAs

The Spearman's rank correlation matrix shows that positive correlations are highly predominant between left-eyedness and MPAs, with multiple statistically significant correlations:

Females

– Looking through a monocle with transversally furrowed tongue ($p<.005$) and Sum 3 MPAs ($p<.05$).
– Hole test with Sum 3 MPAs ($p<.05$), adhered ear lobule left ($p<.05$), transversely furrowed tongue ($p<.05$).

– Sum of 3 eye tests with transversely furrowed tongue (p<.05).
– Some correlations are close to statistical significance:
– Sum of 3 eye tests with Sum 3 MPAs (p=.053).

Males

– Porta test with Sum 3 MPAs (p<.05), transversely furrowed tongue (p<.05).
– Sum of 3 eye tests with transversely furrowed tongue (p<.05).
– Close to statistical significance
– Porta test with Sum of 5 MPAs (p=.066)

Discussion

By selecting three different eye dominance tests, we confirmed the strongly higher prevalence of left-eyedness in schizophrenics versus controls. Another thing that contributed to these strong results was the application of performance assessments, not preference questionnaires.

As in all other aspects, lateralization has gender differences. The male brain is thought to be more lateralized than the female, however, these facts remain the result of the next studies [9,12, 17].

In our data, male schizophrenic patients show a higher frequency of left-eyedness than the same-sex controls for the 3 eye tests separately and as a sum, however, none of these are statistically significant. In contrast, female schizophrenic patients show statistically significantly higher left-eyedness than the same-sex controls in the 3 eye tests separately and as a sum.

This shows that schizophrenic patients are more left-eyed than normal controls in both sexes, but this difference tends to be much more pronounced in women than in men for all three tests. Thus, women contribute the greater part to this overall difference between schizophrenic and control subjects.

Our findings are consistent with those reported by Yan [19], who also found much more pronounced left-eyedness in schizophrenic women than in men, but are opposite to Dane (2009), who found left-eye dominance only in male schizophrenic patients.

It is evident that schizophrenic men in terms of eye dominance become less polarized in eye preference, matching normal women in that regard and schizophrenic women become more polarized in eye preference, matching normal men in that regard.

Considering eye dominance as a continuum shows that, except for homogeneous left dominance, schizophrenic men show twofold more ambilateral eye dominance than schizophrenic women.

Our analysis shows that with respect to the right eye dominance, the frequency arrangement in hierarchical order is as follows: schizophrenic women - 45.2%, 50.0%, 43.2%, schizophrenic men - 35.8%, 35.8%, 41.7%, control women - 21.2%, 17.3%, 19.2%, control men - 16.7%, 23.3%, 23.3%.

Data from the literature concludes that healthy women are less lateralized than healthy men. There is an opposite trend in schizophrenics. Schizophrenic men become less polarized matching normal women in left-eye dominance and schizophrenic women become more polarized matching normal men in left-eye dominance.

The dysfunction in the left hemisphere will determine both schizophrenia and sinistrality- and we may tentatively speculate that this will make schizophrenic men less lateralized than normally and schizophrenic women more lateralized than normally.

Thus, if left hemisphere dysfunction is related to schizophrenia, then eye dominance is directly related to cerebral hemispheric dominance and females with schizophrenia might have a greater chance of showing left eye dominance.

References

1. **Cannon, M., P. Jones, R. M. Murray, M. F. Wadsworth.** Childhood laterality and later risk of schizophrenia in the 1946 British birth cohort. – *Schizophr. Res.,* **26,** 1997, 117-120.
2. **Cannon, M., M. Byrne, B. Cassidy, C. Larkin, R. Horgan, N. P. Sheppard, E. O'Callagham.** Prevalence and correlates of mixed-handedness in schizophrenia. – *Psychiatry Res.,* **59**, 1995, 119-125.
3. **Collinson, S. L., T. Phillips, A. J. Iames, D. J. Quested, T. J. Crow.** Is lateral bias anomalous in early onset schizophrenia? Selected comparisons with normal populations. – *Psychiatry Res.*, **125,** 2004, 219-224.
4. **Dane, S., S. Yildirim, E. Ozan, N. Aydin, E. Oral, N. Ustaoglu, I. Kirpinar.** Handedness, eyedness, and hand eye crossed dominance in patients with schizophrenia: Sex-related lateralization abnormalities. – *Laterality*, **14(1)**, 2009, 55-65.
5. **Giotakos, O.** Crossed hand-eye dominance in male psychiatric patients. *Percept Mot Skills*, **95**, 2002, 728-732.
6. **Gur, R. E**. Motoric laterality imbalance in schizophrenia. A possible concomitant of left hemisphere dysfunction. – *Arch. Gen. Psychiatry*, **34(1)**, 1977, 33-37.
7. **Gureje, O.** Sensorimotor laterality in schizophrenia: which features transcend cultural influences? – *Acta Psychiatr Scand.*, **77**(2)**,** 1988, 188-193.
8. **Liu, Y. C, Y. K. Yang, K. C. Lin, I. H. Lee, K. J. Jeffries, L. C. Lee.** Eye-hand preference in Schizophrenia: sex differences and significance for hand function. – *Percept. Mot. Ski.,* **98**, 2004, 1225-1233.
9. **Maccoby, E. E., C. N. Jacklin.** *The psychology of sex differences*. Stanford, Stanford University Press, **1974.**
10. **Malesu, R. R., M. Cannon, P. B. Jones, K. McKenzie, K. Gilvarry, L. Rifkin, B. K. Toone, R. M. Murray.** Mixed-handedness in patients with functional psychosis. – *Br. J. Psychiatry*, **168,** 1996, 234-236.
11. **Murray, R.** Neurodevelopmental schizophrenia: The rediscovery of dementia praecox. – *Br. J. Psychiatry* **165** (Suppl. 25), 1994, 6-12.
12. **Nielsen, J. A., B. A. Zielinski, M. A. Ferguson, J. E. Lainhart, J. S. Anderson.** An evaluation of the left-brain vs. right-brain hypothesis with resting state functional connectivity magnetic resonance imaging. – *PLoS One*, **8(8)**, 2013, e71275.
13. **Oddy, H. C., T. J. Lobstein.** Hand and eye dominance in schizophrenia. - *Br. J. Psychiatry*, **120**, 1972, 331-332.
14. **Orr, K. G., M. Cannon, C. M. Gilvarry, P. B. Jones, R. M. Murray.** Schizophrenic patients and their first-degree relatives show an excess of mixed-handedness. – *Schizophrenia Res.,* **39,** 1999, 167-176
15. **Piran, N., E. D. Bigler, D. Cohen.** Motoric laterality and eye dominance suggest unique pattern of cerebral organization in schizophrenia. – *Arch. Gen. Psychiatry,* **39(9)**, 1982, 1006-1010.

16. Sakuma, M., A. L. Hoff, L. E. DeLisi. Functional asymmetries in schizophrenia and their relationship to cognitive performance. – *Psychiatry Res.,* **65**, 1996, 1–13.
17. Tomasi, D., N. D. Volkow. Laterality patterns of brain functional connectivity: Gender effects. – *Cereb. Cortex*, **22 (6)**, 2012, 1455–1462.
18. Weinberger, D. R. Implications of normal brain development for pathogenesis of schizophrenia. – *Archives General Psychiatry*, **44**, 1987, 660-669.
19. Yan, S. M., P. Flor-Henry, D. Y. Chen, T. G. Li, S. G. Qi, Z. Ma. Imbalance of hemispheric functions in the major psychoses: a study of handedness in the People's Republic of China. Biol. – *Psychiatry*, **20,** 1985, 906-917.

Institute of Experimental Morphology, Pathology and Anthropology with Museum
Bulgarian Anatomical Society

Acta Morphologica et Anthropologica, 31 (1-2)
Sofia ● 2024

Anatomical Variations of the Articular Surfaces of the Calcaneus among Bulgarian Population

Meglena Angelova, Desislava Marinova*

Medical University Prof. Dr. Paraskev Stoyanov, Varna, Bulgaria

*Corresponding author: angelovameglena@gmail.com

The subtalar joint is formed between talus and calcaneus, has a major role in redistributing the body weight to the distal parts of the foot. Our study showed that the variants with fused anterior and middle facets were widespread among the Bulgarian population. We measured the Gissane's angle, formed between the planes of the anterior and posterior articular surfaces of the calcaneus. The type with three separate articular surfaces was the most common and the angle was the smallest and sharpest. Next in frequency was the variant with fused anterior and middle facets which formed a hourglass shaped surface. On the third place was a spindle-shaped facet, formed by fusion of the anterior and middle ones and the Gissane's angle was the greatest one. In all these variants, the posterior facet of the calcaneus was autonomous and separated from the others.

Key words: calcaneus, articular surfaces, Gissane's angle, subtalar joint.

Introduction

Two anatomically and spatially separate joints are formed between the talus and the calcaneus - art. subtalaris and art. talocalcaneonavicularis by anatomical nomenclature. Because these two joints are functionally linked in a single kinematic chain, it is customary to collectively refer to them as the subtalar joint. This joint has a major role in redistributing the weight of the body to the distal parts of the foot. The anterior and middle articular surfaces of the calcaneus are accepted as part of the medial arch, and the posterior – as part of the lateral arch of the foot. Thus, the anatomy of this joint and its articular facets influence the overall morphology of the foot [6]. According to literature, several different variants of talar articular facets have been described [1, 11]. In type I, the anterior and middle articular surfaces of the calcaneus are fused and the resulting surface is spindle-shaped, remaining separated from the posterior one. Type II is distinguished by three different articular surfaces. The third variant (type III) is characterized by missing anterior facet, and the middle and posterior articular surfaces

are separated from each other. In type IV, the anterior and middle facets are fused, but the resulting surface is hourglass shaped. Type V presents with missing anterior and fused medial and posterior articular surfaces [1, 11] (**Fig.1**).

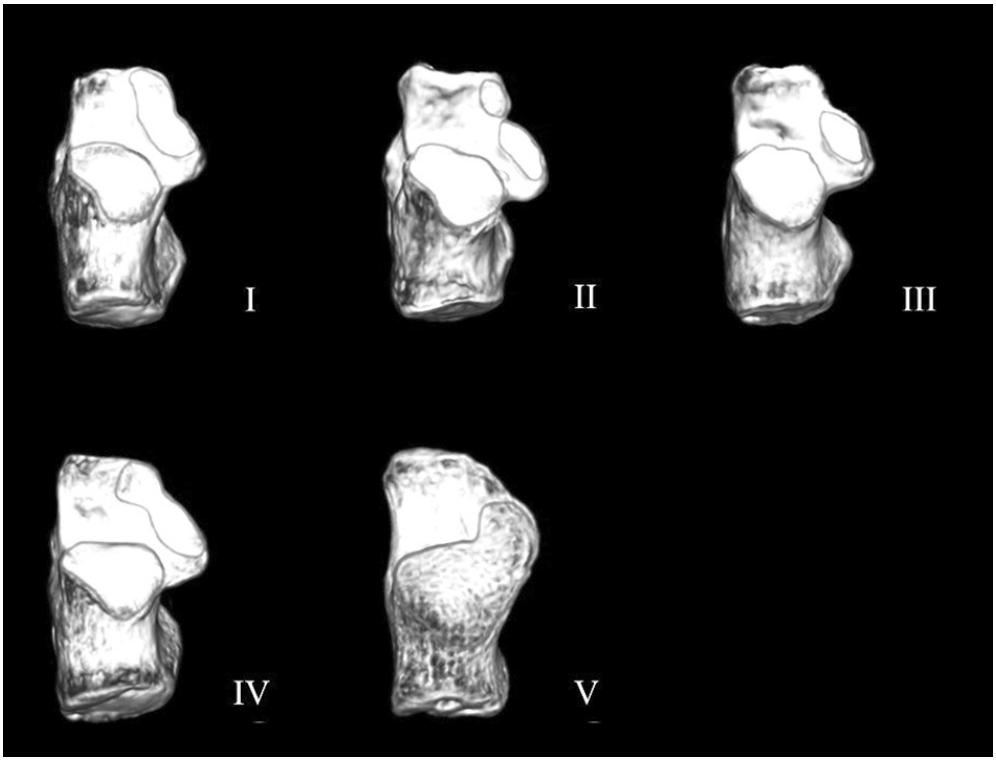

Fig. 1. Types of the talar articular facets of the calcaneus. The articular facets are outlined. Type I – fused anterior and middle facets in an oval-shaped articular surface. Type II – three separated articular surfaces. Type III – a missing anterior articular facet. Type IV – fused anterior and middle facets in an hourglass shaped articular surface. Type V – a missing articular facet and fused middle and posterior articular ones. (Agarwal et al., 2016 – [1]).

Bunning and Barnett have found a significantly higher frequency of the calcaneus type with three separate, autonomous facets, described as Type II by Agarwel, in the European population [3]. In their study significant differences were also indicated in the morphology of the calcaneus in the populations in Europe, Africa and Asia. According to their data, the type with the highest incidence among non-Europeans was that with fused anterior and middle articular surfaces, and its frequency was particularly high in women in African and Asian race. In study of the population in India, fusion of the anterior and middle surfaces has been observed in more than 66% of the examined calcanei. The next most frequent variation, with three separate facets, has been presented in 27.5% of cases [1]. Similar data has been obtained in a study in Turkey, where type I and type IV were dominant, with a total frequency of 58% [10].

Materials and methods

The present study was conducted on 130 calcanei from the bone collection of the Department of Anatomy and Cell Biology of MU-Varna. The bones belonged to Bulgarian citizens and were prepared by maceration according to the department's protocol. The obtained dry specimens were photographed, and the Gissane's angle was measured using open source software ImageJ. The Gissane's angle was defined as the angle between the planes of the anterior and posterior articular surfaces of the calcaneus. The results were statistically processed using Excel.

Results

The conducted study on the calcanei from the collection of bones in MU-Varna showed that the variants with fused anterior and middle facets were widespread among the Bulgarian population.

The type with three separate articular surfaces (Type II by Agarwel) was the most common and represented 40.35% of the studied bones. Next in frequency was the variant with fused anterior and middle facets which formed an hourglass shaped surface (Type IV) and it was observed in 29.82% of the cases. In 22.81%, a spindle-shaped or oval articular surface was found, resulting from the fusion of the anterior and middle ones (Type I). In all three described variants, the posterior facet of the calcaneus was autonomous and separate from the others. An anterior facet was missing in 7.02%, with separate middle and posterior facets (Type III). There were no cases corresponding to type V with fusion of the middle and posterior facets. In addition, the data showed a prevalence of variants with fused anterior and middle articular surfaces, and in total they represent 52.63% of all studied bones (**Fig. 2**).

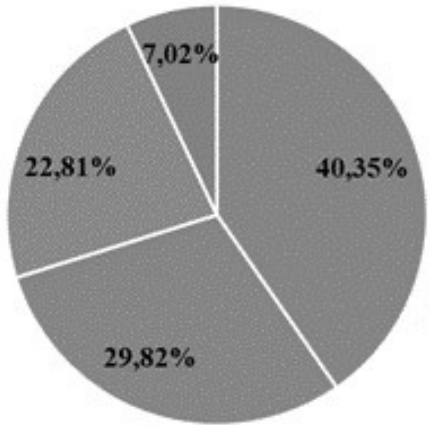

Fig. 2. Incidence of the observed types of calcaneus. 40,35% – three separated articular surfaces; 29,82% – fused anterior and middle facets in a hourglass shaped articular surface; 22,81% – fused anterior and middle facets in an oval-shaped articular surface; 7,02% – a missing anterior articular facet and fused middle and posterior ones.

The type I, type II and type IV Gissane's angle was measured (**Table 1**). The absence of an anterior articular surface in type III was judged to preclude the accurate measurement of the angle. We observed that the angle was the smallest and sharpest in the cases with three different articulation surfaces (Type II). The mean value was 135.26˚ (SD ± 9.25˚). In Type IV it was 148.76˚ (SD ± 7.79 ˚) and it was the greatest one in Type I – 161.38˚ (SD ± 6.66˚). The difference of the value Gissane's angle of these three groups was statistically significant ($p \leq 0.05$) (**Fig. 3**).

Table 1. Comparison of the Gissane's angle measurements. The angle values are presented in degrees (mean value ± SD).

Variants of talar articular facets	Type I	Type II	Type IV
Gissan's angle	161.38˚± 6.66˚	135.26˚± 9.25˚	148.76˚± 7.79 ˚

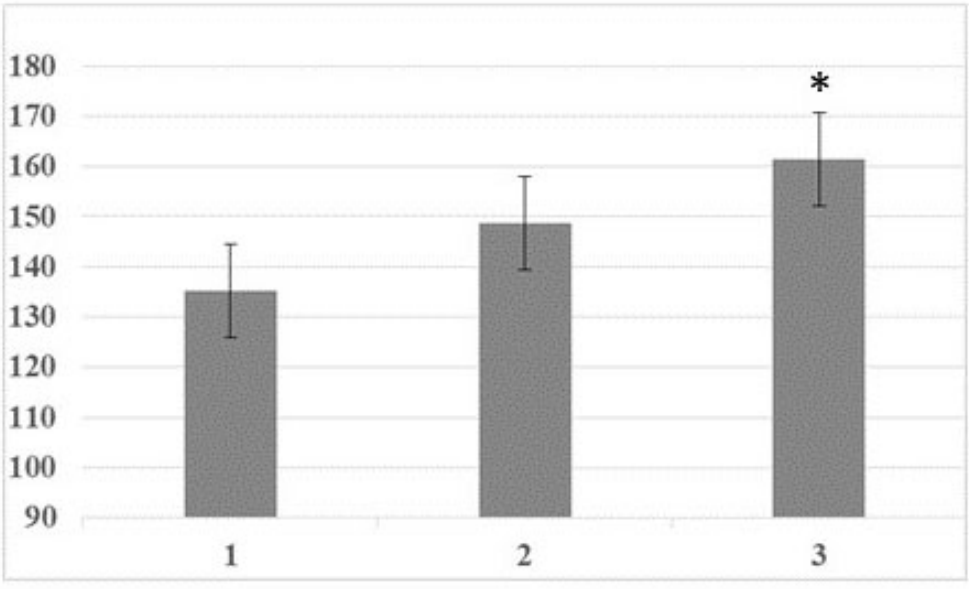

Fig. 3. Gissane's angle in different types of calcaneus in our study. 1 – three separated articular surfaces; 2 – fused anterior and middle facets in an hourglass shaped articular surface; 3 – fused anterior and middle facets in an oval-shaped articular surface.

Discussion

Variations in the articular surfaces between the calcaneus and talus have shown racial and regional differences. They affect mobility in the subtalar joint [2]. The joint is significantly more stable in the presence of three separate facets because in this situation they form a kind of tripod on which the talus is located and prevent excessive movement of its head. The study of Meary's angle (between the axis of the first metatarsal bone and the central axis of the talus) has proved a significant statistical difference in the incidence of flat foot in type I and type IV calcaneus compared to type II. This is in an agreement with the values of Gissane's angle, which are greater in types with fused facets. As larger is the angle, as flatter is the superior surface involved in the subtalar joint. The most obtuse angle has been observed in the cases when the fusion of anterior and middle facets results in an oval-shaped anterior surface [1, 9]. Our results are in unison with the available literature data.

In the cases with fused anterior and middle articular surfaces, the mobility of the subtalar joint is increased, especially the range of rotation of the talar head. It can lead to overstretching of the plantar calcaneonavicular ligament and adjacent muscle tendons, due to their continuous overload. Over time, this type of subtalar joint is predisposed to the development of joint instability and osteoarthritic changes [5] and has been associated with the development of flat foot [2].

In the cases with absence of the anterior articular surface, but middle and posterior one are on their appropriate places, the sustentaculum tali does not provide adequate support for the superiorly located talus. The talar head overrotates anteriorly and inferiorly, with the talus tilting plantarly and the calcaneus in a valgus position. Increased pressure on the anterior part of the subtalar joint, laxity of the capsule and ligaments, and frequent association with flat feet have been reported [8].

The major role of the subtalar joint in the integrity of the foot arches has led to the development of variety of techniques and methods that remodelate foot biomechanics, altering joint morphology. Increased height of the medial foot arch with at least five millimeters after subtalar arthrodesis has been reported [7]. At the same time, variations in the articular surfaces can affect the outcome of operative interventions, such as lateral calcaneus lengthening osteotomy [4].

Conclusions

1. There are three most frequent types of articular surfaces of the calcaneus among the Bulgarian population.
2. The most common type of the articular surfaces of the calcaneus among the Bulgarian population is with three separate articular facets (Type II by Agarwel), but the majority of cases are with fused anterior and middle facets.
3. Gissane's angle correlates with the type of articular surfaces of the calcaneus.

References

1. Agarwal, S., S. Garg, N. Vasudeva. Subtalar joint instability and calcaneal spurs associated with the configuration of the articular facets of adult human calcaneum in Indian population. – *Journal of Clinical and Diagnostic Research*, **10(9)**, 2016, 5-9.

2. Bruckner, J. Variations in the human subtalar joint. – *The Journal of Orthopaedic and Sports Physical Therapy*, **8(10)**, 1987, 489-494.

3. Bunning, P. S., C. Barnett. A comparison of adult and fetal talocalcaneal articulations. – *Journal of Anatomy*, **99(1)**, 1965, 71-76.

4. Canavese, F., A. Dimeglio, F. Bonnel. Postoperative CT-scan 3D reconstruction of the calcaneus following lateral calcaneal lengthening osteotomy for flatfoot deformity in children. Is the surgical procedure potentially associated with subtalar joint damage? – *Foot and Ankle Surgery*, **24(5)**, 2018, 453-459.

5. Drayer-Verhagen, F. Arthritis of the subtalar joint associated with sustentaculum tali facet configuration. – *Journal of Anatomy*, **183 (3)**, 1993, 631-634.

6. Gwani, A. S., M. Asari, Z. Mohd Ismail. How the three arches of the foot intercorrelate. – *Folia Morphologica,* **76(4),** 2017, 682-688.

7. Kitaoka, H., G. Patzer. Subtalar arthrodesis for posterior tibial tendon dysfunction and pes planus. – *Clinical Orthopaedics and Related Research*, **345**, 1997, 187-194.

8. Levangie, P. K., C. Norkin. Joint structure and function: Foundational concepts. In: *Joint structure and function: A comprehensive analysis* (Eds. P. K. Levangie & C. C. Norkin), 5th edition, Philadelphia, PA, F. A. Davis Company McGraw-Hill, 2011.

9. Qiang, M., Y. Chen, K. Zhang, H. Li, H. Dai. Measurement of three-dimensional morphological characteristics of the calcaneus using CT image post-processing. – *Journal of Foot and Ankle Research*, **7(1)**, 2014, 7-19.

10. Uygur, M., F. Atamaz, S. Celik, Y. Pinar. The types of talar articular facets and morphometric measurements of the human calcaneus bone on Turkish race. – *Archives of Orthopaedic and Trauma Surgery*, **129(7)**, 2009, 909-914.

11. Yang, Y., H. W. Cheng, Z. R. Xiong, N. Liu, Y. Liu, Y. Zeng, S. J. Fu, L. Zhang. Classification and morphological parameters of the calcaneal talar facet: which type is more likely to cause osteoarthritis in Chinese population? – *Biomed Res Int.*, 2019 Article ID 6095315.

Institute of Experimental Morphology, Pathology and Anthropology with Museum
Bulgarian Anatomical Society

Acta Morphologica et Anthropologica, 31 (1-2)
Sofia ● 2024

Morphological Variations of Umbilical Cord of Full-Term Foetuses - Correlation with Maternal and Newborn Parameters

Divia Paul A[1], Asha Joselet Mathew[2] , Blessymol Joseph[3]*

[1]Department of Anatomy, Fr Muller Medical College, Kankanady, Mangalore, Karnataka, India
[2]Department of Anatomy, Amrita School of Medicine, Kochi, Kerala, India
[3]Department of Anatomy, Vedantaa Institute of Medical Sciences, Dahanu, Palgar, Maharastra, India

*Corresponding author e-mail: drdiviamanoj@gmail.com

Abnormalities in the development and site of insertion of umbilical cord can cause problems which have the potential to affect maternal and foetal health. The aim of the present study was to assess the gross features of umbilical cord (UC) of singleton pregnancies and to find out the possible association to newborn parameters and maternal parameters at term. An observational, descriptive pilot study was carried out with one hundred placentas. All ethical principles for human research were followed. Adequately preserved placenta with no gross abnormalities were included. Placentae belonging to hypertensive mothers and mothers with gestational diabetes were excluded.The present study had 53% placentas with central, 36% eccentric, 3% furcuate and marginal and 5% with velamentous insertions. Correlation between the umbilical cord insertion site and birth weight was observed. Further investigations are required among velamentous insertion pattern for correlations with maternal blood group.

Key words: Umbilical cord, Insertion patterns, Placentae, Foetus, Maternal Parameters

Introduction

The umbilical cord (UC) connects the foetus with the placenta which contains two arteries and one vein surrounded by Wharton's jelly. Normal development and central pattern of insertion UC is expected, any deviation from the morphology can have potential affect maternal and foetal health [22, 28]. The UC transfers oxygen and nutrients to the growing fetus throughout pregnancy. Numerous studies have pointed out the importance of normal UC morphology with implications on insertion site. Abnormal positioning of UC can be associated with numerous maternal complications and fetal distress [13, 19, 20, 23, 24]. Variations in the site of insertion of umbilical cord are thought to result from the process known trophotrophism in which the chorionic frondosum or the early placenta "migrates" with advancing gestation to ensure a

better blood supply from a more richly vascularised area[24,17]. The UC insertion site can be subdivided into four categories: central, paracentral, marginal/battledore, and velamentous/membranous. The central/paracentral category is considered as the normal condition. It is well accepted that UC insertion is considered aberrant when attached within 2 cms of the edge of the placental disk (marginal/battledore) or when it is inserted into the chorioamniotic membranes (velamentous/membranous), which often leads to fetal death. Incidence of velamentous is 1.1% in singleton births and 8.7 to 16% in twin deliveries [3].Thus umbilical cord insertion to the placenta is divided as central, eccentric, marginal and velamentous, as it is related to the chorionic plates. Another type of variation is furcate insertion, in which umbilical cord branch before its insertion to placenta [8, 15, 24, 27,30].

Complications during delivery and other pathologies i.e; intrauterine growth retardation (IUGR), preterm labour and trophotrophism can be the outcome of peripherally inserted UC [14] Furcate type of insertion with a prevalence of (0.5-1%) has more volume of villi, villous trophoblast and syncytial knots [27]. Early impaired foetal development can be correlated with genetic and environmental associated mechanisms which are associated with and placental functioning and UC parameters [7, 14]. Oxygen and nutrienttransfer capacity of the placenta is highly associated with the vascular network within the chorionic villi. Abnormal UC insertion is associated with smaller placenta [7] and lower placental vessel density [16]. The placental insufficiency and fetal growth is dependent on abnormal cord insertion which may increase the susceptibility to antenatal risk [5, 6]. Optimal placentation will result in a central insertion of the UC which facilitate optimal growth of the foetus throughout gestation. Therefore, the aim of the present study was to evaluate the gross features of UC and correlating it to the newborn parameters and maternal parameters at term.

Materials and Methods

An observational, descriptive pilot study was carried out with one hundred placentas. All ethical principles for human research were followed and ethical approval was obtained from the Institutional Ethics Committee of the medical college from where data was collected. The inclusion criteria were the adequately preserved placenta with umbilical cord after delivery with no gross abnormalities from all pregnant ladies above 18 years of age. Placenta belonging to hypertensive mothers and mothers with gestational diabetes were excluded.

Collection of specimens: We collected a total of 100 specimens (placenta with intact UC) by random method of sample collection for a period of six months obtained from the department of obstetrics and gynecology (OBG). The mode of delivery and birth order were assessed. Samples were preserved in buffered 10% neutral formalin after the analysis at the department of anatomy for future assessments if required any.

Method of study: Specimens were cleared, dissected and observed carefully macroscopically for umbilical parameters namely insertion (central, eccentric, marginal, velamentous, furcuate) by measuring its distance from the placental margin, cord length (Normal between 55-60cm, long >60cm, short <40cm), cord vessels (number of arteries and veins), placental weight (Normal between 500-600gm, Overweight >600gm, Underweight <500gm), placental diameter (Normal between 20-22 cm, long

>23cm, short <19cm) and cord design (Normal, False knots and true knots). Details were photographed, recorded and analyzed.

New born parameters analyzed were baby weight (Normal 2.5-4.2kg, Overweight >4.2kg, Underweight <2.5gm), head circumference (Normal 33-35cm, more>37cm, less<31cm), baby length (Normal 50-52cm, more >55cm, less <45cm). Gestational age is defined as early term: when your baby is born between 37 weeks, 0 days and 38 weeks, 6 days, full term: when your baby is born between 39 weeks, 0 days and 40 weeks, 6 days, late term: when your baby is born between 41 weeks, 0 days and 41 weeks, 6 days. [12].

Maternal parameters assessed were maternal age, birth order, mode of delivery, previous birth manner and blood groups were noted down for further correlations. We have obtained consents from parents of the newborns involved in this study.

Results

The placental attachment of UC and the site of insertion were noted down for 100 samples. We had 74 normal and 26 caesarean section (CS) births. Among the samples, 53 placentas showed the central insertion, 36 eccentrically insertion of cords. In 3 specimens we found furcuated insertion and 5 specimens had velamentous insertion and 3 specimens showed marginal insertion (**Fig. 1 A-E**).

Normal cord length was seen in 89 cases with an average of 53.14 cm. Short cords were noted among 10 cases which had central and eccentric insertions. Single placenta had long cord. Ninety six cases showed normal cord vasculature were four cases showed abnormal vascular pattern with single umbilical artery (SUA) (**Fig. 1 Y**). Placental weight was normal in 70 cases, were 24 placentas weighed less than the normal attached by central and eccentric insertion to UC and 6 placenta had increased weight than normal which had furcuate,velamentous and eccentric insertions of UC.There were 61 placentas with normal diameter, 28 with increased diameter and 11 were decreased diameter. Normal design and pattern of UC were observed in 37 specimens with eccentric insertions predominantly. False knots were seen in 63 cords with central insertions (**Fig. 1 X**). No cord exhibited true knot.

New born parameters analysis showed that 89 infants had normal birth weight with an average of 2.88 Kg. No incidence of large for date baby was observed. 11 babies were underweight with their UC had central (5) and eccentric (6) insertions. Head circumference and baby length of 96 infants was normal with an average of 33.7 cm and 48.4 cm respectively. No incidence of large head circumference and increased baby length was observed. Among 4 babies with decreased head circumference and baby length had central (1) and eccentric (3) insertions of their UC attachment.

We did not find any significant association between the weight of the placentas with either gestational age of the foetus (Pearson's correlation, $r = 0.082$, $P = 0.42$) or the term of birth (Pearson's correlation, $r = 0.084$, $P = 0.40$). We also did not find any significant association between the length of the placental cord with either gestational age of the foetus (Pearson's correlation, $r = 0.064$, $P = 0.53$) or the term of birth (Pearson's correlation, $r = -0.012$, $P = 0.92$).

Considering the birth order, fifty four baby were born from the women who had

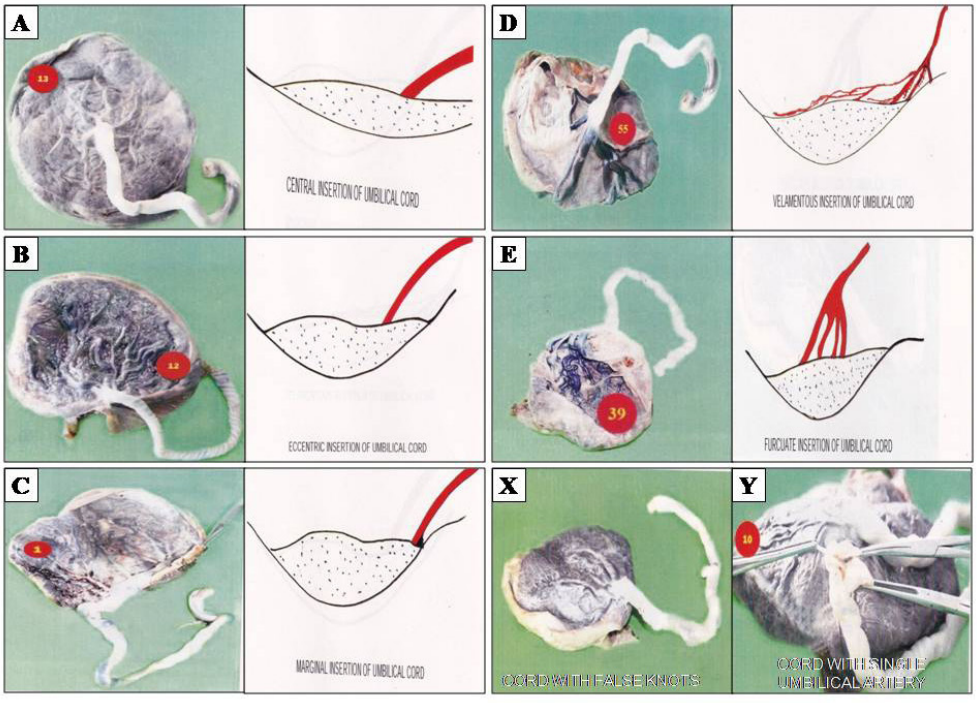

Fig. 1. Umblical cord insertions. A – Central,B – Marginal, C – Eccentric, D-Furcuate, E – Velamentous, X – Cord with false knots, Y – Cord with single umbilical artery

given birth for the first time, thirtyone from second, fourteen from third and one baby from fourth delivery. We did not find any significant association between the age of the mother and the mode of delivery (CS vs. normal). Maternal blood group analysis showed Rh^{+ve}andRh^{-ve}mothers of all blood groups had central, eccentric and marginal insertions. When velamentous insertion of cord was taken in to special consideration because of its complexities associated we had four B^{+ve} mothers and a single O^{-ve} mother. Further investigations are required among this insertion to reach to a conclusion for blood group correlations.

Discussion

The UC morphology and parameters and the deviations from optimal features under certain conditions can affect the foetus. A better understanding of cord function and design is essential for finding solutions to UC related complications. Abnormal UC's design can result in cord rupture, entanglement, complications during of labor and uterine malfunction.

The present study statistics showed 53% placentas with central insertion, 36% eccentric insertion, 3% furcuated and marginal insertions each and 5% specimens with velamentous insertion. Studies of Pilotto et al. [18], Rolschau et al. [25] and Ebbing

et al. [7] had also reported the highest prevalence of central followed by eccentric and marginal insertions.The study samples were more than the present study in other studies by different authors but the percentages of the fore mentioned insertions were similar to the present study. MK SS and MC VM report a high prevalence for eccentric insertions than central insertion in their study [21]. None of the comparative study had furcuate insertion for UC's. When velamentous insertion was taken in to account present study percentage for the same was more than studies of Rolschau et al. of 1.15% of velamentous insertions in their studies. Ebbing et al. had 1.5% and Brouillet et al. [4,7] had 0.95% of velamentous insertions in their sample populations. These percentages when compared to present study show a decreased trend. In the present study infant birth weight at term was reported within normal limits among central and peripheral UC insertions. Brouillet et al. [4] reported an association with fetal growth restriction in terms of low birth weight among UC insertion except central insertion. This result suggests that central UC attachment is relevant for attaining optimal foetal parameters i.e. foetal weight and in peripheral cord insertions there was higher occurrence of foetal growth retardation.

In the present study normal cord length was seen in 89 cases with an average of 53.14 cm. Short cords were noted among 10 cases which had central and eccentric insertions. Single placenta had long cord. Abaidoo et al. [1] reports an average cord length of 47.04 cm and the study also reports 21.56% of short cords which is more than the present study which had only 10% of short cords. When present study was compared to studies of Appiah et al. [2] the percentage of short cords were more in the compared study i.e 29.62%, where increased cord length percentages were similar to the present study. While comparing with the previous study of UC vasculature, it was noted that the SUA was more significant in the present study. The present study had 4% of SUA against 1% in studies of Geipel et al. and 0.2-1.1% in studies of Fernando et al. [9,11].

New born parameters analysis showed that 89 infants had normal birth weight with an average of 2.88 Kg. No incidence of large for date baby was observed.11 babies were underweight with their UC had central and eccentric insertions. Thomson et al. reports that the placental weight and size were not directly proportional to the birth weight [29]. In contrast to this, Shanklin et al.[26] reported low birth weight foetus, when cord is inserted marginally or velamentously. Grbesa et al. [10] reported decreased birth weight in foetus when cord was inserted eccentrically which is similar to the present study but increased birth weight was seen in babies with marginal insertion of cord to placenta. This is not observed in the present study.

Conclusion

In conclusion, correlation between the umbilical cord morphology with maternal and foetal parameters has been highlighted in our study. Extensive studies are required to better understand the pathophysiological mechanisms that facilitate for difference in pattern of UC insertions. To improve neonatal outcome and to avoid maternal complications during delivery, adequate antenatal checkups and ultrasound monitoring for umbilical cord abnormalities is inevitable. Further investigations are required among velamentous insertion to reach to a conclusion for maternal blood group correlations.

References

1. **Abaidoo, C. S., K. A. Boateng, M. A. Warren**. Morphological variations of the "Baby's supply line". – *Journal of Science and Technology (Ghana)*, **28**(2), 2008,1-9.
2. **Appiah, P. K**. Relationship between the morphology of the placenta umbilical cord and perinatal outcome. *PhD thesis*, Kwame Nkrumah University of Science and Technology, 2009.
3. **Benirschke, K., P. Kaufmann, R. Baergen.** Multiple pregnancy. – *Pathology of the Human Placenta,* 2000, 790-902.
4. **Brouillet, S., A. Dufour, F. Prot, J. J.Feige, V. Equy, N. Alfaidy, P. Gillois, P. Hoffmann.** Influence of the umbilical cord insertion site on the optimal individual birth weight achievement. – *BioMedRes.International*, 2014. Article ID 341251
5. **Burton, G. J., E. Jauniaux.** Placental oxidative stress: from miscarriage to preeclampsia. – Journal of the Society for Gynecologic Investigation, **11**(6), 2004, 342-352.
6. **Burton, G. J., E. Jauniaux, A. L. Watson.** Maternal arterial connections to the placental intervillous space during the first trimester of human pregnancy: the Boyd collection revisited. – *American Journal of Obstetrics and Gynecology*,**181**(3),1999, 718-724.
7. **Ebbing, C., T. Kiserud, S. L. Johnsen, S. Albrechtsen, S. Rasmussen.** Prevalence, risk factors and outcomes of velamentous and marginal cord insertions: a population-based study of 634,741 pregnancies. – *PLOS one*, **8**(7), 2013, Article ID70380.
8. **Gavriil, P., E. Jauniaux, F. Leroy.** Pathologic examination of placentas from singleton and twin pregnancies obtained after in vitro fertilization and embryo transfer. – *Pediatric pathology*, **13**(4),1993, 453-462.
9. **Geipel, A., U. Germer, T. Welp, E. Schwinger, U. Gembruch.** Prenatal diagnosis of single umbilical artery: determination of the absent side, associated anomalies, Doppler findings and perinatal outcome. – *Ultrasound in Obstetrics and Gynecology*, **15**(2), 2000,14-117.
10. **Grbeša, Đ., B. Durst-Živković.** Neonatal and placental factors in relation to the mode of umbilical cord insertion: Stereological analysis of chorionic villi. – *Pflügers Archiv*, **431**, 1996, 205-206.
11. **Heredia, F., P. Jeanty.** Umbilical cord anomalies. – *Women's Health Alliance,* 2002, 1149. Available at www. thefetus. net/http://sonoworld. com/fetus/page. aspx?
12. **Kandraju, H., S. Agrawal, K. Geetha, L. Sujatha, S. Subramanian, S. Murki.** Gestational age-specific centile charts for anthropometry at birth for South Indian infants. – Indian paediatrics, **49**, 2012, 199-202.
13. **Liu, C.C., D. H. Pretorius, A. L. Scioscia, A. D. Hull.** Sonographic prenatal diagnosis of marginal placental cord insertion: clinical importance. – *Journal of Ultrasound in Medicine*, **21**(6), 2002, 627-632.
14. **Luo, G., R. W. Redline.** Peripheral insertion of umbilical cord. – *Pediatric and Developmental Pathology*, **16**(6), 2013, 399-404.
15. **McLennan, J. E.** Implications of the eccentricity of the human umbilical cord. – *American Journal of Obstetrics and Gynecology*, **101**(8), 1968, 1124-1130.
16. **Misra, D. P., C. M. Salafia, R. K. Miller, A. K. Charles.** Non-linear and gender-specific relationships among placental growth measures and the fetoplacental weight ratio. – *Placenta,* **30**(12), 2009, 1052-1057.
17. **Monie, I. W.** Velamentous insertion of the cord in early pregnancy. – *American Journal of Obstetrics and Gynecology*, **93**(2), 1965, 276-281.
18. **Piloto, R. F., L. A. Magna, B. Beiguelman.** Factors influencing human birth weight in normal pregnancy: a prospective study in a Brazilian university hospital. – *Rev. Bras. Genet.*, 1993, 457-69.

19. Pinar, H., M. Carpenter. Placenta and umbilical cord abnormalities seen with stillbirth. – Clinical obstetrics and gynecology, **53**(3), 2010, 656-672.
20. Räisänen, S., L. Georgiadis, M. Harju, L. Keski-Nisula, S. Heinonen. Risk factors and adverse pregnancy outcomes among births affected by velamentous umbilical cord insertion: a retrospective population-based register study. – *European Journal of Obstetrics & Gynecology and Reproductive Biology*, **165**(2), 2012, 231-234.
21. Ranga, S. S., V. Mallika. Morphological variations of Umbilical cord in Human placenta. – *Int. J. Ana.t Res.*, **7**(3.1), 2019, 6786-6789.
22. Redline, R. W. The clinical implications of placental diagnoses. – In Seminars in perinatology,WB Saunders, **39**(1), 2015, 2-8.
23. Redline, R. W. Clinical and pathological umbilical cord abnormalities in fetal thrombotic vasculopathy. – *Human pathology*, **35**(12), 2004,1494-1498.
24. Robinson, L. K., K. L. Jones, K. Benirschke. The nature of structural defects associated with velamentous and marginal insertion of the umbilical cord. – *American journal of obstetrics and gynecology*, **146**(2),1983,191-193.
25. Rolschau, J. The relationship between some disorders of the umbilical cord and intrauterine growth retardation. – *Acta Obstetricia et Gynecologica Scandinavica*, **57**(S72), 1978, 15-21.
26. Shanklin, D. R. The influence of placental lesions on the newborn infant. – *Pediatric Clinics of North America*, **17**(1), 1970, 25-42.
27. Singh, I., G. P. Pal. *Human Embryology of The Placenta* (Macmillan Publishers), 8th edition, India Ltd, lndia, 2009, 59-75.
28. Tantbirojn, P., A. Saleemuddin, K.Sirois, C. P. Crum, T. K. Boyd, S.Tworoger, M. M. Parast. Gross abnormalities of the umbilical cord: related placental histology and clinical significance. – *Placenta*, **30**(12),2009,1083-1088.
29. Thomson, A.M., W. Z. Billewicz, F. E. Hytten. The weight of the placenta in relation to birthweight. – *BJOG: An International Journal of Obstetrics & Gynaecology*, **76**(10), 1969, 865-872.
30. Uyanwah-Akpom, P., H. Fox. The clinical significance of marginal and velamentous insertion of the cord. – *BJOG: An International Journal of Obstetrics &Gynaecology*, **84**(12), 1977, 941-943.

Table 1. Morphological features of umbilical cord

CATEGORY	CONDITION	n (%)			
PARAMETERS		C	E	M	F	V
UC Insertion		53	36	3	3	5
UC Length	Normal	48	31	3	3	4
	Long	0	1	0	0	0
	Short	5	4	0	0	1
UC Vasculature	Normal	49	36	3	3	5
	Abnormal	4	0	0	0	0
Placental weight	Normal	35	26	3	2	4
	More	0	4	0	1	1
	Less	18	6	0	0	0
UC Design	Normal	12	24	1	0	0
	False Knots	41	12	2	3	5
	True Knots	0	0	0	0	0

Abbreviations: UC – Umbilical cord, C – Central, E – Eccentric, M – Marginal, F – Furcuate, V-Velementous

Institute of Experimental Morphology, Pathology and Anthropology with Museum
Bulgarian Anatomical Society

Acta Morphologica et Anthropologica, 31 (1-2)
Sofia ● 2024

Superficial Brachial Artery Continuing into the Forearm as a Radial Artery: Case Report

Viktor Ivanov[1], Meglena Angelova[2], Desislava Marinova[2]*

[1]3rd year Medical student, Medical University "Prof. Dr. Paraskev Stoyanov", Varna, Bulgaria
[2]Department of Anatomy and Cell Biology – Medical University "Prof. Dr. Paraskev Stoyanov", Varna, Bulgaria

*Corresponding author e-mail: viktorivanov596@gmail.com

A rare variation of the brachial artery (BA) on the right upper limb was discovered during routine anatomical dissection. The axillary artery bifurcated into two large-sized blood vessels above the teres major muscle - superficial brachial artery (SBA) and deep brachial artery (DBA). The SBA passed between the roots of the median nerve and continued as the radial artery (RA) in the forearm. The deep brachial artery (DBA) was a continuation of the axillary artery (AA). It traversed behind and lateral to the median nerve and in the cubital fossa it turned into the ulnar artery (UA). Detailed knowledge of the variations of the vessels' branching pattern is essential for providing accuracy during vascular diagnosis, reconstructive surgery, and in the evaluation of angiographic images.

Key words: superficial brachial artery, brachial artery variations

Introduction

Accurate knowledge of muscular and neurovascular variations is important for both surgeons and radiologists and may prevent diagnostic errors. The arteries with an abnormal superficial course are often mistaken as superficial veins and accidental injection of certain drugs in these arteries may lead to serious conditions like gangrene or loss of the upper limb. Because their course is superficial, they are more likely to be affected by trauma, which would result in heavy bleeding. According to available medical literature, variations in the branching pattern of the main arteries of the upper limb are discovered in 25% of the studied cases [1, 2, 3].

Material and Methods

The presented case is of a 90-year-old Caucasian male cadaver from the dissection hall of the department of Anatomy and Cell Biology, Medical University-Varna, Bulgaria.

Routine dissection of the axillary fossa and upper limb was performed, according to Vankov's standard dissection guideline. All muscles and neuro-vascular bundles of these regions were exposed, structures were observed for details like origin and orientation, and photographs were taken for documentation. Cadaver material was obtained according to Regulation No 2 from 18.05.2012 of the Bulgarian Ministry of Health.

Results

A variation of the axillary artery was found. It continued as two brachial arteries (BA). Both of them were traced. The superficially located one originated at the level of teres major muscle and went between the lateral and medial roots of the median nerve. In the cubital fossa, this artery moved laterally, gave off the recurrent radial artery and continued as the radial artery (RA) in the forearm between the pronator teres and the brachioradialis muscles **(Fig. 1b)**. The second terminal branch of the axillary artery was located deeper, behind and lateral to the median nerve **(Fig. 1a)**. At the level of the forearm, it divided into the ulnar (UA) and interosseous arteries. The radial and ulnar arteries gave branches and formed the superficial palmar arch **(Fig. 1c)**. The described variation corresponded to cases with superficial brachial artery (SBA), reported in the literature.

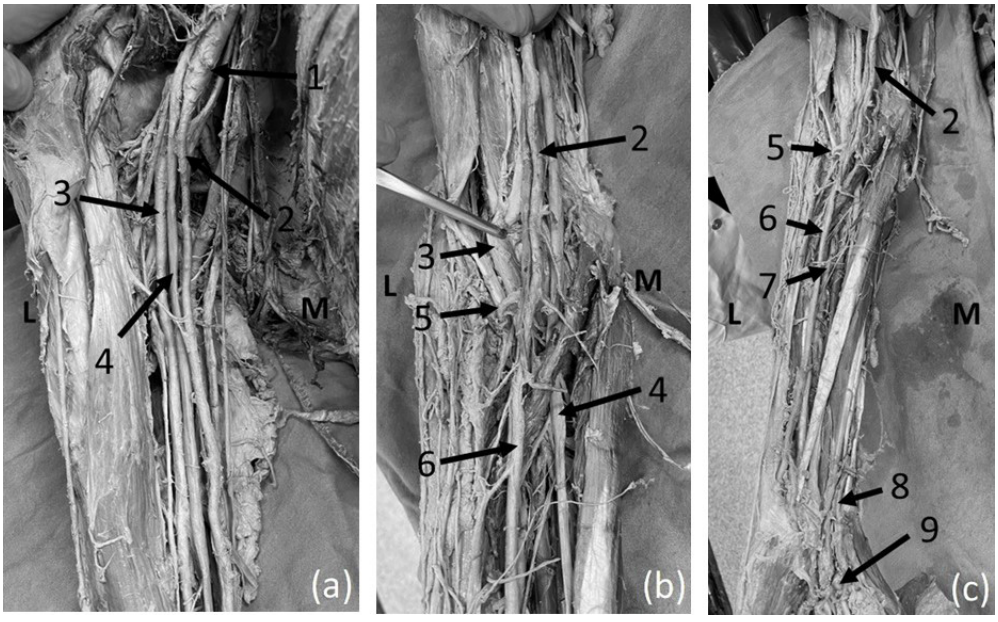

Fig. 1. Formation and orientation of superficial and deep brachial arteries. (a) Anterior brachial region. (b) Cubital fossa. (c) Anterior surface of the forearm and palmar region of the hand. 1. Axillary artery; 2. Superficial brachial artery; 3. Deep brachial artery; 4. Median nerve; 5. Recurrent radial artery; 6. Radial artery; 7. Interosseous artery; 8. Ulnar artery; 9. Superficial palmar arch. M – medial side. L – lateral side.

Discussion

The brachial artery is the major blood vessel of the arm. Variations are important for surgeons and it seems necessary to identify unusual arterial patterns of the upper limb in order to avoid complications with intravenous drug administration and venipuncture. Variations in upper limb arteries have been frequently observed either in routine dissections or in clinical practice.

The most reported variations of the upper limb arteries are described as:

Type 1: This category comprises "normal" anatomy, which is the most common variant – the BA is a continuation of the AA. It is located at the lateral side of the median nerve and ends at the level of the neck of the radius, by dividing into RA and UA [3].

Type 2: SBA is formed as a branch of the AA and distally it gives off the RA and UA of the forearm. The direct continuation of the AA ends as a collateral branch around the elbow joint [3].

Type 3: SBA is formed as a branch of the AA and distally it turns into the RA of the forearm. The AA continues as the deep brachial artery (DBA), which proceeds as the UA [7, 10].

Type 4: SBA is a small vessel that ends in the arm. Its main role is to supply the muscles of the area with blood. DBA follows the "normal" anatomy pattern of the BA [7, 10].

Type 5: Accessory brachial artery (ABA) originating from the BA or AA. After a short course, still within the arm or in the region of the cubital fossa, the ABA rejoins the BA. The fusion of both blood vessels is located proximally to the beginning of RA and UA [7, 10].

Type 6: Superficial brachioradial artery (SBRA) is a RA originating from the upper, middle or lower third of the BA. BA continues as UA [7, 10].

Type 7: Superficial brachioulnar artery (SBUA) has an origin similar to the SBRA but continues as an UA [7, 10].

The findings in our case are corresponding to Type 3 mentioned above.

SBA is observed and reported mostly in the right upper limb [2, 9, 11] with just a few cases in the left upper limb [6]. In our study, we also reported the right location of SBA. In 1961 Keen suggested that the reported variation is a high origin of the radial artery [8]. Such superficial course of accessory brachial artery could be used during coronary catheterization. At the same time existence of a such superficial brachial artery makes it more prone to injuries which can lead to bleeding and ischemia.

Conclusions

Attention has to be given to the branching pattern of the brachial artery while treating the cases of arterio-venous fistulae, aneurysms and abscesses in the axillary area, arm and cubital fossa. The anatomical position of the BA should be considered while performing cardiac catheterization, intra-arterial injections and angiographic procedures using this pathway. Because of all these factors, studies of the vascular variations of the upper limb have significant implications for preventing complications in medical practice.

References

1. **Afroze, M., S. Hayat, S. Shirbadgi.** Branching pattern of brachial artery with accent to high up division and clinical significance. – *Academia Anatomica International*, **5(2)**, 2019, 55-58.
2. **AL-Fayez, M., Z. KaimkhanI, M. Zafar, H. Darwish, A. Aldahmash, A. Al-Ahaideb.** Multiple arterial variations in the right upper limb of a Caucasian male cadaver. – *Int. J. Morphol.*, **28**, 2010, 659-665.
3. **Bagal, G., S. Takale.** A Cadaveric study on division of brachial artery with its embyological basis and clinical significance. – *JMSCR*, **3**, 2015, 8708-8712.
4. **Chakravarthi, K., S. Ks, N. Venumadhav, A. Sharma, N. Kumar.** Anatomical variations of brachial artery - its morphology, embryogenesis and clinical implications. – *J. Clin. Diagn. Res.*, **8(12)**, 2014, 17-20.
5. **Chauhan, K, A. Udainia, C. Bhatt, D. Patil, V. Patel, B. Prajapati.** Morphological study of variations in branching pattern of brachial artery. – *Int. J. Basic & Applied Med. Sci.,* **3**, 2013, 10-15.
6. **Coskun, N, L. Sarikcioglu, B. Donmez, M. Sindel.** Arterial, neural and muscular variations in the upper limb. – *Folia Morphol.,* **64**, 2005, 347-352.
7. **Glin, M., N. Zielinska, K. Ruzik, P. Karauda, M. Konschake, Ł. Olewnik.** Morphological variations of the brachial artery and their clinical significance: a systematic review. – *Surg. Radiol. Anat.*, **45**, 2023, 1125-1134.
8. **Keen, J. A**. A study of the arterial variations in the limb, with special reference to symmetry of vascular patterns. – *Am. J. Anat.,* **108**, 1961, 245-261.
9. **Natsis, K, A. Papadopoulou, G. Paraskevas, T. Totlis, P. Tsikaras.** High origin of a superficial ulnar artery arising from the axillary artery: anatomy, embryology, clinical significance and review of the literature. – *Folia Morphol.,* **65**, 2006, 400-405.
10. **Rodríguez-Niedenführ, M., T. Vázquez, L. Nearn, B. Ferreira, I. Parkin, JR. Sañudo.** Variations of the arterial pattern in the upper limb revisited: a morphological and statistical study, with a review of the literature. – *J. Anat.,* **199(5)**, 2001, 547-566.
11. **Tohno, Y, S. Tohno, C. Azuma, K. Kido, Y. Moriwake.** Superficial brachial artery continuing into the forearm as the radial artery. – *J. Nara Med. Assoc.*, **56**, 2005, 189-193.
12. **Vatsala, A. R., H. Rajashekar, A. Angadi.** Variation in branching pattern of brachial artery: a morphological and statistical study. – *Int. J. Biol. Med. Res*., **4(1)**, 2013, 2920-2923.
13. **Yagain, V., M. Dave, S. Anadkat.** Unilateral high origin of radial artery from axillary artery. – *Folia Morphol.,* **71(2)**, 2012, 121-124.

Institute of Experimental Morphology, Pathology and Anthropology with Museum
Bulgarian Anatomical Society

Acta Morphologica et Anthropologica, 31 (1-2)
Sofia ● 2024

The Titan Submersible Tragedy: physiopathology of the death mechanism and the necessity of prevention for Deep Sea Explorations

Matteo Antonio Sacco[1a], Francesco Maria Galassi[2a], Elena Varotto[3], Pietrantonio Ricci[1], Isabella Aquila[1]*

[1] Institute of Legal Medicine, Department of Medical and Surgical Sciences, "Magna Graecia" University of Catanzaro, Catanzaro, Italy
[2] Department of Anthropology, Faculty of Biology and Environmental Protection, University of Lodz, Lodz, Poland
[3] Archaeology, College of Humanities, Arts and Social Sciences, Flinders University, Adelaide, SA, Australia

***** Correspondence to Francesco M. Galassi, MD PhD, Associate Professor, e-mail: francesco.galassi@biol.uni.lodz.pl
[a] Shared first authorship.

This paper examines the physiopathology of death in the tragedy of the Titan submersible in the light of knowledge on barotrauma and established forensic literature. It also offers practical views on preventive measures against such public health risks. The aim of the work is to reconstruct from a medico-legal point of view the plausible manner of death considering the location and the high depth in the sea reached by the submersible. The case shows the significant environmental risks related to the marine environment at great depths, such as barotrauma and hypothermia, emphasizing the need to prevent these events with strict and suitable safety measures.

Key words: Titan; deep sea exploration; prevention; forensic anthropology; barotrauma

Introduction

The Titan submersible was a groundbreaking creation designed to delve into the depths of the ocean up to 4,000 meters, accommodating up to five individuals [2]. This submersible marked a significant advancement in underwater exploration technology, offering researchers and adventurers the opportunity to explore the mysteries of the deep sea. However, despite its advanced design and capabilities, the Titan submersible encountered a tragic accident during one of its missions. In fact, on June 18, the Titan

began its scheduled dive. The operation seemed to be proceeding smoothly, however after an hour and 45 minutes, the submarine no longer sent the communications that were scheduled every 15 minutes. The submarine was supposed to surface at 2.00 pm EDT without ever doing so. The accident involving the Titan submersible has once again highlighted the risks of deep-sea exploration. Despite the presence of various safety features, the missing submersible still underwent, as per the latest reports, a catastrophic implosion, leading to the presumed fatality of its pilot and four passengers. This occurrence has prompted inquiries regarding the existing safety protocols for deep-sea submersion and the physiological impact of extreme pressure and temperature on the human body. In this paper, we shall investigate the plausible reasons behind the Titan submersible tragedy, the physiological consequences of extreme pressure and extreme low temperature on the human body, as well as methods for avoiding submersible accidents and enhancing safety precautions.

Case presentation: the Titan submersible

The reasons behind the tragic event involving the Titan submersible remain unknown and are currently under investigation. Nonetheless, specialists have been expressing concerns about the safety and development of the Titan submersible since 2018 [5]. Although the submersible had multiple mechanisms designed to bring it to the surface in case of an emergency, but these mechanisms failed to prevent the tragedy [5]. According to experts, the Titan submersible collapsed catastrophically due to the extreme pressure and temperature at the deep-sea level, leading to the instantaneous death of its pilot and four passengers [1, 8]. While the investigation is still ongoing, this incident underlines the possible dangers of deep-sea expeditions.

Discussion

The effects of extreme pressure and temperature on the human body are significant and can pose a threat to life. When an individual submerges in water, the pressure increases with depth and can lead to barotrauma. Barotrauma can cause damage to various parts of the body, including middle ear and paranasal sinuses, pneumothorax, pulmonary hemorrhage, decompression sickness and arterial gas emboli. This damage can be caused by the compression of gas-filled spaces in the body due to the increased pressure. During ascent, gases in the body expand, which can also lead to barotrauma. In such cases, overexpansion of the lungs can occur, resulting in pulmonary barotrauma [3].

There are several factors that are attributed to mechanisms of death related to submersion-related barotrauma. A common cause of death in self-contained underwater breathing apparatus (SCUBA) diving is pulmonary barotrauma. When a diver resurfaces, overexpansion of the lungs can lead to significant injury and death [7]. Tension pneumothorax, which can result in death in just a few minutes, is another cause [7]. Additionally, barotrauma of descent can cause injury in closed spaces in contact with the diver, such as the ear, teeth, and sinuses [3]. We know that the depth of placement of the Titanic is approximately 4,000 m on the bottom of the North Atlantic Ocean. At 4000 meters deep, the pressure is 400 bar [6]. The analysis of the event makes it possible to hypothesize several plausible scenarios from a forensic point of

view. The first detects a possible confinement due to lack of oxygen with accumulation of carbon dioxide and saturation of the rooms of the Titan occupied by passengers.

The second, more likely than the published news, instead concerns a mechanism mainly related to the pressure reached at great depths. In particular, the implosion hypothesized in the last few days by the news would necessarily reveal, from a forensic point of view, a rupture of the Titan such as to allow the achievement of a sudden and very strong pressure imbalance. Such a dynamic would therefore plausibly cause a very high mechanical energy on the victims exerted by the amount of high-pressure water on the passengers, thus determining from a forensic point of view a rapid traumatic crushing with simultaneous drowning. In the dynamics of the events, it is likely to hypothesize a laceration of organs with leakage from the respective anatomical cavities with respect to the greater integrity of other tissues such as the skin and muscles.

In any case, although it is possible to hypothesize a greater integrity of more resistant tissues such as bone, muscles and skin, it is necessary to consider the marine macrofauna at great depths, with the mechanical action of the currents and the thermal variations of the Atlantic Ocean. At these depths, in fact, the macrofauna includes various species of large dimensions, considering the phenomenon of deep-sea gigantism, such as the jellyfish known as *Stygiomedusa gigantea*, the giant isopod, big red jellyfish, giant sea spider, giant ostracod [9]. Finally, as regards the effects of low temperature, the marine depth of 4000 meters would include temperatures between 3/4°C with risk of death in a few minutes due to hypothermia mechanisms. In fact, the human body placed in water loses heat at a much greater rate (about 25 times) than a subject in air. The effects of hypothermia occur when the body temperature drops below 35°C, becoming severe below 28°C with consequent sharp increase in blood pressure, bradycardia, fatal arrhythmias, coma and loss of reflexes [4].

It is crucial to comprehend these mechanisms of death so that prompt and effective treatment can be administered. To prevent accidents involving submersibles and enhance safety measures, it is essential to employ effective strategies such as proper training, equipment maintenance, and safety protocols. Deep-sea exploration entails a considerable level of risk, and safety training is crucial for submersible pilots and passengers to understand these associated risks [10]. By employing adequate safety protocols and maintaining equipment in good condition, it is possible to prevent accidents and promote the safety of submersible expeditions.

Conclusions

The accident involving the Titan submersible evidences to date the perils that accompany deep-sea exploration. The investigation into the causes of the tragedy is still ongoing, but the deleterious effects of extreme pressure and temperature on the human body are widely recognized. To prevent future mishaps, it is crucial that we establish more stringent safety protocols and implement preventative measures to safeguard the well-being of submersible pilots and passengers alike.

References

1. **Associated Press News**. Live updates. Titan's catastrophic implosion likely killed 5 occupants instantly, experts say. June 20th 2023. https://apnews.com/article/missing-sub-titanic-search-live-updates-c2470ab6159caf32ca11010d4f4ce5e7
2. **Bakhtiari, M**. Lessons from the Titan submersible: A wake-up call for radiation oncology. – *J. Appl. Clin. Med. Phys.,* **25(2**), 2024, e14121.
3. **Battisti, A. S., A. Haftel, H. M. Murphy-Lavoie.** Barotrauma. – *StatPearls (Internet)*. June 20th 2023. available at: https://www.ncbi.nlm.nih.gov/books/NBK482348/.
4. **Hleșcu, A. A., A. Grigoraș, V. Ianole, C. Amalinei.** Advanced diagnostic tools in hypothermia-related fatalities – a pathological perspective. – *Diagnostics (Basel),* 2024, **14(7),** 739.
5. **Houston Public Media**. A former passenger details what it's like inside the missing Titan submersible. June 20th 2023. https://www.houstonpublicmedia.org/npr/2023/06/20/1183273102/a-former-passenger-details-what-its-like-inside-the-missing-titan-submersible/
6. **Hu, X., Z. Ma, Z. Gong, F. Zhao, S. Guo, D. Zhang, Y. Jiang**. A Highly sensitive deep-sea hydrodynamic pressure sensor inspired by fish lateral line. – *Biomimetics (Basel),* **9(3),** 2024, 190.
7. **Kennedy-Little, D., T. Sharman.** Pulmonary barotrauma. – *StatPearls (Internet)*, June 20th 2023. available at: https://www.ncbi.nlm.nih.gov/books/NBK559293/
8. **Pittman, R. N.** The circulatory system and oxygen transport. *In: Regulation of tissue oxygenation*, San Rafael, CA, Morgan & Claypool Life Sciences, 2011.
9. **Timofeev, S. F.** Bergmann's principle and deep-water gigantism in marine crustaceans. – *Biology Bulletin,* **28,** 2021, 646–650.
10. **United States Department of Labor**. Occupational safety and health administration, 2023. https://www.osha.gov.

Institute of Experimental Morphology, Pathology and Anthropology with Museum
Bulgarian Anatomical Society

Acta Morphologica et Anthropologica, 31 (1-2)
Sofia ● 2024

Anatomical Features Related to the Locomotion of the Brown Bear (Ursus arctos) Zeugopodium

Iliana Ruzhanova-Gospodinova, Georgi I. Georgiev*

Department "Anatomy, Physiology and Animal science", Faculty of Veterinary Medicine, University of Forestry, Sofia, Bulgaria

* Corresponding author e-mail: iliana_ruzhanova@ltu.bg

The present study aimed to examine the bones and muscles of the Brown bear's (*Ursus arctos*) zeugopodium by macroscopic dissection and identification on 18 thoracic and pelvic limbs, from 5 male and 4 female bears. The features of the muscles and bony structures responsible for the rotation of the antebrachial bones and for the plantar flexion with the eversion of the autopodium in relation to the adaptive mechanisms of the limb to the environment of the Brown bear were investigated. The obtained results were analyzed and compared with the pentadactyl extremity of the dog, cat, rabbit, and human to highlight the specific adaptation of the limbs in the Brown bear. Understanding the locomotion of the limbs is important for veterinary neurology, orthopedics, and traumatology, where the specific adaptation ability should be considered for a better diagnosis and correct treatment.

Key words: Brown bear, supination, pronation, radius, zeugopodium, *m. soleus*

Introduction

As part of the suborder Caniformia of the order Carnivora, the Brown bear has some features of the Canidae family and has been compared to both the dog [14, 26] and the cat [26], but also to the human [9]. In recent years, some morpho-functional and histological studies of the stomach and adrenal glands of the Brown bear have been performed [22, 23]. In our previous research Brown bear arteries, veins, and nerves of the zeugopodium were examined and compared with the dog, cat, and human [20, 21]. Devis 1941 established a similarity between the blood vessels of the thoracic limb of the Red panda (*Ailurus fulgens*) and ursids, while a study on the Spectacled bear (*Tremarctos ornatus*) and Himalayan bear (*Ursus thibetanus*) showed the most appropriate site for blood collecting from the cephalic vein [8, 18]. From an anatomical point of view, the skeletal system of the bear has been widely researched [10, 11, 15, 19]. Sasaki et al. [24] studied the pelvic limb muscles of the Malayan Sun bear

(*Helarctos malayanus*), Polar bear (*Ursus maritimus*), Brown bear, and Giant panda (*Ailuropoda melanoleuca*) concerning their climbing abilities. Amaike et al., 2021 compared the forearm skeletal mobility of Himalayan, Brown, and Polar bears [1]. From the information obtained could be concluded that supination is the movement that is often implemented by the bear. The limited data on the development and function of the musculature related to it drove the authors to study the musculature of the zeugopodium. In the present study the bone structures, the muscles, and their function in the Brown bear were compared with the available data in the literature for the dog, cat, rabbit, and human [1, 2, 5, 6, 7, 11, 13, 28].

Material and Methods

All bear cadavers in the present research are animals from the "Dancing Bear Park" in Belitsa, Bulgaria, who died naturally or were euthanized for medical reasons. The limbs of nine bears were included in the study – 5 male and 4 female, between 30-40 years of age. The skin in the distal part of the limbs was carefully removed. The muscles and their insertion tendons in the regions of interest were dissected and photographed with Lumix DC FZ82 (Panasonic®, Japan). The bones from the same cadavers were prepared by boiling water method with subsequent immersion in diluted with purified water to 15% Hydrogen peroxide (30% Valerus®, Bulgaria) for 24 hours. So prepared bones of the zeugopodium were analyzed and photographed. All terms of the anatomical structures are consistent with Nomina Anatomica Veterinaria [28] and the illustrated nomenclature [5].

Results and Discussion

Craniolaterally on the antebrachium in the Brown bear below *v. cephalica* the strong *m. brachiradialis* was identified, which ends in the distal quarter along the medial edge of the radius, above *proc. styloideus medialis*. Laterally and caudally to it were located the divided in two *m. extensor carpi radialis longus* and *brevis*, as the long ended at the base of the second metacarpal bone, and the short on the third (**Fig. 1A, B; Fig. 2A, B**). Beneath the radial carpal extensors and the common digital extensor, the strong and covered by shiny tendinous sheet *m. supinator* was identified, the insertion of which reached the distal quarter of the radius (**Fig. 2B**). Next to its insertion from the two antebrachial bones started the *m. abductor digiti I [pollicis] longus*, which ended at the base of the first metacarpal bone (**Fig. 1A, B; Fig. 2A, B**). According to Amaike et al. 2021, the ranges of rotation of the radius around the ulna are 74.3° - 80.6° in young Asiatic black bears, and 71° - 80° in adults, while in young Brown bears - 70° - 78.5°, and adult 36.2° - 54.0°. The Polar bear has the most limited movements of about 39.3°. The rotation in dogs is from 20° to 50° and in the cat is over 100° [27]. Belu et al., 2012 established that in humans the angle of rotation is 180°, in dogs is 20°, and in cats 80°. In rabbits, the two bones are strongly curved and fixed together by a fibrous interosseous connection (*syndesmosis*) [6]. Amaike et al. 2021 discuss that there is no significant difference between the studied bear species in bringing food to the mouth, but the difference comes from the natural habitat and food-finding techniques.

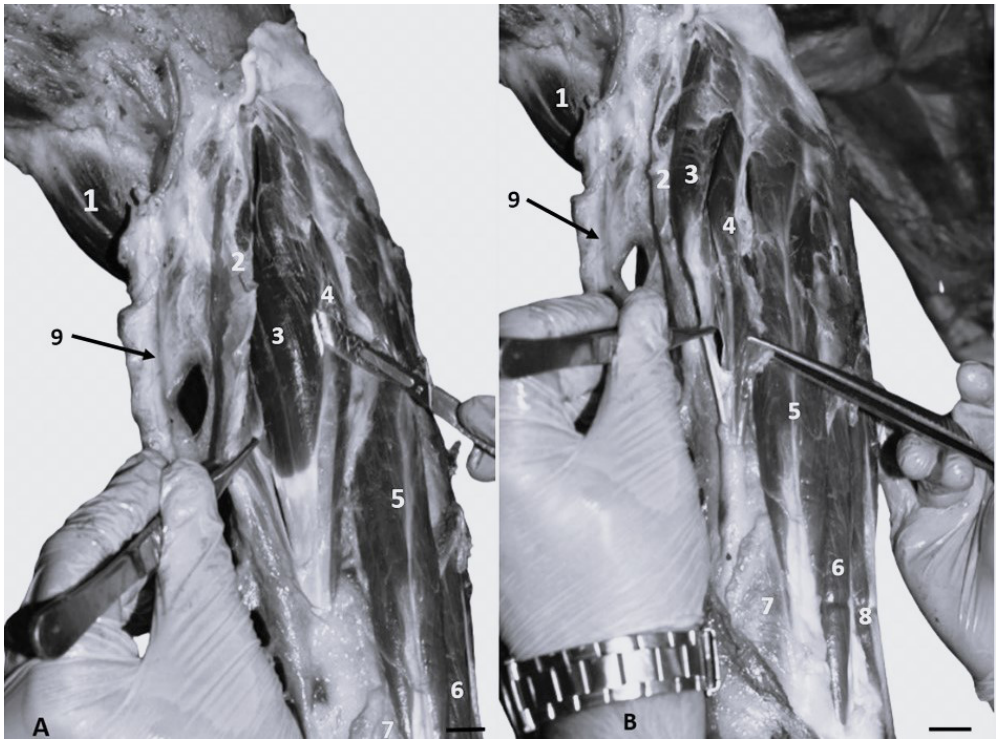

Fig. 1. Craniolateral muscles of the forearm of the Brown bear. **1.** *m. biceps brachii*; **2.** *m. brachioradialis*; **3.** *m. extensor carpi radialis longus*; **4.** *m. extensor carpi radialis brevis*; **5.** *m. extensor digitorum communis*; **6.** *m. extensor digitorum lateralis*; **7.** *m. abductor digiti primi [pollicis] longus*; **8.** *m. extensor carpi ulnaris [m. ulnaris lateralis]*; **9.** *v. cephalica***;** Bar = 2 cm.

The Asiatic black bear is smaller, and its habit is associated with tree climbing at all ages like the Brown bear at a young age, which is accomplished with supination of the forelimbs thus hugging the trees. This ability in Polar and adult Brown bears is lost as they increase in weight and size with the onset of puberty, as the weighting is associated with the colder climate in their habitat [1] and with the reproductive rates in female Brown bears [4, 12]. Inward rotation (pronation) is believed to be limited, occurring when landing from ice floes on snow, other terrain, or water [1]. Bears are good swimmers, but they swim like dogs, which does not include the supination and pronation movement [1]. The rotational movements are also assisted by the carpal bones, being limited in *art. radiocarpea* in humans [2] and situated between the radius and the intermedioradial carpal bone in the bear. This carpal bone moves with the radius during forearm pronation/supination. The carpal joint also allows extension/flexion and abduction/adduction of the thoracic limb at the wrist [17].

From the dissections and analysis conducted by the present study, the authors can point out that the supination is accomplished by several muscles – *m. brachioradialis, m. extensor carpi radialis longus et brevis, m. supinator* and *m. abductor digiti primi [policis] longus*. The brachioradial muscle, which performs semi-pronation and semi-supination in humans [2, 16], is also well developed in the Brown bear with a more distal insertion compared to the dog. It is always present in the cat [5, 27, 28], in 39%

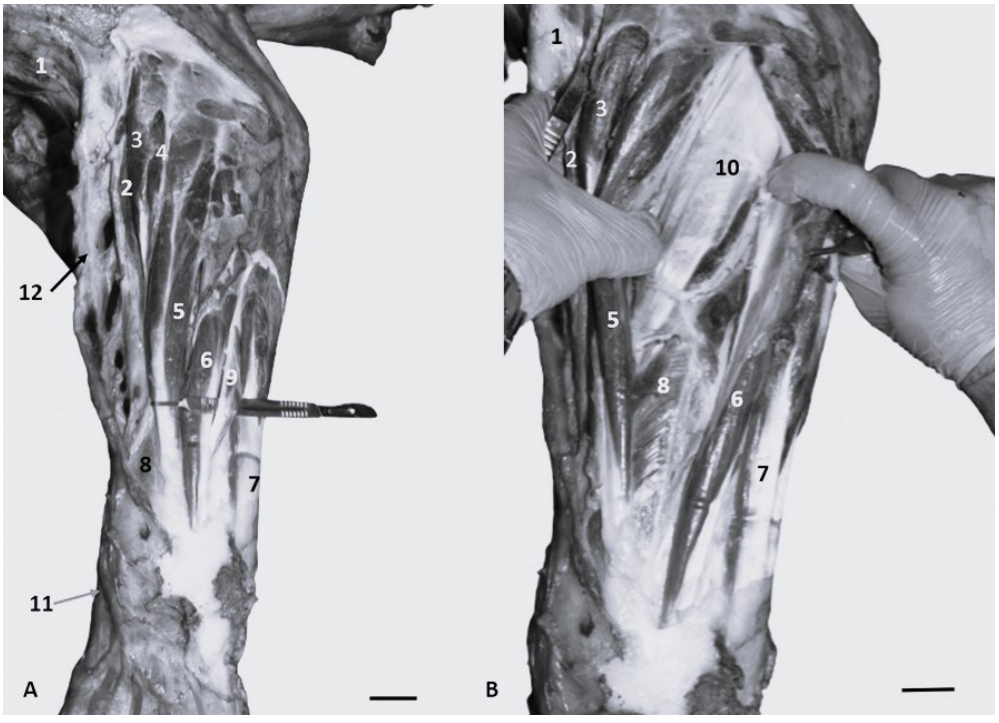

Fig. 2. Superficial (A) and deep (B) craniolateral muscles of forearm of the Brown bear. **1.** *m. biceps brachii*; **2.** *m. brachioradialis*; **3.** *m. extensor carpi radialis longus*; **4.** *m. extensor carpi radialis brevis*; **5.** *m. extensor digitorum communis*; **6.** *m. extensor digitorum lateralis*; **7.** *m. extensor carpi ulnaris [m. ulnaris lateralis]*; **8.** *m. abductor digiti primi [pollicis] longus*; **9.** *m. extensor digiti [pollicis] primi et secundi*; **10.** *m. supinator*; **11.** *v. cephalica accessoria*; **12.** *v. cephalica*. Bar = 2 cm.

of the dogs [13], and absent in the rabbit [7]. *Mm. extensor carpi radialis longus et brevis* are completely separated, they extend and abduct the wrist in humans [2], which is also observed in the Brown bear and cat, while in the dog and rabbit the muscles are partially fused in the region of their bellies and separate only in their insertions [5, 7, 13, 27, 28]. *M. supinator* is limited to the proximal one-quarter of the radius in the dog, to the middle in the cat, and distal in the bears we studied, while in the rabbit the muscle is absent [2, 5, 7, 13, 27, 28]. *M. abductor digiti primi [policis] longus* is well-developed in humans [2] and especially in the Brown bear, where was found attached just next to the insertion of *m. supinator*. In the bear and the cat, the abduction of the wrist is carried out in *art. radiocarpea* and first digit in combination with preceding supination, while in dogs and rabbits, these movements are limited [2, 5, 7, 13, 27, 28]. *M. biceps brachii* is also included in the supination in bears, cats, and humans [2, 6, 27]. Pronation is carried out by only two muscles - *m. pronator teres* and *m. pronator quadratus* [2]. In the Brown bear was found *m. pronator teres*, with a short belly and a long tendon that attaches to the medial edge at the distal third of the radius, approaching the insertion of *m. supinator* (**Fig. 3A, B**). The pronator teres muscle is stronger and longer in the cat compared to the dog [13, 27], where is shorter and functions primarily as a flexor of the elbow joint [13], while in the rabbit is even weaker and rudimentary [7]. This muscle is the largest in humans and consists of the humeral and ulnar head

[2]. *M. pronator quadratus* lies medially on the interosseous antebrachial membrane between the bodies of the radius and ulna. In the Brown bear, as in the cat, the muscle was found covered by a shiny tendon sheath which makes it stronger, being situated distally between the two bones of the forearm [13, 27, 28]. From our observations the small number of muscles performing pronation as a type of movement, although limited, is in great percentage in the cat and young Brown bear.

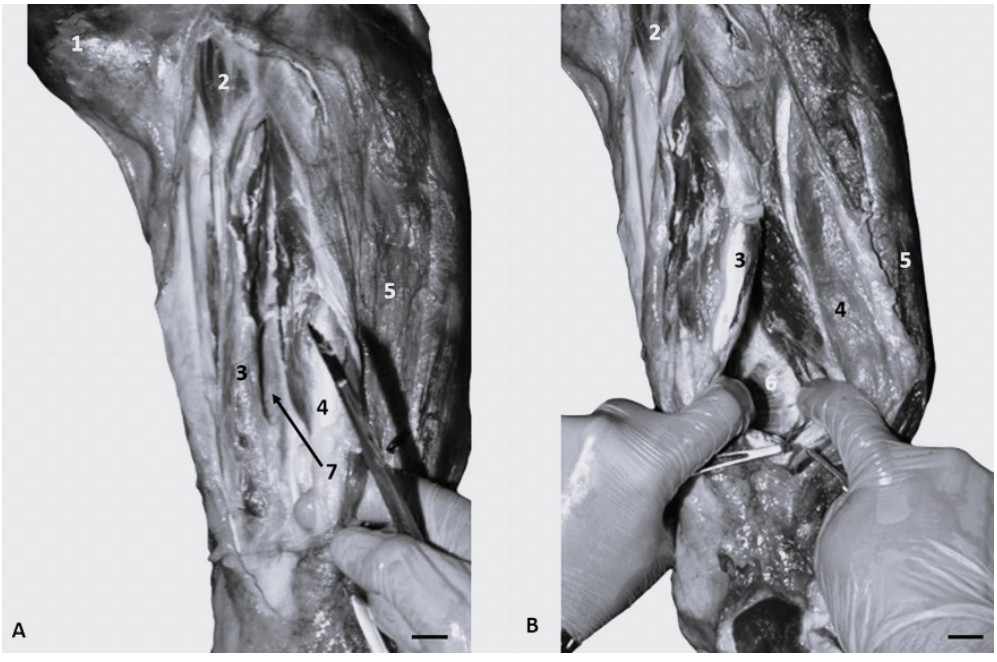

Fig. 3. Superficial (A) and deep (B) caudal muscles of the forearm of the Brown bear, medial view. **1**. *m. biceps brachii*; **2.** *m. pronator teres*; **3.** *m. flexor carpi radialis*; **4.** *m. flexor digitorum superficialis*; **5.** *m. flexor carpi ulnaris*; **6.** *m. pronator quadratus*; **7.** *v. mediana*. Bar = 2 cm.

Proximal rotation of the radius and ulna occurs in-between *cirumferntia atiucularis* of the head of the radius located in *incisura radialis* between the two *proc. coronoideus lateralis et medialis* of the ulna, shown in **Fig. 4A, B, C**, in confirmation of what was established by other authors [6, 11]. The distal rotation is between *cirumferntia artucularis* of the head of the ulna and *incisura ulnaris* of the radius [6, 11], relevant to the preceding abduction of the wrist and finger and supination [2]. In the young to adult Brown bear, the rotation is 36°-78° [1], which is due to the interrupted *cirumferntia articularis* of the radius [1]. This discontinuity was confirmed (**Fig. 4A**), whereas in humans and cats, the radial head is completely round without discontinuity [6, 11], in the dog it is half-complete, and in the rabbit, is presented by two-faceted rudimentary articular surfaces [6, 7, 11]. The greater degree of rotation of the radius in the cat compared to the Brown bear could be explained, in addition to the round *circumferentia articularis*, with the significantly lighter weight, as well as the constant climbing, which is part of their behavior and habit [1, 6, 11].

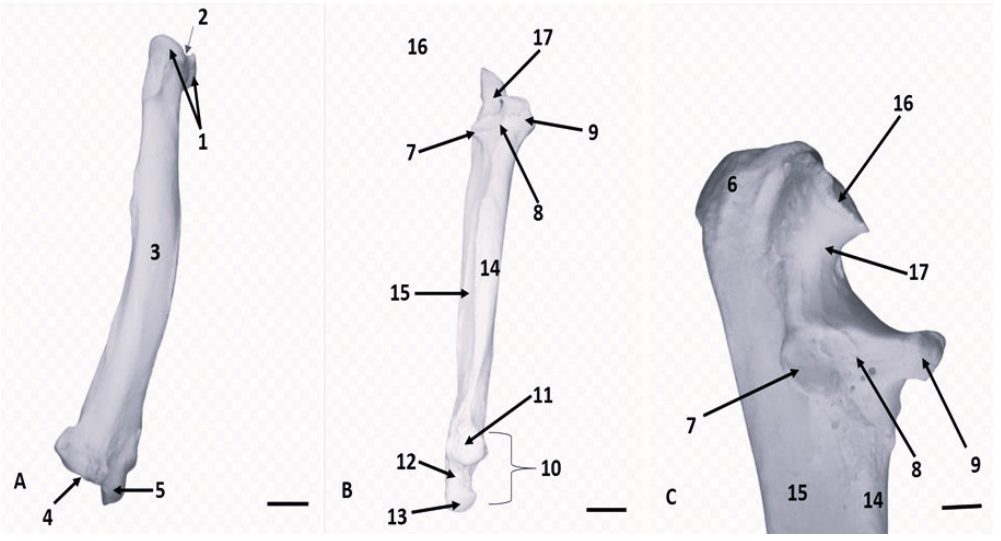

Fig. 4. Bones of the antebrachium in the Brown bear: Radius (A) cranial view; Ulna (B), cranial view; Ulna (C) proximal end, craniolateral view. **1.** *caput radii, circumferentia articularis;* **2.** notch which interrupted *circumferentia articularis*; **3.** *corpus radii*, *facies cranialis*; **4.** *trochlea radii*; **5.** *proc. styloideus medialis*; **6.** *tuber olecrani*; **7.** *proc. coronoideus medialis*; **8.** *incisura radialis*; **9.** *proc. coronoideus medialis*; **10.** *caput ulnae*; **11.** *cirumferentia articularis*; **12.** *proc. styloideus lateralis*; **13.** *facies articularis carpea*; **14.** *facies cranialis, corpus ulnae*; **15.** *facies lateralis*, *corpus ulnae*; **16.** *proc. anconeus*; **17.** *incisura trochlearis*. Bar = 3,1 cm

In **Figure 5A** are observed *m. fibularis [peroneus] longus* and *m. fibularis [peroneus] brevis*, *m. extensor digitalis lateralis* and *m. flexor digitorum lateralis* in the Brown bear. The first two muscles perform plantar flexion with eversion of the foot in humans [2, 16].

They are developed in dogs and cats [5, 28], and in rabbits an additional fourth, *m. fibularis [peroneus] quartus* is presented [7]. In all species, the inversion of the autopodium takes place during bouncing from a place [2, 7, 13, 16, 27]. In the Malayan Sun bear and Giant panda, a larger muscle belly with a short terminal tendon of *m. tibialis cranialis* has been demonstrated and more distal insertion of *m. popliteus* compared to Brown and Polar bears, which is an adaptive mechanism related to climbing and hugging stems with the pelvic limbs [24]. Accordingly, the loss of this ability in Brown and Polar bears has been observed due to the development of larger weight and size [1, 24]. Hugging the trunks is accomplished by turning the autopodium, by the identified muscles of the peroneus group in young Brown bears [1]. In all the bears studied, we observed a strong *m. soleus* [**Fig. 5B**], which started from the head of the fibula and ended in *tendo calcanei* and together with the lateral and medial head of *m. gastrocnemius* thus forming *m. triceps surae* (**Fig. 5B**). *M. soleus* is well developed in humans [2, 16], cats, and rabbits [5, 7, 28], but absent in dogs [5, 13, 28]. This muscle is responsible for the plantar flexion of the foot [2, 16], which in humans is associated with activities such as stepping on the gas pedal, standing on tiptoes, cycling, and dancing, most responsible for pushing off from the ground [16].

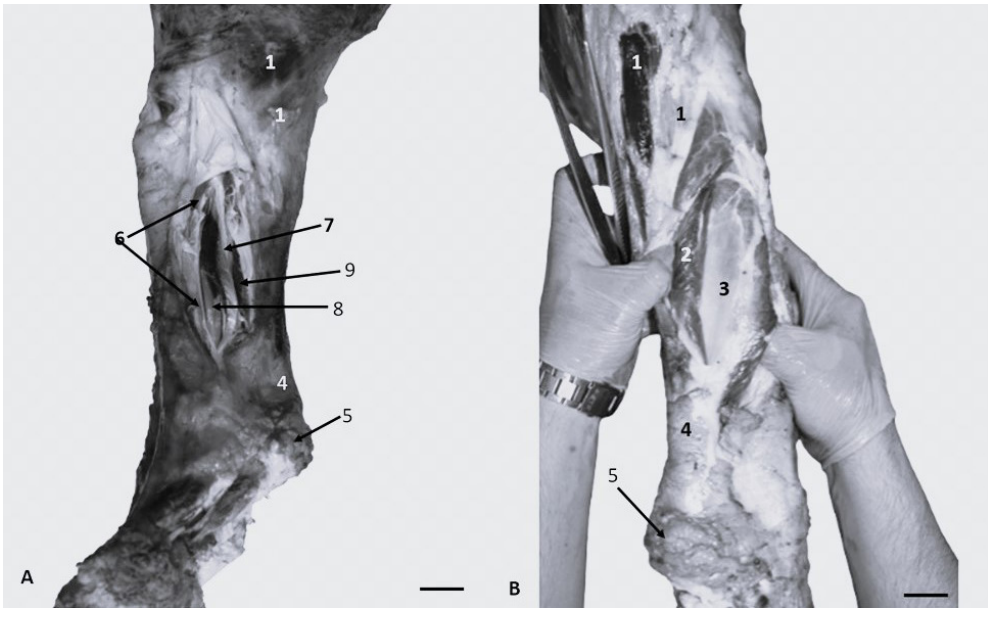

Fig. 5. Craniolateral (A) and caudal muscles (B) zeugopodium on the pelvic limb of the Brown bear. 1. m. biceps femoris; 2. m. gastrocnemius, caput laterale; 3. m. soleus; 4. tendo calacaneus communis; 5. tuber calcanei; 6. m. fibularis (peroneus) longus; 7. m. extensor digitorum lateralis; 8. m. fibularis (peroneus) brevis; 9. m. flexor digitorum lateralis. Bar = 2 cm.

This also explains its strong representation in cats related to high jumping, as well as in rabbits to push off the ground to jump while running [2, 7, 16, 28]. The well-developed muscle in the Brown bear could be associated, in our opinion, with standing on the tip of the toes of the pelvic limbs to reach a high fruit or honeycomb. Dogs lack *m. soleus*, so the primary extensor of the tarsal joint is *m. gastrocnemius* with its two heads. This provides stability when standing and generates propulsive forces during movement in walking, trotting, and galloping [13]. Also, high jumping from a place is not typical for this type of animal.

The tibia of the Brown bear is similar to the human but it is distinguished by deeper concavity of cochlea tibiae *cochlea tibiae* [11], which is confirmed by the present study (**Fig. 6A, B**). In 44% of the adult bears the tibia and the fibula were ossified between the lateral condyle of the tibia, *facies articularis fibularis*, and the head of the fibula, *facies articularis capitis fibulae* in *articulatio tibiofibulris proximalis* [5, 28]. We established a predominant ossification in the male compared to the female Brown bears. Three of the five researched male bears (60%) had fusion on both legs, one on the left only, and one without any. From the four female bears one (25%) was presented with ossification on the right only. It could be assumed that the larger build of the male bears could lead to overloading of this joint, which is also the cause of chronic arthritis of the upper tibiofibular joint in humans [3]. At *articulatio tibiofibulris distalis* [5, 28] no ossification in any of the bears studied was established, neither on the left nor on the right leg.

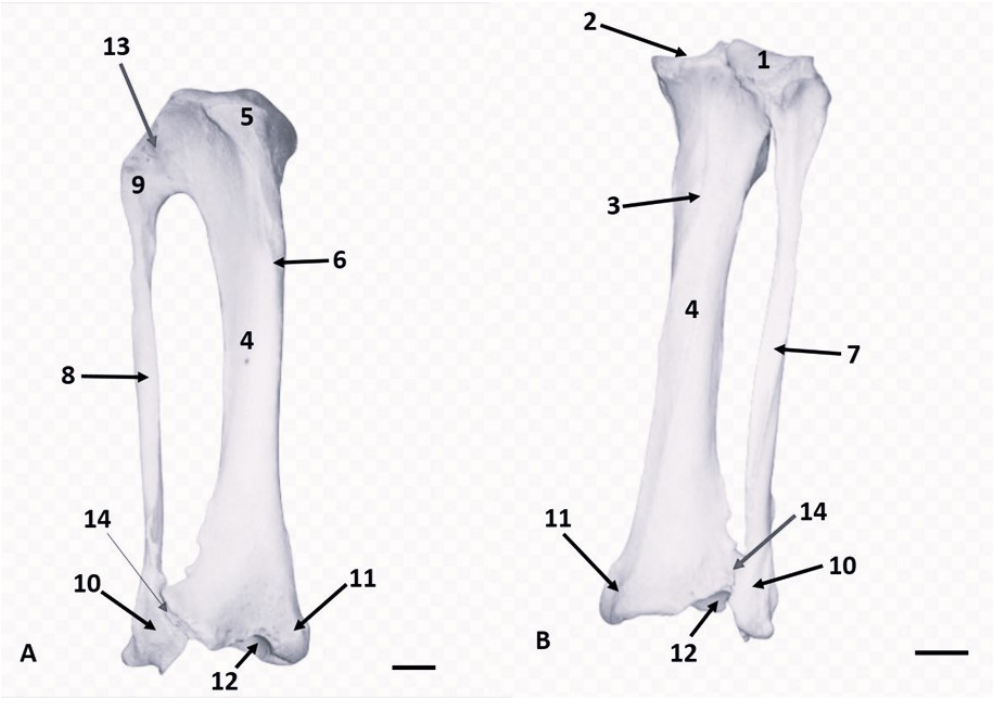

Fig. 6. Crural bones of the Brown bear: Cranial (A) and caudal (B) view. 1. condylus lateralis; 2. condylus medialis; 3. linea m. poplitei; 4. corpus tibiae; 5. tuberosits tibae; 6. margo cranialis; 7. facies caudalis, corpus fibulae; 8. facies cranialis, corpus fibulae; 9. caput fibulae; 10. malleolus lateralis; 11. malleolus medialis; 12. cochlea tibiae; 13. ossified art. tibiofibularis proximalis; 14. art. tibiofibularis distalis: Bar = 2,4 cm.

Conclusion

The rotation of the radius for which the supinator muscles are primarily responsible is greatest in the domestic cat, compared to the Brown bear, and least in the dog. The inability to climb by grasping and hugging would point to a pathology in the innervation (lesion of the *n. musculocutaneous* or *n. radialis*) or rupture of some of the muscles responsible for the supination, also a distortion of the radiocarpal joint might be considered.

The presence of *m. soleus* in the Brown bear, cat and rabbit is associated with plantar flexion necessary for pushing off the ground, and failure to do so during jumping from a place in a cat or during running in a rabbit would point to a lesion of *n. tibialis* or rupture of *m. soleus*.

Acknowledgments*:* The authors thank Bear Park Belitsa for the guidance and assistance in researching the Brown bears.

References

1. **Amaike, H., M. Sasaki, N. Tsuzuki, M. Kayano, M. Oishi, K. Yamada, H. Endo.** Mobility of the forearm skeleton in the Asiatic black (Ursus thibetanus), brown (U. arctos) and polar (U. maritimus) bears. – *Journal of Veterinary Medical Science*, **8**, 2021, 1284-1289.
2. **April, E.** *Clinical anatomy*, 3rd edition (Eds. E. Nieginski) Williams & Wilkins, 1997, 77-99, 209-217.
3. **Batt, M., G. Bhogal**. Superior tibiofibular joint. Oxford textbooks of Reumatology, 2015, 447-449.
4. **Belant, J. L., K. Kielland, E. H. Follmann, L. G. Adams**. Interspecific resource partitioning in sympatric ursids. – *Ecological applications*, **16**, 2006, 2333-2343.
5. **Constantinescu, G. M.** *Ostelology. Arthrology. Myology. Illustrated veterinary anatomical nomenclature.* 4th edition, Stuttgart, Ferdinand Enke Verlag, 2018, 52-55, 68-71, 84-85, 93-95, 118-121, 126, 130.
6. **Belu, C. G. Predoi, B. Georgescu, I. Dumitrescu, A. Șeicaru, P. Roșu, C. Bițoiu.** The antebrachial bone morphology and pronation and supination movement possibilities in domestic mammals and humans. *Scientific Works – University of Agronomical Sciences and Veterinary Medicine, Bucharest Series C, Veterinary Medicine*, **58**, 2012, 12, 3, 13-20.
7. **Craigiae, E. H.** *Bensley`s practical anatomy of the rabbit,* 8th edition, Philadelphia, Canada, The Blakistone Company, 1948, 266-286.
8. **Davis, D. D.** The arteries of the forearm in carnivores. - *Zoological series*, **27**, 1941, 137-227.
9. **Dogăroiu, C., D. Dermengiu, V. Viorel.** Forensic comparison between bear hind paw and human feet. Case report and illustrated anatomical and radiological guide. - *Romanian Journal of Legal Medicine*, 2012, 131-134.
10. **Fosse, P., E. Cregut-Bonnoure.** Ontogeny/growth of (sub) modern brown bear (Ursus arctos) skeleton: A guideline to appraise seasonality for cave bear (Ursus spelaeus) sites. – *Quaternary International*, **339**, 2014, 275-288.
11. **France, D. L.** *Human and nonhuman bone identification. A Color atlas*. CRS Press, 2009, 232, 250, 253, 264, 277, 294, 297, 480.
12. **Hensel, R. J., W. A. Troyer, A. W. Erickson.** Reproduction in the female brown bear. – *The Journal of Wildlife Management*, 1969, 357-365.
13. **Hermanson, J. W., H. Evans, A. Lahunta**. *Miller's anatomy of the dog*, 5th edition, St. Louis, Missouri, Sanders and Elsevier, 2020, 409-410, 571-591, 626-634.
14. **Herrero, S.** Aspects of evolution and adaptation in American black bears (Ursus americanus Pallas) and brown and grizzly bears (U. arctos Linné) of North America – In: *Bears: Their biology and management*, Vol. 2 (Ed. S. Herrero), IUCN Publ., 1972, 221-231.
15. **Li, P., K. K. Smith.** Comparative skeletal anatomy of neonatal ursids and the extreme altriciality of the giant panda. – *Journal of Anatomy*, **236**, 2020, 724-736.
16. **Morrison, W., J. Johnson.** 2023, www. medicalnewstoday.com/articles/31824 #Function-of-plantar-flexion.
17. **Neumann, D. A.** *Kinesiology of the musculoskeletal system: Foundations for rehabilitation*, 3rd ed., Mosby, St. Louis, 2016.
18. **Otaki, Y., N. Kido, T. Omiya, K. Ono, M. Ueda, A. Azumano, S. Tanaka.** A new voluntary blood collection method for the Andean bear (Tremarctos ornatus) and Asiatic black bear (Ursus thibetanus). – *Zoo Biology*, **34**, 2015, 497-500.
19. **Pinto, A. C., F. Etxebarría.** Description of pathological conditions in the skeleton of an adult male brown bear Ursus arctos from the Cantabrian range of mountains. – *Cadernos Lab. Xeolóxico de Lax*, **26**, 2001, 465-477.
20. **Ruzhanova-Gospdinova, I., G. I. Georgiev.** The arteries, veins, nerves of Antebrachium of the brown bear (Ursus arctos). – *Acta Morphol. et Anthropol.*, **30 (1-2)**, 2023, 107-115.

21. Ruzhanova-Gospodinova, I., G. I. Georgiev, I. Georgiev, L. Hristakiev. Morphological studies on the blood vessels and nerves of the crus of the brown bear (Ursus arctos). – *Tradition and modernity in veterinary medicine*, **7(12)**, 2022, 92–98.

22. Sapundzhiev, E., M. Chervenkov, Y. Iliev, S. Mustafa, M. Dimitrova. Morphofunctional investigation of brown bear (Ursus arctus) stomach. – *Tradition and Modernity in Vet, Medicine*, **3**, 2018, 50-54.

23. Sapundzhiev, E., M. Chervenkov, G. Popov, K. Todorova. Adrenal glands histological structure in brown bear (Ursus arctos, Linnaeus, 1758). – *Acta Morphol. et Anthropol.*, **28 (1-2)**, 2021, 32-37.

24. Sasaki, M., H. Endo, O. Wiig, A. E. Derocher, T. Tsubota, H. Taru, M. Yamamoto K. Arishima, Y. Hayashi, N. Kitamura, J. Yamada. Adaptation of the hindlimbs for climbing in bears. – *Annals of Anatomy*, **187**, 2005, 153-160.

25. Sebastiani, A. M., D. W. Fishbeck. *Mammalian anatomy: The Cat*, 2nd edition (Ed. D. Ferguson), Morton Publishing Company, 2005, 145-151.

26. Sienkiewicz, T., A. Sergiel, D. Huber, R. Maslak, M. Wrzosek, P. Podgórski, S. Reljic, L. Pasko. The Brain ´ anatomy of the brown bear (Carnivora, Ursus arctos L., 1758) compared to that of other carnivorans: A cross-sectional study using MRI. – *Frontiers in Neuroanatomy*, **13**, 2019, 79.

27. Singh, B. Dyce, Sack and Wensing`s textbook of veterinary anatomy, 5th edition. Saunders and Elsevie, 2018, 816-818.

28. Staszyk, C. K. –D. Budras, R. Henry, J. W. Maierl, G. M. Constantinescu, P. Sótonyi. *Osteologia et arthrologia, myologia. nomina anatomica veterinaria (N.A.V.), International Committee on Veterinary Gross Anatomical Nomenclature*, Hanover (Germany), Ghent (Belgium), Columbia, MO (U.S.A.), Rio de Janeiro (Brazil), 6th edition, 2017, 19, 22, 32, 34, 42, 43.

Institute of Experimental Morphology, Pathology and Anthropology with Museum
Bulgarian Anatomical Society

Acta Morphologica et Anthropologica, 31 (1-2)
Sofia ● 2024

Trichuriasis in Zoo-Keeping Hamadryas Baboons (*Papio hamadryas*): Case Report and Pathomorphological Findings

Mariana Panayotova-Pencheva, Katerina Todorova*

Institute of Experimental Morphology, Pathology and Anthropology with Museum, Bulgarian Academy of Sciences, Sofia, Bulgaria

* Corresponding author e-mail: marianasp@abv.bg

A case of trichuriasis in three zoo-keeping baboons is described. One of the animals had a high degree of infection and marked clinical symptoms, and the other two - low degree of infection and good general condition. The baboons were treated according to two regimens: 1. Albendazole (7.5 mg/kg) orally for three days; 2. Combination of albendazole (7.5 mg/kg) and ivermectin (0.4 mg/kg), both drugs orally for three days. Despite treatment, the condition of the first baboon deteriorated and he was euthanized. The postmortem examination revealed pathomorphological changes in the intestines, liver, kidneys and lungs. Most of the alterations were associated directly or indirectly with the trichurid infection, and another reflected past diseases that have further worsened the animal‘s condition. The combined treatment and the anti-epidemic measures taken led to a complete and long-lasting elimination of trichuriasis in the animals with a low degree of infection.

Key words: trichuriasis; non-human primates; anthelmintic treatment; gross pathology; pathohistology

Introduction

Trichuriasis is a parasitic zoonosis caused by so-called whipworms of the family Trichuridae, phylum Nematoda. Trichurids are located in the digestive tract of their hosts, mainly the cecum and colon, they are geohelminths with a direct life cycle: The infective stage are larvae within the egg, which develop in 1 or 2 months of being passed in the faeces depending on temperature. Under optimal conditions, these larvated eggs may subsequently survive and remain viable for several years. After ingestion, the plugs of the eggs are digested and the released larvae penetrate the glands of the distal ileum, cecal and colonic mucosa. Subsequently, all four moults occur within these glands, the adults emerging to lie on the mucosal surface with their anterior ends embedded in the mucosa [23].

Trichuris trichiura, the causative agent of trichuriasis in humans, is considered the most common pathogenic parasite in non-human primates [5]. Parasitism of mature *T. trichiura* worms leads to chronic inflammation of mucosa of large intestine. Lacerations of mucosa caused by feeding activities of worms may lead to secondary bacterial infections; in heavily infected or young hosts, rectal prolapse is often seen followed by chronic bloody diarrhea associated with rectal bleeding, iron deficiency anemia and growth deficits [10].

Due to the direct faecal-oral route of transmission and ability to persist in the environment, treatment and control of *T. trichiura* is necessary to maintain healthy baboon colonies [17]. The control of trichuriasis is particularly relevant in animals kept in captivity, in view of reducing the threat of its transmission to humans.

In order to succeed in the fight against parasitoses accumulation of basic knowledge regarding all their aspects is needed [15]. In connection with the above, the aim of the present work was set, namely to document a case of trichurid infection in a group of zoo-keeping Hamadryas baboons (*Papio hamadryas*) and to describe accompanying pathomorphological findings.

Materials and Methods

Sample origin and area of the study.

It concerns a group of three male Hamadryas baboons (*Papio hamadryas*) kept at the Sofia Zoo, Bulgaria for more than 20 years. They lived in an enclosure with an inner part (covered with ceramic tiles) and an outer part covered with concrete on which a soft bedding of sawdust was spread.

Coprological study and treatment.

Individual faecal samples of the animals were collected from the ground of the enclosure. They were microscopically investigated by method of direct smear, common flotation (with solution of sodium chloride, gravity = 1.18) and sedimentation technique [2]. The degree of parasite infection was subjectively assessed according to the number of eggs observed per one microscopic field of view, and the following criteria were adopted for documentation: low degree of infection (2-4 eggs per field of view), medium degree of infection (5-10 eggs per field of view), high degree of infection (more than 10 eggs per field of view) and very high degree of infection (eggs too numerous to count).

Two schemes were used to deworming animals: 1. Albendazole (Zentel® 400 mg tablets) at a dose of 7.5 mg/kg for three consecutive days; 2. Combination of albendazole (Zentel® 400 mg tablets) at a dose of 7.5 mg/kg and ivermectin (Pandex® 1% solution) at a dose of 0.4 mg/kg for three consecutive days. The second treatment was performed 34 days after the end of the first. The drugs were given individually to the animals, orally, mixed with a small amount of their favorite food (boiled rice and dried fruit, sweetened with honey and formed into a ball) after a 12-hour fasting diet. Control examinations of faecal samples were performed on day 7 after treatment according to the first scheme and on days 7, 30 and 90 after treatment according to the second scheme.

Removal of the sawdust litter from the outer enclosure and disinfection of floors (daily) and arrangement (twice a week) with a solution of sodium hypochlorite (1% and 0.05% respectively) were undertaken as anti-epidemic measures.

Pathomorphological study

The carcass of one of the animals was autopsied according to the common way described in the textbooks. Macroscopic changes in the internal organs were described and portions of them (0.5 x 2 x 2 cm) were obtained for histological examination. They were fixed in 10 % phosphate buffered formalin, embedded in paraffin, cut into sections of 5 to 10 μm thick and stained with haematoxylin and eosin according to the routine histological technique. Pictures were taken using a light microscope "Leica DM5000 B", supplied with a camera and software (Leica Application Suite LAS v. 3.1).

Results

Case history

In the summer of 2023, the health condition of one of the baboons deteriorated. Weight loss, malaise and diarrheal stools with traces of blood were observed. The other two animals were in good condition with normal-looking faeces. Examination of faeces using the flotation technique showed the presence of parasitic eggs with morphometric characteristics of *Trichuris* sp. (**Fig. 1**). The degree of infection was subjectively rated as high in the baboon with clinical symptoms and low in the other two animals. All three baboons were treated with albendazole. In their follow-up examination on day 7 after albendazole treatment, trichurid eggs were still found, but they were single, not in all fields of view. Despite the effect of the treatment, the condition of the first baboon continued to deteriorate, became critical and this necessitated his euthanasia. The other two animals were re-treated with a combination of albendazole and ivermectin, and no eggs were found during the all control examinations after this treatment. The euthanized baboon was autopsied.

Fig. 1. Whipworm egg (*Trichuris* sp.) found in faeces of zoo-keeping *Papio hamadryas*.

Gross pathology

External examination: severe cachexia, dehydration and a faeces-stained perianal area. Lungs: small, like pinheads, compacted, gray alterations in the caudal parts of the lung parenchyma (**Fig. 2A**). Liver: adherent with its apical parts to the top of the diaphragm, with colour lighter than normal, covered with tiny dark spots (**Fig. 2B**). Kidneys: different

Fig. 2. Macroscopic view of internal organs, *Papio hamadryas* with *Trichuris* sp. infection: A) lung: small, like pinheads, dark coloured alterations in the caudal parts of the lung parenchyma (arrow), diffuse vessels congestion; B) observation of the abdominal cavity organs: lighter in colour liver, partially adherent to the diaphragm, with subcapsular petechiae; small and large intestines: blood vessels congestion, seen on the serosa, ballooning due to fermentation processes; C) and D) kidneys: different in size and shape, one of them with big perirenal blood coagulum (C), slightly paler in colour cortical part and distinct differences in the renal pelvis sizes (D).

in size and shape, the left one with a big perirenal blood coagulum, slightly paler in colour cortical part and distinct differences in the renal pelvis sizes (**Fig. 2C, D**). Small intestines: strong mucosal hyperemia, blood vessels congestion, seen on the serosa (**Fig. 3A**). Large intestines: pronounced ballooning and blood vessels congestion (**Fig. 3A**); hemorrhages and whitish parasites in the lumen (**Fig. 3B, C**); faeces in the rectum mushy but not diarrheic, of normal colour, without traces of blood.

Pathohistological findings

Lungs: ruptures of the alveolar walls, emphysematous changes, vessels congestion and hemosiderosis (**Fig. 4A**). Liver: space of Disse dilated, sinusoidal dilatation rarely, presence of focal microvesicular fatty changes and parenchymal cells destruction processes as vacuolation, pyknosis, karyorrexis, focal hepatocyte necroses (**Fig. 4B, C**).

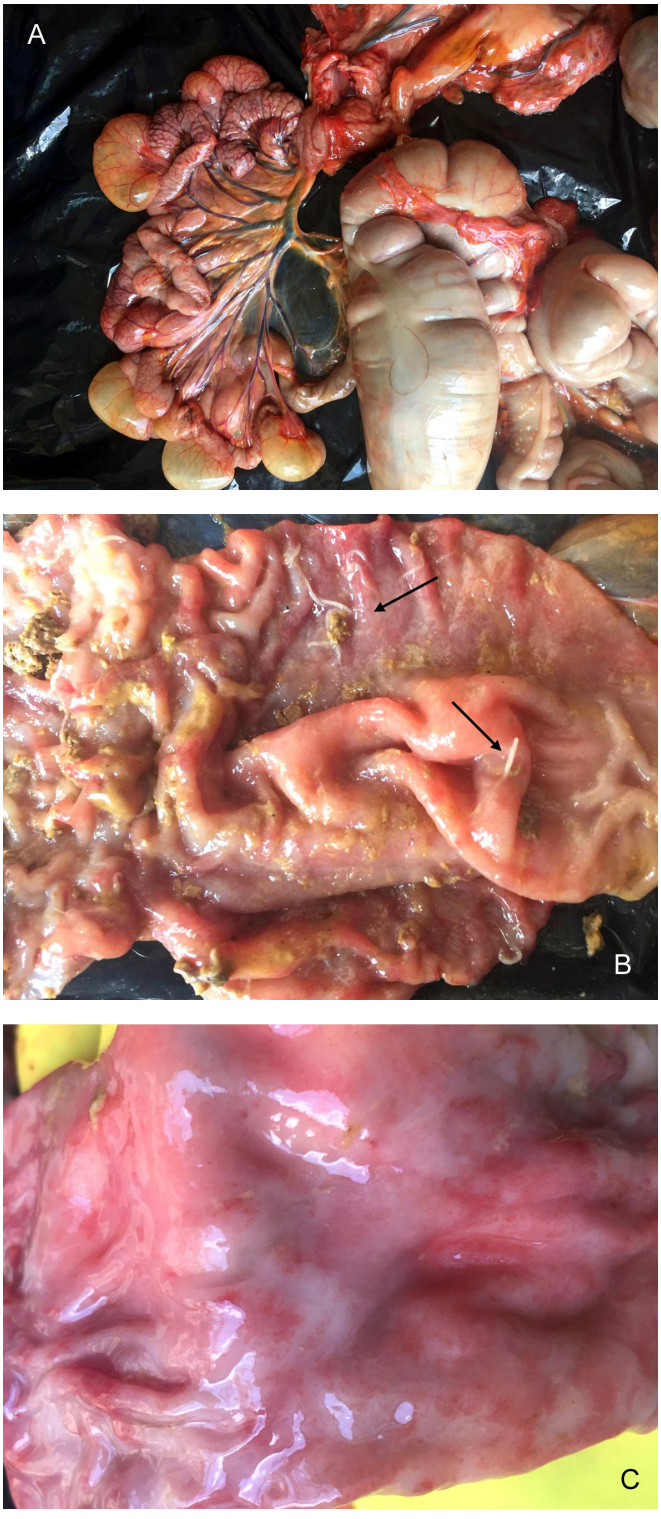

Fig. 3. Macroscopic view of the gut, *Papio hamadryas* with *Trichuris* sp. infection: A) blood vessels congestion and presence of liquid content in the intestinal lumen; B) hemorrhagic colonic mucosa with remnants of intestinal contents and several whipworms (arrows) stuck in it; c) cleaned colonic mucosa with visible diffuse petechial hyperemia.

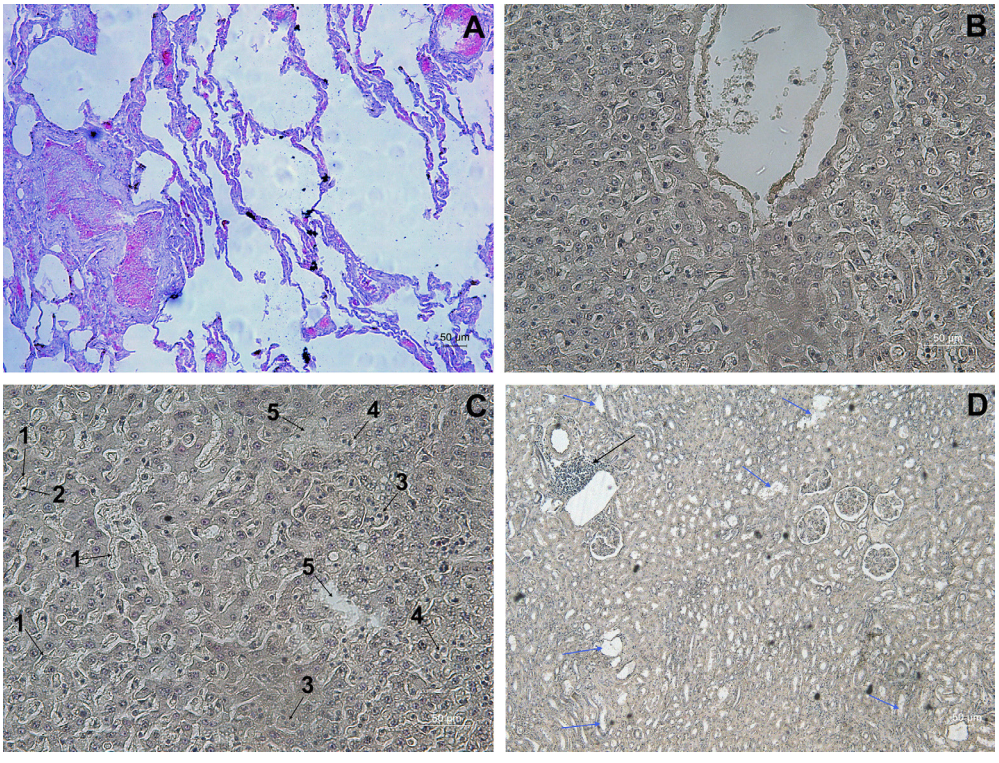

Fig. 4. Parenchymal organs, *Papio hamadryas*: A) lungs: ruptures of the alveolar septum progressing to emphysematous changes, vessels congestion and focal hemosiderosis; B) and C) liver: B) vena centralis in lobulus hepaticus and hepatocytes arranged in irregular cords, C) visible dilated space of Disse (1), sinusoidal lumen (2), karyopyknosis (3), hydropic degeneration of hepatocytes (4), focal islets of cell necrosis and detritus (5), rarely microvesicular fatty changes; D) kidney: blue arrows - cystic tubule dilation and changes in tubular epithelium; black arrow-focal perivascular inflammatory infiltrates; H&E.

Kidney: presence of nonproliferative degenerative lesions like tubular epithelial changes, cystic tubule dilation and focal perivascular inflammatory infiltrates (**Fig. 4D**). Small intestines: lymphoplasmacytic inflammation of lamina propria of the villi, desquamation of the epithelium of the villi and crypts of Lieberkühn (**Fig. 5A**). Large intestines: presence of adult parasite worms in the mucosa, mucosal destruction and cell detritus, neutrophil and lymphoplasmacytic infiltrates in propria mucosae (**Fig. 5B, C, D**).

Discussion

Trichuriasis is a widespread parasitosis caused by more than 70 species of *Trichuris*, each with their own host species [4]. It is a soil-transmitted infection [10]. Factors related with this, such as direct infestation by swallowing eggs from the contaminated environment and the high persistence of eggs and larvae in the soil (infective larvae in egg shell may survive up to 6 years [10]) rank this helminthosis among the persistent

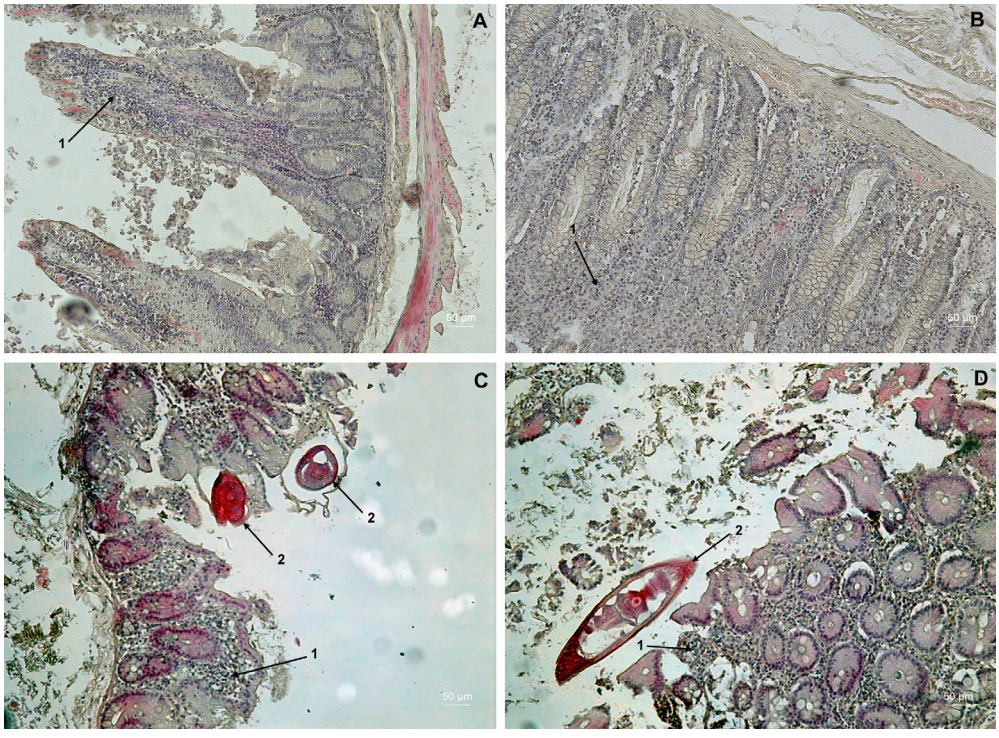

Fig. 5. Tubular organs, *Papio hamadryas*: A) small intestine; B), C), D) colon. Arrows 1- lymphoplasmacytic inflammation of the villus propria and the crypts of Lieberkühn; Arrows 2 – transverse and oblique sections of *Trichuris* sp. adult worms located in the intestinal mucosal tissues; destruction of the columnar epithelium; H&E.

parasitic infections in animals and humans. The nature of the causative agents and the epidemic conditions for their spread, further favored in a zoo environment [14], contribute to the frequent occurrence of the disease in animals kept in captivity. Trichurid infections have been found in a variety of mammal species, including primates, from zoos around the world [1, 3, 7-9, 11, 12, 14,16, 18, 21].

Trichuriasis can be asymptomatic or manifest clinically depending on the degree of infection [10]. We observed this in the present case as well – the two animals in which the infection was in a low degree were in good health status, while the third one, with a high degree of infection, was in a severe condition. The clinical symptoms manifested in this case, such as weight loss, dehydration and diarrhea with possible impurities of blood, are characteristic of the disease and are observed in the various host species of trichurids [10, 23].

Treatment of primates with trichuriasis in previous cases was performed with benzimidazoles and macrocyclic lactones [5, 17]. Reichard et al. [17] found that fenbendazole administered to baboons at a dose of 50 mg/kg orally, once daily for 3 consecutive days was 100% effective (stopped shedding *T. trichiura* eggs within 6 days of treatment, and faecal egg counts remained negative at 65 day after treatment), while the administration of milbemycin oxime in a dose of 1 mg/kg orally at 30-days

intervals for 3 months never totally eliminated eggs of *T. trichiura*. The administration of albendazole in a dosage of 7.5 mg/kg, orally for three consecutive days was completely effective in olive baboons (*Papio anubis*) (faecal egg count reduction was 100% at 28 day post treatment), but with less success (75% reduction of faecal egg count) in vervet monkeys (*Chlorocebus aethiops*), while its application together with ivermectin in a dose of 300µg/kg subcutaneously, each drug for three consecutive days, gave 100% effectiveness in both species of primates [5]. It is interesting to note that the trials of Kagira et al. [5] to treat trichurid infection in these two species of primates with ivermectin alone were completely ineffective (0% faecal egg count reduction at 28 day post treatment). In the present case, the initial treatment of the baboons with albendazole at a dose of 7.5 mg/kg for three consecutive days did not give a completely satisfactory result. However, a long-term 100% elimination of infection in both baboons was achieved after the treatment with albendazole and ivermectin (7.5 mg/kg and 0.4 mg/kg respectively) which confirmed the positive results of combined treatment in a similar situation [5].

Unfortunately, in the present case the condition of the baboon with a high degree of infection worsened regardless of the treatment undertaken and he was euthanized. Obviously, the animal had other health problems in addition to severe infestation. We found evidence of this in the post-mortem examination. Pathological changes were found both in the intestines and in other internal organs - liver, kidneys and lungs.

The cecal and colonic mucosa were inflamed, hemorrhagic with ulceration and formation of diphtheritic membranes. Such kind of alterations are characteristic of the sever cases of trichuriasis [23] and due to the embedding of the adult trichurids with the whiplike anterior portion in the intestinal mucosa [10]. Inflammatory changes in the small intestine can also be associated with trichuriasis, as this is where the larvae hatch and penetrate the intestinal glands remaining there for 2-10 days [3, 23]. It is very likely that the whipworm infection was among the causes that led to the partial liver adhesion to the diaphragm. Supporting this assumption is a study revealed that chronic trichuriasis causes not only a decrease in body weight, but also changes in the abdominal organs and greater visceral adhesion [20].

The mechanisms of internal organ damage in trichuriasis can be associated with general intoxication of the body as a result of resorption of toxins released by trichurid worms and damaged intestinal mucosa [6], intestinal microbiota imbalance and bacterial invasion promoted by the infection [20]. The alterations we observed in the liver, expressed in vacuolization, karyopyknosis and karyorrhexis in the hepatocytes, dilation of the sinusoids and visualization of the perivascular spaces, were not a consequence of autolysis, as we assumed due to the slight delay in performing the autopsy. They had occurred before death and were most likely provoked by chronic exposure to toxins and inflammatory processes associated with the parasitosis [13, 22]. The dilated spaces of Disse, which are a reservoir for stem cells, indicate damage to the liver parenchyma and activation of regenerative processes [19], which testifies to the chronic course in the development of the disease. The emphysematous changes and hemosiderosis in the lungs and the non-proliferative cystic changes in the kidneys cannot be directly related to trichurosis, but they reflect other past diseases that further have worsened the animal‘s condition.

The treatment combined and anti-epidemic measures undertaken apparently led to the overcoming of the infection in the two less infested baboons. This was evident from

the negative coprological tests performed on the 7th and 30th day after treatment. Data on a long prepatent period of 60-90 days in *Trichuris* infection [10, 17] were the reason to the control parasitological examinations performed 90 days after the treatment, which also gave a negative result.

Conclusion

The presented case of trichuriasis in baboons revealed a different course of the infection, related to the degree of infestation and overall health status of the individuals. The combined treatment and anti-epidemic measures taken led to a positive result in the control of trichurid infection in the low infested animals.

Acknowledgements: This research was performed on a voluntary basis, according to an agreement for collaboration between the Institute of Experimental Morphology, Pathology and Anthropology with Museum-Bulgarian Academy of Sciences and the Sofia Zoo.

References

1. Bindke, J. D., A. Springer, M. Böer, **C. Strube.** Helminth fauna in captive European gray wolves (*Canis lupus lupus*) in Germany. – *Front. Vet. Sci., Sec. Parasitol*., **4**, 2017, 228.

2. Foreyt, W. J. *Veterinary Parasitology: Reference Manual. 5th Edition*. Iowa, Blackwell Publishing, 2017, 235 pp.

3. Harvey, W., E. H. Hutto, J. A. Chilton, R. Chamanza, J. V. Mysore, N. M. A. Parry, E. Dick, Z. W. Wojcinski, A. Piaia, B. Garcia, T. D. Flandre, I. D. Pardo, S. Cramer, J. A. Wright, A. E. Bradley. Chapter 3 – Infectious diseases of non-human primates. In: *Spontaneous Pathology of the Laboratory Non-Human Primate* (Eds. A.E. Bradley, J.A. Chilton, B.W. Mahler) Academic Press, 2023, 15-69.

4. Hubbard, I. C., J. S. Thompson, K. J. Else, R. K. Shears. Chapter One – Another decade of *Trichuris muris* research: An update and application of key discoveries. In: *Advances in Parasitology* (Eds. D. Rollinson, R. Stothard) Academic Press, 2023, 1-63.

5. Kagira, J. M., G. Oluoch, K. Waititu, I. Mulei, N. Maingi, M. Ngotho. High efficacy of combined albendazole and ivermectin treatment against gastrointestinal nematodes in Vervet monkeys and baboons. – *Scand. J. Lab. Anim. Sci.,* **38,** 2011, 187-193.

6. Kamburov, P., I. Vasilev, D. Georgieva, I. Kamenov, V. Koinarski. *Veterinary-Medical Parasitology, Agropress,* 1994, Sofia, 463 pp. (in Bulgarian)

7. Kyung-Yeon, E. O., S. E. O. Min-Goo, L. E. E. Hyun-Ho, J. U. N. G. Yeong-Mok, K. W. A. K. Dongmi, K. W. O. N. Oh-Deog. Severe whipworm (*Trichuris* spp.) infection in the hamadryas baboon (*Papio hamadryas*). – *J. Vet. Med. Sci.,* **81**, 2019**,** 53-56.

8. Li, M., B. Zhao, B. Li, Q. Wang, L. Niu, J. Deng, X. Gu, X. Peng, T. Wang, G.Yang. Prevalence of gastrointestinal parasites in captive non-human primates of twenty-four zoological gardens in China. – *J. Med. Primatol.,* **44**, 2015, 168–173.

9. Mahmoud, M. A., O. Azazi. Prevalence of gastrointestinal parasites in captive zoo animals. – *Indian J. Vet. Med.,* **35**, 2014, 29-31.

10. Mehlhorn, H. *Encyclopedia of Parasitology, Third edition.* Springer-Verlag Berlin Heidelberg New York, 2008, 1573 pp.

11. Melfi, V., F. Poyser. *Trichuris burdens* in zoo-housed *Colobus guereza*. – *Int. J. Primatol.*, **28,** 2007, 1449–1456.

12. **Moudgil, A. D., L. Das Singla.** Molecular confirmation and anthelmintic efficacy assessment against natural trichurid infections in zoo-housed non-human primates. – *J. Med. Primatol.*, **47,** 2018, 388-392.
13. **Nayak, N. C., S. A. Sathar, S. Mughal, S. Duttagupta, M. Mathur, P. Chopra.** The nature and significance of liver cell vacuolation following hepatocellular injury – an analysis based on observations on rats rendered tolerant to hepatotoxic damage.– *Vichows. Archiv A. Pathol. Anat.*, **428,** 1996, 353–365.
14. **Panayotova-Pencheva, M.** Parasites in captive animals: a review of studies in some European zoos. – *Der Zool. Gart.*, **82**, 2013, 60–71.
15. **Panayotova-Pencheva, M.** *Strongyloides* sp. infection in a brown capuchin (*Sapajus apella* L.): Case report**.** – *Acta Morphol. Anthropol*., **30**, 2023, 116-121.
16. **Panayotova-Pencheva, M., F. Ponce-Gordo**. Severe parasite co-infection in a captive bactrian camel: case report. – *J. Zool. Bot. Gard.* **4**, 2023, 728–737.
17. **Reichard, M. V., R. F. Wolf, D. W. Carey, J. J. Garrett, H. A. Briscoe**. Efficacy of fenbendazole and milbemycin oxime for treating baboons (*Papio cynocephalus anubis*) infected with *Trichuris trichiura*. – *J. Am. Assoc. Lab. Anim. Sci*. **46**, 2007, 42-45.
18. **Rivero, J., A. M. García-Sánchez, R. Callejón, C. Cutillas**. Characterization of *Trichuris* species from porcupine (*Hystrix cristata*) at zoological garden of Spain. – *Acta Trop*., **228**, 2022, 106276.
19. **Sanz-García, C., A. Fernández-Iglesias, J. Gracia-Sancho, L. A. Arráez-Aybar, Y. A. Nevzorova, F. J. Cubero**. The space of Disse: The liver hub in health and disease. – *Livers,* **1***,* 2021, 3-26.
20. **Schachter, J., D. Alvarinho de Oliveira, C. M. da Silva, A. C. M. de Barros Alencar, M. Duarte, M. M. P. da Silva, A. C. D. P. R. Ignacio, E. J. Lopes-Torres**. Whipworm infection promotes bacterial invasion, intestinal microbiota imbalance, and cellular immunomodulation. – *Infect. Immun*., **88**, 2020, e00642-19.
21. **Shusterman, L., A. E. Marsh, P. H. Joyner.** Detection and differentiation of *Trichuris* in giraffe (*Giraffa camelopardalis*) under human care. – *J. Zoo Wildl. Med*., **53**, 2022, 383-392.
22. **Sunjaya, D. B., G. P. Ramos, M. B. B. Neto, R. Lennon, T. Mounajjed, V. Shah, P. S. Kamath, D. A. Simonetto.** Isolated hepatic non-obstructive sinusoidal dilatation, 20-year single center experience. – *World J. Hepatol*., **10**, 2018, 417–424.
23. **Taylor, M. A., R. L. Coop, R. Wall.** *Veterinary parasitology*, *Third edition*. Oxford, Blackwell Pub., 2007, 2080 pp.

Institute of Experimental Morphology, Pathology and Anthropology with Museum
Bulgarian Anatomical Society

Acta Morphologica et Anthropologica, 31 (1-2)
Sofia ● 2024

Review Articles

Esthetic Anatomy of Hands in Medicine and Art

Tuncay Colak[1], Hande Gurbuz[1,2], Osman Odabas[3]*

[1]Department of Anatomy, Kocaeli University Medical School, Kocaeli, Turkey
[2]Department of Anesthesiology and Reanimation, University of Health Sciences, Bursa City Hospital, Bursa, Turkey
[3]Department of Painting, Faculty of Fine Arts, Kocaeli University, Kocaeli, Turkey

*Corresponding author e-mail: handegrbz@gmail.com

The evolutionary process of the development of hands and fingers has been one of the most distinctive properties of the human species. While no hand, or even fingers of the same hand, is alike, there is no standard size and proportion due to gender, race, geography, repetitive occupations, and genetics. However, generally accepted hand proportions can be used in clothing design, ergonomic design of hand tools, implants used in hand surgery, biomechanical prosthesis development, and forensic research. Some hand characteristics may be similar in some specific populations, especially people with genetic disorders. Additionally, hand anthropometry may change, especially in musicians and sportspeople, because of constantly repetitive movements. Furthermore, hand anatomy has also been a source of inspiration for many artists. They emphasized hands in their art pieces using different methods according to the scope of art movements with which they were impressed. This review aimed to assess the anatomic, medical, and artistic implications of hand proportions.

Key words: artistic anatomy, hand, medicine in art, proportion, regional anatomy, science in art

Introduction

The evolutionary process of the development of hands and fingers has been one of the most distinctive properties of the human species [8]. The appearance of the human hand differs individually. While no hand, or even fingers of the same hand, is alike, there is no standard size and proportion due to gender, race, geography, repetitive occupations, and genetics. However, generally accepted hand proportions can be used in clothing design, ergonomic design of hand tools, implants used in hand surgery, biomechanical

prosthesis development, and forensic research [19; 41]. Some hand characteristics may be similar in some specific populations. For instance, genetic diseases such as Marfan syndrome, Fragile X syndrome, Down syndrome, and achondroplasia also have typical hand appearances [31; 48; 55; 59; 62; 69; 76; 79].

Hand anatomy has also been a source of inspiration for many artists. Furthermore, talented artists and leading scientists collaborated to create realistic images of the dissected anatomical parts. As a result of this collaboration, anatomical paintings and sculptures with high artistic value have emerged. The concept of "artistic anatomy" was born with the fusion of science and art.

This review aimed to evaluate the anatomic, medical, and artistic implications of hand proportions.

Hand Types

Hands hitherto have been classified differently by many authors [3; 45; 84]. The best-known of these classifications is constitutional typology, defined by Kretschmer. Accordingly, body types were defined as asthenic, athletic, and pyknic, and then the measurements of the hands in males and females of these body types were specified [44]. Later on, Sheldon defined somatotypes as endomorphy, mesomorphy, and ectomorphy according to morphological structures [77]. Sheldon's body type sorting is today's most accepted and frequently used classification in academic studies. Accordingly, ectomorph refers to long, thin fingers and weak hands, endomorph refers to short and thick fingers and broad and plump hands, and mesomorph refers to broad and muscular hand types [40] (**Fig.1**). Other subtypes are the combinations of these three somatotypes.

Fig. 1. Hand types according to Sheldon's description. **Left:** ectomorphic hand: a weak hand with long and thin fingers; **Middle:** mesomorphic hand: a muscular hand; **Right:** endomorphic hand: broad and plump hand with short and thick fingers.

In addition to the previously determined classifications for hands, there are some basic rules and approximate ratios for hand proportions:

The hand palm starts from the distal skin fold of the wrist and ends at the apparent base of the fingers. The webs between fingers form the apparent base of the fingers. However, the actual base is formed by the metacarpophalangeal joints. It is difficult to evaluate the hand bones with an external view due to the individual differences in the surrounding soft tissue. Still, hand bones can be better visualized using various radiological imaging methods.

Embryogenesis

Hand development is a complex process orchestrated by a plethora of molecular signals within the upper limb. With both stimulatory and inhibitory effects, these signals regulate cell proliferation and apoptosis, shaping the skeletal structures and spaces of the hand. Understanding the intricacies of hand development is essential for comprehending congenital malformations affecting the hand.

The upper extremity's genesis begins with a lateral bulge in the C5-8 and T1 myotomes around the 27th intrauterine day [11]. This bulge eventually forms a bud comprised of mesenchymal cells originating from both the somitic and lateral plate mesoderm, covered by ectoderm. While the lateral plate mesoderm contributes to cartilage and bone structures, the somitic mesoderm gives rise to limb musculature. By the fourth week of development, arm buds become discernible and expand, vascular structures emerge, and the hand plates take on a paddle-like formation [80]. Around day 36, nerve growth into the limb structure starts, and the digits begin to form as chondrogenic condensations along the distal hand paddle [23].

The first joint (shoulder) appears on the 36th day, and the last appears on the 47th day (in hand) [4]. By around 47 days, digits form as digital rays separated by flattened interdigital tissue, which subsequently undergoes apoptosis, allowing for digit formation. Towards the end of the eighth week (52nd day), separate fingers form with apoptosis of the mesenchymal tissue between the fingers [23; 82]. Within the seven weeks of development, carpal chondrification and muscle group formation commence. The size of the limb bud is influenced by factors such as the number of progenitors, proliferation rate, and cell death, with abnormalities in these factors leading to modifications in digit number and pattern. Chondrification progresses from proximal to distal, and phalanges chondrify around the 50th day [4]. Ossification of cartilaginous elements begins approximately at the sixth week and extends distally to the wrist and hand by the eighth week.

Postnatal growth significantly contributes to upper extremity development. Myelinization is completed around the age of two years, alongside the continuation of ossification of the carpus and epiphyses of the hand.

Key regulatory molecules such as fibroblast growth factor (FGF) 10 and T-box transcription factor-5 play pivotal roles in the bulging and budding on the 27th day [11]. Limb development is guided by specialized signaling centers, including the apical ectodermal ridge (AER), the zone of polarizing activity (ZPA), and the non-ridge ectoderm. These signaling centers secrete molecules regulating coordinated limb growth. The AER guides limb outgrowth along proximodistal through FGFs. A disruption in the FGF pathway leads to transverse limb defects. The ZPA directs the anteroposterior limb growth via Sonic Hedgehog (Shh). An impairment in Shh secretions leads to mirror image duplication on the limb and phalanges. The non-ridge ectoderm controls the limb growth in the dorsoventral axis through the balanced work of the Engrailed-1 transcription

factor. The Engrailed-1 expression directs the ventral patterning by restricting the dorsalization by inhibiting Wnt7a [23; 50]. A disturbance in dorsoventral maturation causes dorsalization defects such as palmar nail syndrome [71].

The chondrogenesis of the digit ray is mainly affected by the Transforming growth factor beta (TGF-β), SRY-related HMG-box (SOX) genes (specifically SOX9), FGFs, and bone morphogenic proteins (BMP) (specifically BMP-2) [2; 43]. The joint formation is dominated by the inhibition of chondrogenesis and apoptosis through the action of the TGF-β superfamily (mainly cartilage-derived morphogenetic protein-1) and the Wnt family (Wnt-4 and Wnt-14) [33; 49; 51]. The formation of separate digit process through programmed cell death is affected by the transcription factors such as muscle segment homeobox (Msx) (Msx-1 and Msx-2) and homeobox (Hox-7), and proteins including BMP-2, BMP-4, and BMP-7 [11]. The interruption of apoptosis of interdigital mesenchymal tissue at any stage of the developmental period results in deformations in interdigital web spaces. This way, congenital web space anomalies such as webbed hands-feet or syndactyly occur [82]. The Hox-D group has a significant role in anteroposterior limb growth, in which the mutations in the Hox-D family can produce various types of synpolydactyly [64]. A mutation in Shh can cause radial polydactyly and thumb anomalies [1].

Hands and Fingers

Interphalangeal and metacarpophalangeal joints are not aligned in a straight line. When three lines passing through the proximal interphalangeal joints, distal interphalangeal joints, and metacarpophalangeal joints are drawn, these lines form a parallel arc. In the resting position, the fingers slightly bend towards the third finger. In the anatomical position, the angle between the first and the fifth metacarpal bones is approximately 90 degrees [61].

Each finger is different in length. The longest finger is the middle finger. The index finger can guide some of the basic measurements of hands. For example, the palm width, the sum of the lengths of the thumb and the first metacarpal bone, and the distance from the second metacarpophalangeal joint to the end of the palm are basically equal to the length of the index finger [25]. The distance corresponding to the longest line of the palm (from the wrist line to the third metacarpophalangeal joint) is equal to the length of the middle finger [65]. These esthetic anatomy rules are the measurements that artists often use in their hand drawings.

Digit proportions show regional, racial, and gender differences. It has also been demonstrated to play a role in functional dexterity and thermoregulation. Thicker index and middle fingers are associated with low dexterity [68; 74]. Furthermore, a shorter and broader first metacarpal bone has been observed in populations living in cold climates [14]. While physical dexterity decreased in people with thick hands and fingers, people with thin hands and fingers could do fine work more efficiently, and physical dexterity increased. Those living in cold regions are thought to adapt to these conditions with thicker hands and fingers, mainly for thermoregulation [14].

Index to Ring Finger Ratio (D2:D4)

The ratio of the index to the ring finger (D2:D4) has been the topic that most attracted the attention of scientists. Although D2:D4 differs individually or regionally, it has

also been used to estimate gender, height, and weight [9]. The D2:D4 ratio has been related to personality, spatial ability, and various diseases (probably due to hormonal relationships).

The D2:D4 ratio is found to be 1.005 in Malaysians, but it is lower than 1 (<1) in other nations [58; 81]. Even though there are minimal differences in hand measurements between both hands according to hand preference, the difference between the two hands in the D2:D4 ratio is insignificant [10; 72]. Additionally, the D2:D4 ratio is lower in males than females, meaning the ring finger is longer in men than women [29; 55; 72].

Intrauterine sexual differentiation takes place towards the end of the first trimester. Thus, it has been suggested that the gender difference in the D2:D4 ratio is due to intrauterine androgen exposure during this period [13; 27; 53]. The D2:D4 ratio also differs within each gender. This difference is attributed to the variation in exposure to intrauterine sex hormones. Namely, while testosterone causes the ring finger to lengthen, contrastingly, estrogen causes the ring finger to shorten [55; 57]. In a study based on this idea, the D2:D4 ratio in male-to-female people was found to be higher than the male control group, while it was similar to the female controls [75]. These results also support the etiology of decreased prenatal androgen exposure in male-to-female people.

Males are suggested to be better at using directional cues to reach a target location in a landscape environment than females. Accordingly, the masculine D2:D4 ratio is thought to be associated with the sense of direction [21]. Physical endurance and sports performance also negatively correlate with D2:D4 [12; 35; 56; 57; 78]. Finally, the studies revealed that the personality traits of people with a male-like D2:D4 ratio are more prone to aggression, anger, violence, smoking, and problem drinking [17; 18; 24; 73].

Hands in Medicine

Many diseases present unique hand appearances specific to the condition. For example, a male-like D2:D4 pattern can be observed in patients with autism spectrum disorder and congenital adrenal hyperplasia as an indicator of intrauterine androgen exposure [15; 52; 70]. Achondroplastic patients have wide palm breadth; however, palm breadth is narrow in Marfan syndrome. The fingers are very short in achondroplasia and very long in Marfan syndrome. In Down syndrome, the hands and feet are small, and the fingers are short and wide. Patients with Down syndrome have clinodactyly (curved fingers), and arachnodactyly is present in a marfanoid appearance. In Fragile-X and Marfan syndrome, the finger joints are hyperextensible [31; 48; 54; 59; 62; 69; 76; 79; 81].

There may be changes in hand anthropometry, especially in musicians and sportspeople, because of constantly repetitive movements [83]. Also, as a result of the overuse of some joints, they may be more prone to some hand injuries [7]. Besides, due to typical hand anthropometry, some medical illnesses like Marfan syndrome may be advantageous to play specific instruments, as with Niccolò Paganini [59; 76].

In medicine, hands are also used as a measurement method to determine the landmarks of some anatomical structures or determine the instruments' estimated sizes to be used. For example, although there is a formula for calculating the pediatric endotracheal tube's diameter, the width and diameter of the little finger of the pediatric patient correspond to the endotracheal tube size suitable for the child [42]. For the femoral nerve blocks, the estimated landmark of the nerve is correlated with the distance from the femoral artery and the width of the little finger [26].

Another area where hand length is used in medicine is estimating the average body size, which is crucial in a clinical setting or forensic science if it is impossible to get specific measurements directly. Hand length and handbreadth are used to predict stature and height [37; 38; 39; 66]. Additionally, hand length is demonstrated to be an excellent independent predictor of body surface area and body mass, and it is accurate for ages two to 17, independent of gender [5; 6]. Furthermore, the hand's palmar aspect is approximately 0.78% of the body surface area [5]. Therefore, hand length is a simple measurement that can be used as a treatment guide, such as estimating the volume of intravenous fluid or packed blood cells. Furthermore, the average age of the children can be estimated by the hand and wrist X-ray, based on the knowledge that the bone maturation and ossification process continue during the child's growth [20].

The Fibonacci Sequence and Golden Ratio

The Fibonacci sequence is a series of numbers starting from 0 and 1 (0, 1, 1, 2, 3, 5, 8, 13, etc.) in which each number is the sum of the two preceding ones. In this sequence, the ratio of two consecutive numbers gives the Golden ratio of approximately 1.618 = phi (ϕ). At the same time, the Golden ratio applies to geometric shapes, such as triangles, rectangles, etc., that have this ratio between their sides. Thus, logarithmically nesting these geometric shapes suitable for this formation creates an equiangular spiral linked to many objects found in nature (nautilus shell, snail, pine cones, sunflower, etc.), architecture, music, and painting.

The esteemed hand surgeon Dr. J. William Littler is the first to discuss the adaptability of the Fibonacci sequence and Golden ratio to hands [47]. After this assertion, a study consisting of a small sample size group demonstrated that the flexion and extension path of the fingertips overlap with an equiangular spiral [28]. Subsequent studies present conflicting results, probably due to measurement differences. In studies measuring the radiographic lengths of the hand bones, the authors stated that the phalangeal ratios are different and do not follow the Fibonacci sequence [32; 67]. Following these results, which failed to prove the previous hypothesis, it has been stated that the measurement method meant by Dr. Littler is not directly measuring the actual bone lengths, but the correct measurement method should be the functional centers of the rotation lengths [60; 67] (**Fig.2**). In another study designed later on this suggestion, and it has been demonstrated that the functional lengths of the phalanges of the fifth finger do follow the exact Fibonacci sequence, while the remaining second, third, and fourth digits follow a specific mathematical pattern very similar to the Fibonacci sequence [36]. According to the results presented by a different research group, the phalanges of all five fingers cannot be ordered according to the same sequential rule [16].

Hands in Art: A Selection from the Most Famous Artists

Hand gestures reflect subtle human emotions, and hands are the most difficult to draw of all the parts of the human body. For this reason, hands have been considered one of the richest and most meaningful elements of the human body in art history and have been given a symbolic meaning. Many artists have emphasized the themes by depicting the hands in their own forms in every era. Hands have a character that offers much information about the psychological and physical condition of the owner by expressing

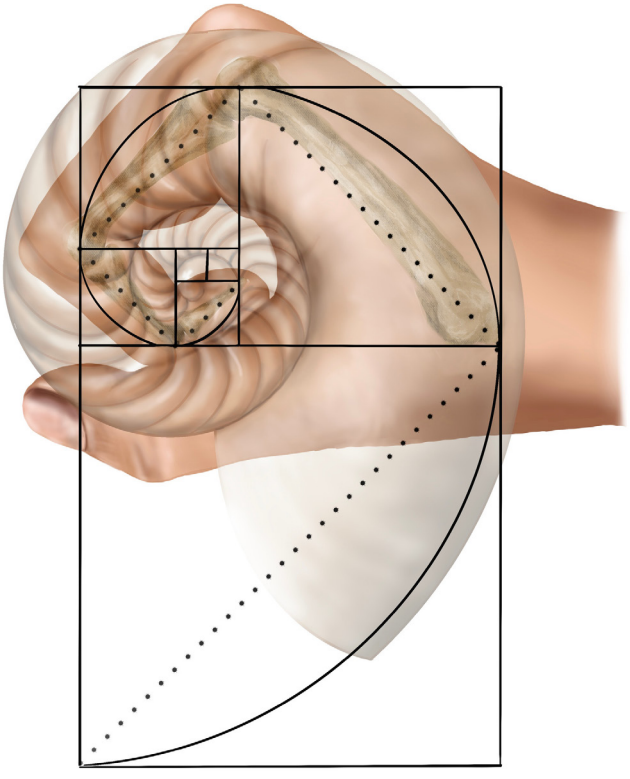

Fig. 2. A hand figure based on William Littler's hypothesis. An equiangular spiral (a nautilus shell) with the corners of the squares passing from the functional centers of rotation.

many emotions with their forms, postures, and gestures. For this reason, hands have been the focus of attention of many artists over the years.

Many nuances in similar movements of the hands can express very different or even opposite emotions. For example, a tightly flexed hand with all fingers aligned may denote someone ready to punch in a fight or a triumphant fist raised excitedly after a hard-fought victory. In contrast, a fist with fingers softly flexed to varying degrees may represent the shape of a resting hand. Again, while a hand gesture -with a taut thumb opened at a wider angle than the hand and a D2 in extension together with a tightly flexed D3, D4, and D5 in such a way that the nails are not visible- expresses a harder emotion (such as authority, tension, excitement, agitation, ...), opening the thumb with a slightly narrower angle and slightly flexing the D3, D4, and D5 with different degrees showing nails in a similar hand movement emphasizes a more natural and softer expression [22]. An example of using hand gestures with another implication is the painting of Leonardo da Vinci, in which Jesus was depicted as Salvator Mundi (Savior of the World) (1490-1500). In this artwork, the right hand with the third finger is extended next to the second finger, and the whole posture represents a blessing hand. At the same time, Leonardo da Vinci used the Golden ratio in both hands, as in many parts of the painting.

Renaissance is the period of coding and symbolism, and the artists frequently used hands and the Golden ratio in their artworks to point out their thoughts. Leonardo da Vinci is indeed one of the artists who frequently used the golden ratio in his paintings during the Renaissance period. It appears in countless places in nature and has been used in architectural structures since the time of the Egyptians. In some of his most famous paintings, such as Mona Lisa (1503), The Annunciation (1472), and The Last Supper (1495-1498), which were depicted using the Golden ratio, character and psychological analyses can be made from the gestures of the carefully drawn hands. One of the famous drawings of hands is Albrecht Dürer's painting Praying Hands

(1503). Although a praying couple of hands has been drawn, it is actually a painting of respect, devotion, sacrifice, effort, and love.

One of the most famous painters of the Renaissance period, as well as a sculptor, poet, and architect, Michelangelo di Lodovico Buonarroti Simoni's painting The Creation of Adam (1505), drawn on the ceiling of the Sistine Chapel, shows the hands of Adam and God stretching out towards each other. The purpose of the hands reaching each other here is not to shake hands or to join hands. The main subject of discussion is the space between the hands, and various theories have been produced on this. Later on, this artwork was adapted to neuroanatomy [63]. Furthermore, if we look at the Statue of David (1501-1504), one of Michelangelo's works of art, what draws our attention here is that David's right hand is incompatible with his body. The reasons behind this disproportionateness made by Michelangelo, who has worked on human anatomy for years and is a great name in body proportions and human anatomy, have been a question of debate. David's statue depicts the shepherd David, who defeated the terrible giant Goliath, an acromegaly patient, only with a tiny sling. It is thought that Michelangelo made this disproportion to emphasize David's nickname "manu fortis", in other words, "strong hand".

Art history and hand anatomy according to art periods

Renaissance, mannerism, baroque

The fact that Lorenzo Ghiberti, Antonio Pollaiuolo, and similar contemporaries began to be interested in the subject of anatomy in the early Renaissance led to the study of anatomy more frequently in the works of artists such as da Vinci, Michelangelo, and Vasari and to the production of pieces with scientific findings on the subject in the later years. At the same time, Andreas Vesalius, an anatomist, corrected the mistakes in the works of Claude Galen (Galen of Pergamon) (which has been considered valid for the last thousand years) and created the book "De Humani Corporis Fabrica Libri Septem (1543)", which was recognized as the most comprehensive scientific study on anatomy ever made to that date. The drawings and engravings in the book were made by the painters in the workshop of the famous artist of the period, Titian.

The anatomical treatment of body parts separately in art in the Renaissance period has made human hand drawings one of the indicators and criteria of concepts such as mastery and virtuosity for artists. Along with the mannerism period, which can be considered a transitional stage between the Renaissance and Baroque periods, new artistic proposals and forms were created about hand drawings and anatomy, such as exaggerating body lines and deliberately deforming them. It is possible to see the traces of Albrecht Dürer in the paintings of Hendrick Goltzius, one of the master engravers of the Early Baroque and Mannerist period, as in Peter Paul Rubens, one of the greatest painters of the Baroque period, bear traces of Hendrick Goltzius. Influenced by Michelangelo and Dürer, these two names created their unique style and form based on these artists' understanding of deformation due to the period's thought movement. Hands have become one of the most prominent indicators of this unique style in the drawings and paintings they made using exaggerated lines, form, and mass, considering each part of the human body separately. The painting of another great artist of the Baroque period, Rembrandt, "The Anatomy Lesson of Dr. Nicolaes Tulp (1632)", which depicts Dr. Tulp's lecture showing his students the muscles and bones of the human hand, has been accepted as one of the masterpieces of the period [34].

The weakening of the dogmatic thought movement of the Middle Ages and the changes experienced with the Renaissance, together with the confidence of the artists' scientific experiences in anatomy, enabled the artists to reflect the forms of the figure more freely in the Baroque and Mannerist periods.

Neoclassicism and Romantism

Hand figures and drawings from the Neoclassical and Romantic periods are a new representation of the concept of imitating nature in the forms and shapes of the classical period. In the artworks of painters such as Eugene Delacroix and Jacques Louis David, the use of figures and, therefore, hands, as a reflection of the period's intense military and political climate, seems to have undertaken a task similar to that of the classical period. In most of the paintings of Jean-Auguste-Dominique Ingres, one of the most famous portrait painters of the neoclassical period, the hands are the complements of the portrait. Due to the conditions of the period, the revival of the classical style and portraying it with surgical precision is necessary. Ingres' paintings are the most prominent examples of this. Hands and faces, which are more visible among the details and ornaments in Ingres' dull, monumental, smooth brush technique, are the last and most magnificent challenge of classicism, perhaps in the history of painting [30].

Realism

Since the mid-1800s, within the scope of the realism movement, hands have appeared differently from the fictional or symbolic style in previous periods. The hand figure is a symbol that supports the expression in artworks, mainly dealing with concepts such as religion, monarchy, and feudalism. Due to the structure of the classical period, in the realism movement, people working in the fields, greeting each other, or combing their hair are depicted as a part of real daily life in the works of painters such as Gustave Courbet and Francois Millet.

Modernism

Towards modern art, the figure begins to diverge from the classical style in the periods of Expressionism and Impressionism. Contrary to the old great ideologies and movements, when personal feelings, opinions, and self-concepts come to the fore in this period, the depiction of the figure and hands changes accordingly. Imagination forces not only the subject but also the form of the artwork. The anatomical structure is shown on the hands and the whole-body figure, with a unique deformation understanding specific to the artist. In the works of Gustav Klimt and Egon Schiele, the artists of this period, the hands are like the reflection of the feelings and thoughts of the depicted figure [46].

Cubism and surrealism

In modernism and later, the search for new ideologies and an understanding apart from formal concerns and esthetic diversity, the figure has been depicted using primitive, distorted, or geometric forms. Painters who carried out these studies, such as Picasso and Dali, the pioneers of the Cubism and surrealism movements, also made anatomic studies in their early periods; thus, they were able to distort or deform the shape in line with these classical studies. In this period, artists like Neşet Günal presented their sense of art with a social context, with deformed and disproportionately sized hands and feet.

Conclusion

Hands constitute an important place in art as well as in medicine. The shape and proportions of the hands and fingers may be typical features of people of different races living in various geographies. The shape and proportions of the hands and fingers may present the phenotype of many genetic diseases and reflect people's physical and personality traits. Additionally, hands have been considered one of the richest and most meaningful elements of the human body in art history and have been given a symbolic meaning. Many artists have depicted different emotions and events in their paintings using the characters of the hands.

References:

1. **Afshar, A.** An update on embryology of the upper limb. – *J. Hand. Surg. Am.,* **38**, 2013, 2304.
2. **Akiyana, H., M. C. Chabeissier, J. F. Martin, A. Schedl, B. de Crombrugghe.** The transcription factor Sox9 has essential roles in successive steps of the chondrocyte differentiation pathway and is required for expression of Sox5 and Sox6. – *Genes. Dev*., **16**, 2002, 2813–2828.
3. **Alpenfels, E. J.** The anthropology and social significance of the human hand. – *Artificial Limbs*., **2**, 1955, 4-21.
4. **Al-Qattan, M. M., Y. Yang, S. H. Kozin.** Embryology of the upper limb. – *J. Hand Surg.*, **34**, 2009, 1340-1350.
5. **Amirsheybani, H. R., G. M. Crecelius, N. H. Timothy, M. Pfeiffer, G. C. Saggers, E. K. Manders.** The natural history of the growth of the hand: I. Hand area as a percentage of body surface area. – *Plast. Reconstr. Surg*., **107**, 2001, 726-733.
6. **Amirsheybani, H. R., G. M. Crecelius, N. H. Timothy, M. Pfeiffer, G. C. Saggers, E. K. Manders.** Natural history of the growth of the hand: part II - hand length as a treatment guide in the pediatric trauma patient. – *J. Trauma*, **49**, 2000, 457-460.
7. **An, K. N., F. J. Bejjani.** Analysis of upper-extremity performance in athletes and musicians. – *Hand. Clin*., **6**, 1990, 393-403.
8. **Andrews, P.** Last common ancestor of apes and humans: morphology and environment. – *Folia Primatol. (Basel)*., **91**, 2020, 122-148.
9. **Barut, C., U. Tan, A. Dogan.** Association of height and weight with second to fourth digit ratio (2D:4D) and sex differences. – *Percept. Mot. Skills,* **106**, 2008, 627-632.
10. **Barut, C., O. Sevinc, V. Sumbuloglu.** Evaluation of hand asymmetry in relation to hand preference. – *Coll. Antropol*., **35**, 2011, 1119-1124.
11. **Baykal, B., S. Turkkan.** Development of the hand. – *J. Embryol.*, **1,** 2017, 1-5.
12. **Bennett, M., J. T. Manning, C. J. Cook, L. P. Kilduff.** Digit ratio (2D:4D) and performance in elite rugby players. – *J. Sports. Sci.,* **28**, 2010, 1415-1421.
13. **Berenbaum, S. A., K. K. Bryk, N. Nowak, C. A. Quigley, S. Moffat**. Fingers as a marker of prenatal androgen exposure. – *Endocrinology,* **150**, 2009, 5119–5124.
14. **Betti, L., S. J. Lycett, N. Von Cramon-Taubadel, O. M. Pearson.** Are human hands and feet affected by climate? A test of Allen's rule. – *Am. J. Phys. Anthropol*., **158**, 2015, 132–140.
15. **Bloom, M. S., A. S. Houston, J. L. Mills, C. A. Molloy, M. L. Hediger**. Finger bone immaturity and 2D:4D ratio measurement error in the assessment of the hyperandrogenic hypothesis for the etiology of autism spectrum disorders. – *Physiol. Behav*., **100**, 2010, 221-224.
16. **Buryanov, A., V. Kotiuk**. Proportions of hand segments. – *Int. J. Morphol*., **28**, 2010, 755-758.

17.Butovskaya, M., V. Burkova, D. Karelin, V. Filatova. The association between 2D:4D ratio and aggression in children and adolescents: cross-cultural and gender differences. – *Early. Hum. Dev*., **137**, 2019, 104823.
18. Canan, F., C. Tegin, O. Gecici. The second to fourth digit (2D:4D) ratios, smoking, and problem drinking in a young adult university student sample. – *Neurol. Psychiatry. Brain Res*., **32**, 2019, 63-67.
19. Case, D. T., A. H. Ross. Sex determination from hand and foot bone lengths. – *J. Forensic Sci.,* **52**, 2007, 264-270.
20. Cavallo, F., A. Mohn, F. Chiarelli, C. Giannini. Evaluation of bone age in children: a mini-review. – *Front. Pediatr*., **9**, 2021, 580314.
21. Chai, X. J., L. F. Jacobs. Digit ratio predicts sense of direction in women. – *PLoS. One*., **7**, 2012, e32816.
22. Civardi, G. *Art of drawing: drawing hands and feet: form, proportions, gestures and actions.* United Kingdom, Search Press, 2005.
23. Cole, P., Y. Kaufman, D. A. Hatef, L. H. Hollier Jr. Embryology of the hand and upper extremity. – *J. Craniofac. Surg*., **20**, 2009, 992-995.
24. Dogan, A., C. Barut, N. Konuk, Y. Bilge. Relation of 2D:4D ratio to aggression and anger. – *Neurol. Psychiatry. Brain Res*. **14**, 2008, 151–158.
25. How to draw realistic hands. Dragoart, 2011. Available at: https://dragoart.com/tut/how-to-draw-realistic-hands-draw-hands-9019
26. Frković, V., S. K. T. S. Wärmländer, A. Petaros, I. Španjol-Pandelo, J. Ažman. Finger width as a measure of femoral block puncture site: an ultrasonographic anatomical-anthropometric study. – *J. Clin. Anesth*., **27**, 2015, 553-557.
27. Galis, F., C. M. A. Ten Broek, S. Van Dongen, L. C. D. Wijnaendts. Sexual dimorphism in the prenatal digit ratio (2D:4D). – *Arch. Sexual. Behavior*, **39**, 2010, 57–62.
28. Gupta, A., G. S. Rash, N. N. Somia, M. P. Wachowiak, J. Jones, A. Desoky. The motion path of the digits. – *J. Hand Surg*., **23**, 1998, 1038–1042.
29. Gupta, S., V. Gupta, N. Tyagi, Ettishree, S. Bhagat, M. Dadu, N. Anthwal, T. Ashraf. Index/ring finger ratio, hand and foot index: gender estimation tools. – *J. Clin. Diagn. Res.*, **11**, 2017, 73-77.
30. Guran, L. The aesthetic dimension of American-Romanian comparative literary studies. – *The Comparatist*, **27**, 2003, 94-115.
31. Hamada, Y., K. Sairyo, N. Yasui. Locking of the metacarpophalangeal joint as a result of the shape of the metacarpal head in achondroplasia. – *J. Hand Surg. Eur. Vol*., **32**, 2007, 588-590.
32. Hamilton, R., R. A. Dunsmuir. Radiographic assessment of the relative lengths of the bones of the fingers of the human hand. – *J. Hand Surg. Br*. **27**, 2002, 546-548.
33. Hartmann, C., Tabin, C. J. Wnt14 plays a pivotal role in inducing synovial joint formation in the developing appendicular skeleton. – *Cell*, **104**, 2001, 341–351.
34. Hollingsworth, M. *Art in world history*. Florence, Giunti Editore, 2008.
35. Hönekopp, J., M. Schuster. A meta-analysis on 2D:4D and athletic prowess: substantial relationships but neither hand outpredicts the other. – *Pers. Individ. Dif*., **48**, 2010, 4–10.
36. Hutchison, A. L., R. L. Hutchison. Fibonacci, littler, and the hand: a brief review. – *Hand (New York)*, **5**, 2010, 364-368.
37. Ibegbu, A. O., E. T. David, W. O. Hamman, U. E. Umana S. A. Musa. Association of hand length with height in Nigerian school children. – *J. Biol. Life Sci.,* **4**, 2013, 83.
38. Ibegbu, A. O., E. T. David, W. O. Hamman, U. E. Umana, S. A. Musa. Height determination using hand length in Nigerian school children. – *J. Morphol. Sci.,* **31**, 2014, 193-198.
39. Ibegbu, A. O., E. T. David, W. O. Hamman, U. E. Umana, S. A. Musa. Hand length as a determinat of height in school children. – *Adv. Life Sci.*, **5**, 2015, 12-17.

40. Jakubietz, R. G., M. G. Jakubietz, D. Kloss, J. G. Gruenert. Defining the basic aesthetics of the hand. – *Aesthetic Plast. Surg*., **29**, 2005, 546-551.
41. Kanchan, T., P. Rastogi. Sex determination from hand dimensions of North and South Indians. – *J. Forensic Sci*., **54**, 2009, 546-550.
42. King, B. R., M. D. Baker, L. E. Braitman, J. Seidl-Friedman, M. S. Schreiner. Endotracheal tube selection in children: a comparison of four methods. – *Ann. Emerg. Med*., **22**, 1993, 530-534.
43. Kornak, U., S. Mundlos. Genetic disorders of the skeleton: a developmental approach. – *Am. J. Hum. Genet.,* **73**, 2003, 447– 474.
44. Kretschmer, E. Types of physique. – In: *Physique and character,* 1st ed. Berlin, Springer. 1931, 16-36.
45. Krogman, W. M. The anthropology of the hand. – *Ciba Symposia*, **4**, 1942, 1294-1321.
46. Latimer, T. T. Discrepant Modernisms. – *American Art.,* **30**, 2016, 2-6.
47. Littler, J. W. On the adaptability of man's hand (with reference to the equiangular curve). – *Hand (New York)*, **5**, 1973, 187–191.
48. Loesch, D. Z., D. A. Hay, L. J. Sheffield. Fragile X family with unusual digital and facial abnormalities, cleft lip and palate, and epilepsy. – *Am. J. Med. Genet.,* **44**, 1992, 543-550.
49. Logunathan, P.G., S. Nimmagadda, R. Huan, M. Scaal, B. Christ. Comparative analysis of the expression patterns of Wnts during chick limb development. – *Histochem. Cell. Biol.,* **123**, 2005, 195–201.
50. Loomis, C. A., R. A. Kimmel, C. X. Tong, J. Michaud, A. L. Joyner. Analysis of the genetic pathway leading to formation of ectopic apical ectodermal ridges in mouse Engrailed-1 mutant limbs. – *Development*, **125**, 1998, 1137-1148.
51. Luyten, F. P. Cartilage-derived morphogenetic protein-1. – *Int. J. Biochem. Cell. Biol.,* **29**, 1997, 1241-1244.
52. Mackus, M., D. de Kruijff, L. S. Otten, A. D. Kraneveld, J. Garssen, J. C. Verster. The 2D:4D digit ratio as a biomarker for autism spectrum disorder. – *Autism. Res. Treat*., **2017**, 2017, 1048302.
53 Malas, M. A., S. Dogan, E. H. Evcil, K. Desdicioglu. Fetal development of the hand, digits, and digit ratio (2D:4D). – *Early Hum. Dev*., **82**, 2006, 469–475.
54. Mankin, H. J., J. Jupiter, C. A. Trahan. Hand and foot abnormalities associated with genetic diseases. – *Hand (New York),* **6**, 2011, 18-26.
55. Manning, J. T., L. Barley, J. Walton, D. I. Lewis-Jones, R. L. Trivers, D. Singh, A. Szwed. The 2nd:4th digit ratio, sexual dimorphism, population differences, and reproductive success: Evidence for sexually antagonistic genes? – *Evol. Hum. Behav*., **21**, 2000, 163–183.
56. Manning, J. T., R. P. Taylor. Second to fourth digit ratio and male ability in sport: implications for sexual selection in humans. – *Evol. Hum. Behav*., **22**, 2001, 61-69.
57. Manning, J., L. Kilduff, C. Cook, B. Crewther, B. Fink. Digit ratio (2D:4D): a biomarker for prenatal sex steroids and adult sex steroids in challenge situations. – *Front. Endocrinol.,* **5**, 2014, 9.
58. Manning, J. T., B. Fink, R. Trivers. Digit ratio (2D:4D) and gender inequalities across nations. – *Evol. Psychol*., **12**, 2014, 757-768.
59. Mantero, R. The marfan hands of Niccolò Paganini. – *Ann. Chir. Main*., **7**, 1988, 335-340.
60. Markley, J. M. The Fibonacci sequence: relationship to the human hand. – *J. Hand Surg. Am*., **28**, 2003, 704-706.
61. Human anatomy fundamentals: how to draw hands, 2014. Available at: https://design.tutsplus.com/tutorials/human-anatomy-fundamentals-how-to-draw-hands--cms-21440
62. Meryash, D. L., C. E. Cronk, B. Sachs, P. S. Gerald. An anthropometric study of males with the fragile-X syndrome. – *Am. J. Med. Genet*., **17**, 1984, 159-174.
63. Meshberger, F. L. An interpretation of Michelangelo's Creation of Adam based on neuroanatomy. – *JAMA*., **264**, 1990, 1837-1841.

64. Muragaki, Y., S. Mundlos, J. Upton, B. R. Olsen. Altered growth and branching patterns in synpolydactyly caused by mutations in HOXD13. – *Science*, **272**, 1996, 548-551.
65. The various proportions of human hand and fingers, 2021. Available at: https://www.joshuanava.biz/hands/proportions-and-measurements.html
66. Numan, A. I., M. O. Idris, J. V. Zirahei, D. S. Amaza, M. B. Dalori. Prediction of stature from hand anthropometry: a comparative study in the three major ethnic groups in Nigeria. – *Br. J. Med. Med. Res.,* **3**, 2013, 1062-1073.
67. Park, A. E., J. J. Fernandez, K. Schmedders, M. S. Cohen. The Fibonacci sequence: relationship to the human hand. – *J. Hand Surg. Am.,* **28**, 2003, 157-160.
68. Payne, S., A. Macintosh, J. Stock. The influence of digit size and proportions on dexterity during cold exposure. – *Am. J. Phys. Anthropol*., **166**, 2018, 875-883.
69. Pedrazzini, A., A. Martelli, S. Tocco. Niccolò Paganini: the hands of a genius. – *Acta Biomed*., **86**, 2015, 27-31.
70. Puts, D. A., M. A. McDaniel, C. L. Jordan, S. M. Breedlove. Spatial ability and prenatal androgens: meta-analyses of congenital adrenal hyperplasia and digit ratio (2D:4D) studies. – *Arch. Sex. Behav*., **37**, 2008, 100-111.
71. Ridder, M. A. Congenital palmar nail syndrome. – *J. Hand Surg.,* **17**, 1992, 371–372.
72. Robertson, J., W. Zhang, J. J. Liu, K. R. Muir, R. A. Maciewicz, M. Doherty. Radiographic assessment of the index to ring finger ratio (2D:4D) in adults. – *J. Anat.,* **212**, 2008, 42-48.
73. Romero-Martínez, A., M. Lila, P. Sariñana-González, E. González-Bono, L. Moya-Albiol. High testosterone levels and sensitivity to acute stress in perpetrators of domestic violence with low cognitive flexibility and impairments in their emotional decoding process: a preliminary study. – *Aggress. Behav*., **39**, 2013, 355-369.
74. Sahin, F., N. S. Atalay, N. Akkaya, S. Aksoy. Factors affecting the results of the functional dexterity test. – *J. Hand Ther*., **30**, 2017, 74-79.
75. Schneider, H. J., J. Pickel, G. K. Stalla. Typical female 2nd-4th finger length (2D:4D) ratios in male-to-female transsexuals-possible implications for prenatal androgen exposure. – *Psychoneuroendocrinol.*, **31**, 2006, 265-269.
76. Schoenfeld, M. R. Nicolo Paganini - musical magician and Marfan mutant? – *Med. Times,* **108**, 1980, 117-125.
77. Sheldon, W. H., S. S. Stevens, W. B. Tucker. *The varieties of human physique.* New York, Harper, 1940.
78. Sudhakar, H. H., U. B. Veena, R. N. Tejaswi. Digit ratio (2D:4D) and performance in Indian swimmers. – *Ind. J. Physiol. Pharmacol*., **57**, 2013, 72-76.
79. Sureshbabu, R., R. Kumari, S. Ranugha, R. Sathyamoorthy, C. Udayashankar, P. Oudeacoumar. Phenotypic and dermatological manifestations in Down Syndrome. – *Dermatol. Online J*., **17**, 2011, 3.
80. Tickle, C. Molecular basis of limb development. – *Biochem. Soc. Trans*., **22**, 1994, 565-569.
81. Hand index correlates with genetic variation and genetic distance. Hand research news & reports, 2017. Available at: http://www.handresearch.com/news/hand-shape-hand-index-correlates-with-genetic-variation-genetic-distance.htm
82. Vogel, A., C. Rodriguez, J. C. Izpisua-Belmonte. Involvement of FGF-8 in initiation, outgrowth and patterning of the vertebrate limb. – *Development*, **122**, 1996, 1737-1750.
83. Wagner, C. H. The pianist's hand: anthropometry and biomechanics. – *Ergonomics*, **31**, 1988, 97-131.
84. Wolff, C. The form of the hand. – In: *The human hand*. London, Routledge, 1942.

Author Guidelines

Acta Morphologica et Anthropologica is an open access peer review journal published by Bulgarian Academy of Sciences, Prof. Marin Drinov Publishing House.
Corporate contributors are Bulgarian Academy of Sciences, Institute of Experimental Morphology, Pathology and Anthropology with Museum and Bulgarian Anatomical Society.

Acta Morphologica et Anthropologica is published in English, 4 issues per year.

The journal accepts manuscripts in the following **fields**: experimental morphology, cell biology and pathology, anatomy and anthropology.

Publication types: original articles, short communications, case reports, reviews, Editorial, letters to the Editors.

Acta Morphologica et Anthropologica is the continuation of Acta cytobiologica et morphologica

The **aim** of the Journal is to disseminate current interdisciplinary biomedical research and to provide a forum for sharing new scientific knowledge and methodology. The general editorial policy is to optimize the process of issuing and distribution of *Acta Morphologica et Anthropologica* in line with modern standards for scientific periodicals focusing on content, form, and function.

Scope – experimental morphology, cell biology and pathology (neurobiology, immunobiology, tumor biology, environmental biology, reproductive biology, etc.), new methods, anatomy and pathological anatomy, anthropology and paleoanthropology, medical anthropology and physical development.

Acta Morphologica et Anthropologica is published twice a year as one volume with 4 issues. For the first two issues (1-2) the deadline for manuscript submission is March 15th and for the next two issues (3-4), the deadline is September 15th. Electronic version for issues 1-2 is uploaded on the website till June 30th and for issues 3-4 – till December 30th.

Contact details and submission

Manuscript submission is electronical only. The manuscripts should be sent to the Managing Editor's e-mail address ygluhcheva@hotmail.com with copy to iempam@bas.bg

All correspondence, including notification for Editor's decision, requests for revision, is sent by e-mail.

Article structure

Manuscripts should be in English with total length not exceeding 10 standard pages, line-spacing 1.5, justified with 2.5 cm margins. The authors are advised to use Microsoft Word 97-2003, Times New Roman, 12 pt throughout the text. Pages should be numbered at the bottom right corner of the page.

The article should be arranged under the following headings: Introduction, Material and Methods, Results, Discussion, Conclusion, Acknowledgements and References.

Title page – includes:

- **Title** – concise and informative;
- **Author(s)' names and affiliations** – indicate the given name(s) and family name(s) of all authors. Present the authors' affiliation addresses below the names. Indicate all affiliations with a lower-case superscript after the author's name and in front of the appropriate address. Provide the full postal address information for each affiliation, including the country name.
- **Corresponding author** – clearly indicate who will handle the correspondence for refereeing, publication and post-publication. An e-mail should be provided.
- **Abstract** – state briefly the aim of the work, the principal results and major conclusions and should not exceed 150 words. References and uncommon, or non-standard abbreviations should be avoided.
- **Key words** – provide up to 5 key words. Avoid general, plural and multiple concepts. The key words will be used for indexing purposes.

Introduction – state the objectives of the work and provide an adequate background, avoiding a detailed literature survey or summary of the results.

Material and Methods – provide sufficient detail to allow the work to be reproduced. Methods already published should be indicated as a reference: only relevant modifications should be described.

Results – results should be clear and concise.

Discussion – should explore the significance of the results in the work, not repeat them. A combined *Results and Discussion* section is often appropriate. Avoid extensive citation and discussion of published literature.

Conclusions – the main conclusions of the study should be presented in a short section.

Acknowledgements – list here those individuals who provided help during the research and the funding sources.

Units – please use the International System of Units (SI).

Math formulae – please submit math equations as editable text, not as images.

Electronic artwork – number the tables and illustrations according to their sequence in the text. Provide captions for them on a separate page at the end of the manuscript. The proper place of each figure in the text should be indicated in the left margin of the corresponding page. **All illustrations (photos, graphs and diagrams)** should be referred to as "figures" and given in abbreviation "Fig.", and numbered in Arabic numerals in order of its mentioning in the manuscript. They should be provided in grayscale as JPEG or TIFF format, minimum 300 dpi. The illustrations should be submitted as separate files.

References – they should be listed in alphabetical order, indicated in the text by giving the corresponding numbers in parentheses. The "References" should be typed on a separate sheet. The names of authors should be arranged alphabetically according to family names. In the reference list titles of works, published in languages other than English, should be translated, original language must be indicated at the end of reference (e.g., [in Bulgarian]). Articles should include the name(s) of author(s), followed by the full title of the article or book cited, the standard abbreviation of the journal (according to British Union Catalogue), the volume

number, the year of publication and the pages cited, for books - the city of publication and publisher. In case of more than one author, the initials of the second, third, etc. authors precede their family names. Ideally, the names of all authors should be provided, but the usage of "et al" after the fifth author in long author lists will also be accepted.

For articles: **Davidoff, M. S., R. Middendorff, G. Enikolopov, D. Riethmacher, A. F. Holstein, D. Muller**. Progenitor cells of the testosterone-producing Leydig cells revealed. – *J. Cell Biol.,* **167**, 2004, 935-944.

Book article or chapter: **Rodriguez, C. M., J. L. Kirby, B. T. Hinton. The development of the epididymis.** – In: *The Epididymis – from molecules to clinical practice* (Eds. B. Robaire, B. T. Hinton), New York, Kluwer Academic Plenum Publisher, 2002, 251-269.

Electronic books: **Gray, H.** *Anatomy of the human body* (Ed. W.H.Lewis), 20th edition, NY, 2000. Available at http://www.Bartleby.com.

PhD thesis: **Padberg, G**. Facioscapulohumeral diseases. *PhD thesis*, Leiden University, 1982, 130 p.

Website: National survey schoolchildren report. National Centre of Public Health and Analyses, 2014. Available at http://ncphp.government.bg/files

Page charges

Manuscript publication is free of charges.

Ethics in publishing

Before sending the manuscript the authors must make sure that it meets the Ethical guidelines for journal publication of Acta morphologica et anthropologica.

Human and animal rights

If the work involves the use of human subjects, the authors should ensure that work has been carried out in accordance with *The Code of Ethics of the World Medical Association* (Declaration of Helsinski). The authors should include a statement in the manuscript that informed consent was obtained for experimentation with human subjects. The privacy rights of human subjects must always be observed.
All animal experiments should comply with the *ARRIVE guidelines* and should be carried out in accordance with the U.K. Animals (Scientific procedures) Act, 1986 and the associated guidelines *EU Directive 2010/63/EU* for animal experiments, or the National Institutes of Health guide for the care and use of Laboratory animals (NIH Publications No. 8023, revised 1978) and the authors should clearly indicate in the manuscript that such guidelines have been followed.

Submission Details

Acta morphologica et anthropologica is published twice a year as one volume with 4 issues. For the first two issues (1-2) the deadline for manuscript submission is March 15th and for the next two issues (3-4), the deadline is September 15th. Electronic version for issues 1-2 is uploaded on the website till June 30th and for issues 3-4 – till December 30th.

Manuscript submission is electronical only.

The manuscripts should be sent to the Managing Editor email address ygluhcheva@hotmail.com with copy to iempam@bas.bg

All correspondence, including notification for Editor's decision, requests for revision, is sent by e-mail.

Submission declaration

Submission of the manuscript implies that the work described has not been published previously, is not considered under publication elsewhere, that its publication is approved by all authors, and that if accepted, it will not be published elsewhere in the same form, in English or in any other language, including electronically, without the informed consent of the copyright-holder.

Contributors

The statement that all authors approve the final article should be included in the disclosure.

Copyright

http://www.iempam.bas.bg/journals/acta/Author%20Copyright%20Agreement_last.pdf

Upon acceptance of an article, the authors will be asked to complete a "**Copyright Transfer Agreement**".

http://www.iempam.bas.bg/journals/acta/Copyright_Transfer_Agreement_Form_AMA.doc

Peer review

Once a manuscript is submitted, the Managing Editor (or the Editor-in-Chief) briefly checks the manuscript for conformance with the journal's Focus, Scope, Policies and style requirements and decide whether it is potentially suitable for publication and can be processed for review, or rejected immediately, or returned to the author for improvement and re-submission.
Manuscripts are peer-reviewed by the Editors, Editorial Board members, and/or external experts before final decisions regarding publication are made. The entire editorial workflow is performed in the following steps:

1. The submitted manuscript is checked in the editorial office whether it is suitable to go through the normal peer review process.

2. If deemed suitable, the manuscript is sent to 2 reviewers for peer-review. The choice of reviewers depends on the subject of the manuscript, the areas of expertise of the reviewers, and their availability.

3. Each reviewer will have 2 weeks to provide evaluation of the manuscript. The Editor may recommend publication, request minor, moderate or major revision, or provide a written critique of why the manuscript should not be published (rejected).

4. In case only one reviewer suggests rejection of the manuscript, the latter is subjected to additional evaluation by a third reviewer.

5. The manuscript will be published in a revised form provided that the authors successfully answer the critics received. The Editor-in-Chief is the final authority on all editorial decisions.

Open Access

This journal provides immediate open access to its content on the principle that making research freely available to the public supports a greater global exchange of knowledge.

After acceptance

Proof correction

The corresponding author will receive proofs by e-mail in PDF format and will be requested to return it with any corrections within two weeks.